# PORE STRUCTURE AND DIFFUSIONAL PROPERTIES OF HARDENED CEMENT PASTES

VITALIS TATA NGALA

Doctor of Philosophy

THE UNIVERSITY OF ASTON IN BIRMINGHAM

September 1995

THE UNIVERSITY OF ASTON IN BIRMINGHAM

**Pore Structure and Diffusional Properties of Hardened Cement Pastes**

**Vitalis Tata NGALA** **Doctor of Philosophy 1995**

# ABSTRACT

This study has investigated the inclusion of pulverised fuel ash (PFA) and blast furnace slag (BFS) into hardened cement pastes (HCP) in retarding the ingress of chloride ions and oxygen molecules from the external environment.

The rates of diffusion of chloride ions through HCP is thought to be influenced by the proportion of capillary pores, and by their connectivity and tortuosity. Pore structure data in HCP were obtained by the desorption technique and mercury intrusion porosimetry. An alternative method of measurement, the low temperature calorimetry, was developed to provide information regarding porosity and ice formation in HCP and other porous materials.

The chloride diffusion coefficients were determined by a concentration gradient steady state method while the oxygen diffusion coefficients were determined by a steady state electrochemical technique. The diffusion coefficients obtained for the OPC, OPC/30%PFA and OPC/65%BFS hardened pastes were related to their corresponding pore structure.

The influence of environmental factors such as drying and carbonation on the pore structure and diffusional properties of OPC, OPC/30%PFA and OPC/65%BFS hardened pastes was investigated. Specimens were desorbed from a saturated surface dry condition to a near constant weight at 65% relative humidity (RH) while others were simultaneously exposed to a 65% RH atmosphere and a carbon dioxide atmosphere of up to 5% by volume until there were fully carbonated.

The presence of the interfacial zone at the cement paste-aggregate interface was critically reviewed and identified. The influence of the interfacial zone on porosity and chloride ingress in assumed periodic composites of glass bead mortars was also studied.

The investigations have demonstrated the following;

(a) The use of fly ash and slag in blended cement pastes has resulted in a marked reduction in capillary porosity and rate of chloride ingress.

(b) The ratio of oxygen to chloride diffusion coefficients increased from values close to 1 in permeable pastes, to values of around 15 in low-permeability blended fly ash and slag pastes. This supports the view that the diffusion of chloride ions is retarded by the surface charge of the hydrated cement gel in low-permeability pastes.

(c) Compared with plain OPC pastes, the carbonation of blended fly ash and slag pastes resulted in a marked increase in the coarse capillary porosity and a corresponding increase in the oxygen and chloride diffusion rates.

**KEY WORDS:** **Blended Pastes, Chloride Ion, Oxygen Molecule, Carbonation, Pore Structure, Interfacial Zone, Ice Formation**

**TO MY PARENTS**

**Ephraim Ngala FAISON and Mary Kwabu FAISON**

# ACKNOWLEDGEMENTS

The author is deeply indebted to his supervisor Professor C L Page over the whole duration of the research project. His knowledge and expertise, guidance, encouragement and support were greatly appreciated.

I am very grateful to the trustees of the Overseas Research Students (ORS) Award Scheme and the James Watt Memorial Foundation for financing this research. Thanks are due to British Cement Association for supporting the development of the low temperature calorimeter; in particular to Dr L J Parrott who was also my co-supervisor. His comments, advice and useful discussions were invaluable.

The entire technical staff of the Civil Engineering Department, in particular Mr C J Thompson are thanked for their help and assistance in the laboratory work. Mr Robert Poole's assistance in computing was immensely appreciated.

I wish to thank my research colleagues and friends, especially G Chadbourn, Drs S Yu, G Sergi, G Seneviratne, M Maleki and R G Sibbick for their stimulating discussions and help during the course of this project.

I am particularly grateful to my dear friend Martin Fienkeng who have stood by me and encouraged me at difficult times during my life in the UK. To all my relatives and friends, especially Polycarp Tarla, Cletus Njobe, Tantoh Shieh, Ebob Eta, Lily Abila, George Nche, Betty Achonduh, Patience and John Ajongwen, Felicite and Yvonne Ndikum and Josephine Ngong, thank you for your support. Thanks are also due to Dr Evaristus Mainsah for his effort and patience in reading through this thesis.

Finally, and more importantly, I am eternally grateful to my parents, brothers and sisters for their loving moral support. I will always remain deeply indebted to my parents for their love and understanding throughout my life and for their encouragement and financial support during my school years at Sacred Heart College, Bamenda, Cameroon.

# GLOSSARY OF ABBREVIATIONS

| | | |
|---|---|---|
| ABS | - | Absorption |
| AgI | - | Silver Iodide |
| ASR | - | Alkali Silica Reaction |
| BCC | - | Body-centred cubic |
| BFS | - | Ground Granulated Blast Furnace Slag or GGBFS or slag |
| BFS5NCS | - | OPC/65%BFS, water/binder ratio of 0.5, non-carbonated and saturated, etc. |
| BFS6NCD | - | OPC/65%BFS, water/binder ratio of 0.6, non-carbonated and partially dried, etc. |
| BFS7C | - | OPC/65%BFS, water/binder ratio of 0.7, carbonated, etc. |
| C | - | Carbonated |
| C-S-H | - | Calcium Silicate Hydrate |
| $C_2S$ | - | Dicalcium Silicate ($2CaO.SiO_2$) |
| $C_3A$ | - | Tricalcium Aluminate ($3CaO.Al_2O_3$) |
| $C_3S$ | - | Tricalcium Silicate ($3CaO.SiO_2$) |
| $C_4AF$ | - | Tetracalcium Aluminoferrite ($4CaO.Al_2O_3.Fe_2O_3$) |
| $Ca(OH)_2$ | - | Calcium Hydroxide |
| $CaCl_2$ | - | Calcium Chloride |
| $CaCO_3$ | - | Calcium Carbonate |
| Cap. | - | Capillary |
| $CO_2$ | - | Carbon dioxide gas |
| D | - | Diffusion Coefficient |
| $D_{cl}$ | - | Chloride Diffusion Coefficient |
| $D_{eff}$ | - | Effective Diffusion Coefficient through glass bead mortars |
| $D_o$ | - | Oxygen Diffusion Coefficient |
| $D_s$ | - | Diffusion Coefficient through spheres or glass beads |
| DSC | - | Differential Scanning Calorimetry |
| FCC | - | Face-centred cubic |
| HCP | - | Hardened Cement Paste |
| KCl | - | Potassium Chloride |
| KOH | - | Potassium Hydroxide |

| | | |
|---|---|---|
| LTC | - | Low Temperature Calorimetry |
| MIP | - | Mercury Intrusion Porosimetry |
| NaCl | - | Sodium Chloride |
| $NaNO_2$ | - | Sodium Nitrite |
| NaOH | - | Sodium Hydroxide |
| NC | - | Non-carbonated |
| NCD | - | Non-carbonated and partially dried |
| NCS | - | Non-carbonated and saturated |
| OPC | - | Ordinary Portland Cement |
| OPC4NCS | - | Ordinary Portland Cement, water/cement ratio of 0.4, non-carbonated and saturated, etc. |
| OPC5NCD | - | Ordinary Portland Cement, water/cement ratio of 0.5, non-carbonated and partially dried, etc. |
| OPC6C | - | Ordinary Portland Cement, water/cement ratio of 0.6, carbonated, etc. |
| PFA | - | Pulverised Fuel Ash or Fly Ash |
| PFA5NCS | - | OPC/30%PFA, water/binder ratio of 0.5, non-carbonated and saturated, etc. |
| PFA6NCD | - | OPC/30%PFA, water/binder ratio of 0.6, non-carbonated and partially dried, etc. |
| PFA7C | - | OPC/30%PFA, water/binder ratio of 0.7, carbonated, etc. |
| PRT | - | Platinum Resistance Thermocouple sensors |
| $\Phi_b$ | - | Volume fraction of glass beads |
| r | - | pore radius |
| RH | - | Relative Humidity |
| SCE | - | Saturated Calomel Electrode |
| SEM | - | Scanning Electron Microscopy |
| W/C | - | Water/Cement Ratio |
| W/S | - | Water/binder Ratio |

# TABLE OF CONTENTS

# LIST OF TABLES

# LIST OF FIGURES

## LIST OF PLATES

# CHAPTER ONE

# INTRODUCTION

## 1.1 FIELD OF STUDY

Since the invention of portland cement in the early nineteenth century, concrete has become the most widely used construction material. The idea of embedding steel bars in concrete to form reinforced concrete was later realised in the second half of that century. Henceforth, the application of the composite material grew rapidly, with reinforced concrete being used extensively in buildings, highway bridges, car parks, industrial plants and other engineering structures.

In recent years, the durability of reinforced concrete structures has been a subject under constant investigation. These structures are under threat from factors such as sulphate attack, alkali-silica reaction, carbonation and the presence of aggressive chemicals such as chloride ions. The most important cause of widespread structural damage to reinforced concrete is the attack of steel by the aggressive chloride ions. When chloride ions are present in sufficient quantities in the pore solution, they destroy the passive film often causing localised corrosion in the form of pits (Andrade and Page, 1985; Hansson, 1984; Holden *et al.*, 1983).

Corrosion of reinforcement has been identified as being due mainly to the ingress of chloride ions from external sources such as de-icing salts (New Civil Engineer, 1991) or sea water (Gjorv and Vennesland, 1979). There has been increased use of de-icing salts on highways (Figure 1.1) due to the increasing traffic density and general road construction and development associated with it. In the UK, the use of de-icing salts on highway structures not designed to have protection against chloride ingress has increased, with

consequent increase in reinforcement corrosion (Lawrence, 1986). Furthermore, there has been increasing need for the construction of coastal and offshore structures, most of these structures being made of reinforced concrete.

Thus corrosion of reinforcement in concrete is a severe problem, one which engineers have been trying to tackle over the last two to three decades. A number of solutions have been proposed, some of which have been successfully implemented in practice while others are still under development. These solutions which are either preventive or repair techniques include cathodic protection, polymer impregnation of concrete, protective surface coating of concrete, galvanizing or coating of reinforcement with zinc or epoxy, realkalisation and desalination. Some of these solutions have met with varying degrees of success, most are complicated and are practically not cost-effective. It could be argued that the most practical solution to the problem of reinforcement corrosion is likely to involve exploiting fully the useful properties offered by the various available cements.

In order to develop a very durable concrete, it is vital to understand the pore structure of the hardened cement pastes involved. Engineering properties of concrete such as strength, permeability, diffusivity, shrinkage and creep are known to be associated with pore structure. There are a number of experimental techniques available today for the analysis of pore structure of HCP, with the most widely used being MIP and capillary condensation for large and small pores respectively. The major problem with these techniques is that the specimens have to be dried to obtain the measurements (Feldman, 1972), and this may lead to changes in the microstructure of the material (Parrott, 1983, 1981; Marsh and Day, 1983). Thus there is the need for the development of an alternative or supplementary method of measurement.

It is thought that refining the pore structure of cement pastes may improve the resistance of concrete to chloride ingress. Incorporating pulverised fuel ash (PFA) and ground

granulated blast furnace slag (GGBFS or BFS) as cement replacement material has been employed in a broad spectrum of concrete projects, from highway bridges to marine structures. Fly ash is obtained by electrostatic or mechanical means from the exhaust fumes of coal-fired power stations while slag is a by-product obtained during the manufacture of pig iron in the blast furnace. The use of PFA or BFS in blended concrete is beneficial economically, allowing a reduction of the OPC content in the concrete, and providing an economical means of discarding these waste materials.

The use of blended cements constituting OPC and fly ash or slag forms additional C-S-H gel and other hydration products, improving the microstructure of the hardened concrete, thereby enhancing its resistance to chloride ions and other aggressive chemicals. Researchers (Dhir *et al.*, 1991; Kumar *et al.*, 1986; Roy *et al.*, 1986; Page *et al.*, 1981) have shown that the use of fly ash or slag can reduce the rate of chloride ingress significantly. The authors ascribed these beneficial effects to the physical properties and the chemical composition of the cement blends and their effect on the solid phase and pore solution of the resulting concrete.

The kinetics of chloride ion transport in cementitious materials is not fully understood. It is thought that chloride ingress would be affected considerably by the interaction between the negatively charged chloride ions and pore walls at the cement matrix-pore solution interface. Current research at Aston University (Ngala *et al.*, 1995; Yu and Page, 1991) has supported this hypothesis and suggested that the surface charge effect on ionic diffusion is mainly associated with transport through micropores.

A portland cement consists basically of the following compounds: $C_3S$, $C_2S$, $C_3A$, $C_4AF$ and gypsum. When water is added to cement, several complicated reactions are initiated which finally lead to the formation of a hardened mass. Hydrating portland cement gives rise to several morphological forms including C-S-H gel, $Ca(OH)_2$, calcium aluminate

trisulphate hydrate (ettringite), calcium aluminate monosulphate hydrate, tricalcium aluminate hydrate and other minor constituents. These phases of the microstructure all vary in proportion depending on the type of cement and degree of hydration (Taylor, 1984). The $C_3A$ phase of cement is one of the constituents that protects steel against corrosion. It can react with free chloride in the water forming tricalcium chloroaluminate hydrate, a complex insoluble salt, thus removing the aggressive ions from the pore solution.

Steel may also become susceptible to corrosion if it becomes depassivated by a reduction in the alkalinity of the concrete at the location of the steel. The most common way of neutralization is by carbonation. Carbonation of concrete normally involves a chemical reaction between atmospheric $CO_2$ and products of cement hydration. Carbonation can also initiate corrosion by reacting with the insoluble tricalcium chloroaluminate hydrate, thereby releasing a substantial amount of the bound chloride into pore solution. Previous studies (Bier, 1986; Hilsdorf *et al.*, 1984; Pihlajaavara, 1968) have shown that carbonation generally modifies the pore structure of the exposed material. Sergi (1986) and Dhir *et al.* (1993) have reported that sequential carbonation and chloride attack is a worse degradation problem than either process acting separately. The authors demonstrated that the good qualities of slag and fly ash concretes in resisting the penetration of chloride ions are lost on carbonation.

The performance of plain concrete is governed by the properties of both the hardened cement paste and the aggregate, and by the nature of the interface between them. Compared to the bulk cement matrix, the microstructure of the interfacial zone is characterised by coarser crystals, less cement paste, more capillary pores and preferred orientation of the calcium hydroxide crystals (Scrivener and Gartner, 1988; Scrivener and Pratt, 1986; Grandet and Ollivier, 1985; Barnes *et al.*, 1979, 1978; Hadley, 1972), and is thought to influence fluid transport and other durability-related properties of concrete.

Young (1988) indicated that the permeability coefficients for concrete are generally about 100 times higher than those for comparable pastes and about 3-10 times higher than those for comparable mortars.

## 1.2 PURPOSE OF STUDY

It has been recognised that the properties and performance of concrete are more sensitive to the volume and geometry of the larger pores. The most commonly used and easily available method of measurement of pore structure is MIP. However, due to the limitations of MIP (outlined in Section 3.4.3.2) there is the need for the development of an alternative or supplementary method of measurement. In addition, the use of fly ash and slag as partial cement replacement materials has been shown to modify the microstructure of the resulting paste and retard chloride ingress, but the kinetics of chloride ingress in these concretes are not fully understood. Furthermore, the influence of the cement paste-aggregate interfacial zone and environmental factors such as carbonation and cyclic wetting and drying on the pore structure and transport capabilities of the various cementitious materials are in need of further investigations. In an effort to gain an improved understanding of these phenomena, the present study has been undertaken with the following main objectives;

(1) To establish the differences in pore structure between non-carbonated OPC pastes and the corresponding non-carbonated OPC/30%PFA and OPC/65%BFS blended pastes.

(2) To determine the effects of drying and carbonation on the pore structure of OPC, OPC/30%PFA and OPC/65%BFS pastes.

(3) To contribute towards the development of a low temperature calorimeter for the analysis of large pores in cementitious systems and other porous materials.

(4) To compare the rates of diffusion of chloride ions through OPC pastes with those through blended fly ash and slag cement pastes.

(5) To compare the rates of diffusion of dissolved oxygen molecules through

water-saturated OPC pastes with those through the corresponding blended fly ash and slag cement pastes.

(6) To identify the effect of the surface charge/pore wall interactions of chloride ions by comparing their diffusion rates through non-carbonated OPC, OPC/30%PFA and OPC/65%BFS pastes with those of the similarly-sized neutral oxygen molecules.

(7) To relate the rate of diffusion of both the oxygen molecule and chloride ion through non-carbonated and carbonated pastes to the pore structure of these pastes. This may provide an insight into the binding capabilities of chloride ions or their reaction with the cement hydrates.

(8) To examine the effect of the interfacial zone between cement paste and model aggregates (glass beads) on the rate of chloride ingress and the influence of the volume fraction of glass beads on the interfacial zone properties. This may provide an improved understanding of the continuous phase in mortars and concrete responsible for the transport of chloride ions.

## 1.3 OUTLINE OF THESIS

This thesis is divided into eight chapters. Following this introductory chapter are;

Chapter Two describes the overall experimental programme undertaken: details of materials, preparation of specimens and experimental techniques employed in this study.

Chapter Three describes the experimental work undertaken to determine the porosity and pore structure of cement pastes using desorption at 90.7% relative humidity, oven drying at 105°C and MIP. It outlines the differences in pore structure between OPC pastes and blended fly ash and slag pastes, and describes the development of the low temperature calorimeter, an alternative technique for measuring the pore structure of cement pastes and other porous materials.

Chapter Four describes the steady state method used for determining the effects of w/s ratio and cement type on the rate of chloride diffusion in HCP. This chapter relates the rate of chloride ingress through cement pastes to their pore structure.

Chapter Five describes the steady state electrochemical technique employed for determining the effects of w/s ratio and cement type on the rates of diffusion of dissolved oxygen molecules in HCP. It relates the differences in oxygen diffusion rates between OPC, OPC/30%PFA and OPC/65%BFS pastes to their pore structure and pore continuity or tortuosity. It also examines the ratio ($D_O/D_{Cl}$) of oxygen diffusion coefficient, $D_O$, to chloride diffusion coefficient, $D_{Cl}$, for the various pastes thus identifying the effect of surface charge of chloride ions on pore walls.

Chapter Six outlines the process of carbonation and the factors influencing carbonation in cementitious materials. It determines the influence of carbonation on pore structure of cement pastes and measures the subsequent rate of diffusion of both the oxygen molecule and chloride ion through these carbonated pastes.

Chapter Seven reviews and identifies the presence of the interfacial zone at the cement paste-aggregate interface. It points out the influence of varying volume fraction of glass beads on the porosity and chloride ion transport in glass bead mortars.

Chapter Eight summarises the general conclusions and outlines recommendations for further investigations.


**Figure 1.1: Increase in the use of de-icing salts in the UK and the USA (Lawrence, 1986 and New Civil Engineer, 1991)**

# CHAPTER TWO

# MATERIALS, SAMPLE PREPARATION AND EXPERIMENTAL TECHNIQUES

## 2.1 MATERIALS

All the investigations in this project were carried out using cement pastes and mortars. The main materials used for paste and mortar formulation were Ordinary Portland Cement (OPC), Pulverised Fuel Ash (PFA), Ground Granulated Blast Furnace Slag (GGBFS or BFS), and glass beads. All the mortars used in the investigations contain OPC and glass beads, while blended cement pastes consist of either OPC/30%PFA or OPC/65%BFS for fly ash and slag blended pastes respectively. Other main requirements for specimen curing and conditioning, and for diffusion studies were sodium chloride, sodium hydroxide, sodium nitrite, barium chloride, oxygen gas, nitrogen gas and 5% carbon dioxide gas. Also, silver iodide, ethanol and porous glasses of varying pore diameters were used for the calibration of the low temperature calorimeter.

### 2.1.1 Ordinary Portland Cement

Ordinary portland cement is manufactured by mixing together argillaceous or other silica-, alumina-, and iron oxide-bearing materials, burning them at a clinkering temperature and grinding the resulting clinker. No material other than gypsum, water and grinding aids may be added after burning. OPC is an excellent general cement and is the most widely used since it is readily available. The portland cement used during this investigation was obtained from Blue Circle Cement, and its chemical analysis and Bogue compositions are shown in Table 2.1.

### 2.1.2 Pulverised Fuel Ash

Pulverised fuel ash is the most common artificial pozzolan and is obtained by electrostatic or mechanical means from the exhaust fumes of coal-fired power stations. The fly ash particles are spherical and of at least the same fineness as cement so that the silica is readily available for reaction.

Fly ash is composed of individual unlike particles that are collected, rather than ground from a larger mass, with each particle being derived independently from an individual ground fragment of coal. Different fly ashes also vary considerably from one source to another, depending both on the coal being burned and details of the power plant operating system. A distinction is customarily made between low-calcium content fly ashes (Class F) derived mostly from bituminous coals and high-calcium ashes (Class C) which are derived from sub-bituminous and lignite coals.

The ASTM specification C618-84 describes a pozzolan as a "siliceous or siliceous and aluminous material which in itself produces little or no cementitious value but will, in finely divided form and in the presence of moisture, chemically react with calcium hydroxide (librated by hydrating portland cement) at ordinary temperatures to form compounds possessing cementitious properties". The chemical composition of the fly ash used during this study is shown in Table 2.1.

### 2.1.3 Ground Granulated Blast Furnace Slag

Ground granulated blast furnace slag is a glassy material constituted essentially of the same main oxides as a portland cement, namely lime (CaO), silica ($SiO_2$) and alumina ($Al_2O_3$), but in different proportions. It is a waste product obtained during the manufacture of pig iron in the blast furnace. Slag can be used as lightweight aggregate or granular base, or as cement replacement material depending on its hydraulic properties, which in turn, depend on the cooling process and treatment of the molten slag.

For use as a partial replacement for portland cement, the molten slag is granulated when it is removed from the blast furnace and then ground to a fineness of about 300-550 $m^2/kg$ (Blaine) with a minimum of 250 $m^2/kg$ in the U.K (BS 4550, 1970). This fine product is largely amorphous but reactive when mixed with portland cement and water. The hydration of slag is initiated when $Ca(OH)_2$ liberated in the hydration of portland cement provides the correct alkalinity; subsequent hydration does not depend on $Ca(OH)_2$. The chemical analysis of the slag used during this study is shown in Table 2.1.

### 2.1.4 Glass Beads

Non-porous glass beads used for this investigation were supplied by English Glass Ltd. The specific gravity of the beads was 2.95 while the size range was 0.925-1.292 mm diameter, with at least 80% of the beads within 1.01-1.275 mm diameter range and the rest within 0.927-1.292 mm diameter range.

## 2.2 PREPARATION OF SAMPLES

All the binders used during this investigation were sieved through a 150 μm mesh in order to remove coarse particles. The required proportions of the binders were weighed, and in the case of blended mixes, OPC was added to the fly ash or slag as necessary. Deionised water was added to the mix to produce a paste of the desired water-to-solid ratio (w/s). The mixture was blended thoroughly by hand for about 5 minutes with a spatula. It was then poured into cylindrical PVC containers (49 mm diameter by 75 mm in height), which were vibrated for 2-4 minutes to get rid of any trapped air bubbles. On at least two occasions, the "foamy" layer that had accumulated on the surface was removed and replaced with fresh paste. A polythene sheet was placed on the surface of the paste in each of the cylinders to prevent the entrapment of air by the cap which was subsequently fitted on top.

The cylinders were rotated end over end at a speed of 8 rpm for at least 24 hours in order to minimise segregation and bleeding enabling the production of "as-cast" uniform cement pastes. The specimens were stored in a high humidity curing room at a temperature of 22°C for 2 weeks. Finally, the specimens were demoulded, immersed in a 35mM NaOH solution and stored in another curing room at a temperature of 38±2°C for 10 weeks. This was to ensure that all the samples produced achieved a high level of hydration, especially in the case of blended cements where the fly ash and slag require longer times or higher temperatures than OPC to achieve full hydration (BS 4550, 1970).

When the cylindrical samples were fully cured as expected, thin discs required for diffusion experiments were cut from the central regions. This process was achieved with the use of a Cambridge Microslice-2, an accurate diamond wheel saw, and deionised water for lubricating the blade. The discs obtained were approximately 3 mm thick. Their specimen surfaces were ground with grade 600 emery paper, rinsed with deionised water, and dried with a lens tissue before being fitted into the diffusion cells.

## 2.3 EXPERIMENTAL TECHNIQUES

### 2.3.1 Solvent Replacement

Solvent replacement technique is considered the most effective way of removing water from cement pastes without causing considerable damage to the pore structure (Feldman and Beaudoin, 1991). The alcohol used for this study was propan-2-ol (iso-propanol) because it affects the pore structure to a lesser extent than other solvents, as recommended in the previous investigations (Konecny and Naqvi, 1993; Feldman and Beaudoin, 1991). The specimen was broken into small pieces and immersed into propan-2-ol. The jar containing the sample was vibrated in an ultrasonic waterbath for approximately 5 minutes and the cloudy alcohol discarded. The process of vibration was repeated until the alcohol ceased to become cloudy. It was then assumed that, most of the water in the sample had been removed, since water is miscible with alcohol producing the cloudy appearance.

Following the last vibration, the sample was dried using a cold air blower, and stored in a vacuum desiccator until required for MIP testing.

### 2.3.2 Analysis of Chloride Ion

The concentration of chloride ion and its variation with time of diffusion was determined by withdrawing 100 µl aliquots of the solution in compartment 2 of the diffusion cell (Figure 4.2), and analyzing for chloride ion by a standard spectrophotometric technique (Vogel, 1978). Then 9.9 ml of deionised water was added to each 100 µl aliquot solution followed by 2 ml of 0.25M ferric ammonium sulphate ( $Fe(NH_4)(SO_4)_2.12H_2O$ ) in 9M nitric acid, and 2 ml of saturated mercuric thiocyanate in ethanol.

Chloride ions displace thiocyanate ions which, in the presence of iron (III) ions form a highly coloured complex by the following reaction (Vogel, 1978);

$$2Cl^- + Hg(SCN)_2 + 2Fe^{3+} = HgCl_2 + 2Fe(SCN)^{2+} \qquad \text{.....(2.1)}$$

The coloured solution obtained was lightly shaken and left undisturbed for about 10 minutes for full reaction to occur before pouring into test cell. The intensity of the colour which is related to the original chloride ion concentration, was determined by use of a spectrophotometer which measures the absorption of light at a specific wavelength. A Beckman Model-24 spectrophotometer was employed in this study.

A sample and a reference cell containing the coloured solution and deionised water respectively were placed in appropriate enclosures within the spectrophotometer. A beam of light was passed through the cells at a wavelength of 460 nm. In this case, the difference in absorption of the two cells is an indication of the amount of chloride ion that was present in the original solution. Chloride concentrations were estimated from the calibration curve in Figure 2.1, constructed by plotting a curve of concentration of standard

chloride solutions against corrected absorption (ABS) spectrophotometric values.

### 2.3.3 Phenolphthalein pH Indicator

The phenolphthalein pH indicator solution was adopted for monitoring the carbonation of the thin discs used in Chapter Six because of its convenience and reproducibility (RILEM CPC-18, 1984; Forrester, 1976; Verbeck, 1958). In order to ensure that all the discs were fully carbonated, the thickest one was broken and the phenolphthalein solution sprayed on to the broken surfaces. The phenolphthalein remains colourless for fully carbonated samples and gradually changes from colourless to red for partially carbonated samples for a pH greater than about 9. The carbonation process was continued until the partially carbonated samples were fully carbonated, in which case the sprayed phenolphthalein remained colourless.

### 2.3.4 Determination of Bulk Density

Bulk density measurements were conducted on all discs used for diffusion studies in order to monitor any major variations between replicate specimens. After a diffusion experiment, the specimen was dismantled from the diffusion cell and its weight immersed in water was measured and recorded ($W_1$). The specimen was then removed from the water, lightly wiped with a lens tissue, reweighed in air and the saturated surface dry weight ($W_2$) recorded. The bulk density was determined according to Archimedes' principle as the ratio of weight in air to loss of weight in water;

$$\underset{Density}{Bulk}\,(g/cm^3) = \frac{W_2}{W_2 - W_1} \qquad \text{.....(2.2)}$$

### 2.3.5 Porosity and Pore Structure Measurements

After determining weights $W_1$ and $W_2$ as in Section 2.3.4, the specimen was exposed to an atmosphere of 90.7% relative humidity (RH) at 22°C until a near-constant weight ($W_3$) was recorded. The 90.7% RH atmosphere was controlled by the use of a saturated solution

of barium chloride in an air-tight vacuum desiccator. The specimen was then finally dried at 105±5°C for 24 hours and weight ($W_4$) measured. If the specimen is saturated with water and then dried, the loss in weight is a direct reflection of the void volume since water has a density of about 1 g/cm$^3$. Porosity is given by the ratio of the void volume to the total volume. The total volume as calculated during density measurement is the loss in weight of a sample when weighed in water to that saturated with water but weighed in air. Therefore using notations in Section 2.3.4 and above, the capillary porosity is given by;

$$\underset{Porosity}{Capillary}(\%)=(\frac{W_2-W_3}{W_2-W_1})x100 \qquad \text{.....(2.3)}$$

where the capillary porosity, as measured, represents the pores of size greater than approximately 30 nm (Parrott, 1992), while the total porosity is given by;

$$\underset{Porosity}{Total}(\%)=(\frac{W_2-W_4}{W_2-W_1})x100 \qquad \text{.....(2.4)}$$

The pore structure analyses by means of mercury intrusion porosimetry and low temperature calorimetry are described in Chapter Three.

### 2.3.6 Identification of ASR gel

The glass bead mortar discs were obtained using a diamond wheel saw as described in Sections 2.2 and 7.3.2. One surface of the mortar discs were ground for about 10-15 minutes on a 15 μm and a 9 μm lapping plates. The ground surfaces were polished for about 10 minutes on a 6 μm and a 1 μm polishing plates. The disc surfaces were properly cleaned between each grind or polish. The polished surfaces of the discs were then placed under a Reflected Light Polarising Microscope and an image analyzing system was used to check for the existence of any ASR gel formed.

**Table 2.1(a): Chemical Analysis of OPC, PFA and SLAG cements.**

| Material | OPC | PFA | BFS |
|---|---|---|---|
| CaO | 63.53 | 1.45 | 40.09 |
| $SiO_2$ | 21.20 | 48.2 | 35.51 |
| $Al_2O_3$ | 5.34 | 32.2 | 12.59 |
| $Fe_2O_3$ | 2.62 | 8.02 | 0.58 |
| $SO_3$ | 3.38 | 0.52 | 0.15 |
| MgO | 1.30 | 0.66 | 9.11 |
| $Na_2O$ | 0.09 | 0.98 | 0.24 |
| $K_2O$ | 0.75 | 2.85 | 0.54 |
| Cl | 0.015 | - | 0.09 |
| $TiO_2$ | - | 0.79 | 0.70 |
| L.O.I. | 1.53 | 3.84 | 0.91 |

**Table 2.1(b): Bogue composition of ordinary portland cement (Neville and Brooks, 1987).**

| | $C_3S$ | $C_2S$ | $C_3A$ | $C_4AF$ |
|---|---|---|---|---|
| OPC | 48.2 | 24.5 | 9.7 | 8.0 |

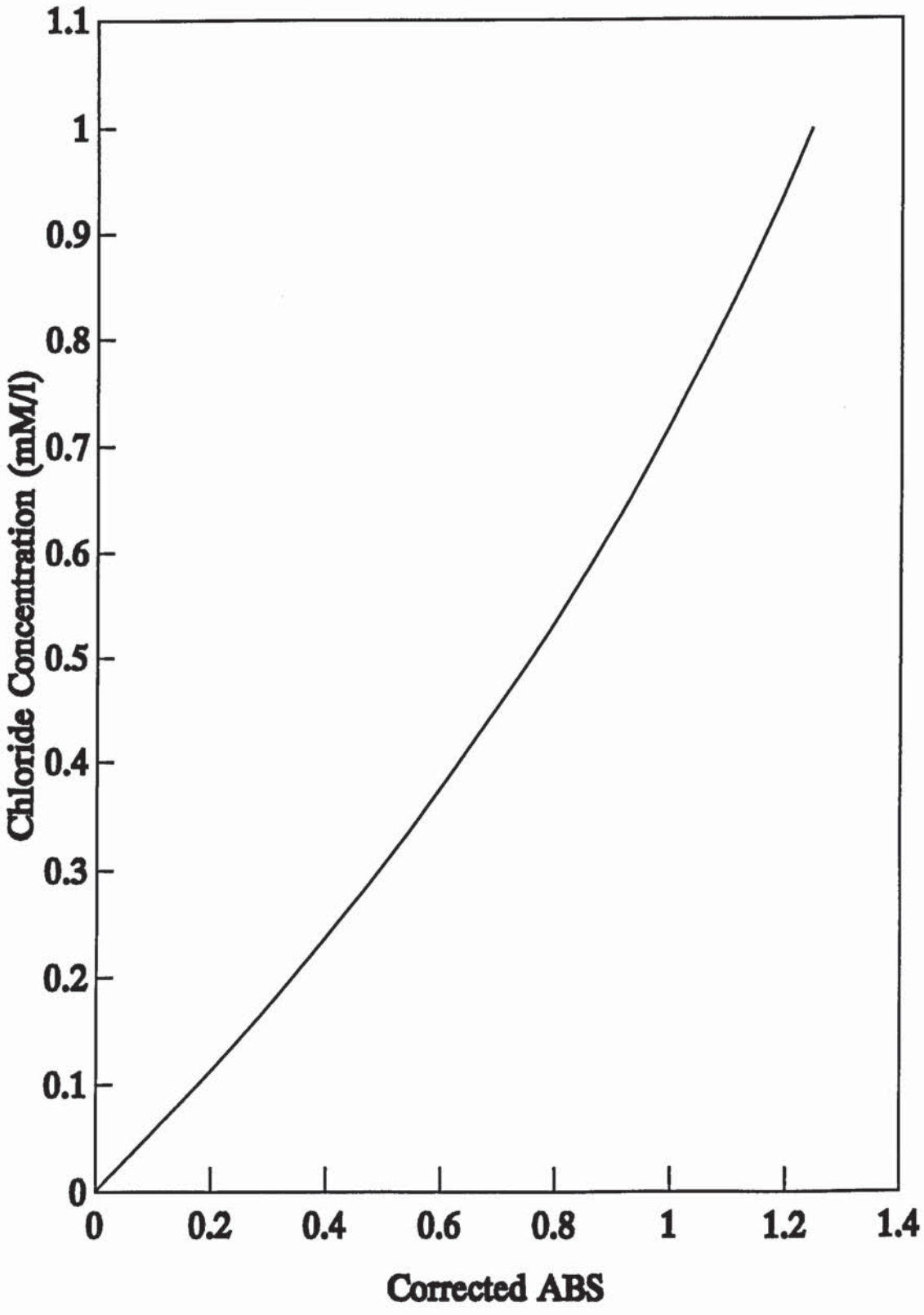


**Figure 2.1: Chloride Calibration Curve**

# CHAPTER THREE

# PORE STRUCTURE OF HYDRATED CEMENT PASTES

## 3.1 INTRODUCTION

Engineering properties of concrete such as strength, permeability, diffusivity, shrinkage and creep are known to be associated with pore structure. There are four aspects of pore structure that might influence ionic and molecular diffusion rates in HCP; porosity or pore volume, pore size distribution, pore geometry and the interconnectivity of the pores. These properties vary in cement pastes and concrete containing different cements such as OPC, PFA, BFS, metakaolin and microsilica. Furthermore, the pore structure of any cementitious material is known to be altered by reactions occurring around or within the material. Some of the well known factors influencing the pore structure of cement paste and concrete are drying and carbonation which have been investigated in Chapter Six. Therefore, from an engineering point of view, there is a distinct advantage in being able to characterise pore structure using simple test methods.

There are a number of experimental techniques that are available today for the analysis of pore structure of HCP, with the most widely used being Mercury Intrusion Porosimetry (MIP) and Capillary Condensation for large and small pores respectively. The major difficulty with these techniques is that the water residing in the pores has to be removed in order to obtain the measurement (Feldman, 1972). In addition, the removal of the water may lead to changes in the microstructure of the material (Marsh and Day, 1988; Parrott, 1983, 1981). Another difficulty is that the application of the measuring technique may lead to changes in these sensitive materials during testing, thus influencing the results obtained.

The desorption of water from saturated or partially saturated specimens and MIP have been employed in this Chapter to analyse the pore structure of the hardened cement pastes under investigation. Furthermore, the development of the low temperature calorimetry is envisaged to assist in this analyses.

## 3.2 LITERATURE REVIEW

Researchers (Konecny and Naqvi, 1993; Feldman and Beaudoin, 1991; Day and Marsh, 1988; Marsh and Day, 1985; Marsh *et al.*, 1985) have shown that with HCP, the method of drying affects the pore size distribution data obtained. Marsh and co-workers (Day and Marsh, 1988; Marsh and Day, 1985; Marsh *et al.*, 1985) found out that solvent exchange drying seemed better to preserve the fine pore structure of plain and blended cement pastes, in comparison to oven-drying at 105°C. Marsh and Day (1985) pointed out that differences between porosity measured by mercury intrusion and that measured by helium pycnometry were noticeable only when there was evidence of significant pozzolanic reaction. The authors also showed that MIP data obtained correlated well with compressive strength. Pore structure determined by helium pycnometry (Marsh *et al.*, 1985) was found to measure only the immediately accessible porosity and was related to the permeability of the paste. The differences in porosity from the two methods was attributed to a discontinuous pore structure or pore-blocking, as a result of pozzolanic reaction. Their results were demonstrated by Feldman (1984) who found out that, for blended cement pastes, mercury intrusion at high pressure gives an unrealistic estimate of pore structure because of the damage it causes. Nevertheless, it was suggested that oven drying blasts open the pores giving a true picture of the actual pore volume because of its effective water removal power (Moukwa and Aitcin, 1988). In so doing, oven drying alters the pore structure mainly by rearranging the hydration products.

Feldman and Beaudoin (1991) investigated the pre-treatment of HCP for mercury intrusion measurements and concluded that;

(a) the method of drying which results in the least influence on the pore structure is iso-propanol replacement followed by immediate evacuation and heating at 105°C for 20 hours;

(b) it is not possible to obtain actual pore size distribution of HCP by MIP because of the sensitivity of the material to stress; and

(c) unlike iso-propanol, solvent replacement by methanol increases the threshold pore diameter of the pore distribution curve by changing surface characteristics of the solid cement hydrate.

Recently, Konecny and Naqvi (1993) agreed with the findings of Feldman and Beaudoin (1991) pointing out that solvent replacement technique is best with respect to preserving the pores in the finest pore size region. The authors also pointed out that freeze drying techniques should be sufficient for evaluating properties related to larger pores such as strength and permeability.

Capillary condensation methods are frequently used to study the characteristics of small pores in HCP and there are well developed techniques for measurement and analysis (Dullien, 1979; Gregg and Sing, 1967). It has been shown (Parrott, 1981 and Parrott *et al.*, 1980) that, using adsorption methods, the reduction in volume of small pores with drying is not fully recoverable with saturation. Litvan (1976) reported that solvent exchange drying could increase the accessibility of the smaller pores in HCP to nitrogen such that, both nitrogen and water adsorption yielded approximately the same surface areas.

An alternative technique that does not require pre-drying of the test specimens is Low Temperature Calorimetry (LTC). Sellevold and co-workers (Bager and Sellevold, 1986c, 1986b, 1986a, 1980; Le Sage De Fontenay and Sellevold, 1980; Sellevold and Bager, 1980) have indicated that LTC is an essential tool for assessing the effects of w/c ratio,

cement hydration, elevated curing temperatures and drying upon larger pores in HCP. Le Sage de Fontenay and Sellevold (1980) demonstrated that cyclic freezing and melting does not seem to cause any significant change in the pore structure of HCP. Investigating the effect of drying on pore structure Bager and Sellevold (1986c and 1986b) concluded that;

(a) drying and resaturation of HCP affects the ice formation pattern, and by implication, the pore structure and,

(b) drying introduces large irreversible structural changes in the pore structure of hardened cement pastes.

In the past, a great deal of research has been directed towards the examination of the smaller pores in HCP, mainly because the adsorption methods of characterization were well developed. However, it has recently been recognised that the properties and performance of concrete are more sensitive to the volume and geometry of the larger pores. As a result, MIP is supplanting adsorption techniques and because of its limitations (outlined in Section 3.4.3.2), there is the need for the development of an alternative or supplementary method of measurement. Consequently, part of this author's study was directed towards the development of the low temperature calorimetry for the analysis of large pores in cementitious systems and other porous materials. The project (described in Section 3.4.4) was pursued in conjunction with the British Cement Association (BCA), who through some of their staff, initiated and designed the main components of the calorimeter a few years ago.

## 3.3 MODELS OF PORE STRUCTURE OF HYDRATED CEMENT PASTES

Hydrated cement paste (HCP) is composed of C-S-H gel and other hydration products of $C_3S$, $C_2S$, $C_3A$ and $C_4AF$, and contains a wide range of pore sizes. Powers' model (Powers, 1958) of pore structure considers two classes of pores; gel and capillary pores, in which the gel pores are visualized as the spaces between gel particles of the matrix. Any spaces not filled by the cement gel are called capillary cavities or pores.

However, Powers' model is now thought to be oversimplified since pastes contain a continuous distribution of pores classified by their behaviour in water (Young, 1988), as shown in Figure 3.1. Micropores and the smaller mesopores are considered to form the intrinsic porosity of the gel. Water in these pores is absorbed and becomes involved in structural bonding, whereas in the larger mesopores and macropores, the water present acts as bulk water.

A totally different model of pore structure to that of Powers' was proposed by Feldman and Sereda (1970). In this Feldman-Sereda model (Figure 3.2), the C-S-H structure is considered to be an irregular array of single layers which may come together randomly to create interlayer spaces. These layers are considered to be bonded together through solid-solid contacts, whose strength is thought to lie between the weak Van der Waals' forces and the strong ionic covalent bond. Water that enters the interlayer spaces becomes part of the structure and contributes to the rigidity of the system. Most of this water cannot be removed from the system on drying until relative humidities of less than 10% are achieved.

Diamon *et al.* (1977) modified the Feldman-Sereda model based on adsorption studies on hydrated $C_3S$ paste after the removal of calcium hydroxide. Adsorption measurements indicated the existence of two kind of pores; a wider inter-gel-particle pore which can be seen even in the inner C-S-H by Scanning Electron Microscopy (SEM) and a smaller intra-gel pore existing within the gel particles which cannot be observed by SEM. The intra-gel pores are further classified into intra-crystalline pores corresponding to the interlayer spaces in the Feldman-Sereda model, and inter-crystalline pores. The authors also suggested that, some relatively large pores in dense pastes are accessible to water only through interlayer spaces.

## 3.4 TECHNIQUES FOR ANALYSIS OF PORE STRUCTURE

### 3.4.1 Introduction

Pore structure is one of the major factors controlling durability of reinforced concrete and other cementitious materials. An accurate determination of the pore structure of a material is necessary, and can lead to a basic understanding of the many phenomena occurring within the material. A variety of techniques such as mercury intrusion porosimetry (MIP), low temperature calorimetry (LTC), sorption, capillary condensation, electron microscopy and image analysis, and small-angle x-ray scattering (SAXS) have been used, but only water desorption, MIP and LTC have been employed in the present investigations.

### 3.4.2 Desorption

#### 3.4.2.1 Experimental Procedure

Similar specimens to those used in diffusion experiments were tested for both capillary and total porosities. The capillary porosity was obtained by exposing saturated surface dry specimens to a an atmosphere with an relative humidity (RH) of 90.7% until a near-constant weight was achieved. The weight, $W_3$, was recorded and the weight loss on drying ($W_2$-$W_3$) was converted to the volume fraction of bulk paste as demonstrated in Section 2.3.5. The 90.7% RH was achieved by placing a saturated salt solution of hydrated barium chloride ($BaCl_2.2H_2O$) in an airtight vacuum desiccator. Air into the desiccators was passed through a jar containing a mixture of carbosorb and silica gel to absorb any $CO_2$, thereby minimizing any possible carbonation. This loss in weight was associated to the evaporation of water from large unconstricted capillary pores and was termed the "capillary" porosity. This simple measure of coarse capillary porosity was adopted because;

(i) it avoided unrealistic drying, which can produce porosity artefacts (Parrott, 1987) and

(ii) it was found to correlate with another transport property, the rate of water absorption (Parrott, 1992). The author demonstrated that water absorption by

cement paste prisms from 91% RH to saturation corresponds to the filling of pores greater than about 30 nm in width.

At the end of the exposure period, the specimens were dried in an oven at a temperature of 105±5°C for about 24 hours and weight, $W_4$, measured. The total porosity was then calculated using Equation 2.4 as described in Section 2.3.5.

### 3.4.2.2 Porosity Results for non-carbonated HCP

The capillary and total porosities obtained for hydrated non-carbonated OPC, PFA and BFS pastes are shown in Tables 4.3, 4.4 and 4.5 respectively, but the average values for each set of specimens are shown in Table 3.1 together with the MIP data. Figures 3.3 and 3.4 illustrate the relationships between the various pastes and the w/s ratio.

Figures 3.3 and 3.4 show that the porosity of all the non-carbonated pastes investigated increase with increasing w/s ratio. However, the porosity of the OPC pastes increases much more rapidly than that of blended fly ash and slag pastes. These figures also indicate that, at the same w/s ratio, the percentage of capillary pores (which plays a vital role in transport properties) is variable depending on the composition and cementitious properties of the material in question.

Figure 3.3 demonstrates that, although the total porosity of the blended OPC/65%BFS pastes are slightly greater than those of plain OPC pastes of the same w/s ratio, the reverse is true for capillary porosity. Furthermore, the difference in capillary porosity between the two types of pastes increases from about 49% at a w/s ratio of 0.4 to 61% at a w/s ratio of 0.7, in comparison to total porosity where the difference is fairly constant at all w/s ratios investigated. This observation between the porosities of the two pastes is very similar to that reported by Ngala *et al.* (1995) between the capillary and total porosities of OPC and blended OPC/30%PFA pastes. This similarity between fly ash and slag pastes

is clearly illustrated in Figure 3.4. This figure indicates that the capillary and total porosities of fly ash and slag pastes are almost identical except at w/s ratios greater than 0.6, where the capillary porosity of fly ash pastes becomes significantly greater than that of slag pastes.

### 3.4.3 Mercury Intrusion Porosimetry

#### 3.4.3.1 Experimental Procedure

The specimens used for MIP were prepared as described in Section 2.3.1. MIP determines the pore size distribution of accessible pores in hydrated cement pastes by measuring the volume of mercury penetrating a sample of paste, as a function of the increasing applied pressure, P. The total volume of mercury indicates the total porosity of paste while the pressure at which the pores are penetrated is related to the pore diameter (d) by the Washburn equation;

$$P = -\frac{4\gamma\cos\theta}{d} \qquad \text{.....(3.1)}$$

where $\gamma$ is the surface tension and $\theta$ is the contact angle

MIP testing was achieved by means of a micromeritics pore sizer 9310 which applies a maximum pressure of 30,000 psi, using samples of 2-3 grammes in weight depending on the properties. A contact angle of 117° was adopted for this study based on earlier work by Winslow and Diamond (1970) where it was reported that, the contact angle for cylindrical pores in hydrated cement pastes oven-dried at 105°C was approximately 117°. Although the contact angle of 117° is not strictly correct for specimens dried by alcohol replacement, the results are considered satisfactory since they are used for comparison and not for purposes of providing exact pore size distributions.

### 3.4.3.2 Limitations of MIP

Although predrying of test samples prior to measurement is the main drawback of MIP, there are a number of other additional factors that require careful consideration when using this technique:

Any pores or groups of pores that are accessible only via narrow entrances or necks (ink-bottle pores) are intruded at a pressure corresponding to the entrance diameter. These ink-bottle pores lead to an overestimate of the volume of small pores.

The high pressures sometimes required for the intrusion of the smaller pores can distort and damage the original pore structure. Feldman (1984) showed that during mercury intrusion, pores in cement pastes (especially blended pastes) were disrupted by the pressure, and on reintrusion were filled at much lower pressures. The author achieved this by distilling the specimens after the first intrusion to remove mercury, and then reintruding them. Following Feldman's work, Shi and Winslow (1985) later found out that, the heat required to remove the mercury after the first intrusion also alters the pore structure. They therefore pointed out that the alteration observed by Feldman was produced not solely by the high pressure involved, but by a combination of the pressure and the heating during mercury removal.

Hydrated portland cement paste does not have a unique contact angle that is applicable for mercury intrusion. A study by Shi and Winslow (1985) revealed that failure to consider changes in the operant contact angle may produce significant distortions in the pore size distribution data. The simplified geometrical assumptions that pores are cylindrical, non-interacting and connected to the surface, necessary for analysis of results are not representative of the HCP pore structure. Winslow and Diamond (1970) demonstrated that there was a "missing" pore volume in pores too fine to be intruded with the limited pressure available. However, further experiments using higher pressures led Diamond

(1971) to conclude that most of the missing pore volume is not in ultra fine pores, but rather in encapsulated pockets. The author suggested that, there is no reason to envisage that the distribution of pore sizes in such encapsulated portions of the paste was much different from the portions not so isolated from the surface. If this be the case, the pore size distribution data obtained using MIP should be reasonably representative of the entire sample.

Despite its disadvantages, MIP is still a valuable tool for obtaining pore size distribution data over a wide range of pores, and is useful for comparing pore size distribution data in different materials or cement pastes because;

(a) the equipment is readily available as opposed to other alternatives, and

(b) the method is fairly quick and convenient to apply.

### 3.4.3.3 MIP Results for non-carbonated HCP

Specimen characteristics for various cement pastes are given in Table 3.1. The table also includes results obtained for the threshold diameter and the total penetration volume intruded by mercury. Figures 3.5 to 3.7 illustrate the cumulative pore size distribution for OPC, PFA and BFS pastes respectively. Each curve shows the total penetration pore volume which resides in pores greater than a given diameter. The distribution curves in Figures 3.5 to 3.7 demonstrate that negligible intrusion takes place in pores with diameters above the "threshold" value, but immediately below, the greatest portion of the intrusion occurs. Winslow and Diamond (1970) interpreted this diameter to be the minimum diameter of pores which are geometrically continuous throughout the HCP sample.

Figure 3.5 shows that for OPC pastes, the total pore volume increases with increasing w/c ratio, from a value of approximately 0.10 $cm^3/g$ at a w/c ratio of 0.4 to 0.26 $cm^3/g$ at a w/c ratio of 0.7. This figure also points to an increase in the threshold diameter with increasing w/c ratio. These results suggest that there is a greater volume of larger

continuous pores in pastes of higher w/c ratio as mentioned in Section 3.4.2.2. These findings between total penetration volume and pore diameter in OPC pastes are similar to those obtained for blended fly ash and slag pastes as illustrated in Figures 3.6 and 3.7 respectively. Nevertheless, this increase in the threshold diameter with w/s ratio is much greater for the OPC pastes than for the blended pastes.

Table 3.1 and Figure 3.12 show that the threshold pore diameter increases from 43 to 147 nm and 26 to 90 nm for PFA and BFS pastes respectively, when the w/s ratio increases from 0.4 to 0.7. These results suggest that the PFA pastes contain slightly more larger pores than the BFS pastes at all w/s ratios investigated. This slight difference should be treated with caution, in the light of the limitations of the technique used, and the fact that these threshold diameters are approximate values. However, both blended pastes reveal a comparatively less coarser pore structure than plain OPC pastes whose threshold diameter increases from 43 to 307 nm for the same range of w/s ratios.

Figures 3.8 to 3.11 demonstrate that, although the BFS pastes have slightly higher total penetration volume than the PFA pastes, the reverse is true for the threshold pore diameter at the various w/s ratios. Despite this, there is a more significant difference between OPC pastes and blended fly ash and slag pastes. Figure 3.8 highlights a large difference of 29% between the penetration volume of OPC and the blended pastes at a w/s ratio of 0.4. This difference gradually reduces with increasing w/s ratio, getting down to as low as 10% and 1% for BFS and PFA pastes respectively at a w/s ratio of 0.7 (Figure 3.11). On the other hand, the difference in the threshold pore diameter of the pastes is almost negligible at a w/s ratio of 0.4, but gradually increases with w/s ratio. A large difference in threshold diameter is more noticeable at w/s ratios of 0.6 and 0.7 (Figures 3.10 and 3.11 respectively). Figure 3.11 shows that at a w/s ratio of 0.7, the threshold pore diameter of OPC is approximately 52% and 70% higher than that of PFA and BFS pastes respectively, indicating a much higher volume of larger continuous pores in the OPC pastes. The

differences discussed above regarding the threshold diameter and total pore volume of the various hydrated pastes are summarised in Figures 3.12 and 3.13.

The intrusion curves for BFS pastes at low w/s ratios of 0.4 and 0.5 (Figures 3.8 and 3.9 respectively) seem to indicate a much higher volume of large pores than was expected. This behaviour, though difficult to account for, may be associated to the disruption of the microstructure of the paste caused either by the drying technique used or by the high pressures encountered during intrusion. This behaviour, however, was not noticeable in BFS pastes with higher w/s ratios of 0.6 and 0.7 (Figures 3.10 and 3.11 respectively).

### 3.4.4 Low Temperature Calorimetry (LTC)

#### 3.4.4.1 Introduction

The pore structure of a fully or partially saturated material can be studied using LTC to monitor heat changes associated with the freezing of pore water or the melting of ice. The heat change is a measure of the quantity of water (and thus the volume of pores) while the temperature indicates the range of pore diameters in which the water freezes. The smaller the pore diameter, the lower the temperature at which water in it is expected to freeze. The major advantage of the LTC over other techniques is that it does not require pre-drying of the test specimen. The removal of water from materials have been shown by researchers (Marsh and Day, 1988; Parrott, 1983, 1981) to cause considerable changes to the microstructure of the material.

Measurement of ice formation in HCP, concrete and other porous materials is essential in view of the fact that the data obtained can be related not only to pore structure parameters, but also to length change, frost resistance and dynamic mechanical behaviour. However, insufficient research has been pursued to measure the extent of ice formation in HCP and concrete, partly due to the lack of readily available equipment. In the beginning, Powers and Brownyard (1947) used an indirect method of calculating amounts of ice from

measured volume changes. Since then, researchers have used various methods to measure heat flow, mainly on porous materials other than concrete (Fagerland, 1974). Sellevold and co-workers (Bager and Sellevold, 1986c, 1986b, 1986a, 1980; Le Sage De Fontenay and Sellevold, 1980; Sellevold and Bager, 1980) performed extensive studies on ice formation patterns in HCP using the Low Temperature Calvet Microcalorimeter. Their findings are summarised in Section 3.4.4.3.

### 3.4.4.2 Freezing Point of Pore Water

The Kelvin equation relates the meniscus radius of capillary condensed water to the relative vapour pressure it exerts. An analogous equation given by Defay *et al.* (1966) relates the meniscus radius to the freezing point of water. Both equations are diagramatically represented in Figure 3.14. This theory, relating pore size to the freezing point of water assumes that the pores are cylindrical and that the contact angle between condensed water and pore wall is zero.

Generally, freezing at high temperatures is associated with large pores. From Figure 3.14, the amount of ice formed to -5°C is equal to the volume of pores with radii greater than 11 nm.

### 3.4.4.3 Literature Review

Sellevold and co-workers (Sellevold and Bager, 1980; Le Sage De Fontenay and Sellevold, 1980; Bager and Sellevold, 1980, 1986a, 1986b and 1986c) studied ice formation patterns in HCP using the low temperature Calvet Microcalorimeter which is described in detail by Le Sage De Fontenay and Sellevold (1980). During the initial investigations, Sellevold and Bager (1980) found out that no freezing of pore water (even with pure water) took place at temperatures greater than -10°C. This behaviour, associated with supercooling, was reduced in further experiments by sprinkling a few milligrams of powdered silver iodide (AgI) on the specimens to seed ice nucleation. One of the main drawbacks of the

Calvet Microcalorimeter was, that the block temperature differed from the specimen temperature during tests. Separate experiments showed that the lag could be between 0.4 to 0.8°C in normal runs and during periods of freeze/thaw activity, or could reach several degrees during periods of high activity.

However, it was the work of Le Sage de Fontenay and Sellevold (1980) that formed the basis of the research on ice formation at their laboratory in Denmark. The authors measured ice formation in hardened cement pastes and concluded that;

(a) little ice forms below a temperature of about -55°C;

(b) the rate of ice formation is not a simple function of temperature, but contains three well defined peaks centred around -8°C, -23°C, and -40°C. The relative magnitude of the peaks is a function of the w/c (Figure 3.15);

(c) melting takes place continuously from -55°C, but by far the majority of the ice melts close to 0°C (Figure 3.15);

(d) the rate of cooling (in the range 1.7 to 13.3°C/hour) has relatively little influence on the amount of ice formed at a given temperature;

(e) the frozen part of the evaporable water varies from 20% (w/c-0.4) to 57% (w/c-0.7);

(f) by far the major part of the ice forms in the pore system.

Bager and Sellevold (1986c, 1986b and 1986a) later investigated the effect of drying on pore structure. The specimens were dried by desorption at room temperature to equilibrium at different relative water vapour pressures, and then resaturated. It was demonstrated that the amount of non-frozen water at -55°C decreases with increasing severity of drying. This was attributed to either a decrease in the amount of pores in which the water is non-freezable, or a decrease in internal surface area due to a collapse of the pore structure. The authors therefore concluded that drying causes an increase in the volume of larger pores as a result of the collapse of the smaller pores.

The heating and cooling cycles obtained for hardened cement pastes using differential scanning calorimetry (DSC) (Beddoe and Setzer, 1990; Dorner, 1984; Dorner and Setzer, 1980) showed good agreement with the thermograms published by Bager and Sellevold (1986c, 1986b and 1986a). However, it has been demonstrated (Dorner and Setzer, 1980; Dorner, 1984) that phase transition of free water in capillary pores occurs at between -10°C and -25°C for pores with radius, r, greater than 10 nm and between -43°C and -52°C for water in the medium gel pores with r values in the range 3 nm < r < 10 nm. Bager and Sellevold observed two or three well-defined phase transitions of pore water in HCP depending on w/c ratio, while Dorner and Setzer could show only two well-defined freezing peaks.

Despite this promising outcome using low temperature calorimetry, the Calvet Microcalorimeter was very expensive to maintain and hence not cost effective to perform experiments. As such the calorimeter could neither be marketed to other researchers at affordable prices, nor used by the authors for further investigations. Since the work of Sellevold and co-workers, very little research has been directed towards the understanding of the connection between ice formation and frost durability, and of the relationship between pore structure, water content, the rate of temperature change and ice formation in HCP and concrete. Consequently, this section is aimed at developing or paving a way for the development of a suitable low temperature calorimeter for the measurement of ice formation in porous materials.

### 3.4.4.4 Development of the Low Temperature Calorimeter

#### 3.4.4.4.1 The Calorimeter

The development of the low temperature calorimeter was initiated at the British Cement Association (BCA) as early as 1986, but was only pursued intermittently thereafter. It was this author and Aston University's interest that reinstated BCA's initial interest in developing this apparatus. The design work and initial stages in the assembly of the

calorimeter were carried out at the former BCA premises in Slough, while the final development to the present state has been achieved at Aston University in Birmingham.

The purpose of the calorimeter is to measure heat flow out or into a sample as it is cooled or heated at a predetermined rate. This would indicate the rate of heat flow as a function of temperature from which information on porosity and pore size distribution could be obtained. This information is envisaged to produce an improved understanding of ice formation patterns and frost durability in cementitious and other porous materials.

The calorimeter shown in Figure 3.16 measures differential heat flow and presently operates in a constant current mode. The calorimeter consists of the following main parts or sections;

(i) sample and reference holders, which are circular copper containers of approximately 15 mm in diameter and 10 mm in height.

(ii) distribution plate, which is a copper plate of size 80 x 30 x 10 mm (L x W x H) and distributes the cooling or heating effect from the main pump uniformly into the sample and reference holders.

(iii) heat sink, made up of solid copper top layer for supporting the components and vertical copper plates below. The copper plates are perforated for easy circulation of water in the water bath.

(iv) water bath, in which the lower part of the calorimeter sits and is maintained at a constant temperature of approximately 5°C prior to and during an operation.

(v) insulation cover, which constitutes a 2 mm thick copper plate on the inside for heat distribution and a 15 mm thick polystyrene on the outside to provide thermal insulation.

The calorimeter block is cooled using main and backup pumps (and power supplies) which are located on the heat sink as shown in Figure 3.16. The temperature is measured by

platinum resistance thermocouple (PRT) sensors which are located directly beneath the sample and reference holders. Heat flow is measured by heat flow sensors on which the holders sit. When operated in a differential mode the heat flow sensors are connected such that the output signal of the calorimeter is proportional to the difference between the heat flow from the sample holder and the reference holder. The heat capacities of the identical holders are thus eliminated from the output signal.

Data collection and treatment are achieved by means of a control circuit box and a computer programme. The data (which consists of time, sample and reference heat flows, differential heat flow, applied voltage and temperature) is collected, treated continuously and stored in a named disk file.

The calorimeter block is cooled or heated by a constant rate of current from the power supplies. This constant current tends to depress or increase the temperature at varying rates during an operation depending on the temperature of the calorimeter as shown in Figure 3.17. This figure shows a fairly steady decrease in cooling rate (for a typical cooling-heating cycle) from approximately 8°C/hour at the start of run to about 1°C/hour towards the end. Similarly, a fairly steady increase in the heating rate from about 1°C/hour to approximately 8°C/hour is also demonstrated in Figure 3.17. However, the faster cooling and heating rates of about 7°C/hour and 7.5°C/hour respectively during periods of phase transition are deemed satisfactory for the purposes of this study. Temperature variations between different cooling-heating cycles were minimal, with a maximum of about 0.3°C and 0.4°C observed during cooling and heating modes respectively. Nevertheless, it would be desirable for future work to enhance the control computer programme such that a constant cooling and heating rate of between 3 to 4°C/hour is maintained throughout a run.

#### 3.4.4.4.2 Calibration

Cooling-heating cycles were run with the specimen and reference holders empty. The differential thermopile signal drifted occasionally, at times reaching absolute values of about 0.3 mV, corresponding to not more than 5% of the output in a typical experiment with a HCP specimen. However, due to the occasional nature of these drifts and the steady nature of the heat flow during experiments, this study can serve as a demonstration that the differential signal in an experiment originates mainly from the specimen.

Control experiments were run using water and water/ethanol mixtures to determine the capability of the calorimeter to monitor phase transitions at different temperatures. In all experiments carried out, powdered silver iodide was used for the purpose of providing nucleation sites for the solutions during ice formation. The cooling and heating cycles for water are shown in Figure 3.18. It can be seen from this figure that, whereas most of the ice melted close to 0°C, the freezing peak of water occurred at about -3.8°C. This behaviour could be associated mainly with the temperature lag between temperature sensors and the sample, and also probably with lack of nucleation sites for ice formation. It must be pointed out that without the presence of AgI, the ice was formed at about -7°C.

Ethanol was used to depress the freezing point of water by making various water/ethanol mixtures (CRC, 1977) as shown in Table 3.2. The cooling curves for the water/ethanol mixtures are shown in Figure 3.19. This figure demonstrates the potential of the LTC to produce and monitor phase changes at temperatures as low as -35°C. The temperatures at which the solutions are expected to freeze are compared in Table 3.2 with the actual values obtained from the cooling runs. The difference between the two temperature values, which seem to decrease with decreasing ice formation temperatures, could be ascribed to properties such as temperature lag and nucleation.

### 3.4.4.5 Results and Discussion

Granular porous glasses with known pore diameters of 36, 81, 149, 205 and 313 nm were used to determine the influence of pore diameter on phase changes using the LTC. Unfortunately, the difference in freezing point depression for the range of porous diameters investigated is almost negligible as shown in Figure 3.14, with a value of about -1.7°C for the pore diameter of 36 nm. The cooling and heating curves for the various porous glasses are shown in Figures 3.20 and 3.21 respectively, while the freezing and melting peak temperatures are shown in Table 3.3. It can be seen from this table and from Figures 3.20 and 3.21 that,

(a) there is a slight variation between the freezing and melting points for the various pore diameter porous glasses;

(b) the freezing of water occurs at about -4°C while the majority of the ice melts close to zero degrees centigrade;

(c) the freezing peak seems to occur at slightly higher temperatures with increasing pore diameters (except in the case of the 313 nm diameter porous glasses).

The potential of the calibrated calorimeter was demonstrated on a few hardened OPC pastes with w/c ratios of 0.5, 0.6 and 0.7. The cooling and heating cycles for 0.788g of pastes for the three w/c ratios are shown in Figures 3.22 and 3.23 respectively. A number of observations can be made:

(a) For the temperature range investigated (+5 to -35°C), there was only one freezing peak observed. The amount of heat flow during this freezing may be associated with the capillary pore volume of these cement pastes.

(b) The relative magnitude of the heat flow peaks for the OPC pastes seems to increase with increasing w/c ratio.

(c) The freezing peaks for the OPC pastes of 0.6 and 0.7 occurred at almost the same temperature (approximately -3.4°C compared to -4.2°C for pastes of 0.5 w/c ratio).

(d) The heat flow curves for the three pastes in Figure 3.23 are slightly different in

shape from those obtained for water/ethanol mixtures or porous glasses. Although some of the ice seems to melt at about -2.5°C, the majority melts close to 0°C. It would be necessary to perform these runs at a slower cooling rate in order to provide a better understanding of the shape of these curves, especially considering that only one peak was observed during the cooling cycles.

The heat flow curves obtained in this study for HCP showed one freezing peak at a temperature of approximately -4°C. This heat flow was associated with the capillary pore volume since water in large pores is thought to freeze at higher temperatures than water in smaller pores. Within the range of temperatures (+5 to -35°C) achieved with this calorimeter, no secondary peak was observed. This suggests that temperatures down to -35°C are probably not low enough to freeze water in the micropores, thus supporting previous conclusions (Dorner, 1984; Dorner and Setzer, 1980; Le Sage de Fontenay and Sellevold, 1980) that the freezing of water in the smaller pores occurs at temperatures below -40°C. It is thus evident that further developments are required in order to achieve temperatures as low as -55°C, where ice formation in the smaller pores is likely to be realised.

Figures 3.20 and 3.21 demonstrate the potential of the present calorimeter to monitor phase changes in porous glasses. It has also been demonstrated in Figure 3.22 that, for the same weight of pastes the amount of heat flow increased with increasing w/c ratio. This heat flow is associated with the capillary pore volume which has been shown in Sections 3.4.2 and 3.4.3 (using Desorption and MIP techniques respectively) to increase with increasing w/c ratio of the pastes. This indicates the potential of the LTC to characterise porosity in HCP and other porous materials and provides scope for further developments.

## 3.5 DISCUSSION

Both techniques employed in this study (desorption and MIP) reveal similar information about the pore structure of HCP, but in slightly different manners. The drying of specimens from a saturated surface dry condition down to 90.7% RH was related to pores with diameters greater than 30 nm (Parrott, 1992) and termed the capillary porosity. The total porosity was further determined by drying the specimens in an oven at 105±5°C. On the other hand, MIP data produces information concerning the pore size distribution, and the threshold diameter and total intrusion volume which could be related respectively to the capillary porosity and the total porosity from the desorption technique. All the properties measured by the two techniques indicate a similar variation with w/s ratio for the different pastes investigated.

It is well established that capillary porosity plays a vital role in the transport properties of cement pastes and concrete. However, the extent to which this capillary porosity affects the transport properties depends not only on the pore volume, but also on the pore size distribution and pore connectivity and tortuosity. Although drying and MIP techniques provide information regarding the pore volume, pore size distribution and to a certain extent the continuity of the pores, they do not identify the tortuosity of the pores, and this is likely to vary in the different cement systems, thereby, influencing the transport properties.

The capillary porosity for PFA and BFS blended pastes is relatively smaller than that for OPC pastes despite the greater total pore volume in these blended pastes. This is a reflection of the greater gel porosity due to the production of additional C-S-H gel associated with the pozzolanic reaction of the fly ash or the hydraulicity of the slag. The reaction of the glass phase (silica and alumina) of fly ash and slag with $Ca(OH)_2$ released by the hydration of OPC, contributes towards the refinement of the pore structure by forming additional C-S-H gel and possibly an aluminate phase. This results in reduced

capillary porosity but increased total porosity. In hydrated OPC pastes, $Ca(OH)_2$ is dispersed throughout the pore structure, causing a better continuity of the pores because of either inhomogeneity of the composite and poor bonding at the C-S-H/$Ca(OH)_2$ interface, or the inherent porosity of the coarse $Ca(OH)_2$ crystals themselves.

There is a significant difference in the pore size distribution and total pore volume between the hydrated fly ash and slag blends. This may be associated mainly with the variation in the chemical composition of the two blends, and the fineness and percentage replacement of the binders used. The influence of these factors on the ultimate pore structure is in turn dependent on the curing temperature (38°C) used and the level of hydration attainable at the end of the 90 days' curing period. Moreover, varying the w/s ratio of the various mixes would inevitably affect the hydration and resulting pore structure of the three cement systems to varying extents as shown in Figures 3.3 to 3.13.

Hydrating portland cement gives rise to several morphological forms: C-S-H gel, $Ca(OH)_2$, ettringite or ettringite-like AFt phases, calcium aluminate monosulfate hydrate or related AFm phases, *etc.*. These combined with residues of unhydrated clinker components and the pore spaces between (and possibly within) the solid particles comprise the microstructural elements making up cement paste. These phases of the microstructure all vary in proportion depending on the type of cement and the degree of hydration. Taylor (1984) calculated the weight and volume proportion of each of the phases in several specific portland and fly ash pastes. A w/c ratio of 0.5 OPC paste hydrated for 3 months was found to have, in its saturated state, 40% C-S-H gel, 16% AFm product, 12% $Ca(OH)_2$, 8% of residual unhydrated cement, and a total of 24% of pore space. It is generally appreciated that the presence of PFA and BFS both limit the amount of $Ca(OH)_2$ that deposits in the early stages of hydration. As such, Feldman (1984) reported that the differences in the pore structure of the OPC pastes and hydrated PFA and BFS blends could be explained simply in terms of their $Ca(OH)_2$ content, which is approximately 18%

for OPC paste, 6% for PFA paste and 2.5% for BFS paste. The extent to which the refined pore structure of OPC and blended pastes and the resulting diffusion kinetics are influenced by natural processes such as drying and carbonation is the subject of investigations in Chapter Six.

Whereas the high curing temperature of 38°C used for this investigation was aimed at accelerating the pozzolanic reaction of fly ash and the hydraulicity of the slag, thereby refining the pore structure, there is the possibility of a contrary effect on OPC paste. Detwiler *et al.* (1991) reported that in plain portland cement concretes, elevated curing temperatures result in a coarser pore structure and a corresponding decrease in the resistance to chloride diffusion. The lower the w/c ratio, the more pronounced the effect of the curing temperature.

These results should be treated with caution since MIP tends to give a misleading image of the pore size distribution. This is more evident in hydrated blended pastes where relatively large pores are connected by narrow entrances leading to an overestimation of the small pore volume. Furthermore, the technique has been proven to cause structural damage during measurement and this would be expected to affect the blended pastes to a greater extent than OPC pastes. Despite these limitations, the MIP technique has been employed by many researchers for comparing the pore size distribution of different cement pastes and other cementitious materials for reasons outlined earlier (Section 3.4.3.2).

## 3.6 CONCLUSIONS

(1) There is a general increase in the capillary and total pore volumes of OPC, OPC/30%PFA and OPC/65%BFS pastes with increasing w/s ratio. However, the rate of increase with w/s ratio varies between the three cement systems.

(2) Compared to plain OPC pastes, the pozzolanic reaction of fly ash and the hydraulicity of slag result in reduced capillary porosity, but increased total pore volume in the various blended pastes.

(3) There is a significant difference in the pore size distribution between the hardened OPC/30%PFA and OPC/65%BFS blends, with the fly ash pastes indicating higher values of capillary porosity and slightly lower values of total porosity. This difference may be associated with the variation in chemical composition and physical properties such as fineness and percentage replacement between the two materials.

(4) The microcalorimetric measurements of heat flow in porous glasses and hardened cement pastes demonstrates the great potential of the low temperature calorimeter developed in this study for characterising the state of pore water in porous materials and providing information regarding the proportion of coarse pores in these materials. This provides an incentive for the further development of the calorimeter and a basis for the interpretation of the mechanical properties of ice formation in porous materials.


**Figure 3.1: Pore size classification for cement pastes (Young, 1988)**

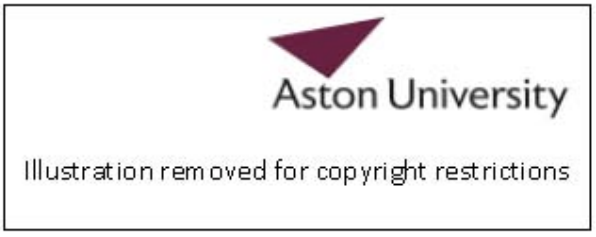


**Figure 3.2: Schematic presentation of Feldman-Sereda pore structural model (Feldman and Sereda, 1970)**

**Table 3.1: Porosity data for non-carbonated hydrated cement pastes.**

| Sample | Bulk Density ($g/cm^3$) | Threshold Diameter (μm) | Total Pen. Volume ($cm^3/g$) | Capillary Porosity (%) | Total Porosity (%) |
|---|---|---|---|---|---|
| OPC4NCS | 1.985 | 0.043 | 0.098 | 4.32 | 41.58 |
| OPC5NCS | 1.886 | 0.115 | 0.161 | 8.36 | 47.48 |
| OPC6NCS | 1.795 | 0.188 | 0.225 | 18.83 | 52.94 |
| OPC7NCS | 1.736 | 0.307 | 0.260 | 24.86 | 55.53 |
| PFA4NCS | 1.945 | 0.043 | 0.139 | 3.07 | 43.27 |
| PFA5NCS | 1.854 | 0.064 | 0.194 | 5.31 | 48.69 |
| PFA6NCS | 1.773 | 0.070 | 0.248 | 9.13 | 55.26 |
| PFA7NCS | 1.705 | 0.147 | 0.262 | 13.60 | 59.02 |
| BFS4NCS | 1.978 | 0.026 | 0.143 | 2.21 | 42.96 |
| BFS5NCS | 1.874 | 0.034 | 0.206 | 4.95 | 48.03 |
| BFS6NCS | 1.786 | 0.064 | 0.278 | 6.76 | 54.50 |
| BFS7NCS | 1.733 | 0.090 | 0.290 | 9.61 | 57.16 |

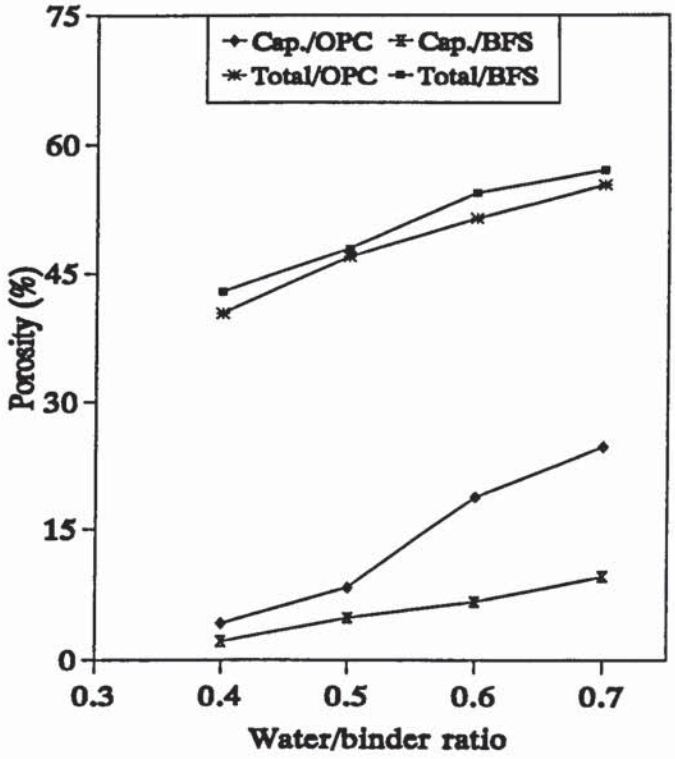


**Figure 3.3: Capillary and total porosities of hydrated OPC and slag pastes**

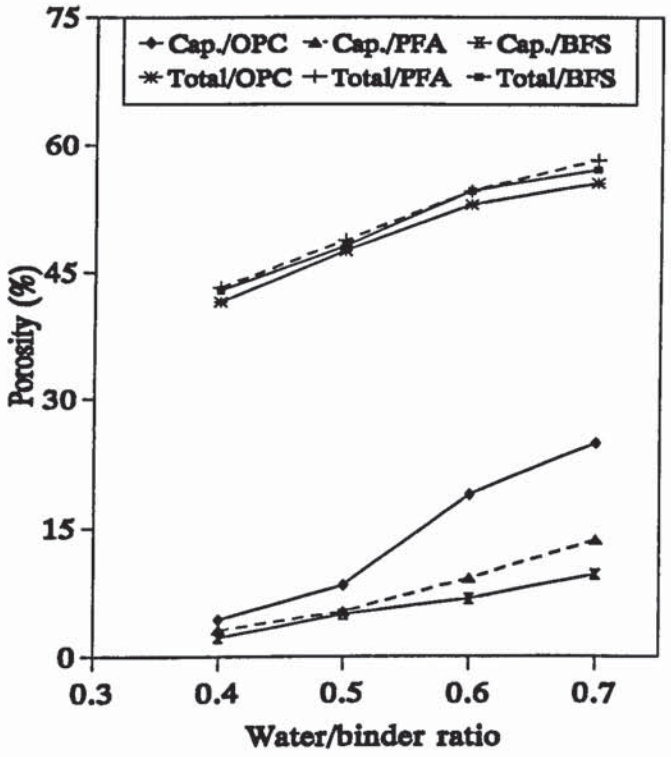


**Figure 3.4: Capillary and total porosities of hydrated cement pastes**

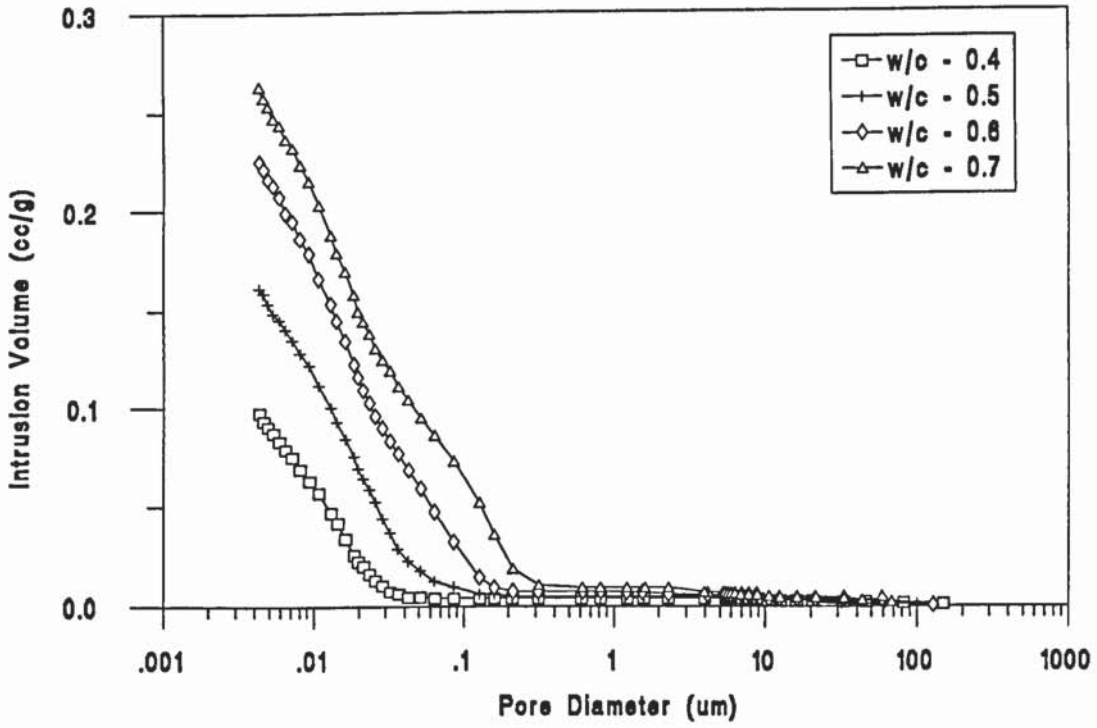


**Figure 3.5: Pore size distribution curves for non-carbonated OPC pastes**

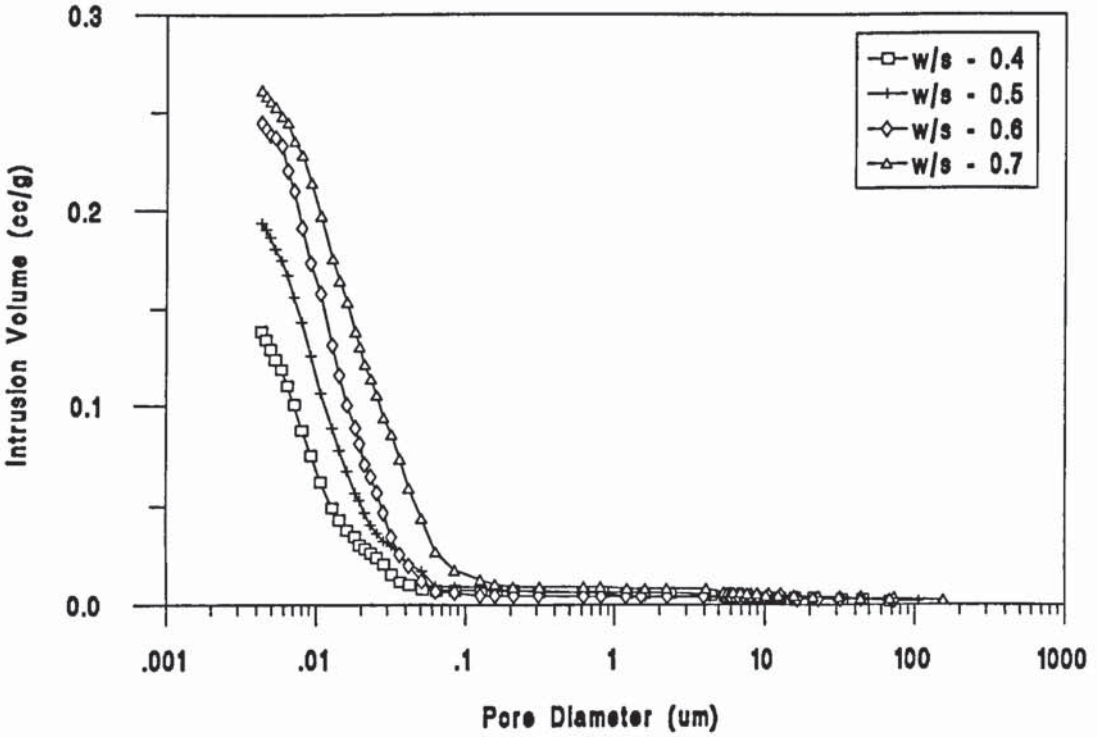


**Figure 3.6: Pore size distribution curves for non-carbonated fly ash pastes**

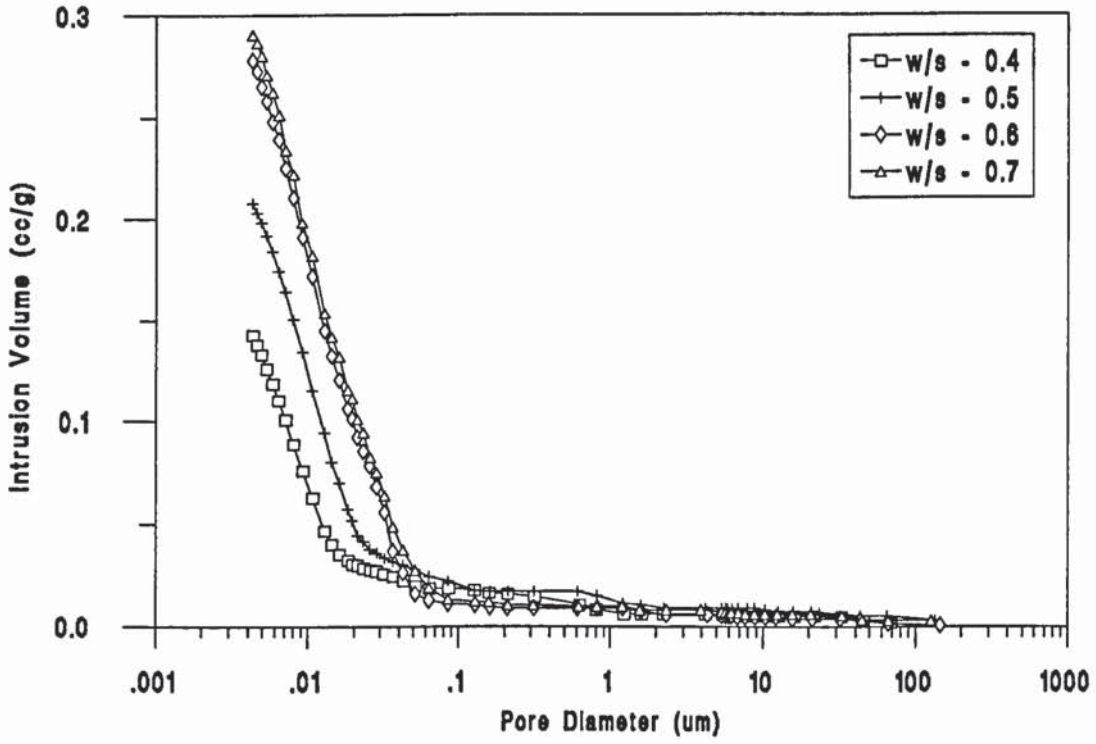


**Figure 3.7: Pore size distribution curves for non-carbonated slag pastes**

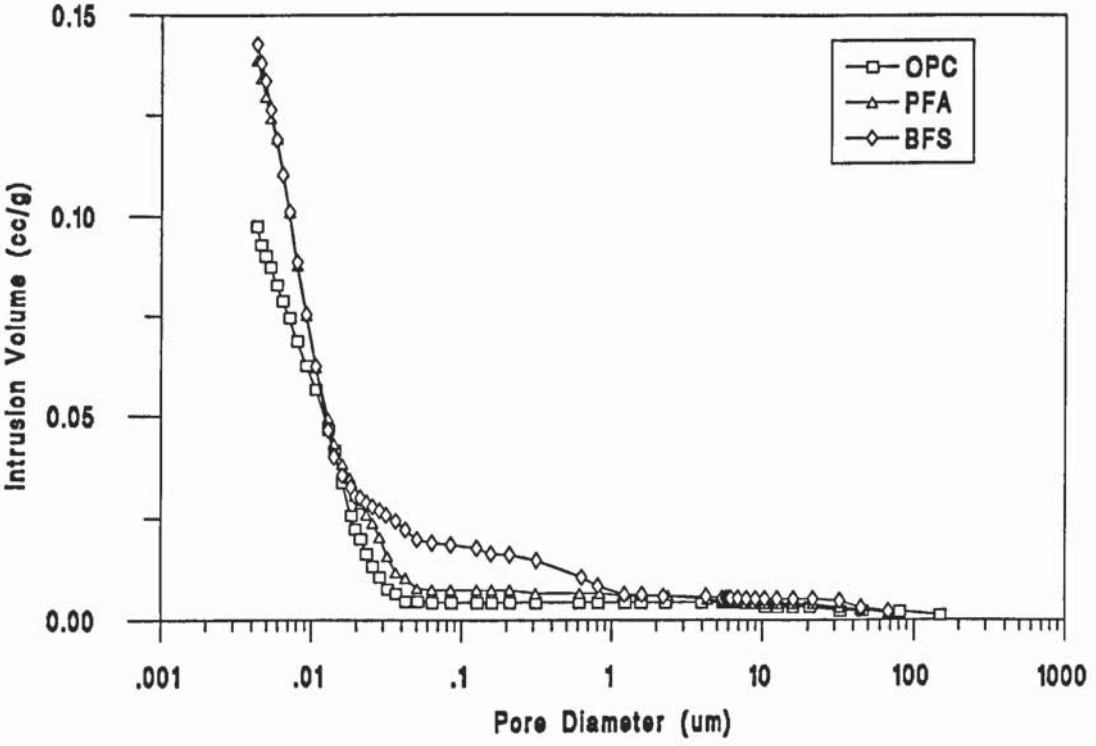


**Figure 3.8: Pore size distribution curves for non-carbonated HCP of 0.4 w/s**

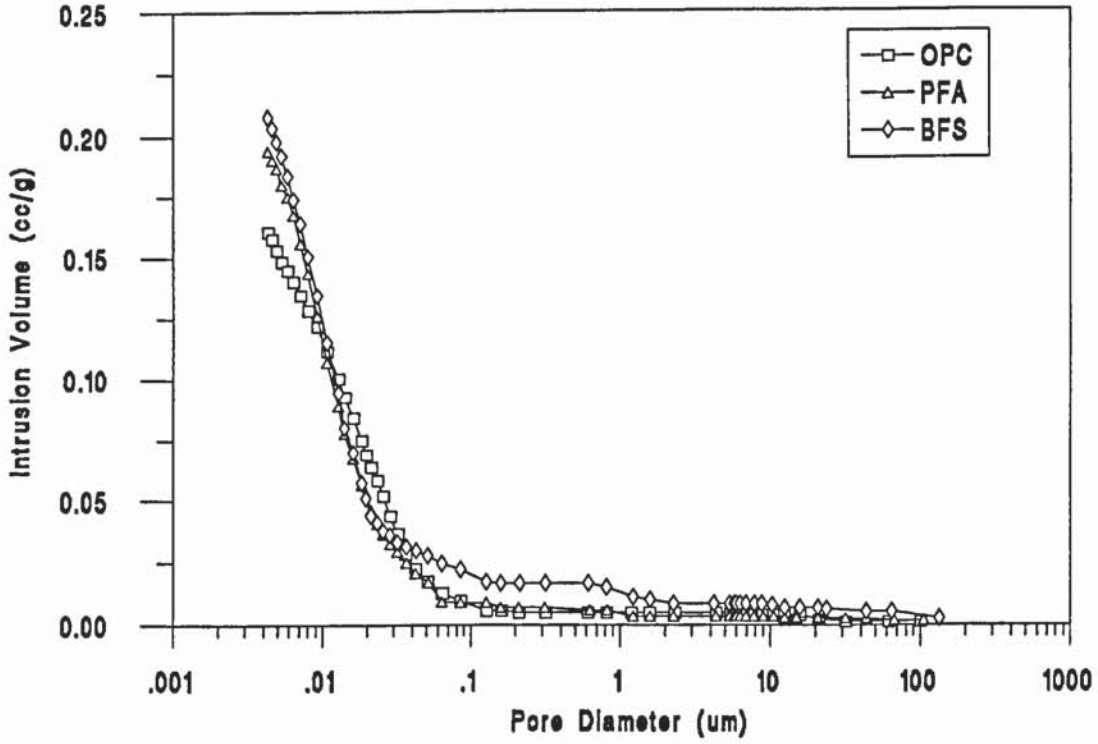


**Figure 3.9: Pore size distribution curves for non-carbonated HCP of 0.5 w/s**

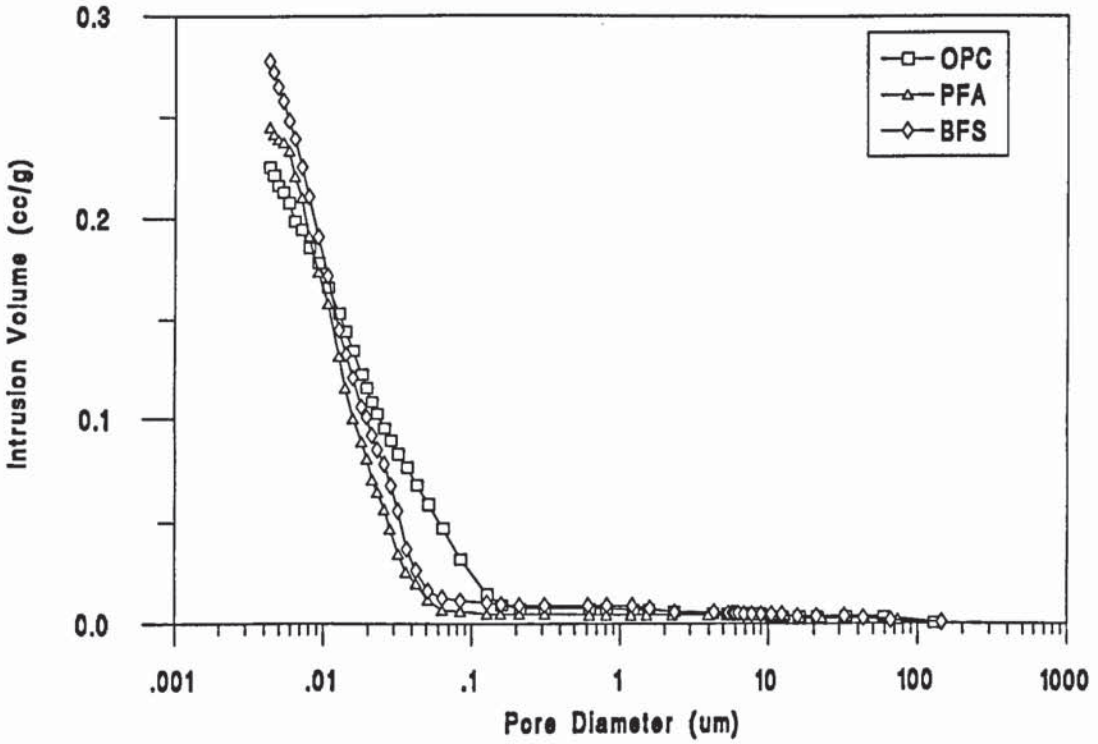


**Figure 3.10: Pore size distribution curves for non-carbonated HCP of 0.6 w/s**

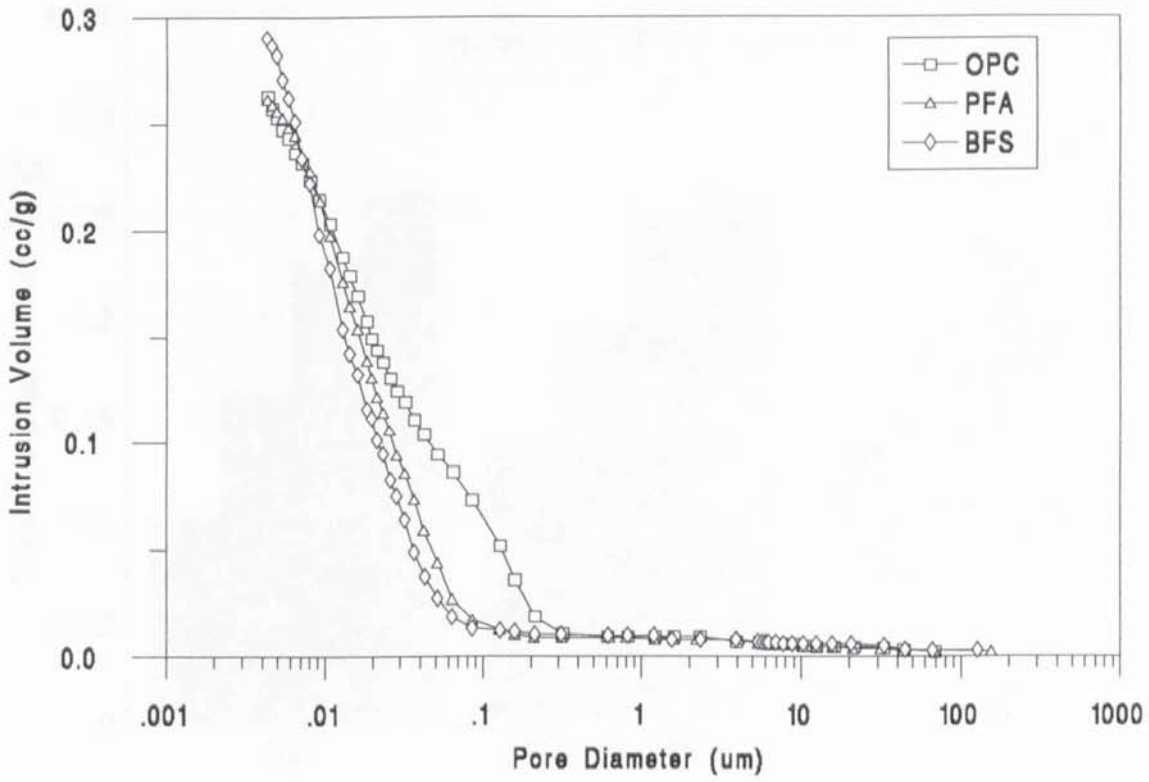


**Figure 3.11: Pore size distribution curves for non-carbonated HCP of 0.7 w/s**

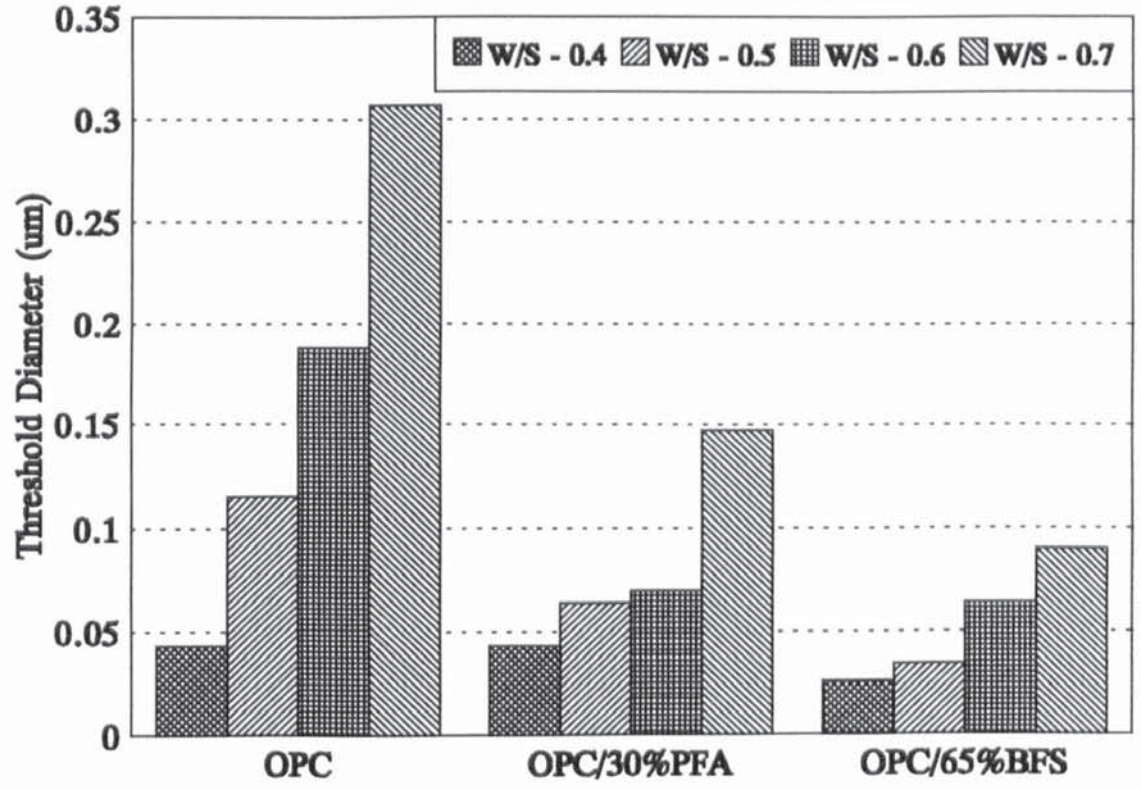


**Figure 3.12: Threshold diameters for non-carbonated HCP samples**

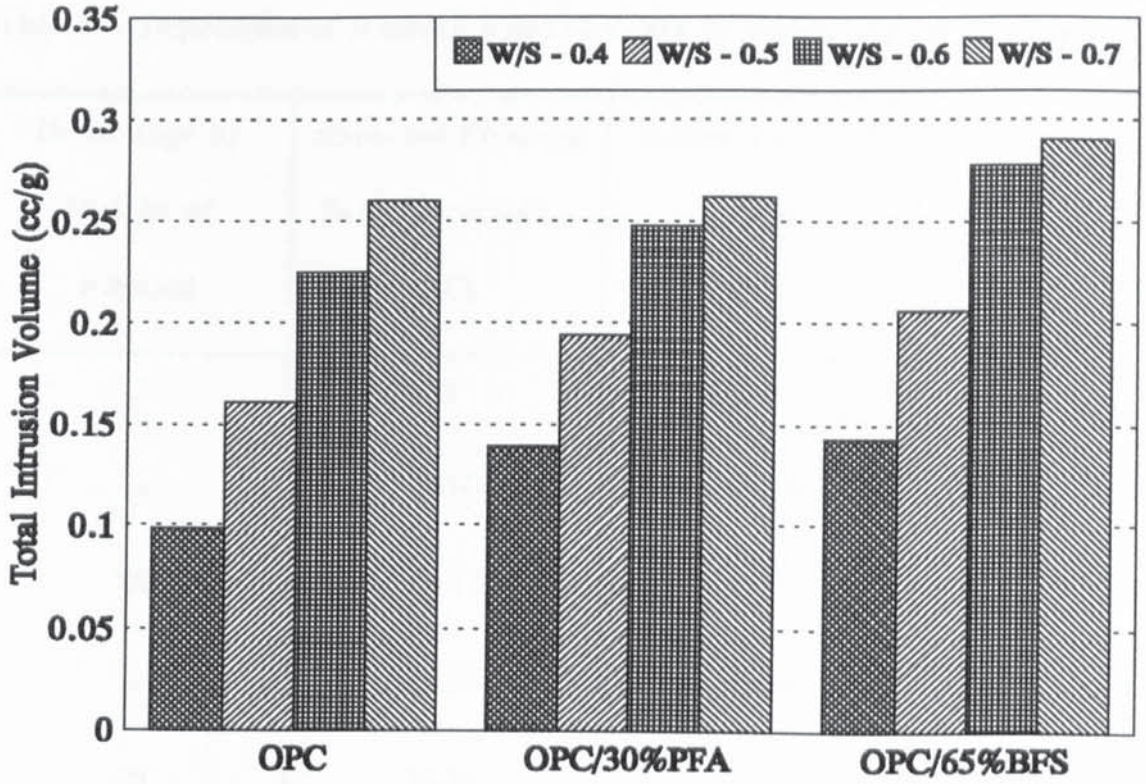


**Figure 3.13: Total intrusion volumes for non-carbonated HCP samples**

**Table 3.2: Depression of freezing point of water by water/ethanol mixtures**

| Percentage by Weight of Ethanol | Expected Freezing Point Depression (°C) | Actual Freezing Peak (°C) |
|---|---|---|
| 0 | 0 | -3.81 |
| 16 | 8.01 | -10.55 |
| 28 | 18.43 | -20.60 |
| 36 | 25.98 | -28.09 |
| 46 | 34.36 | -35.65 |

**Table 3.3: Freezing and melting points for granular porous glasses**

| Pore Diameter (nm) | Freezing Peak (°C) | Melting Peak (°C) |
|---|---|---|
| 36 | -4.68 | -0.75 |
| 81 | -4.48 | -0.31 |
| 149 | -3.85 | -0.75 |
| 205 | -3.49 | -0.31 |
| 313 | -4.18 | -0.19 |


**Figure 3.14: Relationship between meniscus radius of capillary condensed water ($r_k$) and freezing point (Sellevold and Bager, 1980).**


**Figure 3.15: Apparent heat capacity curves (Bager and Sellevold, 1986a) A: Cooling and B: Heating. a, b, c, d and e represent w/c ratios of 0.35, 0.4, 0.45, 0.5 and 0.6.**

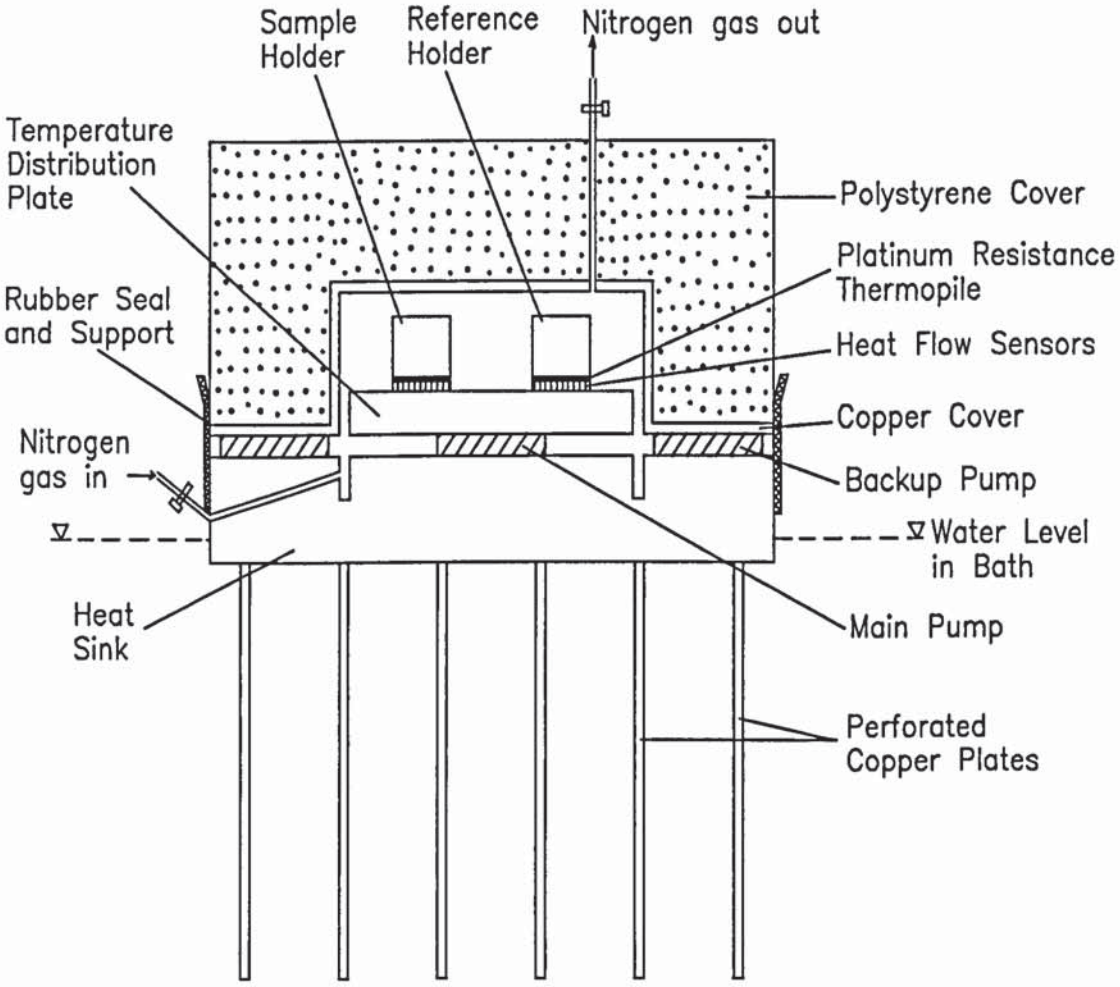


**Figure 3.16: The Low Temperature Calorimeter**

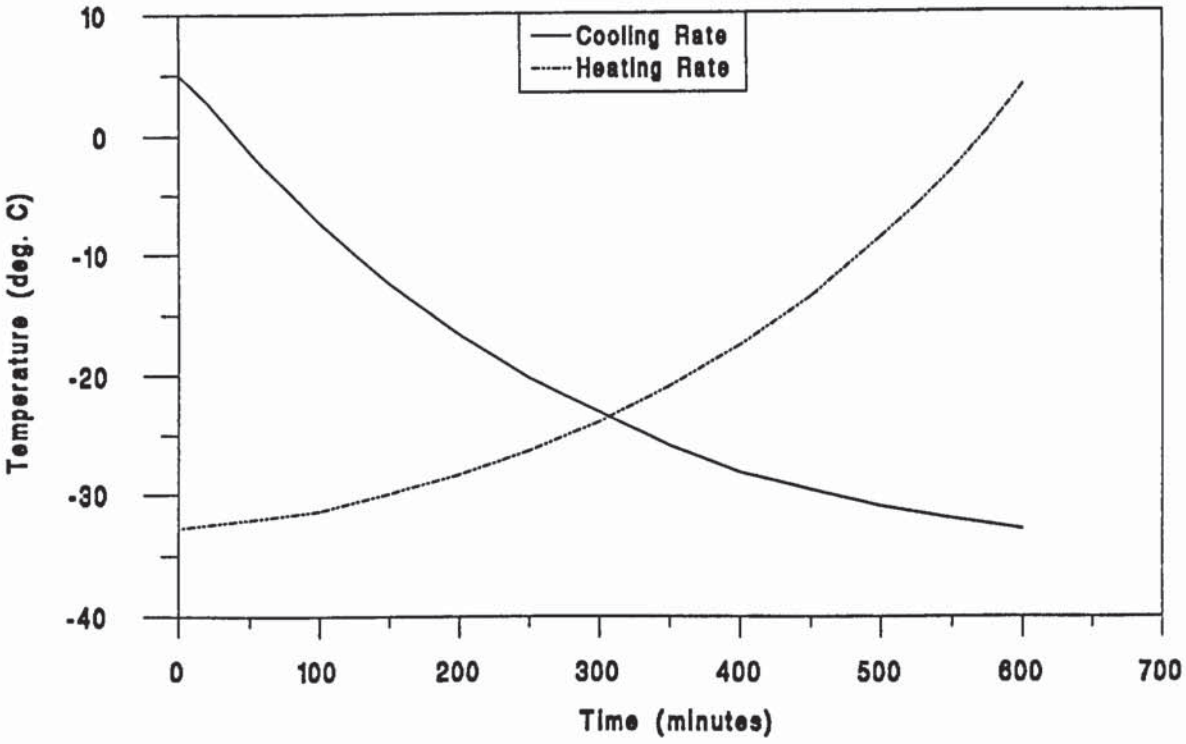


**Figure 3.17: Variation of cooling and heating rates during a typical LTC run**

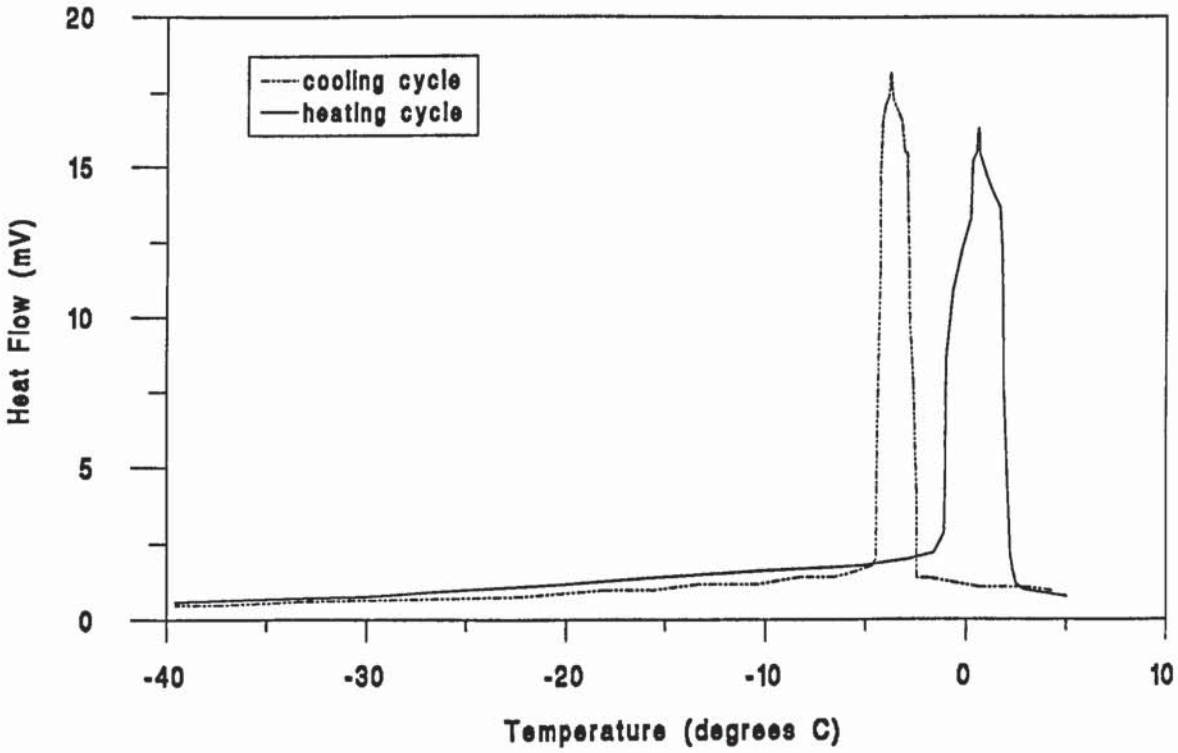


**Figure 3.18: Heat flow curves for water**

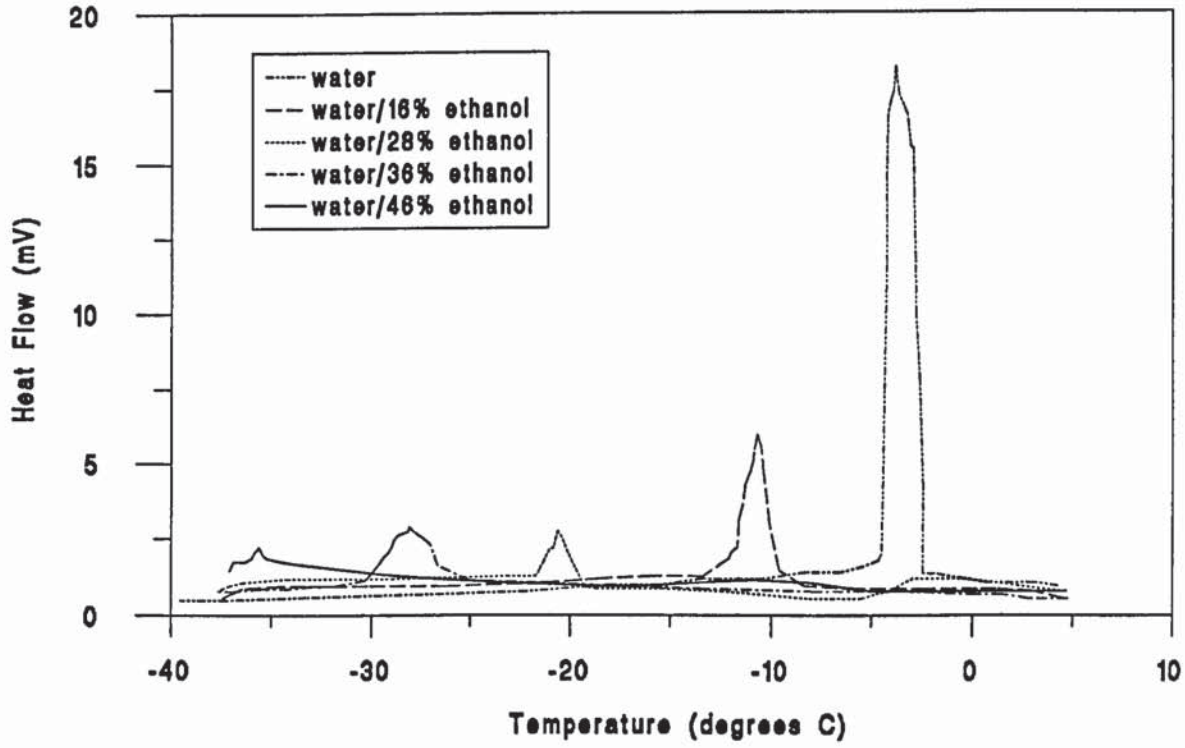


**Figure 3.19: Heat flow curves for water/ethanol mixtures during cooling cycles**

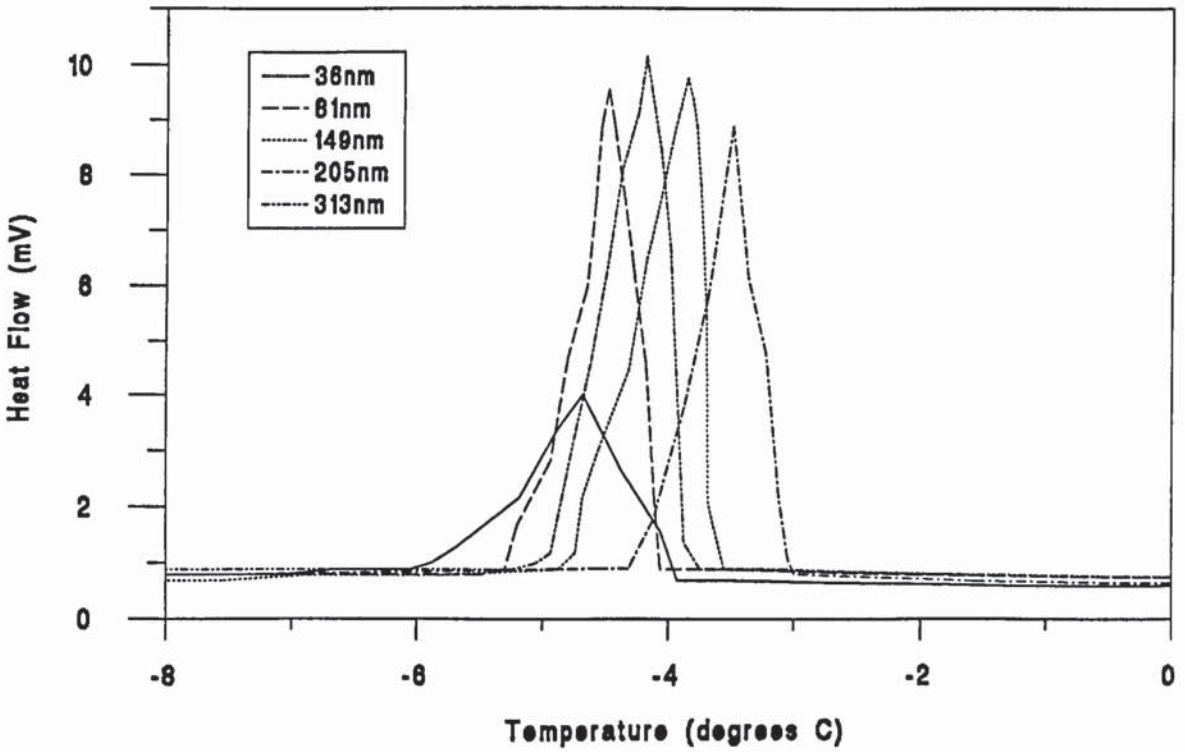


**Figure 3.20: Heat flow curves for porous glasses during cooling cycles**

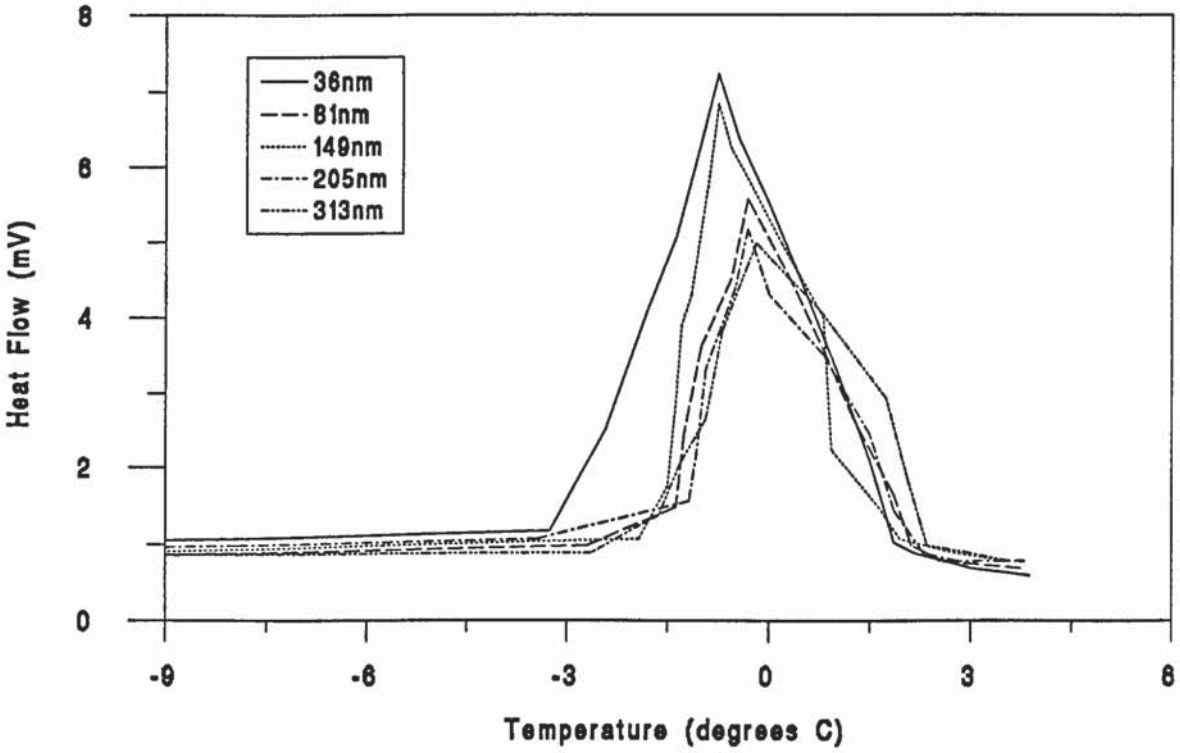


**Figure 3.21: Heat flow curves for porous glasses during heating cycles**

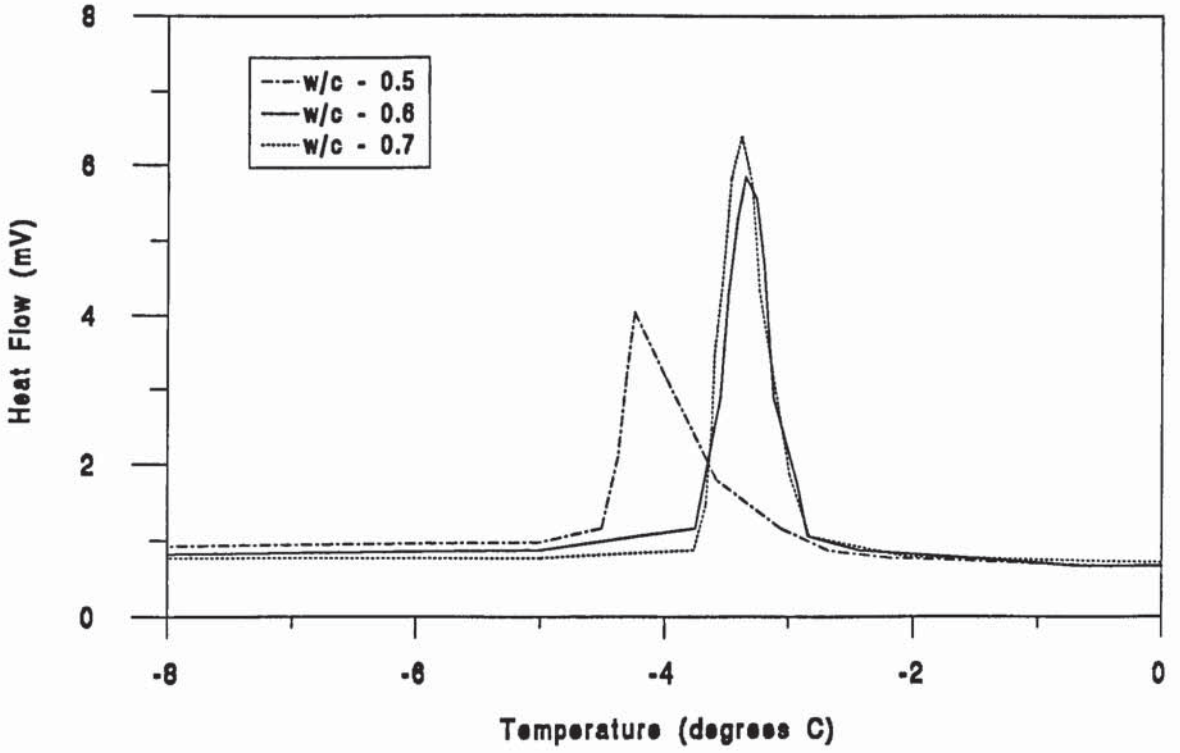


**Figure 3.22: Heat flow curves for OPC pastes during cooling cycles**

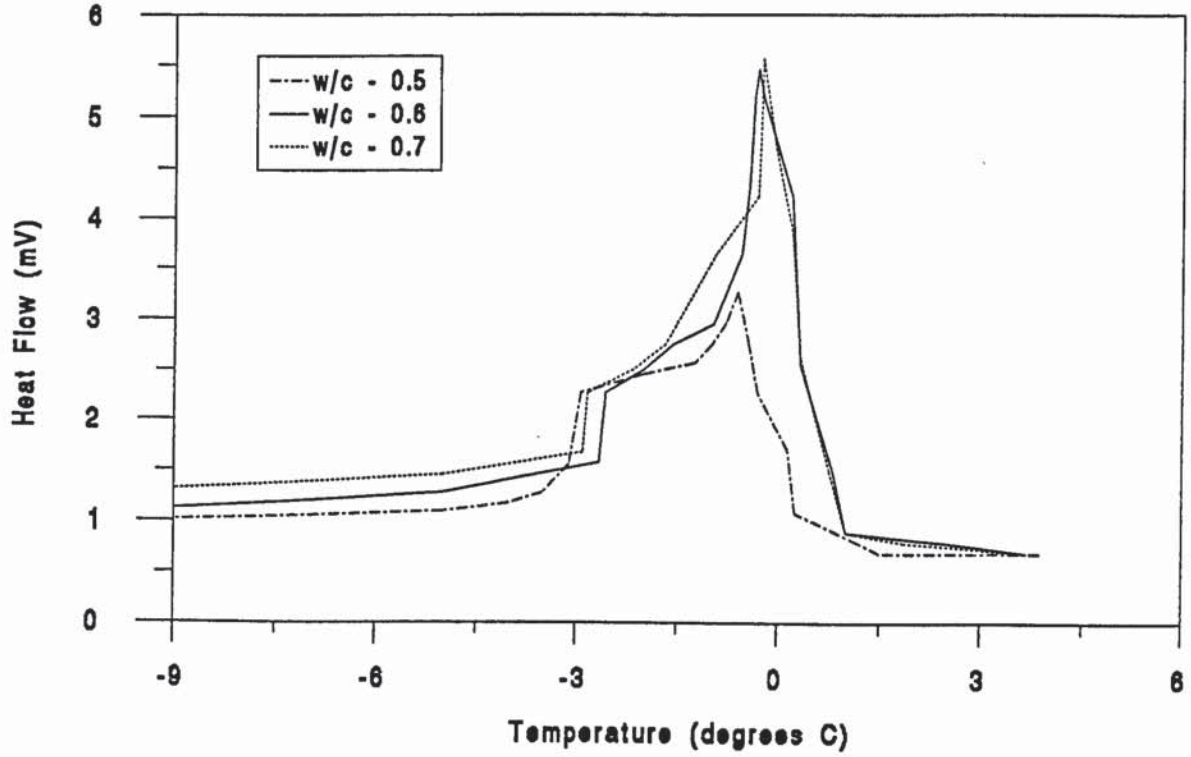


**Figure 3.23: Heat flow curves for OPC pastes during heating cycles**

# CHAPTER FOUR

# IONIC DIFFUSION IN HYDRATED CEMENT PASTES

## 4.1 INTRODUCTION

Reinforced concrete has become the most widely used composite construction material in buildings, bridges and other structures. Nevertheless, these structures are under threat from factors such as sulphate attack, alkali-silica reaction, and the presence of aggressive chemicals such as chloride ions in the cement matrix. The most important cause of widespread structural damage in reinforced concrete is chloride attack. The extent of the attack and subsequent failure due to corrosion of embedded steel is related to the rate of diffusion or permeation of the chloride ions. The cement constituents, the w/c ratio, the pore size distribution, temperature and carbonation are some of the factors that might influence chloride ingress. However the extent to which these factors influence chloride ingress separately or in combination with each other, together with the kinetics of chloride ion diffusion are not fully understood, and thus require further investigation.

The aim of this study is to provide an improved understanding of the mechanism of chloride ingress into cementitious materials by examining the effects of pore size distribution on chloride diffusion in well-cured cement pastes. The use of blended cement pastes constituting OPC/30%PFA and OPC/65%BFS for determining diffusion rates of chloride ions and oxygen molecules (Chapter Five), is envisaged to provide a better insight into some of the factors influencing the kinetics of chloride ion diffusion through hardened cement paste, mortar and concrete.

## 4.2 LITERATURE REVIEW

The environmental sources of chlorides, the mechanism of chloride ion transport in HCP, mortar and concrete as well as the occurrence of chlorides in cementitious materials have all been subjects of previous studies (Section 4.2.1). The investigations undertaken on the use of PFA and BFS concrete have concentrated on bulk engineering properties (e.g., strength) and only recently has attention been directed towards durability in general, and chloride ingress in particular.

### 4.2.1 Availability of Chlorides

Following the abolition of the use of chloride-containing admixtures for reinforced concrete in 1977 (CP110, 1972), chlorides can only be introduced into concrete by salt-contaminated constituent materials, such as sea-dredged aggregates and mixing water, or by the ingress of chlorides from external sources. Since restrictions were imposed on the use of chloride-contaminated constituent materials (BS 8110, 1985), external sources of chloride ions, mainly road de-icing salts and the marine environment, have become the major origins of chloride ions in reinforced concrete.

The problem of the corrosion of reinforcement in concrete structures, especially bridge decks and associated structures due to the ingress of chloride ions from de-icing salts have been identified and reported (New Civil Engineer, 1989; Wallbank, 1989; Collepardi *et al.*, 1972). However the use of de-icing salts is considered necessary in order to keep roads free of ice during the cold winter periods. There has also been a recent increase in the number of coastal and offshore structures, most of these structures constituting reinforced concrete. Nevertheless, the marine environment is one of the most naturally aggressive, in terms of corrosion of reinforcement (Gjorv and Vennesland, 1979). Therefore, it is of vital importance, that new methods are developed in an attempt to limit the destructive nature of chlorides from these sources on steel reinforcement.

### 4.2.2 Mechanism of Chloride Ion Transport in Concrete

Chloride ions may enter concrete either as constituents of the original mix, or by subsequent diffusion into the hardened concrete from external sources. The former has been restricted (BS 8110, 1985), leaving the latter as the more important source of degradation. However, there are circumstances where the use of locally available resources is necessary, rendering the inclusion of chlorides in the original mix inevitable.

Transport of chloride ions in concrete is a rather complicated process which involves diffusion, capillary suction and convective flow with flowing water, accompanied by physical and chemical binding. These complications are usually neglected and pure diffusion, sometimes with binding capacity, is adopted as a predominant transport process in the evaluation of the chloride ion transport property. There are many methods reported for evaluating ion diffusion in HCP, mortar and concrete. They can be classified in three categories: steady state, non-steady state and electrical methods.

#### 4.2.2.1 Steady State Method

The steady state method is generally referred to a diffusion cell experiment of the type adopted in this work and described in Section 4.3. Assuming Fick's first law of diffusion to be applicable after a steady state flow of ions is reached, the diffusion coefficient can be calculated from experimental data as demonstrated in Section 4.3.3.

The steady state method was first reported by Gordon (1945), but it was Ushiyama and Goto (1974) who first used this method to publish a detailed study of the diffusion of chloride ions in HCP. Page *et al.* (1981) presented a detailed procedure of the chloride diffusion experiment (Section 4.3) and carried out an extensive study of chloride diffusion through HCP at various w/c ratios and temperatures. A simpler type of diffusion cell with the added advantage of immersing several specimens in a single tank containing NaCl was proposed by Hansson *et al.* (1985). Roy *et al.* (1986) also developed another simpler type

of diffusion cell, but this required a longer testing period than the previous ones.

#### 4.2.2.2 Non-Steady State Method

The non-steady state method is generally referred to as an immersion experiment. This method usually involves; (i) sealing all except one surface of the specimen to prevent multi-directional penetration; (ii) immersing the specimen in a solution containing the specific ion of interest for a certain period of time; (iii) measuring the penetration depth or concentration profile of the specific ion in the specimen. Assuming Fick's second law of diffusion to be applicable, the diffusion coefficient (D) is calculated from the experimental data by using Equation 4.1 for penetration depth (Collepardi et al, 1970) or Equation 4.2 for concentration profile (Crank, 1975).

$$X_d = 4\sqrt{Dt} \qquad \text{.....(4.1)}$$

$$C = C_o\left[1 - erf\left(\frac{x}{2\sqrt{Dt}}\right)\right] \qquad \text{.....(4.2)}$$

where $X_d$ - penetration depth (m)

t - duration of immersion (s)

C - ion concentration at the distance x ($kg/m^3$)

$C_o$ - ion concentration at the exposed surface ($kg/m^3$)

erf - error function

x - distance from the exposed surface (m).

It is very important that the specimen is well saturated prior to immersion, in order to avoid secondary processes such as capillary suction and moisture transport occurring. This ensures that the assumption of pure diffusion is appropriate. The immersion period may be several months or even years depending on the properties of the specimen.

The penetration depth is usually determined by a colorimetric method (Collepardi *et al.*, 1970) and concentration profiles can be obtained as described by Sergi *et al.* (1992). Poulsen (1990) proposed a method to calculate diffusion coefficient by sophisticated curve fitting of Equation 4.2 to concentration profiles using a portable calculator. The only standardized test procedure of an immersion experiment so far is the AASHTO Designation T259-80 (1980).

#### 4.2.2.3 Electrical Method

The electrical method involves the application of an external electric field across the specimen and the measurement of certain parameters which are considered to be related to the diffusion coefficient of the ions.

Whiting (1981) proposed a first type of electrical method for determining chloride permeability of concrete called the "Coulomb test", which involved the application of a 60V D.C. potential across the specimen. Hansen *et al.* (1986) introduced another method using a weak electric field and thus, involving a longer testing period which is almost similar to that of the pure immersion experiments. Dhir *et al.* (1990a) modified Whiting's method by measuring the increment of chloride concentration in the anodic cell. They calculated a "potential difference (PD) index" on the basis of Fick's first law, but realised that the PD index was about a hundred times larger than the diffusion coefficient obtained with the conventional diffusion cell method. Tang and Nilsson (1992), established a mathematical model of ion diffusion under the action of an electric field and proposed a new type of electrical method for directly and quickly determining the chloride diffusion coefficient in concrete.

Recently, Andrade (1993) critically reviewed the Rapid Chloride Permeability Test standardized by AASHTO, pointing out its limitations and errors but recognising its contribution to the development of a simple and quick test for chloride migration. The

author also reviewed the electrochemical fundamentals of the processes developed in concrete under the influence of an electric field and presented the limitations and assumptions needed for the simplified resolution of the Nernst-Planck and Nernst-Einstein equations. In order to determine the accuracy of the migration method to measure the diffusion coefficient of chlorides, Andrade and Sanjuan (1994) performed preliminary experiments and concluded that;

(i) migration tests resulted in a practical method of accelerating chloride diffusion across concrete, thereby considerably shortening the time required to calculate the effective chloride diffusivity;

(ii) the effective chloride diffusivity values calculated from migration experiments were about two to four times smaller than those calculated from natural diffusion tests.

Garboczi and Bentz (Garboczi and Bentz, 1992; Bentz and Garboczi, 1991) have recently shown that, the diffusivity of cement pastes can be studied by using computer simulation to generate digital image-based microstructural models.

For comparison, some experimental results from different researchers and different methods are listed in Table 4.1. It can be seen from Table 4.1 that the results from non-steady state methods and electrical methods are consistently higher than those obtained from the steady state method.

Conventionally, the steady state method is the most appropriate laboratory method for determining the rate of diffusion of a particular ion in the concrete being studied (Buenfeld and Newman, 1987). However, the results are questionable since the method is strongly influenced by factors such as, disc thickness, temperature, concentration of solution and co-existing ions. Although the non-steady state method provides diffusion coefficients of the concrete being tested, it is very time consuming and labour intensive. The electrical

method provides the possibility of rapid evaluation, but cannot be used for determining the diffusion coefficient of a specific ion of interest. Consequently, the steady state method has been adopted and used in the present study for both chloride and oxygen diffusion measurements.

### 4.2.3 Influence of Concrete Properties

Atkinson and Nickerson (1984), using the diffusion cell technique, termed their diffusivities the "intrinsic diffusion coefficients" because they do not represent the flux flowing through a cross sectional area of the liquid, but that through the area of the medium. They were also critical that an osmotic flow of liquid may result from the low to the high concentration side. They pointed out that temperature had at least two effects on diffusion; one was the temperature-induced changes in the pore structure and the other, the basic temperature dependence of the diffusion mechanism.

Powers *et al.* (1958, 1954) studied the effect of w/c ratio on the permeability of mature OPC pastes. They concluded that varying the w/c ratio resulted in a change in total porosity and pore size distribution. Goto and Roy (1981b) later confirmed this and found out that varying the w/c ratio affects the pore structure and permeability in hardened cement pastes. Powers *et al.* (1954) had showed that permeability is related to capillary porosity; gel pores control the permeability for pastes with w/c ratio below 0.4 since the capillary pores are only interconnected by the gel pores. When capillary porosity is relatively high, the capillaries are a continuous interconnected network through the gel. Thus for mature pastes with w/c ratio above 0.5, capillary porosity determines permeability. Goto and Roy (1981b) then pointed out that for w/c ratios below 0.5, the w/c ratio and curing age had relatively negligible effects on the diffusion of sodium and chloride ions, thus confirming Powers' postulate.

Page *et al.* (1981) demonstrated similar effects of the pore structure on chloride diffusion. They showed that for diffusion in mature OPC pastes, the activation energy was substantially higher than that of ions in normal aqueous solutions. Their results indicated a fairly constant value of activation energy for pastes with w/c ratios of 0.4 and 0.5 but showed a significant decrease in activation energy in pastes with a w/c ratio of 0.6. They attributed this to the availability in pastes of 0.6 w/c ratio of relatively large unconstricted capillaries which were absent in pastes of lower w/c ratios. Midgley and Illston (1980 and 1984) have demonstrated that w/c ratio affects the penetration of chloride ions and that chloride ions alter the pore structure and reduce the average pore size after penetration.

Temperature has been shown to have a significant effect on diffusional properties in concrete and cement pastes (Lambert *et al.*, 1989; Goto and Roy, 1981). Page *et al.* (1981) found that for pastes of the same w/c ratio, the effective diffusivity of chloride ions depends on the temperature at which the diffusion was taking place. Detwiler *et al.* (1991) demonstrated that elevated curing temperatures result in a coarser pore structure and a corresponding decrease in the resistance to chloride diffusion. This effect was found to be more pronounced in concretes of lower water/cement ratios. Cement paste has been found to behave as an electronegative semi-permeable membrane for temperatures up to 70°C (Goto and Roy, 1981; Ushiyama and Goto, 1974), but for temperatures above 70°C, it may be assumed to be an electropositive semi-permeable membrane (Goto and Roy, 1981).

### 4.2.4 Effect of Blending Materials

In blended cement mixes, the blending materials such as PFA and BFS form additional C-S-H gel and other hydration products, improving the microstructure of the hardened concrete, thereby enhancing its resistance to chloride ions and other aggressive chemicals. The diffusion of chloride ions has been found to be strongly influenced by the type of cement, and the type and proportion of the blending materials (Roy, 1986). Blended

cement pastes containing appropriate amounts of PFA, BFS and silica fume exhibit substantially lower diffusion rates than does the corresponding OPC paste (Malek *et al.*, 1989, 1987; Li and Roy, 1986; Roy *et al.*, 1986; Page *et al.*, 1981).

Page *et al.* (1981) reported that blended cement pastes containing PFA or BFS sustained lower diffusion rates at 25°C than OPC pastes of the same w/c ratio. This was attributed to the variation in the pore structure of the materials. Kumar *et al.* (1986) also showed that the addition of PFA results in a lower chloride ion diffusion rates at temperatures of 38°C and 60°C. They associated this with the decrease in the interconnectivity of the porous matrix within the blended paste. Collepardi *et al.* (1972b) explained that the differences in chloride diffusivity in the different types of cement pastes was due to the interaction occurring between chloride ions and the pore surface of the various pastes. Roy *et al.* (1986) pointed out that blending OPC with PFA or BFS leads to lower porosities and finer pore structure. It was reported by Dhir *et al.* (1991) that it is PFA quantity and not quality that affects chloride diffusion, and that in some extreme cases, the value of the diffusion coefficient was reduced by up to 70%.

The use of PFA and BFS blended cements has been proven to reduce chloride diffusion dramatically compared with that in OPC. The mechanism of chloride ingress into hardened cement pastes and concrete has been associated partly with the interaction or binding of chloride ions to the pore walls and partly with the properties of the cement gel. However, the extent to which these properties affect ionic diffusion in the different types of cementitious materials is not fully understood. The use of PFA and BFS blended cement, as well as varying w/s ratio would provide well-cured cement pastes with distinct pore structures and material properties. Determining the chloride diffusivity and pore structure in these cement pastes and comparing them with the corresponding diffusivity of neutral oxygen molecule (Chapter 5), is expected to pave the way for a better understanding of surface charge effects on ionic diffusion and other related transport properties.

### 4.2.5 Occurrence of Chlorides in Concrete

Chlorides occur in concrete in three distinct forms; chemically bound, physically adsorbed and as free chlorides in pore fluid (Arya and Newman, 1990; Dhir *et al.*, 1990b; Tuutti, 1980), as shown in Figure 4.1. The relative proportion of chlorides present in each of these forms is a property of the cement type and content, w/c ratio, curing temperature and age (Arya *et al.*, 1990). Cements with high $C_3A$ content and pozzolanic additives show low levels of free chloride concentration for the same total chloride content (Glasser *et al.*, 1988; Byfors, 1986). This was associated with the ability of $C_3A$ to react with chloride ions forming Friedel's salt as demonstrated by Equations 4.3 and 4.4.

Free chloride ions are known to be the most significant form of chloride present in concrete since they alone can cause reinforcement corrosion. The physically adsorbed chloride ions are those adsorbed onto the pore walls and built into the structures of the hydration products (Ramachandran, 1971). Thus the amount of physically adsorbed chlorides would depend on the availability of the adsorption sites and the nature of the hydration products.

Hydrated $C_3A$ has been reported to react rapidly with chlorides to form calcium chloro-aluminate hydrates ($3CaO.Al_2O_3.CaCl_2.10H_2O$), generally in the mineralogical form of Friedel's salt (Hoffman, 1984; Mehta, 1980; Midgley and Illston, 1980), as follows;

$$Ca(OH)_2 + 2NaCl \rightarrow CaCl_2 + 2NaOH \qquad \text{.....(4.3)}$$

$$CaCl_2 + 3CaO.Al_2O_3 + 10H_2O \rightarrow 3CaO.Al_2O_3.CaCl_2.10H_2O \qquad \text{.....(4.4)}$$

In addition to $C_3A$ in cement, there may be other components contributing towards the binding of chloride ions since cements with no $C_3A$ have been found to show significant binding capacity (Verbeck, 1975; Monfore and Verbeck, 1960).

#### 4.2.5.1 Effects of Chlorides on Hydrates

It has been reported that prolonged exposure of specimens to chloride ions results in a decrease in the rate of chloride ingress (Dhir *et al.*, 1991; Page and Lambert, 1986), suggesting some modifications in both the microstructure and binding properties of the specimens with time. Hoffman (1984) observed a decrease in the gel pore content in chloride-exposed cement mortar specimens and attributed this to the formation of Friedel's salt and other complex minerals affecting a reduction in the amount of gel pores. It has been observed in the present study, that the rate of chloride diffusion through blended cement pastes with w/s ratios below 0.5 decreased significantly with long exposure periods. This could be associated to the blocking of the pores as a result of chloride binding. The formation of smaller pores of a discontinuous nature as a result of chloride ingress has provided practical evidence of reduced permeability (Kayyali, 1989; Kayyali and Haque, 1988; Midgley and Illston, 1984).

#### 4.2.5.2 Effects of Chlorides on Pore Solution

The main parameters of the chemistry of the cement pore solution are; (i) ionic strength, which affects ion exchange reactions with solid phases, (ii) pH, which determines the degree of hydrolysis, and (iii) cation composition. The main cations in the pore solution are generally those of potassium ($K^+$), sodium ($Na^+$) and calcium ($Ca^{2+}$).

It was reported by Tritthart (1989) that the binding capabilities of cement pastes to chloride ions increase with increasing pH ($OH^-$ concentration) of the chloride solution and *vice versa*. The introduction of chloride ions would result in an increase in free chloride concentration in pore fluid with time. The concentration would vary depending on the associated cations added to the mix. It has been observed that the addition of NaCl produces a higher percentage of free chloride ions in pore solution than $CaCl_2$ (Al-Hussaini *et al.*, 1990; Kawamura *et al.*, 1988; Andrade and Page, 1986), and produces more C-S-H gel for high w/c ratios (Midgley and Illston, 1980). On the other hand, it was reported by

Hansson *et al.* (1985) that the addition of $CaCl_2$ to OPC mortar resulted in higher corrosion rates than the addition of NaCl or KCl. This effect was attributed to a combination of a coarsening of the pore structure and a decrease in the pH of the pore solution by $CaCl_2$. However, this effect was not related to the concentration of chloride ions remaining in the pore solution.

## 4.3 EXPERIMENTAL PROCEDURE

### 4.3.1 Sample Preparation and Experimental Set-up

The specimens or discs used for the chloride diffusion experiments were prepared as outlined in Section 2.2. After obtaining the thin discs and hand grinding them on grade 600 emery paper, each one was mounted into a glass diffusion cell similar to that used by Page *et al.* (1981), as shown in Figure 4.2. Each disc was mounted between the ground flanges of the two compartments and sealed with lightly greased rubber gaskets placed between the disc and the flanges. The flange joint was well wrapped with PTFE tape to ensure isolation of the cell contents from each other or from any external contaminants. A layer of PVC insulation tape was wound round to provide additional strength in holding the assembly together, the seal being completed with a final layer of PTFE tape.

The high concentration side (compartment 1) of each cell was filled with 1M NaCl in 35mM NaOH solution, while the low concentration side (compartment 2) was filled with a known volume of 35mM NaOH solution. The controlling parameter for the type and concentration of solution used (NaOH) was the curing solution, as the two had to be identical to avoid leaching of other ions which could interfere with diffusion. Five cells were set up for each condition being investigated, and placed in a waterbath at a constant temperature of 25°C. The experimental set-up is shown in Figure 4.3.

### 4.3.2 Chloride Ion Measurement

Chloride ion diffusion across the thin discs was determined by means of a spectrophotometer. 100 ul aliquot of the solution in compartment 2 of each cell was withdrawn on a regular basis and analyzed for chloride ion as described in Section 2.3.2. The withdrawn solution was not replaced as the overall reduction in volume was negligible. These measurements were carried out over a period of about 2 to 5 weeks for OPC pastes and about 2 to 6 months for blended PFA and BFS pastes, depending on the w/s ratio of the pastes being investigated. At the end of each experiment, the diffusion cells were dismantled, and the diffusion areas of the discs determined by measuring the diameter of the marks left by the grease. The thicknesses of the discs were measured by means of a micrometer gauge.

### 4.3.3 Chloride Diffusivity

After an initial time, $t_o$, during which steady state chloride ion diffusion becomes established across the thickness of the disc, there is a linear increase in the chloride ion concentration with time in compartment 2 of the diffusion cell. The time required to achieve a steady state condition, varied from a few days to months, depending on the properties of the specimens under investigation. The concentration of chloride ions in compartment 2 was analyzed by the spectrophotometric technique as described in Section 2.3.2, and presented in Table 4.2 for sample OPC7NCS. A typical example of the increase in chloride ion concentration with time in compartment 2 is shown in Figure 4.4. Throughout the period of measurement, the concentration of chloride ion in compartment 1 is assumed to remain effectively constant since the concentration of diffused chloride ion in compartment 2 is negligible comparatively.

The flux, J, of chloride ion entering compartment 2 is given by;

$$J=\frac{V}{A}\frac{dC_2}{dt}=\frac{D}{l}(C_1-C_2) \qquad \text{.....(4.5)}$$

where D is the diffusion coefficient of chloride ion, V is the volume of the solution in compartment 2, A is the cross-sectional area of diffusion, l is the thickness of the disc and $C_1$ and $C_2$ are the concentrations of the solutions in compartments 1 and 2 respectively.

Rearranging Equation 4.5 gives;

$$\frac{dC_2}{C_1-C_2}=\frac{DA}{Vl}dt \qquad \text{.....(4.6)}$$

Integrating Equation 4.6 for $t>t_o$ and $C_1>>C_2$ yields;

$$C_2\approx\frac{DAC_1}{Vl}(t-t_o) \qquad \text{.....(4.7)}$$

Thus the chloride ion diffusion coefficient, D, can be calculated from the slope, S, of the plot of $C_2$ against t as follows;

$$D\approx\frac{Vl}{AC_1}S \qquad \text{.....(4.8)}$$

## 4.4 CHLORIDE DIFFUSION RESULTS

Using Equation 4.8 and experimental measurements, the chloride diffusivities were calculated for OPC, OPC/30%PFA and OPC/65%BFS pastes and are shown in Tables 4.3, 4.4 and 4.5 respectively. These tables also contain values of the bulk densities, the capillary porosities and total porosities of the various specimens tested for chloride

diffusion. The values show very close consistency between the replicate specimens, thereby validating the sample preparation and measurement techniques employed in this study.

The average values of the chloride diffusion coefficients are plotted in Figure 4.5 against the w/s ratios. Compared with the OPC paste of the same w/s ratio, the OPC/30%PFA and OPC/65%BFS pastes provide greater resistance to the diffusion of chloride ions as previously reported (Ngala *et al.*, 1995; Lambert *et al.*, 1984; Page *et al.*, 1981). This figure, however, also points out that for blended cement pastes, fly ash has slightly higher diffusion rates than slag at all w/s ratios investigated.

Chloride diffusion coefficients are shown in Figure 4.6 to diminish as the capillary porosity diminishes for OPC, fly ash and slag pastes. Chloride diffusion coefficients for the three cement systems tend to zero as the capillary porosities approach zero. This relationship is better illustrated in Figure 4.7 by an approximate linear extrapolation of the plot of chloride diffusion coefficient versus capillary porosity. This figure (best fit lines) suggests that as the capillary porosity approaches zero, the cement systems provide almost complete resistance to the diffusion of chloride ions. Also, the chloride diffusion coefficients for the blended pastes are markedly smaller than those for OPC pastes for the same capillary porosity. Though both blended pastes show considerably reduced chloride diffusivity compared to OPC pastes, PFA pastes are slightly more permeable to chloride ions than BFS pastes for the same capillary porosity.

The linear plot of chloride diffusion coefficients against total porosity in Figure 4.8 demonstrates, that as the chloride diffusion coefficient diminishes to zero, it approaches a total pore volume with very low chloride diffusion. This total pore volume is approximately 35% for the three cement systems and probably represents the proportion of gel pores which are completely impermeable to chloride ions. This figure in itself

suggests that, a cement matrix comprising either OPC, OPC/30%PFA or OPC/65%BFS with a total pore volume of approximately 35% will provide almost total resistance to the penetration of chloride ions. However, it is unlikely that such a system would be practicable and economically viable for construction purposes.

## 4.5 DISCUSSION

In this study, it has been observed that the chloride diffusion coefficient for well-cured cement pastes diminished markedly with the w/s ratio. This is more noticeable in OPC pastes where the chloride diffusion coefficient at a w/c ratio of 0.4 is 81% smaller than that at a w/c ratio of 0.7, compared to 62% and 69% for PFA and BFS pastes respectively. The chloride diffusion coefficients for blended fly ash and slag pastes are considerably less than those for OPC pastes for a given w/s ratio. The results indicate that the diffusion of chloride ions in HCP is strongly influenced by the type of cement used. They confirm the conclusions of previous investigations, which have shown that blended cements containing pozzolans (Ngala *et al.*, 1995; Kumar *et al.*, 1986; Page *et al.*, 1981) or slag (Page *et al.*, 1981) limit chloride diffusion more effectively than portland cements. However, the blended cement pastes limit chloride diffusion to slightly different extents. These differences in chloride diffusion between the three cement systems can be associated to the differences in the pore size distribution outlined in Chapter Three and the surface interaction between the diffusing chloride ion and pore walls which is to be investigated in Chapter Five.

Chloride diffusion coefficients for the three cement systems tend to zero as the capillary porosities approach zero (Figures 4.6 and 4.7). This implies that the cement hydrates which comprise the gel pores, have a low permeability to chloride ions. Also, the diffusion coefficients for the blended pastes are markedly smaller than those for OPC pastes for the same capillary porosity. This suggests that there is a greater continuity of the capillary pore volume in the OPC pastes than in the blended pastes. Thus it is not

only the proportions of large pores present that influence diffusion, but also the connectivity and tortuosity of these large pores. This suggestion is consistent with the findings of Chapter Three, that is, there is a greater continuity of the capillary pore volume in OPC pastes than in the blended pastes. However, the tortuosity of the pores in either of the three cement systems could not be characterized, but is thought to vary, thereby influencing chloride diffusion to different extents. Feldman (1984) pointed out that hydrated cement blends have lower permeabilities than hydrated portland cements owing to a discontinuous pore structure, in which relatively large pores are connected by narrow entrances.

In Chapter Three, it was concluded that the chemical composition of the cements and the curing temperature of 38°C used would influence the pore structure of the resulting pastes and consequently, their diffusion properties. Detwiler *et al.* (1991) reported that in plain portland cement concretes, elevated curing temperatures result in a coarser pore structure and a corresponding decrease in the resistance to chloride diffusion. However, this is not the case with blended cement pastes where a curing temperature of 38°C was intended to accelerate the slow pozzolanic reaction of fly ash and the hydraulic reaction of slag, resulting in a finer pore structure in both blended cement systems. These reactions produce extra C-S-H gel and less $Ca(OH)_2$ during hydration, refining the microstructure probably by blocking the pores instead of just forming as a surface layer on the solid pore surfaces. The chemical compositions of the hydrates formed in these blended cement pastes and the low proportion of large continuous pores might tend to influence the predominant interactions between diffusing chloride ions and the pore surface/bound water layer. This is the subject of investigation in Chapter Five, where a comparative study of the diffusion kinetics of chloride ions and neutral oxygen molecules is to be undertaken.

## 4.6 CONCLUSIONS

(1) The diffusion rate of chloride ions through mature saturated cement pastes diminishes markedly with a reduction in the w/s ratio and tends to a very low value as the capillary porosity approached zero.

(2) For a given w/s ratio or given capillary porosity, the chloride diffusion rates at 25°C for blended OPC/30%PFA and OPC/65%BFS pastes are about one order of magnitude smaller than those for OPC pastes.

(3) For blended cement pastes, the OPC/65%BFS pastes provide slightly greater resistance to the diffusion of chloride ions than OPC/30%PFA pastes for a given w/s ratio or given capillary porosity.

**Table 4.1 : Chloride Diffusion Coefficients for OPC Pastes**

| Researchers | Method | w/c | Age (days) | Temp. (°C) | D ($x10^{-12}m^2/s$) |
|---|---|---|---|---|---|
| Page et al (1981) | Steady state | 0.4 | 60 | 25 | 2.6 |
| | | 0.5 | 60 | 25 | 4.47 |
| | | 0.6 | 60 | 25 | 12.35 |
| Gautefall (1986) | Steady state | 0.5 | 180 | 20 | 5.79 |
| | | 0.7 | 180 | 20 | 9.28 |
| | | 0.9 | 180 | 20 | 19.1 |
| Tang & Nilsson (1992) | Steady state | 0.4 | 45 | 22 | 2.9 |
| | | 0.6 | 45 | 22 | 9.4 |
| | | 0.8 | 45 | 22 | 21.0 |
| | | 0.5 | 90 | 20 | 16.0 |
| Gautefall (1989) | Non-steady state | 0.7 | 90 | 20 | 17.0 |
| | | 0.9 | 90 | 20 | 39.0 |
| | | 0.4 | 90 | 22 | 9.3 |
| Tang & Nilsson (1992) | Electric | 0.6 | 90 | 22 | 17.5 |
| | | 0.8 | 90 | 22 | 25.4 |


**Figure 4.1: Occurrence of three different forms of chlorides in hardened concrete (Tuutti, 1980)**

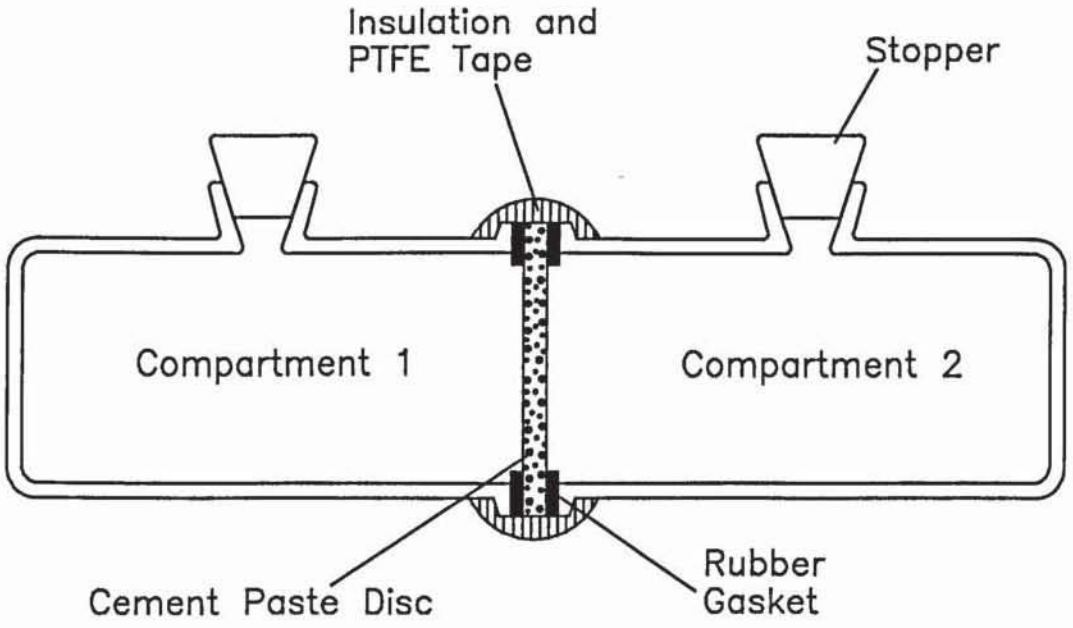


**Figure 4.2: The Ionic Diffusion Cell**

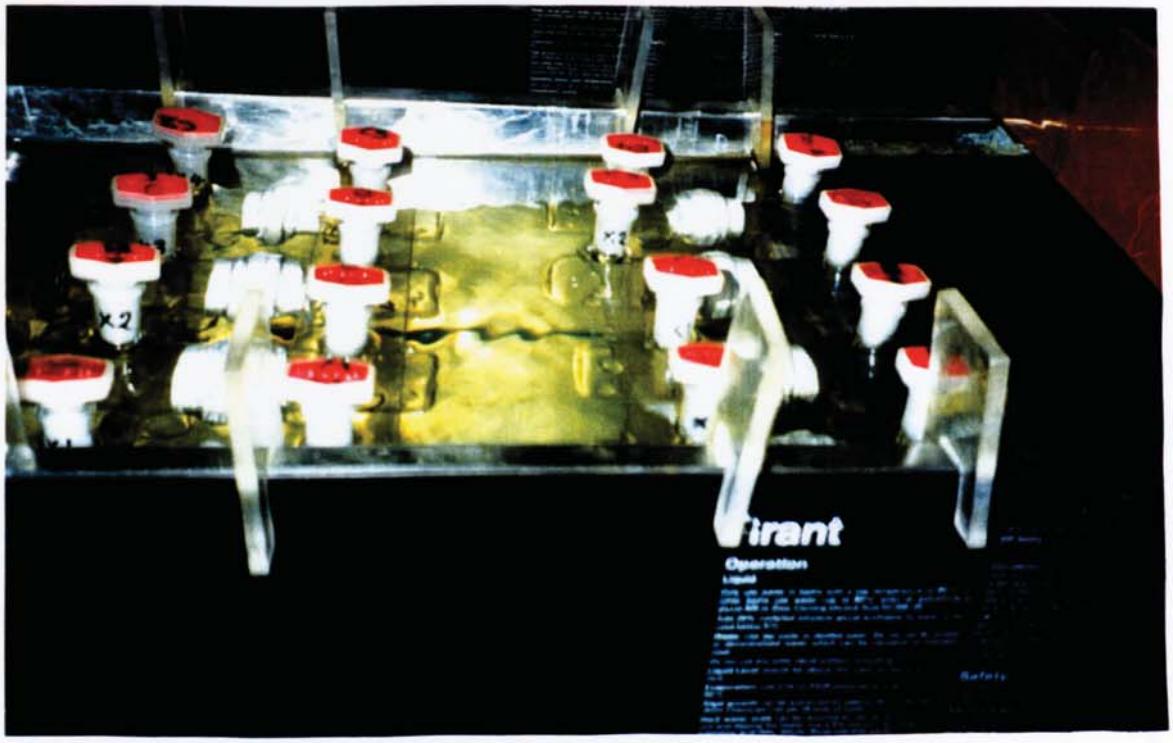

Figure 4.3: Set-up of chloride diffusion experiments

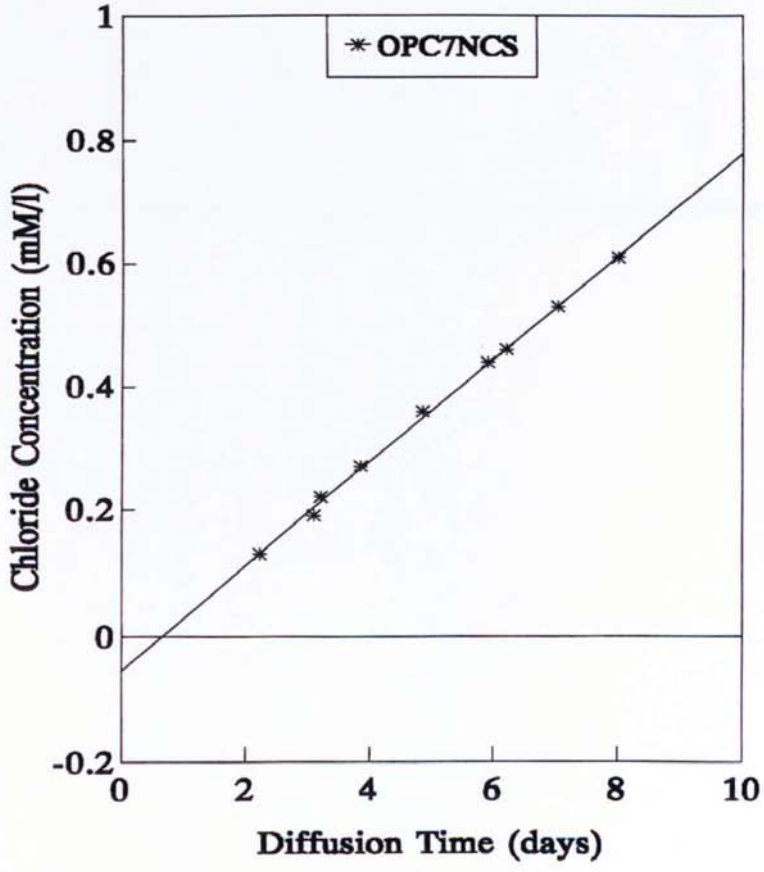


Figure 4.4: Increase with time of chloride ion concentration in compartment 2 of ionic diffusion cell

**Table 4.2: Chloride ion concentration results for OPC7NCS paste**

| Diffusion Time (days) | ABS | Corrected ABS | Chloride Conc. (mM/l) |
|---|---|---|---|
| 1.10 | 0.134 | 0.072 | 0.040 |
| 1.94 | 0.260 | 0.197 | 0.115 |
| 2.23 | 0.293 | 0.230 | 0.130 |
| 3.10 | 0.391 | 0.329 | 0.190 |
| 3.21 | 0.439 | 0.375 | 0.220 |
| 3.85 | 0.518 | 0.454 | 0.270 |
| 4.85 | 0.632 | 0.572 | 0.360 |
| 5.90 | 0.739 | 0.680 | 0.440 |
| 6.19 | 0.772 | 0.709 | 0.460 |
| 7.02 | 0.850 | 0.787 | 0.530 |
| 8.00 | 0.952 | 0.885 | 0.610 |

**Table 4.3: Experimental results obtained for hydrated OPC pastes.**

| W/C | Chloride Diffusivity ($x10^{-8}cm^2/s$) | Bulk Density ($g/cm^3$) | Capillary Porosity (%) | Total Porosity (%) |
|---|---|---|---|---|
| 0.4 | 4.35 | 1.982 | 4.33 | 42.35 |
| | 3.75 | 1.987 | 4.32 | 41.20 |
| | 3.99 | 1.987 | 4.05 | 41.11 |
| | 4.01 | 1.987 | 4.56 | 41.15 |
| | 3.65 | 1.981 | 4.32 | 42.09 |
| **Average** | 3.95 | 1.985 | 4.32 | 41.58 |
| 0.5 | 7.16 | 1.888 | 8.34 | 47.37 |
| | 7.93 | 1.889 | 8.34 | 48.05 |
| | 8.06 | 1.884 | 8.30 | 47.05 |
| | 8.06 | 1.882 | 8.48 | 47.43 |
| **Average** | 7.80 | 1.886 | 8.36 | 47.48 |
| 0.6 | 12.99 | 1.807 | 19.73 | 51.63 |
| | 13.81 | 1.791 | 19.77 | 52.59 |
| | 12.45 | 1.797 | 17.83 | 51.06 |
| | 10.40 | 1.799 | 17.47 | 51.67 |
| | 13.37 | 1.783 | 19.34 | 52.94 |
| **Average** | 12.60 | 1.795 | 18.83 | 52.94 |
| 0.7 | 19.65 | 1.750 | 24.29 | 54.59 |
| | 19.86 | 1.750 | 24.51 | 55.10 |
| | 22.16 | 1.738 | 25.18 | 55.16 |
| | 21.28 | 1.733 | 24.15 | 55.81 |
| | 24.35 | 1.707 | 26.19 | 56.97 |
| **Average** | 21.46 | 1.736 | 24.86 | 55.53 |

**Table 4.4: Experimental results obtained for hydrated OPC/30%PFA pastes.**

| W/S | Chloride Diffusivity ($x10^{-8}cm^2/s$) | Bulk Density ($g/cm^3$) | Capillary Porosity (%) | Total Porosity (%) |
|---|---|---|---|---|
| 0.4 | 0.33 | 1.947 | 3.11 | 43.37 |
| | 0.52 | 1.943 | 3.10 | 43.29 |
| | 0.33 | 1.948 | 2.96 | 43.20 |
| | 0.39 | 1.941 | 3.11 | 43.22 |
| **Average** | 0.39 | 1.945 | 3.07 | 43.27 |
| 0.5 | 0.35 | 1.855 | 5.15 | 48.84 |
| | 0.57 | 1.856 | 5.25 | 48.30 |
| | 0.42 | 1.852 | 5.88 | 49.26 |
| | 0.43 | 1.850 | 4.95 | 48.36 |
| | 0.39 | 1.857 | 5.30 | 48.70 |
| **Average** | 0.43 | 1.854 | 5.31 | 48.69 |
| 0.6 | 1.04 | 1.771 | 8.83 | 55.46 |
| | 0.82 | 1.777 | 9.28 | 54.83 |
| | 0.72 | 1.768 | 8.74 | 55.00 |
| | 1.01 | 1.772 | 9.68 | 55.68 |
| | 0.93 | 1.778 | 9.10 | 55.34 |
| **Average** | 0.90 | 1.773 | 9.13 | 55.26 |
| 0.7 | 0.89 | 1.707 | 13.06 | 58.64 |
| | 1.06 | 1.699 | 13.92 | 59.41 |
| | 1.10 | 1.704 | 13.68 | 58.76 |
| | 1.14 | 1.699 | 13.75 | 59.32 |
| | 0.96 | 1.714 | 13.58 | 58.96 |
| **Average** | 1.03 | 1.705 | 13.60 | 59.02 |

**Table 4.5: Experimental results obtained for hydrated OPC/65%BFS pastes.**

| W/S | Chloride Diffusivity ($x10^{-8}cm^2/s$) | Bulk Density ($g/cm^3$) | Capillary Porosity (%) | Total Porosity (%) |
|---|---|---|---|---|
| 0.4 | 0.32 | 1.973 | 2.27 | 43.05 |
| | 0.24 | 1.971 | 2.14 | 43.30 |
| | 0.18 | 1.983 | 2.20 | 42.91 |
| | 0.28 | 1.985 | 2.07 | 42.79 |
| | 0.26 | 1.976 | 2.38 | 42.77 |
| **Average** | 0.26 | 1.978 | 2.21 | 42.96 |
| 0.5 | 0.24 | 1.875 | 4.84 | 48.52 |
| | 0.35 | 1.873 | 5.00 | 47.58 |
| | 0.40 | 1.870 | 5.18 | 47.59 |
| | 0.21 | 1.878 | 4.78 | 48.19 |
| | 0.45 | 1.874 | 4.94 | 48.29 |
| **Average** | 0.33 | 1.874 | 4.95 | 48.03 |
| 0.6 | 0.61 | 1.784 | 6.95 | 54.51 |
| | 0.54 | 1.786 | 6.70 | 54.76 |
| | 0.55 | 1.783 | 7.13 | 54.59 |
| | 0.38 | 1.788 | 6.61 | 54.50 |
| | 0.46 | 1.787 | 6.39 | 54.14 |
| **Average** | 0.51 | 1.786 | 6.76 | 54.50 |
| 0.7 | 0.92 | 1.731 | 10.04 | 57.28 |
| | 0.78 | 1.739 | 8.97 | 56.87 |
| | 1.04 | 1.728 | 10.53 | 57.65 |
| | 0.81 | 1.727 | 9.23 | 56.76 |
| | 0.72 | 1.737 | 9.29 | 57.24 |
| **Average** | 0.85 | 1.733 | 9.61 | 57.16 |

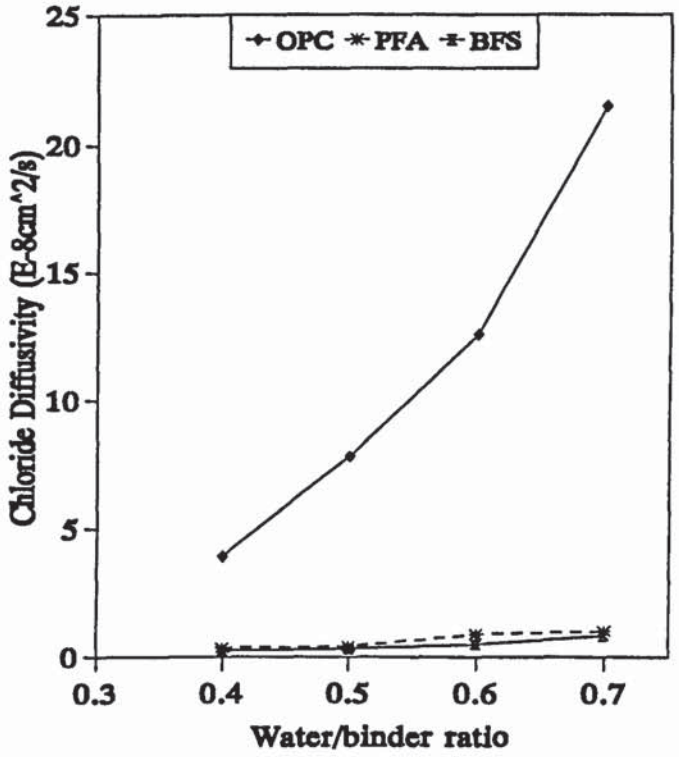


**Figure 4.5: Plot of chloride diffusion coefficient versus water/binder ratio**

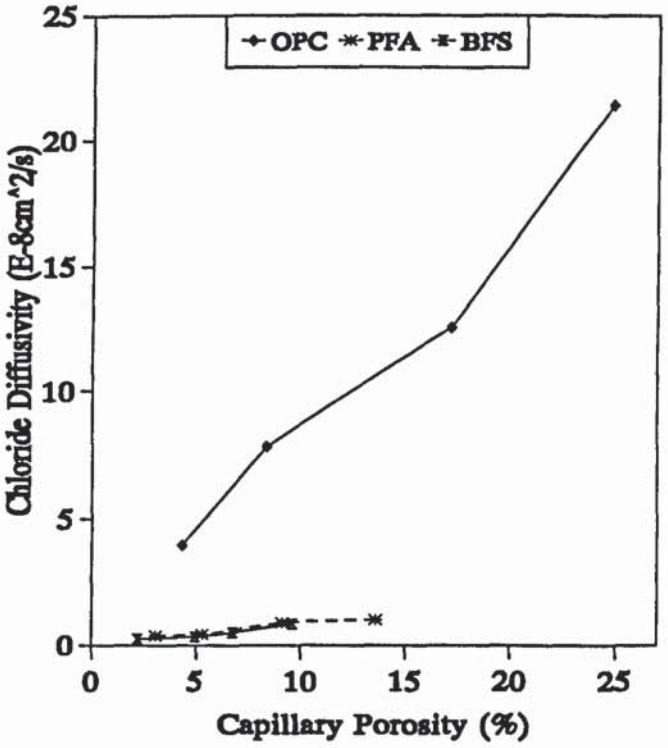


**Figure 4.6: Plot of chloride diffusion coefficient versus capillary porosity**

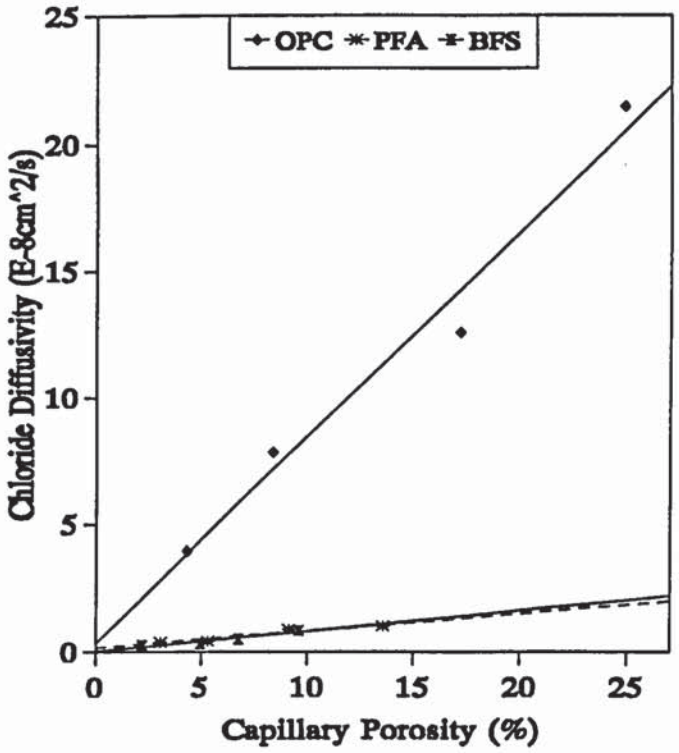


**Figure 4.7: Linear plot of chloride diffusion coefficient versus capillary porosity**

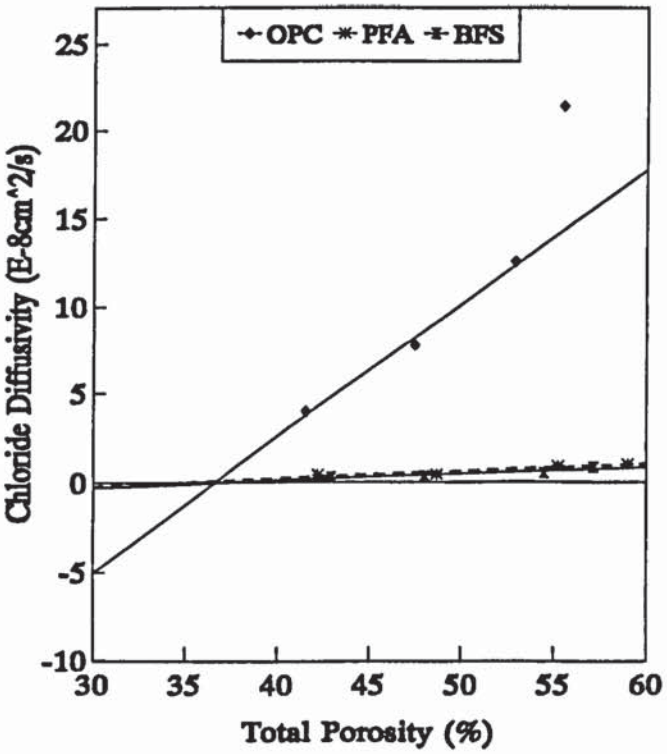


**Figure 4.8: Linear plot of chloride diffusion coefficient versus total porosity**

# CHAPTER FIVE

# OXYGEN DIFFUSION IN HYDRATED CEMENT PASTES

## 5.1 INTRODUCTION

When steel is embedded in concrete or other cementitious materials, it is usually in a passive state, protected from significant corrosion by a surface film of iron(iii)oxide ($Fe_2O_3$). There are two common circumstances that may give rise to the breakdown of this thermodynamically stable passive film; (a) carbonation, which lowers the pH towards neutral values rendering $Fe_2O_3$ unstable, and (b) the presence of chloride salts, which may stimulate the local disruption of the $Fe_2O_3$ film leading to pitting corrosion (Page and Treadaway, 1982).

At the surface of the steel in an active state, corrosion reaction progresses by an electrochemical mechanism such as indicated below. In effect, an anodic reaction in which Fe is ionized and a cathodic reaction in which the dissolved oxygen is reduced will proceed at the surface of the steel at mutually equal speeds as indicated by Equations 5.1 and 5.2 respectively.

$$Fe = Fe^{2+} + 2e^- \qquad \text{.....(5.1)}$$

$$O_2 + 2H_2O + 4e^- = 4OH^- \qquad \text{.....(5.2)}$$

It is clear from Equations 5.1 and 5.2 that, oxygen plays the role of stimulating cathodic reaction in the corrosion of steel and governs the corrosion reaction of steel. Therefore, for corrosion of steel to occur in concrete, the existence of oxygen at the surface of the steel is as fundamentally important as the presence of chloride ions or the lowering of the pH.

In comparison with chloride diffusion, oxygen diffusion would be considerably less affected by the surface charge or the double layer at the pore/solution interface. The pore structure of the hydrated cement paste and the viscosity of the pore solution are the main factors expected to determine the diffusion rates of dissolved oxygen. Since oxygen and chloride have similar diffusion coefficients in infinitely dilute solutions, $2.1 \times 10^{-5}$ and $2.03 \times 10^{-5}$ $cm^2/s$ at 25°C respectively (Cussler, 1984), they should have similar sizes, and accordingly, may be expected to diffuse through similar pores in HCP. Comparing the rates of diffusion for the two species in a range of well-cured hydrated cement systems would lead to a greater understanding and evaluation of the extent of surface interaction on ionic diffusion. Oxygen, however, being a neutral molecule without dipolar character, is not expected to encounter electrostatic surface interactions of the kind that may influence the transport of chloride ions in HCP.

The electrochemical technique employed was developed at Aston University in Birmingham and involves the cathodic consumption of the diffused oxygen in a steady state condition enabling the determination of the effective diffusion coefficient. The design of the diffusion cell was based on the theory initially proposed by Lingane (1967 and 1958), and reviewed in Section 5.2.1.

## 5.2 LITERATURE REVIEW

### 5.2.1 Current Decay at the Electrode/Solution Interface

The criterion for a virtually complete consumption of an electrochemical substance at a constant potential with respect to a reference electrode, is the decay of current from a high value to a very low value close to zero. Such a system was considered by Lingane (1967) in his earlier work. Lingane considered the rate of the electrode process to be limited by the diffusion and the electro-migration of the reacting species from the bulk solution to the electrode surface. The instantaneous current (I) was derived from Fick's first law and Faraday's law;

$$I=\frac{nFDA_eC_2}{L} \qquad \text{.....(5.3)}$$

where n is the number of electrons transferred per molecule of the reacting substance, F is the Faraday number, D and $C_2$ are respectively, the diffusivity and concentration of the substance in the solution, L is the thickness of the diffusion layer and $A_e$ is the effective surface area of the electrode. This equation is based on the assumption that the substance which diffuses through the diffusion layer to the electrode surface is immediately consumed.

The decay current resulting from the gradual consumption of a single reactant having an initial concentration, $C_o$ (moles) in a solution of fixed volume, V was derived from Equation 5.3 by Lingane (1967 and 1958);

$$I=I_o e^{-(\frac{DA_e}{VL})t} \qquad \text{.....(5.4)}$$

for a constant value of L, where t is the polarisation time in seconds, $I_o$ is the initial current at $t=t_o$, and $t_o=0$.

Lingane (1967 and 1958) also showed that the extent to which the electro-active specie has been consumed at a certain polarisation time can be explicitly expressed by the ratio of the consumed quantity (Q) to its initial quantity ($Q_o$);

$$\frac{Q}{Q_o}=1-e^{-(\frac{DA_e}{VL})t} \qquad \text{.....(5.5)}$$

where Q can be obtained by integrating Equation 5.4 over time and has the same units (charge passed in coulombs) as $Q_o$.

### 5.2.2 Potentiostatic Measurement of Oxygen Diffusivity

Gold (Newton, 1988), platinum and steel (Gjorv *et al.*, 1976) cathodes have been used in studies of oxygen diffusion in water-saturated cement paste, mortar and concrete. Oxygen diffusivity can be determined potentiostatically from the flux and diffused amount during steady state diffusion.

Two types of test systems have been designed for experimental measurements. The first type is an electrochemical cell composed of two compartments joined together by a specimen. One compartment contains an anode and is filled with a solution of known oxygen concentration, while the other compartment contains an initially oxygen-free solution and a cathode. The diffusion of oxygen from the high concentration side to the low concentration side during steady state is monitored electrochemically (Section 5.3.3). This test system is similar to the one described in Chapter Four for ionic diffusion in the manner in which the diffusion process is established. The alternative approach for determining oxygen diffusivities employs a cathode buried in the test sample. This second type of system may be considered to be more realistic if the effect of oxygen transport on reinforcement corrosion is to be examined. Gjorv *et al.* (1976) and Newton (1988) used this test system to determine the quantity of accumulated oxygen around the buried cathode during an interruption of steady state diffusion.

With the first type of test system, the cathode is polarized at a potential such that the reduction of oxygen is the only significant cathodic reaction to take place. If diffusion of oxygen is at a steady state, it is possible to obtain a stable flux current, $I_d$. Since at this flux current, the diffused amount is the same as that being consumed, the total flux, $J_o$ (mM/sec) is given by;

$$J_o = \frac{I_d}{nF} \qquad \text{.....(5.6)}$$

and the flux current is related to the intrinsic diffusivity by Fick's first law, viz

$$I_d = nFD_o A\frac{dC}{dx} \qquad \text{.....(5.7)}$$

where $D_o$ is the oxygen diffusivity, A is the diffusion area, and dC/dx is the gradient of the oxygen concentration. Using this method, Gjorv *et al.* (1976) obtained oxygen diffusivities within the range $10^{-6}$ to $10^{-5}$ $cm^2$/sec for some mortar and concrete specimens. One disadvantage of this method was that prolonged polarization period of up to 4 weeks was required to achieve such a stable current.

Page and Lambert (1987) used an electrochemical cell similar in scale to the cell described in Chapter Four for chloride diffusion experiments. The authors measured the accumulated amount of diffused oxygen instead of the steady-state diffusion current. The important features of the cell design were the efficiency of the stirring system and the relatively large size of the cathode employed (approx. 10 $cm^2$). Using this cell the authors studied the influence of w/c ratio and temperature on the effective diffusivity of oxygen in HCP and found that;

(a) activation energies for the diffusion of oxygen in hardened portland cement pastes were smaller than those reported for ionic diffusion (Page *et al.*, 1981), but showed a similar pattern of variation as a function of w/c ratio;

(b) the activation energy recorded for mature hydrated paste with a w/c ratio of 0.6 was significantly lower than those of specimens with a w/c ratio of 0.5 or less.

Recent research at Aston University by Yu and Page (1991) used a modified and improved version of the electrochemical cell used earlier by Page and Lambert (1987). The major difference between the two cells is the reduced volume of the cathode compartment (approx. 35 ml) compared to that (approx. 130 ml) used by Page and Lambert. Equation 5.5 indicates that the efficiency of the cell can be exponentially improved by increasing

the ratio of the electrode area to the solution volume. Yu (1990) achieved this by decreasing the volume of the cathode compartment as opposed to increasing the surface area of the electrode. Using this technique, Yu and Page (1991) concluded that the ratio of oxygen to chloride diffusion coefficients increases with decreasing chloride diffusion coefficient. This supported the hypothesis that ionic diffusion in HCP is affected by the surface charge or the electrical double layer at the cement matrix-pore solution interface. The authors suggested that the surface charge effect on ionic diffusion is mainly associated with transport through micropores.

Whereas, Yu and Page (1991) carried out their studies on a limited range of cement pastes and pore systems, the present study is aimed at investigating the effect of surface interactions over a wider range of well-cured cement pastes and pore systems. Therefore measurement of diffusion of both oxygen and chloride ion in OPC paste and blended pastes constituting OPC/30%PFA and OPC/65%BFS of w/s ratio of 0.4, 0.5, 0.6 and 0.7, as well as in carbonated pastes (Chapter Six) was undertaken. Chloride diffusion was determined by the steady state diffusion technique described in Chapter Four. Oxygen diffusivity was electrochemically measured by consuming the total amount of diffused oxygen during steady state conditions at 25°C. The cell used is described in Section 5.3.1 and is similar to the one used by Yu and Page (1991). In order to assist in the interpretation of the diffusion data, porosity and pore size distribution measurements were made on the specimens used for diffusion experiments.

## 5.3 EXPERIMENTAL PROCEDURE

### 5.3.1 The Oxygen Diffusion Cell

The glass diffusion cell used in this study is illustrated in Figure 5.1. It is very similar to that used by Yu and Page (1991), the only modification being the manner in which the oxygen gas is bubbled through the solution. The diffusion cell is made up of two main compartments; compartment 1 (the anode compartment) and compartment 2 (the cathode

compartment), with compartment 2 having a much smaller volume than compartment 1. Compartment 1 contains an activated titanium anode and a saturated calomel reference electrode (SCE) while compartment 2 contains a cathode comprising a platinum foil attached to a platinum wire. A magnetic bar follower coupled with an external stirrer is added to the cathode compartment, enabling the stirring of the solution during an electrochemical measurement. The external stirrer consists of a magnet driven by a small motor connected to a d.c. generator.

In order to improve the efficiency of saturation and minimize the introduction of air bubbles and loss of solution due to bubbling of the oxygen gas, this study has modified the diffusion cell by connecting a glass bottle to one side of the anode compartment. The glass bottle has two entrances and one outlet and its sole function is to saturate the solution in compartment 1 with oxygen, ensuring that saturation occurs without and not within compartment 1. The solution from compartment 1 enters the glass bottle through one of the entrances and is bubbled with oxygen gas from the gas supply coming in through the other entrance. The resulting oxygen-saturated solution exits the glass bottle through the outlet before being returned to the compartment. This was an on-going process once the experiment was set up ensuring that the solution was always oxygen-saturated during the course of the experiment.

### 5.3.2 Experimental Set-Up

Specimens used for oxygen diffusion experiments were prepared as described in Section 2.2. Thin discs (usually 2.5 to 3 mm thick) were cut and immersed in the curing solution at least a week before the start of the diffusion experiment. This was to ensure that the pores in the samples were entirely water-saturated, as diffusion of oxygen in air-filled pores would be much faster than in water-filled pores.

To assemble a cell, a specimen was mounted between the flanges of the two compartments as described for ionic diffusion in Section 4.3. The anode compartment was filled with 35mM NaOH and bubbled with oxygen as described in Section 5.4.1. The cathode compartment was filled with de-aerated 35mM NaOH solution which had been purged with purified nitrogen in a de-aeration cell for at least 12 hours. Care was taken to ensure that no gas bubbles were present in either of the compartments. Any small volume of gas phase in the cathode compartment may contain a comparatively high quantity of oxygen in a vapour-solution system, thus affecting the accuracy of the measurements obtained. The cell was finally placed in a waterbath controlled at a constant temperature of 25°C. Four or Five replicate cells were set up for each condition under investigation as shown in Figure 5.2.

At the end of each experimental set-up, the cells were disassembled, the diffusion areas of the discs determined from the marks left by the grease and their thicknesses measured using a micrometer gauge. The cells were then washed with deionised water, ready for the next experimental set-up. At times, dilute nitric acid (0.01M) was required in order to clean the cells and electrodes properly, thereby getting rid of any precipitated NaOH crystals.

### 5.3.3 Electrochemical Measurements

It was noticed that it took about 4 to 7 days for diffusion to reach steady state for most of the specimens investigated, except in the case of non-carbonated OPC/65%BFS pastes, where a duration of at least 14 days was required. Cathodic polarisation at -600 mV Vs SCE was carried out every 1 to 3 days during the period of non-steady state diffusion but the current and charge were not recorded. A Multistat System supplied by Thompson Electrochem Ltd was used for the electrochemical measurements and consists of five potentiostats, a Master Control Unit and a BBC Master Computer. The current was measured every second with the programmed measurement range of 0.3 to 1538 μA, and

the charge passed was integrated numerically through the computer program.

Diffused oxygen was determined at diffusion time intervals of between 1 to 3 days depending on the properties of the specimens. A constant ratio of the charge passed to the diffusion time interval would indicate steady state conditions and a reasonably complete consumption of the diffused oxygen. The cathodic polarisations were carried out by holding the potential at -600 mV Vs SCE for a pre-determined period of time. The polarisation time in the range 6000 to 20000 seconds used in this study was chosen such that all the diffused oxygen was completely consumed. Typical examples of current time curves for the cathodic consumption of diffused oxygen are shown in Figure 5.3 for polarisation times of 6000 and 8000 seconds.

During steady state diffusion, the charge passed (Q) or the accumulative charge ($Q_t$) should respectively be proportional to the time interval ($t_i$) or the total time ($t_d$) of diffusion. The ratio $Q_t/t_d$ was adopted for this work to calculate the flux by Faraday's law. The diffusion experiments were stopped when the calculated ratio, $Q/t_i$, showed little variation for 6 or more consecutive measurements. Table 5.1 shows the recorded charge, $Q_t$, passed and the end current, $I_e$, for 9 consecutive measurements obtained from sample OPC6NCS. The first measurement, A, in Table 5.1 was assumed to be the reference zero point for the calculation of the accumulative charge and total diffusion time. The accumulative charge, $Q_t$, was then plotted against the total diffusion time, $t_d$, as shown in Figure 5.4 for OPC6NCS paste, and the slope of the straight line was used in Equation 5.8 to calculate the oxygen diffusivity.

### 5.3.4 Oxygen Solubility in 35mM NaOH Solution

In order to calculate the diffusivity of oxygen, it was necessary to know its concentration in the anode compartment, that is, its solubility in 35mM NaOH solution. The solubility at 25°C was determined as follows. The 35mM NaOH solution was initially bubbled with

oxygen for at least 6 hours. The gas was passed through a spiral glass tube containing the solution and placed in the waterbath. Three cells were set up in a similar manner as described in Section 5.3.2. The cathode compartments were filled with known volumes of the prepared solution, while the anode compartment contained air-saturated solution. The cathodes were polarized at -600 mV Vs SCE for 11.11 hours, and the two measurement ranges of the current, 0.3 to 1500 μA and 1500 μA to 1A, were controlled through the computer software. The integrated charged passed for the three cells are shown in Table 5.2, together with the corresponding end current and actual volume of solution in the cathode compartments.

The calculated solubilities for the three cells are shown in Table 5.2, with an average value of $1.27 \times 10^{-3}$M. Compared with the value of $1.23 \times 10^{-3}$M of oxygen solubility in water (Dean, 1985), the experimentally determined value for 35mM NaOH solution is about 3.2% higher. As such, oxygen solubility in 35mM NaOH solution is very similar to that in water. This is in reasonable agreement with Yu (1990), who found out that oxygen solubility in saturated $Ca(OH)_2$ was $1.25 \times 10^{-3}$M, only 1.6% higher than that in water.

### 5.3.5 Oxygen Diffusivity

The oxygen diffusivity, $D_o$, is calculated from Fick's first law and Faraday's law as;

$$D = \frac{L\left(\frac{Q_t}{t_d}\right)}{4FAC_o} \qquad \text{.....(5.8)}$$

where L is the specimen thickness, $Q_t/t_d$ (mA) is the slope determined from the $Q_t$-$t_d$ plot, A is the diffusion area of the sample, $C_o$ is the solubility, and $C_o/L$ is the assumed concentration gradient.

## 5.4 DIFFUSIVITY RESULTS

### 5.4.1 Oxygen Diffusion

Using Equation 5.8 and the experimental measurements obtained, the oxygen diffusion coefficients calculated for OPC, OPC/30%PFA and OPC/65%BFS pastes are shown in Tables 5.3, 5.4 and 5.5 respectively. These tables reveal very close consistency in oxygen diffusivity between the replicate specimens, thereby validating the measurement technique used. These tables also contain the bulk density, capillary porosity and total porosity data for the various specimens.

The average values of the oxygen diffusion coefficients are plotted in Figure 5.5 against the water/binder ratio. This figure demonstrates that, at all the w/s ratios investigated, the resistance of the OPC/30%PFA pastes to the diffusion of neutral oxygen molecule is greater than that of OPC pastes as reported by Ngala *et al.* (1995), but less than that of OPC/65%BFS pastes. It can also be seen from this figure that, at a high w/s ratio of 0.7, oxygen diffuses substantially faster through OPC pastes than through the blended fly ash and slag pastes. This suggests that at this w/s ratio, there is a greater continuity of the pore system in the OPC pastes than in the blended pastes.

Oxygen diffusion coefficients are shown in Figure 5.6 to diminish as the capillary porosity diminishes for both OPC and fly ash pastes, but remains fairly constant for slag pastes. This figure also indicates that as capillary porosity approaches zero, the three cement systems still show considerable permeability to the diffusion of the neutral oxygen molecule. This relationship is better illustrated in Figure 5.7 by an approximate linear plot of the oxygen diffusion coefficient versus capillary porosity. However, the figure seems to suggests that the permeability of OPC/65%BFS pastes to the diffusion of oxygen is fairly constant irrespective of the volume of capillary pores present in these pastes. Also, the oxygen diffusion coefficients for the three cement systems are all different for the same capillary porosity (Figures 5.6 and 5.7). Furthermore, the results suggest that

OPC/30%PFA hydrates are slightly more permeable to oxygen than those of OPC/65%BFS, but less permeable than those of OPC. This may be associated with the proportion of $Ca(OH)_2$ in the three cement systems since $Ca(OH)_2$ is coarsely crystalline in comparison with C-S-H gel. Feldman (1984) pointed out that the $Ca(OH)_2$ content of hydrated pastes were approximately 18% for OPC paste, 6% for PFA pastes and 2.5% for BFS pastes for a w/s ratio of 0.45.

The linear extrapolation of oxygen diffusion coefficient against total porosity in Figure 5.8 demonstrates that, as the oxygen diffusion coefficient diminishes to zero for OPC and fly ash pastes, it approaches a total pore volume with a very low oxygen diffusivity. This total pore volume is approximately 15% for both cement systems. However, this behaviour could not be ascribed to the slag pastes where the oxygen diffusivity seems constant and independent of the total or capillary porosity.

### 5.4.2 Chloride Diffusion

Chloride diffusion experiments were carried out in parallel with oxygen diffusion experiments for a set of accompanying specimens. This was achieved by the use of the steady state ionic diffusion cell described in Section 4.3. The chloride diffusion coefficients were calculated as demonstrated in Section 4.3.3 and the results obtained were listed in Tables 4.3, 4.4 and 4.5 for OPC, fly ash and slag pastes respectively.

### 5.4.3 Comparing oxygen and chloride diffusion coefficients

The average values of diffusion coefficients of oxygen and chloride ion are plotted in Figure 5.9 against the w/s ratio. Oxygen is shown to have a greater diffusion coefficient than chloride ion for the OPC, OPC/30%PFA and OPC/65%BFS pastes. For the OPC paste, the difference between oxygen and chloride diffusion coefficients is very large at lower w/s ratios but becomes almost zero at a w/s ratio of 0.7, whilst for PFA and BFS pastes, this difference is very large at all the w/s ratios investigated.

Chloride and oxygen diffusion coefficients are shown in Figure 5.10 to diminish as the capillary porosity diminishes for OPC, PFA and BFS pastes. Chloride diffusion coefficients for the three cement systems tend to zero as the capillary porosity approaches zero while, the oxygen diffusion coefficients do not tend to zero as the capillary porosity approaches zero.

## 5.5 DISCUSSION

In this study it has been observed that the oxygen diffusion coefficients for well-cured cement pastes decrease with the water/binder ratio. The oxygen diffusion coefficients for OPC, OPC/30%PFA and OPC/65%BFS pastes all vary for a given water/binder ratio. This result indicates that, like chloride ions, the diffusion of oxygen molecules in HCP is strongly influenced by the type of binder or cement used. These differences in oxygen diffusion coefficient between the three cement systems may be associated solely with the differences in the pore geometry since oxygen, being a neutral molecule without dipolar character, is not expected to encounter electrostatic surface interactions of the kind that may influence the transport of chloride ions in HCP.

Cement hydrates in OPC, OPC/30%PFA and OPC/65%BFS pastes have been shown to be considerably permeable to oxygen molecules, compared to their permeability for chloride ions reported in Chapter Four. Figure 5.7 indicates that the oxygen diffusion coefficient at zero capillary porosity is about 59%, 50% and 79% of its value at 18% capillary porosity for OPC, OPC/30%PFA and OPC/65%BFS pastes respectively. On the other hand, it was pointed out in Figure 4.7 that the chloride diffusion coefficient for all the three cement systems tend to zero for zero capillary porosity. This suggests that, whereas the cement hydrates in the three cement systems are permeable to oxygen molecules, they show very low permeability to the diffusion of chloride ions. However, the slag pastes show a fairly constant value of oxygen diffusivity as the capillary porosity diminishes.

The sizes of the oxygen molecule and the chloride ion are similar and their diffusion coefficients in bulk aqueous solutions are comparable. Thus the two species might be expected to diffuse at similar rates in very porous, hydrated cement pastes. However, large differences between oxygen and chloride diffusion coefficients have generally been observed for all the blended fly ash and slag pastes, and OPC pastes of low w/s ratio or capillary porosity (Figures 5.9 and 5.10). These differences suggest that chloride diffusion kinetics in these pastes are greatly restricted by the interactions between the migrating chloride ion and the electrostatically charged pore walls or by the electrical double layer at the interface between the pore walls and pore solution.

The ratio of oxygen to chloride diffusion coefficients ($D_O/D_{Cl}$) may be considered as a numerical measure of the effect of the surface charge as demonstrated for OPC and fly ash pastes by previous investigations at Aston University (Ngala *et al.*, 1995; Yu and Page, 1991). The ratio of oxygen to chloride diffusion coefficients for OPC, OPC/30%PFA and OPC/65%BFS is summarised in Tables 5.6, 5.7 and 5.8 respectively. These tables generally indicate an increase in the ratio ($D_O/D_{Cl}$) with decreasing w/s ratio for each cement system. These results suggest that the rate-controlling factors of diffusion in all three types of pastes are not the same for chloride as an anion and oxygen as a neutral molecule. Figure 5.11 illustrates the variation of the ratio ($D_O/D_{Cl}$) with chloride diffusion coefficient, together with data from the earlier study (Yu and Page, 1991) for OPC/20%PFA pastes at w/s ratios of 0.35, 0.5 and 0.6. It may be seen from this figure that as the pastes become less permeable to chloride ions, they provide progressively more resistance to the diffusion of chloride ion than to the diffusion of the neutral oxygen molecule. This implies there could be some fundamental differences in the kinetics of oxygen and chloride diffusion, especially in the dense pastes.

The ratio ($D_O/D_{Cl}$) approaches 1 for continuous capillary pore systems with very high values of chloride diffusion coefficient, but can be as great as 15 at very small values of

chloride diffusion coefficient. This suggests that the diffusion rates of chloride ions in pastes of low permeability are predominantly determined by the effect of the surface charge on pore walls rather than purely geometrical restrictions such as pore volume, pore size distribution, pore connectivity and tortuosity.

It has been demonstrated that the diffusion of chloride ions appears to be retarded compared to the diffusion of oxygen molecules. This may point to one of three causative factors: firstly, the surface charge effect of chloride ions; secondly, physical and chemical binding of chloride ions to cement hydrates, and thirdly, a greater diffusion area or diffusion path for oxygen. The latter implies that chloride and oxygen do not share all of their diffusion paths and that oxygen can diffuse through more pores. However, since the two species have comparable sizes and diffuse at similar rates in dilute aqueous solutions, they may be expected to diffuse at similar rates in very porous hydrated cement pastes. For chloride to have a smaller effective diffusion area, it must either be (i) repelled from some of the pores that contribute to the diffusion of oxygen or (ii) prevented from permeating some of the pores by partial or complete blockage of these pores.

In (i) above, the separation of diffusion paths could be achieved only through the electrical field existing at the pore/solution interface of some of the small pores, which presumably, repels chloride ions, thereby reducing the effective diffusion area. This hypothesis is consistent with the findings of previous researchers (Goto and Roy, 1981; Ushiyama and Goto, 1974), who pointed out that cement pastes behave as an electronegative semi-permeable membrane for temperatures of up to 70°C. Ottewill (1983) has reported that the electrical field generally extends from the surface to a distance of approximately twice the double layer thickness.

Also, chloride ions can be physically adsorbed on to the pore walls (Ramachandran, 1971) or can chemically bind with $C_3A$ and other hydration products forming mainly Friedel's

salt (Hoffman, 1984; Mehta, 1980; Migley and Illston, 1980). These binding effects may clog up the pores, blocking them completely or constricting them to sizes through which diffusion cannot take place. Consequently, the diffusion area is reduced, resulting in low chloride diffusion coefficient and a high oxygen to chloride diffusion coefficient ratio.

Therefore, a smaller diffusion area or diffusion path for chloride ions compared to oxygen molecules, is primarily due to surface charge effects on chloride diffusion. This effect manifests itself either (a) directly, where the chloride ions are repelled from some of the pores depending on the sizes, or (b) indirectly, where the chloride ions bind with cement hydrates, blocking the pores, thereby resulting in a reduction in the diffusion path for the chloride ions. Further investigations are necessary to determine the magnitude of the binding effect of chloride ions on the pore structure of cement pastes.

## 5.6 CONCLUSIONS

(1) The diffusion of dissolved oxygen molecules in well-cured pastes diminishes with a reduction in the water/binder ratio but does not tend to very low values as the capillary porosity approaches zero. On the other hand, the diffusion rate of chloride ions tends to very low values as the capillary porosity approaches zero.

(2) For a given water/binder ratio or a given capillary porosity, the oxygen diffusion rates for OPC/30%PFA pastes are about 25% smaller than those for OPC pastes but about 35% higher than those for OPC/65%BFS pastes.

(3) In comparison with the diffusion kinetics in dilute aqueous solutions, the oxygen molecule diffuses relatively faster than the chloride ion through hydrated OPC, OPC/30%PFA and OPC/65%BFS pastes.

(4) The ratio of oxygen to chloride diffusion coefficients increases from values close to one in permeable pastes, to values of around 15 in low-permeability, blended fly ash and slag pastes. This supports the view that the diffusion of chloride ions is retarded by the surface charge of the hydrated cement gel in pastes with low capillary porosities. In contrast, the hydrated cement gel is much more permeable to the similarly-sized, neutral oxygen molecules.

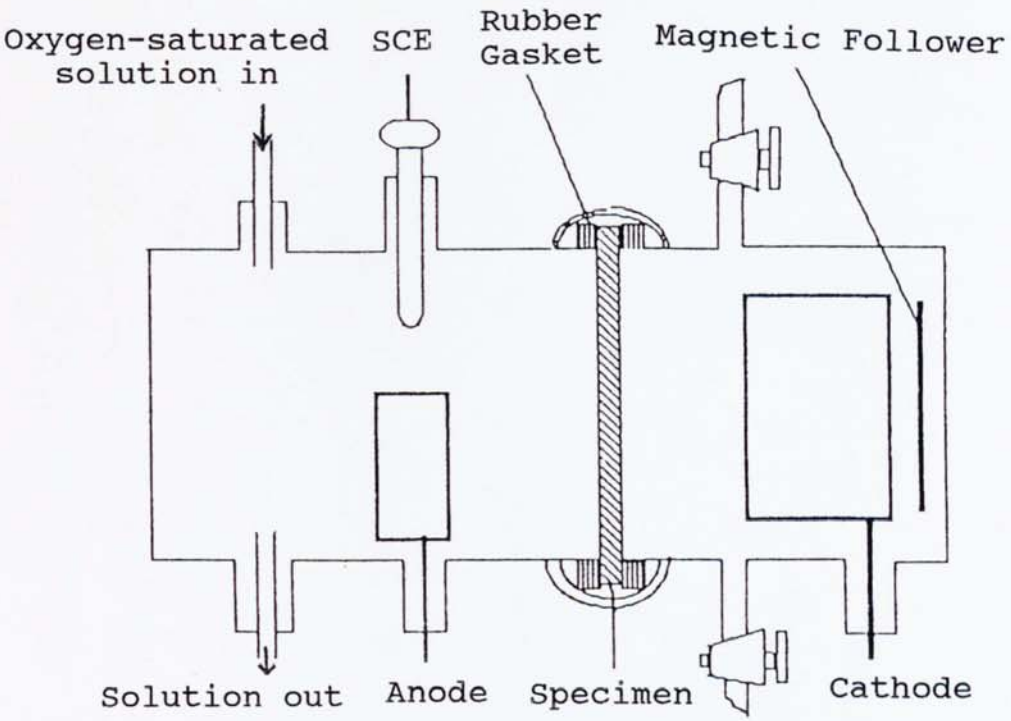


**Figure 5.1: The Oxygen Diffusion Cell**


**Figure 3.2: Set-up of oxygen diffusion experiment**

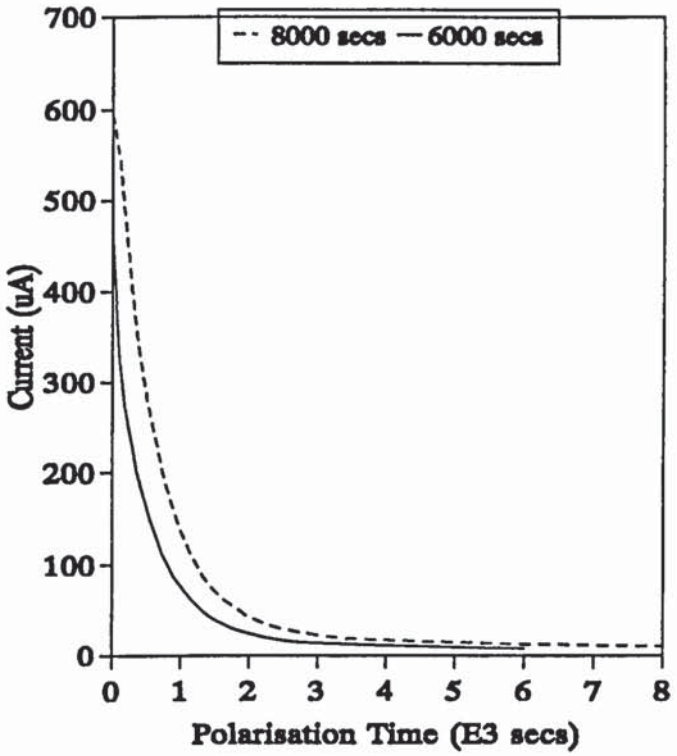


**Figure 5.3: Decay of cathodic current with polarisation time**

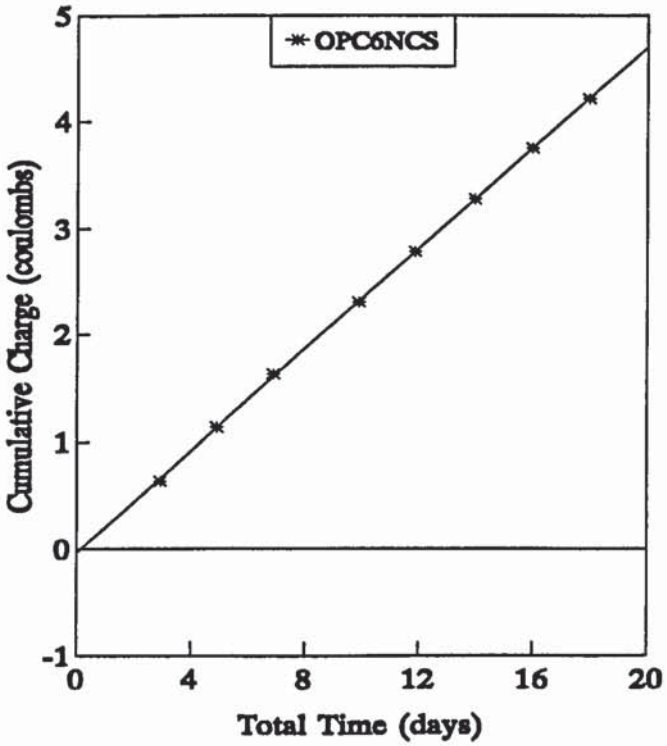


**Figure 5.4: Plot of cumulative charge against total time**

**Table 5.1: Oxygen diffusion data for hydrated OPC6NCS paste.**

| Test | $t_p$ (sec) | $I_e$ (μA) | Q (Coul) | $t_i$ (days) | $Q/t_i$ (Coul/day) | $t_d$ (days) | $Q_t$ (Coul) |
|---|---|---|---|---|---|---|---|
| A | 6000 | 16.2 | 0.517 | | | | |
| B | 8000 | 15.0 | 0.638 | 2.93 | 0.218 | 2.93 | 0.638 |
| C | 6000 | 16.4 | 0.495 | 1.99 | 0.248 | 4.92 | 1.133 |
| D | 6000 | 16.5 | 0.492 | 1.99 | 0.247 | 6.91 | 1.625 |
| E | 8000 | 16.1 | 0.673 | 3.00 | 0.224 | 9.91 | 2.298 |
| F | 6000 | 16.5 | 0.482 | 1.97 | 0.245 | 11.88 | 2.780 |
| G | 6000 | 17.0 | 0.496 | 2.10 | 0.236 | 13.98 | 3.276 |
| H | 6000 | 16.5 | 0.471 | 2.01 | 0.234 | 15.99 | 3.747 |
| J | 6000 | 16.4 | 0.463 | 1.97 | 0.235 | 17.96 | 4.210 |

**Table 5.2: Solubility of oxygen in 35mM NaOH solution**

| Cell Number | 1 | 2 | 3 |
|---|---|---|---|
| Weight of Cell (g) | 218.2 | 233.5 | 213.3 |
| Weight of Cell + Solution (g) | 245.9 | 267.2 | 244.6 |
| Volume of Solution in Cathode (ml) | 27.7 | 33.7 | 31.3 |
| Charge (coulombs) | 13.756 | 16.284 | 15.334 |
| End Current (uA) | 12.7 | 14.8 | 14.5 |
| Solubility ($x10^{-3}M$) | 1.287 | 1.252 | 1.269 |
| **Average Solubility ($x10^{-3}M$)** | **1.269** | | |

**Table 5.3: Experimental results obtained for hydrated OPC pastes.**

| W/C | Oxygen Diffusivity ($x10^{-8}cm^2/s$) | Bulk Density ($g/cm^3$) | Capillary Porosity (%) | Total Porosity (%) |
|---|---|---|---|---|
| 0.4 | 9.78 | 2.019 | 4.33 | 40.18 |
| | 10.00 | 2.020 | 4.32 | 40.40 |
| | 8.49 | 2.012 | 4.05 | 40.43 |
| | 9.00 | 2.018 | 4.56 | 40.56 |
| | 9.40 | 2.018 | 4.32 | 40.59 |
| **Average** | 9.33 | 2.017 | 4.32 | 40.41 |
| 0.5 | 9.63 | 1.891 | 8.34 | 47.16 |
| | 10.41 | 1.893 | 8.34 | 47.02 |
| | 10.87 | 1.898 | 8.30 | 47.19 |
| | 10.68 | 1.891 | 8.48 | 47.01 |
| **Average** | 10.40 | 1.893 | 8.36 | 47.10 |
| 0.6 | 14.24 | 1.794 | 19.73 | 52.20 |
| | 11.37 | 1.813 | 17.83 | 50.97 |
| | 12.67 | 1.810 | 17.47 | 50.89 |
| | 16.65 | 1.792 | 19.34 | 52.17 |
| | 13.29 | 1.794 | 19.77 | 51.57 |
| **Average** | 13.64 | 1.801 | 18.83 | 51.56 |
| 0.7 | 19.08 | 1.729 | 24.29 | 55.26 |
| | 17.37 | 1.734 | 24.51 | 54.95 |
| | 24.47 | 1.724 | 25.18 | 55.51 |
| | 20.99 | 1.724 | 24.15 | 55.18 |
| | 26.84 | 1.712 | 26.19 | 56.25 |
| **Average** | 21.75 | 1.725 | 24.86 | 55.43 |

**Table 5.4: Experimental results obtained for hydrated OPC/30%PFA pastes.**

| W/S | Oxygen Diffusivity ($x10^{-8}cm^2/s$) | Bulk Density ($g/cm^3$) | Capillary Porosity (%) | Total Porosity (%) |
|---|---|---|---|---|
| 0.4 | 6.33 | 1.938 | 3.11 | 43.37 |
| | 5.54 | 1.941 | 3.10 | 43.29 |
| | 6.24 | 1.938 | 2.96 | 43.20 |
| | 5.56 | 1.939 | 3.11 | 43.22 |
| | 5.36 | 1.942 | 3.07 | 43.25 |
| **Average** | 5.79 | 1.940 | 3.07 | 43.27 |
| 0.5 | 7.00 | 1.827 | 5.15 | 48.84 |
| | 6.62 | 1.824 | 5.25 | 48.30 |
| | 6.41 | 1.828 | 4.95 | 48.36 |
| | 6.63 | 1.825 | 5.88 | 49.26 |
| **Average** | 6.67 | 1.826 | 5.31 | 48.69 |
| 0.6 | 8.80 | 1.746 | 8.83 | 54.28 |
| | 6.94 | 1.740 | 9.28 | 54.58 |
| | 7.58 | 1.740 | 9.68 | 54.73 |
| | 6.72 | 1.743 | 8.74 | 54.53 |
| **Average** | 7.51 | 1.742 | 9.13 | 54.53 |
| 0.7 | 9.25 | 1.676 | 13.92 | 58.29 |
| | 9.30 | 1.681 | 13.06 | 58.26 |
| | 8.63 | 1.677 | 13.68 | 58.46 |
| | 8.35 | 1.675 | 13.75 | 58.22 |
| **Average** | 8.88 | 1.677 | 13.60 | 58.31 |

**Table 5.5: Experimental results obtained for hydrated OPC/65%BFS pastes.**

| W/S | Oxygen Diffusivity ($x10^{-8}cm^2/s$) | Bulk Density ($g/cm^3$) | Capillary Porosity (%) | Total Porosity (%) |
|---|---|---|---|---|
| 0.4 | 3.15 | 1.965 | 2.27 | 43.05 |
| | 2.85 | 1.964 | 2.14 | 43.30 |
| | 2.77 | 1.963 | 2.20 | 42.91 |
| | 2.28 | 1.966 | 2.07 | 42.79 |
| | 3.01 | 1.961 | 2.38 | 42.77 |
| **Average** | 2.81 | 1.964 | 2.21 | 42.96 |
| 0.5 | 2.33 | 1.848 | 4.84 | 48.52 |
| | 3.66 | 1.847 | 5.00 | 47.58 |
| | 3.16 | 1.851 | 5.18 | 47.59 |
| | 2.29 | 1.851 | 4.78 | 48.19 |
| | 3.01 | 1.859 | 4.94 | 48.29 |
| **Average** | 2.89 | 1.851 | 4.95 | 48.03 |
| 0.6 | 2.73 | 1.769 | 6.95 | 54.51 |
| | 2.63 | 1.764 | 6.70 | 54.76 |
| | 2.75 | 1.766 | 7.13 | 54.59 |
| | 3.77 | 1.761 | 6.61 | 54.50 |
| | 2.30 | 1.766 | 6.39 | 54.14 |
| **Average** | 2.84 | 1.765 | 6.76 | 54.50 |
| 0.7 | 2.83 | 1.723 | 8.97 | 56.87 |
| | 2.88 | 1.718 | 10.04 | 57.28 |
| | 3.39 | 1.712 | 10.53 | 57.65 |
| | 3.01 | 1.725 | 9.23 | 56.76 |
| | 3.16 | 1.726 | 9.29 | 57.16 |
| **Average** | 3.05 | 1.721 | 9.61 | 57.16 |

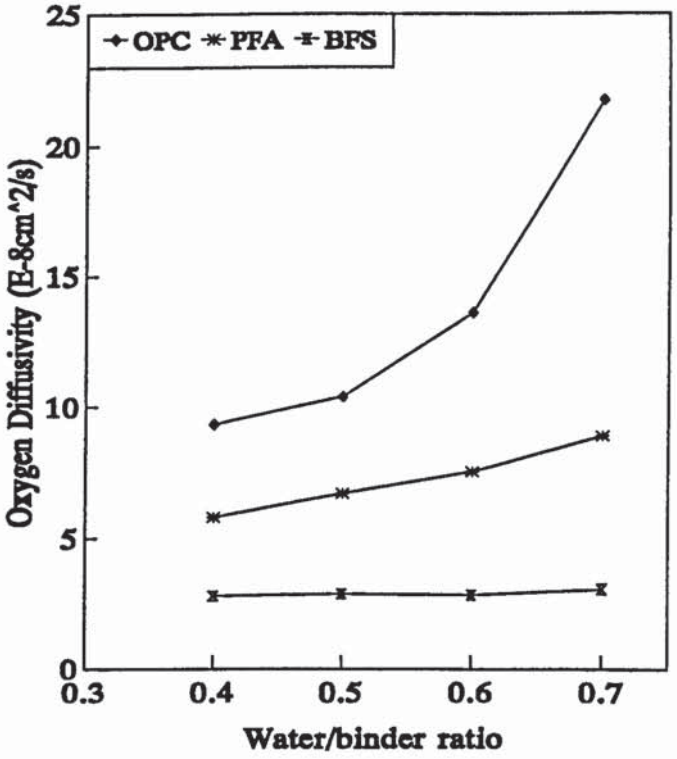


**Figure 5.5: Plot of oxygen diffusion coefficient versus water/binder ratio**

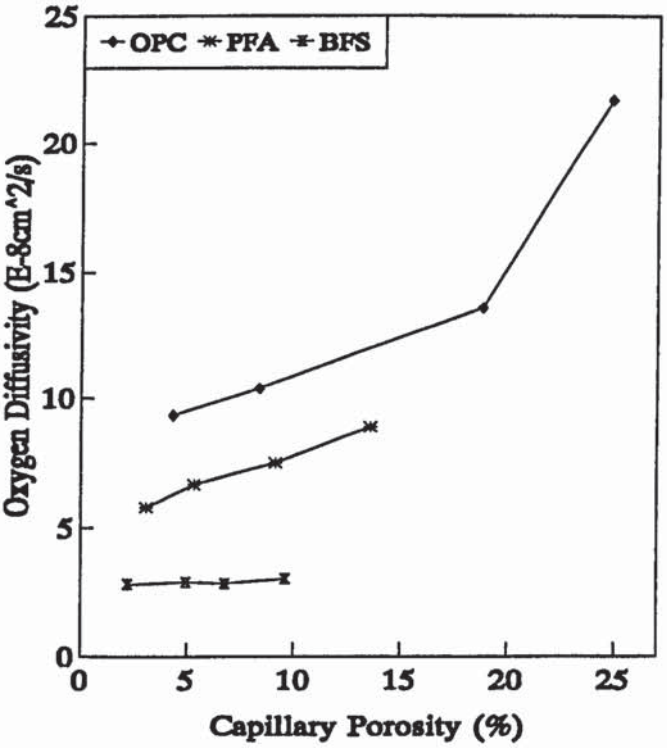


**Figure 5.6: Plot of oxygen diffusion coefficient against capillary porosity**

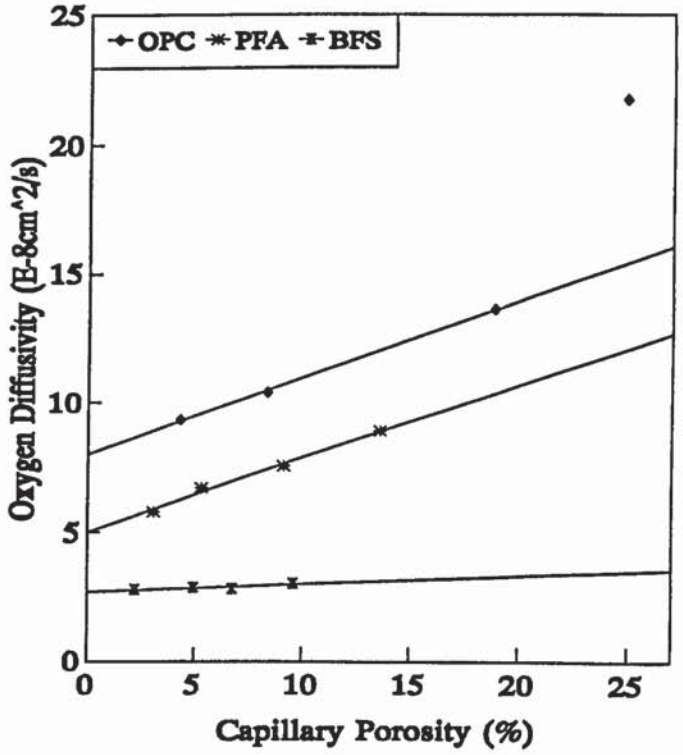


**Figure 5.7: Linear plot of oxygen diffusivity versus capillary porosity**

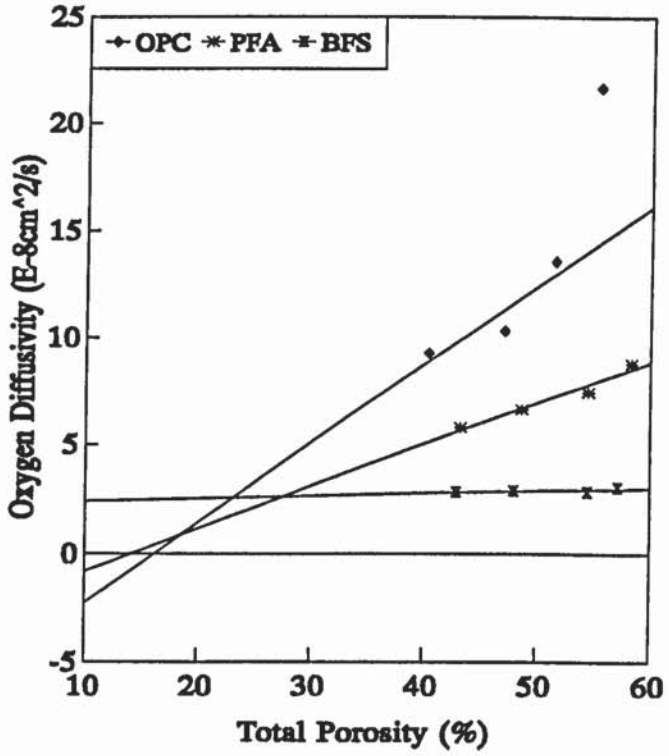


**Figure 5.8: Linear plot of oxygen diffusion coefficient against total porosity**

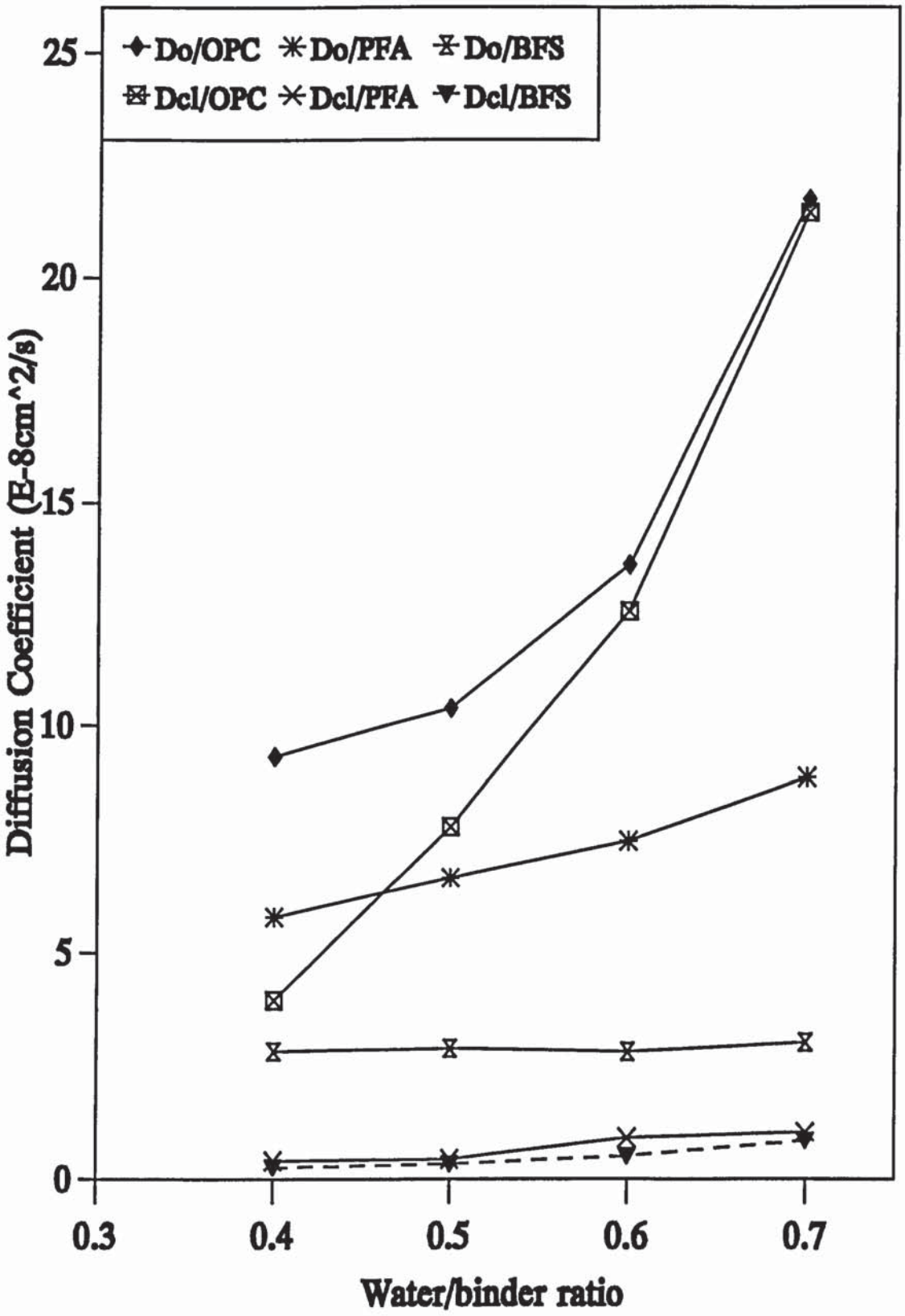


**Figure 5.9: Variation of oxygen and chloride diffusion coefficients with water/binder ratio**

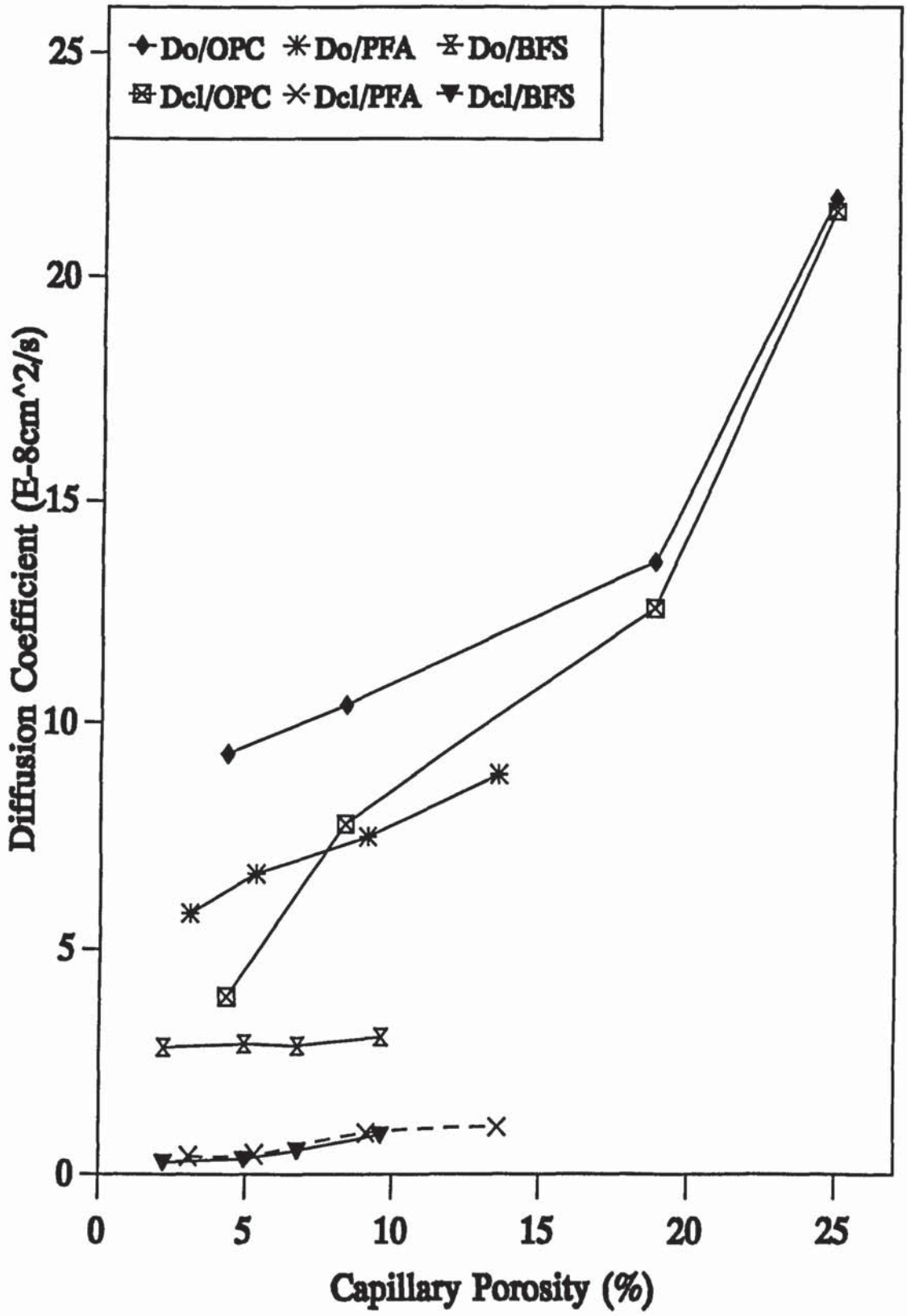


**Figure 5.10: Variation of oxygen and chloride diffusion coefficients with capillary porosity**

**Table 5.6: Ratio of oxygen to chloride diffusion coefficient for hydrated OPC pastes.**

| W/C | Oxygen Diffusivity ( $D_o$ ) ( $x10^{-8}cm^2/s$ ) | Chloride Diffusivity ( $D_{cl}$ ) ( $x10^{-8}cm^2/s$ ) | $D_o/D_{cl}$ |
|---|---|---|---|
| 0.4 | 9.33 | 3.95 | 2.362 |
| 0.5 | 10.40 | 7.80 | 1.333 |
| 0.6 | 13.64 | 12.60 | 1.083 |
| 0.7 | 21.75 | 21.46 | 1.014 |

**Table 5.7: Ratio of oxygen to chloride diffusion coefficient for hydrated OPC/30%PFA pastes.**

| W/S | Oxygen Diffusivity ( $D_o$ ) ( $x10^{-8}cm^2/s$ ) | Chloride Diffusivity ( $D_{cl}$ ) ( $x10^{-8}cm^2/s$ ) | $D_o/D_{cl}$ |
|---|---|---|---|
| 0.4 | 5.79 | 0.39 | 14.846 |
| 0.5 | 6.67 | 0.43 | 15.511 |
| 0.6 | 7.51 | 0.90 | 8.344 |
| 0.7 | 8.88 | 1.03 | 8.621 |

**Table 5.8: Ratio of oxygen to chloride diffusion coefficient for hydrated OPC/65%BFS pastes.**

| W/S | Oxygen Diffusivity ( $D_o$ ) ( $x10^{-8}cm^2/s$ ) | Chloride Diffusivity ( $D_{cl}$ ) ( $x10^{-8}cm^2/s$ ) | $D_o/D_{cl}$ |
|---|---|---|---|
| 0.4 | 2.81 | 0.26 | 10.807 |
| 0.5 | 2.89 | 0.33 | 8.758 |
| 0.6 | 2.84 | 0.51 | 5.568 |
| 0.7 | 3.05 | 0.85 | 3.588 |

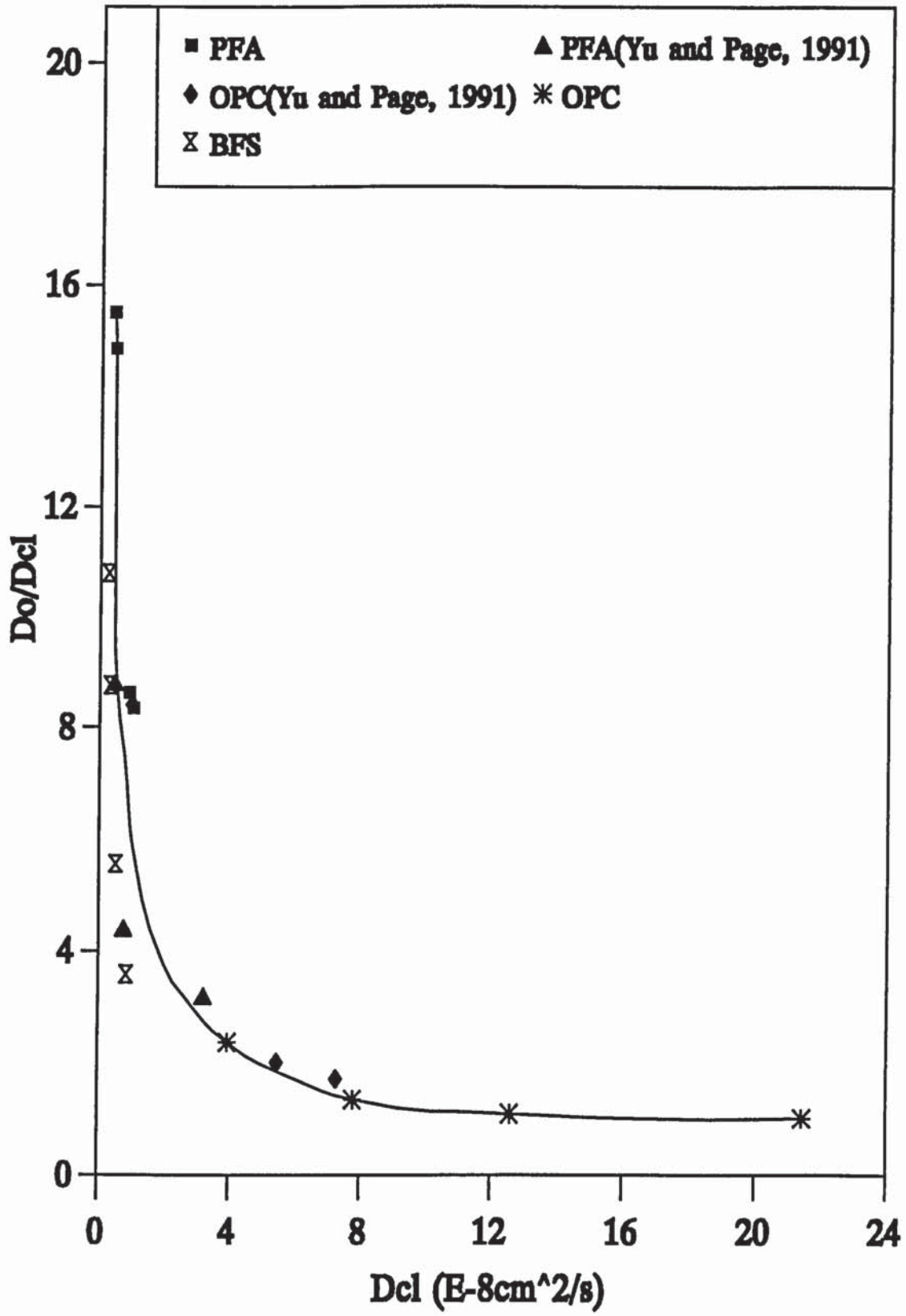


**Figure 5.11: Ratio of oxygen to chloride diffusion coefficients**

# CHAPTER SIX

# THE NEUTRALIZATION OF CEMENTITIOUS MATERIALS

## 6.1 INTRODUCTION

The most common cause of deterioration in reinforced concrete is the corrosion of steel reinforcement. In hardened concrete, steel is normally protected from corrosion by a highly alkaline medium which stabilises a passive layer of oxide on the metal surface. However, steel may become susceptible to corrosion in the presence of chloride ions due to either depassivation or a reduction in the alkalinity of the concrete at the location of the steel. This reduction in alkalinity can occur either by severe leaching of hydroxyl ions into a more neutral solution like seawater, or by carbonation of the cement matrix. The more common and important way of neutralization is carbonation, which is investigated in Part I of this Chapter on a variety of cement pastes.

Atmospheric carbon dioxide can only react with cement hydrates where there is sufficient pore water to first dissolve it. As such, hydrated cement dried to very low relative humidity would not carbonate to any significant extent. Although the carbonation reaction can readily occur under saturated conditions when carbon dioxide is freely available, in practice, it is necessary for the carbon dioxide to diffuse through the carbonated surface layer to reach the reaction zone. This gaseous diffusion is a slow process if the pores of the cement paste are filled with water. Thus, the maximum rate of carbonation is achieved at an intermediate moisture content. This entails drying the specimens to an appropriate relative humidity. However, the drying process itself tends to affect the pore structure of cementitious materials. Consequently, Part II of this Chapter investigates the influence of initial drying prior to carbonation on the pore structure and chloride diffusion kinetics of cement pastes and concrete.

# PART I: CARBONATION OF HYDRATED CEMENT PASTES

## 6.2 INTRODUCTION AND LITERATURE REVIEW

Carbonation is a readily occurring process since carbon dioxide is available at normal atmospheric concentrations of about 0.03% by volume. Nevertheless, the neutralization process can only occur when conditions are favourable as outlined in Section 6.2.2. Accelerated carbonation can be achieved by increasing the concentration by volume of $CO_2$ to a desired level.

### 6.2.1 Carbonation Reactions

Carbonation of concrete normally involves a chemical reaction between atmospheric carbon dioxide and products of cement hydration. Carbon dioxide penetrates the pores and dissolves in the moisture present forming carbonic acid. The carbonic acid reacts with the basic components of the matrix forming calcium carbonate and water as shown below;

$$Ca(OH)_2+CO_2+H_2O \rightarrow CaCO_3+2H_2O \qquad \text{.....(6.1)}$$

The main cement hydrates of calcium silicate hydrate, calcium hydroxide and various calcium aluminate or ferro-aluminate hydrates react to produce calcium carbonate, silica gel and hydrated aluminium and iron oxides, while the sulphate originally present in the cement reverts to gypsum after complete carbonation (Suzuki *et al.*, 1985; Manns and Wesche, 1968; Verbeck, 1958). At the other extreme, the unhydrated cement compounds can also react where $CO_2$ is present at high concentrations. Manns and Wesche (1958) showed that ettringite would carbonate as follows;

$$C_3A.3CaSO_4.32H_2O+3CO_2+3H_2O \rightarrow 3CaCO_3+2Al(OH)_3+3CaSO_4.2H_2O+30H_2O \qquad \text{.....(6.2)}$$

Under normal atmospheric conditions these hydrated cement compounds would be regarded as unreactive, thereby rendering Equation 6.2 impossible.

### 6.2.2 Factors Influencing Carbonation

Carbonation of the surface layer of concrete occurs readily but for deeper or complete neutralization to take place, continuous pores are required for easy penetration by the $CO_2$ gas. Daimon *et al.* (1981) demonstrated that pores can be classified as closed, accessible and continuous. The transport of ions, moisture and gases is controlled mainly by the continuous pores. If the cement matrix is completely dry, most continuous pores would allow easy air permeability, but the $CO_2$ present in the air would not neutralize the solid alkaline matrix in the absence of the aqueous phase, resulting in minimal carbonation. On the other hand, if the pores are completely saturated with water, as might be the case with a fully submerged structure, $CO_2$ cannot enter the pores directly. It would have to dissolve in the water near the surface in the form of weak carbonic acid, resulting in a negligible carbonation rate. Consequently, there is an intermediate moisture content at which a maximum carbonation rate would be achieved. At this moisture content, the majority of the pores would be empty for easy $CO_2$ penetration, but enough moisture would be present to dissolve the $CO_2$ and neutralize the cement matrix. It is generally agreed by researchers (Thomas and Matthews, 1992; Tuutti, 1982; Sauman, 1972, 1971; Powers, 1962) that this intermediate relative humidity where the fastest carbonation rate can be achieved is between 60% and 70%. This relationship is illustrated in Figure 6.1 after Tuutti (1982) who demonstrated that even at 99.9% RH, there are still a substantial volume of capillary pores which are not completely filled with water. Tuutti also pointed out that small changes in the relative humidity at this high value necessitate considerable changes in the moisture content of the concrete. An increase in temperature would increase the diffusivity of $CO_2$ but would also promote drying. Thus depending on the degree of hydration, elevated temperatures could increase or decrease the later rate of carbonation (Daimon *et al.*, 1981).

The neutralization of concrete occurs at different rates depending on the composition of the mix and the water/solid ratio. It was reported that rate of carbonation of concrete

depended on the compressive strength and w/c ratio (Treadaway *et al.*, 1983). The authors also obtained a relationship between cement content and depth of carbonation, thereby confirming the fact that, generally, higher cement content concretes resulted in lower carbonation depths. Other studies (Hamada, 1968; Mayer, 1968) have also reported similar findings to those of Treadaway *et al.*. Hamada (1968) observed faster carbonation rates for BFS and pozzolanic cement concretes and attributed the effect to the reduced amount of $Ca(OH)_2$. Mayer (1968) carbonated concretes with varying amounts of BFS to illustrate the effect of slag cements. The author showed that higher BFS additions resulted in increases in the carbonation rates and demonstrated that a reduction in the w/s ratio greatly reduces the measured depth of carbonation. Recent studies have shown that concretes containing 15-30% fly ash, carbonated to a slightly greater extent than OPC concretes of the same strength grade (Haque and Kawamura, 1992; Thomas and Matthews, 1992). Haque and Kawamura (1992) further pointed out that concretes containing 50% fly ash carbonated faster than concretes with lower proportions (15-30%) of fly ash. This increase in the carbonation rate was linked to the reduced $Ca(OH)_2$ levels in higher fly ash concretes as a result of the dilution of the OPC and the consumption of the $Ca(OH)_2$ in the pozzolanic reaction.

The curing conditions as well as the $CO_2$ concentration or partial pressure to which cement paste or concrete is exposed would affect its degree of carbonation. Short term curing increases the depth of carbonation (Thomas and Matthews, 1992; Nagati *et al.*, 1986). Nagati *et al.* (1986) reported that the effect of curing was more pronounced with drier exposure conditions. Slow reacting systems with PFA or BFS in the binder benefit more from prolonged moist curing (Bier, 1986; Mayer, 1968). The rate of carbonation increases with increasing concentration of $CO_2$ by volume (Hamada, 1968; Verbeck, 1958), owing to a higher concentration of the dissolved $CO_2$ in the pore solution and easier penetration within the particles. However, Verbeck (1958) illustrated (Figure 6.2) that, there is only a small increase in the amount of weight gained beyond 1% by volume of carbon dioxide

gas.

When carbonation occurs, the $CaCO_3$ modifications exist in three possible forms; vaterite, calcite and aragonite, with aragonite being the least common. It is commonly speculated that the finer crystalline vaterite would form more readily where the carbonation reactions are faster and where the nucleation of calcium carbonate in the form of vaterite crystals is easier opposed to the slower but more stable large crystalline calcite. Where conditions permit, the vaterite could then slowly recrystallize to the coarser morphology of the calcite.

Sauman (1971) established that, the C-S-H gel when carbonated, initially formed vaterite which then transformed either partly or fully to the more stable calcite. A relative humidity of 100% resulted in the rapid and complete transformation of the vaterite into calcite. Higher $CO_2$ levels of up to 30% also facilitated a more complete transformation, however, aragonite was formed to only a small extent. Kondo *et al.* (1968) showed a relative variation of the $CaCO_3$ modifications with increasing depth by carbonating mortar prisms through one surface only. At the deeper parts of the prisms where carbonation had been relatively fresh, the carbonate formed was comparable to the amorphous calcite found at intermediate depths. Nearer the surfaces, however, the amount of calcite decreased at the expense of the increasing vaterite. The authors claimed that calcite was formed more readily during early carbonation, but vaterite was more likely at the later stages as the unhydrated $C_3S$ starts to carbonate.

From the above discussions, it can be summarised that apart from weather conditions, the rate of carbonation depends on the following;

(a) relative humidity with a maximum between 60 and 70%

(b) carbon dioxide partial pressure in the atmosphere

(c) water/binder ratio of the original mix

(d) amount of carbonatable material which in turn depends on:

(i) type of cement

(ii) amount of cement in the mix

(iii) degree of hydration

By monitoring and considering these factors, it may be possible to minimize the rate of carbonation of concrete and its subsequent influence on concrete properties.

### 6.2.3 Effects of Carbonation on Concrete Properties

The carbonation reaction generally modifies the pore solution composition and porosity of the cementitious material in which it occurs. Equation 6.1 shows that there is a resultant increase in weight since effectively, one mole of $H_2O$ is replaced by a heavier mole of $CO_2$. However, considerable weight loss would be expected in Equation 6.2 as 27 moles of water are lost compared with a gain of 3 moles of $CO_2$. Thus after carbonation, mass can either increase or decrease depending on the balance between water lost and carbon dioxide gained in the reaction. Researchers (Bier *et al.*, 1989; Bier, 1986; Hilsdorf *et al.*, 1984; Pihlajavaara, 1968) have observed that carbonation generally causes a reduction in the porosity of exposed material because the volume of $CaCO_3$ formed exceeds that of the parent hydrate. Pihlajavaara (1968) showed that carbonation affected the larger pores more than the smaller pores. Hilsdorf *et al.* (1984) and Bier (1986) pointed out that carbonation increases the capillary porosity of BFS cements despite the reduction in total porosity. This behaviour was attributed to the presence of more silica gel formed by the decomposition of the C-S-H gel. The reduction in total porosity following carbonation consequently leads to an increase in the compressive strength of concrete as demonstrated by Mayer (1968) and Manns and Wesche (1968). However, the authors showed that the compressive strength of concrete made with BFS decreased with carbonation. Generally, the higher the OPC content of the carbonated paste as opposed to BFS, the higher the final strength gained.

A reduction in the pH is the most obvious change when $CO_2$ from the atmosphere reacts with NaOH and KOH in pore solution. This affects steel reinforcement as the passive medium is destroyed. Carbon dioxide can also initiate corrosion by reacting with insoluble complex calcium chloroaluminate salt (Friedel's salt) as follows;

$$3CaO.Al_2O_3CaCl_2.10H_2O+3CO_2+3H_2O \rightarrow 3CaCO_3+2Al(OH)_3+CaCl_2+10H_2O$$

.....(6.3)

This reaction releases a substantial amount of $CaCl_2$ back into solution, thereby increasing the initially low $[Cl^-]/[OH^-]$ ratio as the $OH^-$ concentration is reduced.

Carbonation has been reported to increase the modulus of elasticity (Pihlajavaara, 1976), surface hardness (Amasaki, 1984) and creep (Parrott, 1975), and to cause significant shrinkage (Verbeck, 1958). Hilsdorf *et al.* (1984) found an increase in resistance to frost attack and a reduction in permeability as a result of carbonation. Sulphate attack (Regourd, 1976) and chloride penetration (Dhir *et al.*, 1993; Sergi, 1986) have been found to be accelerated by carbonation. Recently, Dhir *et al.* (1993) reported that sequential carbonation and chloride attack is a worse degradation problem than either process acting separately. The authors demonstrated that PFA resistance to chloride diffusion is almost completely lost on carbonation. Similar results were reported by Sergi (1986) using BFS cement pastes. In general, concrete property changes due to carbonation are consistent with changes in porosity.

The above literature indicates that carbonation has been and will continue to be a problem in reinforced concrete structures. Considering the factors influencing carbonation (Section 6.2.2), it is possible that carbonation can be reduced dramatically by using say a high CaO content portland cement with sufficiently low w/c ratio and a high cement content

especially if accompanied by a thick reinforcement cover. However, such measures would not be practically and economically viable. Furthermore, there may be instances where special cements are required for a particular property such as low ionic diffusivity or where a thin depth of cover may be unavoidable. As a result, a continued study of carbonation is necessary to try and address these problems. Consequently, this Section of Chapter Six will attempt to deal with some of the key questions regarding carbonation such as;

(a) effect of carbonation on porosity of OPC, PFA and BFS cement pastes and its influence on chloride diffusion, and

(b) resistance of carbonated cement pastes to diffusion of the neutral oxygen molecule in comparison to chloride diffusion. This is expected to give an insight into the binding capabilities of chloride ions or their reaction with the cement hydrates and could help evaluate the effect of carbonation on the known advantages of using fly ash and slag to reduce chloride ingress and reinforcement corrosion.

## 6.3 EXPERIMENTAL PROCEDURE

### 6.3.1 Sample Preparation and Experimental Set-up

The samples were prepared as described in Section 2.2 and the thin discs obtained were approximately 2.5 mm thick. The disc surfaces were ground with grade 600 emery paper, rinsed with deionised water and dried with a lens tissue before being placed in a standing position on specially made perspex racks. These racks were placed above a saturated solution of sodium nitrite in semi air-tight containers at room temperature as illustrated in Figure 6.3, thus maintaining the relative humidity at about 65% as recommended by the RILEM permanent committee (RILEM CPC-18, 1984).

### 6.3.2 Monitoring Carbonation

Carbonation of the specimens during this investigation was carried out in an artificial $CO_2$ atmosphere ranging from the atmospheric concentration of 0.03% to a maximum of 5% by volume. This range of $CO_2$ concentration was achieved by passing a 5% $CO_2$ gas for

about 30 minutes daily through the specimens in the semi air-tight containers. After an appreciable time period, the thickest discs from each set of specimens were removed from the containers and tested for full carbonation by means of a pH indicator (Section 2.3.3). This was repeated at regular intervals until all the discs were fully carbonated.

### 6.3.3 Diffusional and Pore Structural Characteristics

When the discs were fully carbonated, some were further dried for MIP studies by using iso-propanol as outlined in Section 3.4.3. The rest were completely saturated in water with the aid of a vacuum pump. Some of the saturated samples were used for porosity determination by the drying technique (Section 3.4.2) while the rest were used for diffusion studies. Chloride and oxygen diffusion experiments were set up and carried out on 4 or 5 replicate specimens as described in Chapters Four and Five respectively and the corresponding diffusion coefficients determined. In this case of carbonated pastes, one molar NaCl in deionised water and deionised water were respectively used as electrolytes in compartments 1 and 2 of the ionic diffusion cell (Figure 4.2). Similarly, de-aerated deionised water and deionised water were respectively used as electrolytes in the cathode and anode compartments of the oxygen diffusion cell (Figure 5.1).

## 6.4 CARBONATION RESULTS

### 6.4.1 Porosity and Pore Structure

The desorption and MIP techniques were used to measure the porosity and pore size distribution of carbonated cement pastes. Table 6.1 contains the specimen characteristics for various carbonated pastes and results obtained for the threshold pore diameter and total penetration volume of mercury. The porosity and density values in Table 6.1 are a summary of the average values from Tables 6.2, 6.3, 6.4 and 6.5. Compared to Table 3.1, Table 6.1 shows considerably higher bulk densities for corresponding specimens of the three cement systems investigated.

#### 6.4.1.1 Desorption Technique

Figures 6.4, 6.5 and 6.6 respectively, indicate that, whereas there is a considerable reduction in the total porosity of OPC, OPC/30%PFA and OPC/65%BFS pastes as a result of carbonation, the reverse is true for capillary porosity. These figures show that in blended fly ash and slag pastes where the capillary porosities are initially much smaller than those of the corresponding OPC pastes, carbonation causes a greater increase in the volume of large continuous pores than in the OPC pastes. This observation is clearly illustrated in Figure 6.7 where the average increase in capillary porosity following carbonation is almost negligible for OPC pastes (about 5%), compared with approximately 145% and 230% for OPC/30%PFA and OPC/65%BFS pastes respectively. On the other hand, Figures 6.4 to 6.6 also indicate that, the reduction in total porosity of HCP, though substantial in all three systems, is slightly greater in the OPC pastes than in the corresponding fly ash and slag pastes (approximately 25%, 18% and 17% for OPC, PFA and BFS pastes respectively).

#### 6.4.1.2 MIP Technique

The pore size distribution curves obtained by MIP are illustrated in Figures 6.8 to 6.10 for OPC pastes, Figures 6.11 to 6.14 for blended fly ash pastes and Figures 6.15 to 6.18 for blended slag pastes. These figures show the variation of the pore size distribution curves for carbonated and non-carbonated pastes at w/s ratios of 0.4, 0.5, 0.6 and 0.7. It can be seen from these figures that, generally, the threshold diameter or the volume of pores filled down to 30 nm diameter tends to increase after carbonation while the total intrusion volume of mercury tends to decrease. This implies that whereas there is a reduction in the total porosity of carbonated pastes, there is also a considerable coarsening of the pore structure as mentioned in Section 6.4.1.1 for measurements carried out using the desorption technique. Furthermore, the figures show that the difference in proportion of large pores between carbonated and non-carbonated pastes increases with increasing w/s ratio. Likewise, the reduction in total volume of pores with carbonation decreases with increasing

w/s ratio.

Figures 6.19 and 6.20 illustrate respectively, the variation of the threshold diameter and total intrusion volume of mercury for the various cement systems. Compared to the corresponding non-carbonated cement systems (Figures 3.12 and 3.13), the threshold diameters and total intrusion volumes are respectively higher and lower for the carbonated pastes. Although Figure 6.19 indicates minimal change in threshold diameter with increasing w/s ratio for the carbonated slag pastes, the volumes of mercury intruded for pores greater than 30 nm in these pastes are approximately 0.038, 0.053, 0.114 and 0.143 cc/g for w/s ratios of 0.4, 0.5, 0.6 and 0.7 respectively. This is just a preliminary observation, the implications of which are still not very clear. Consequently, further work is necessary to provide an improved understanding of this observation as recommended in Chapter Eight.

### 6.4.2 Diffusional Properties

#### 6.4.2.1 Chloride Diffusion

The chloride diffusion coefficients determined using Equation 4.8 for carbonated OPC, OPC/30%PFA and OPC/65%BFS pastes are shown in Tables 6.2, 6.3 and 6.4 respectively. The tables also contain values of bulk density, capillary porosity and total porosity for the various specimens used for diffusion experiments or an accompanying set of specimens. These values show very close consistency between the replicate specimens.

The average vales of the chloride diffusion coefficients are plotted in Figure 6.21 against the w/s ratio for OPC, OPC/30%PFA and OPC/65%BFS pastes. Compared with non-carbonated pastes of the same w/s ratio, the carbonated pastes all show a considerably higher permeability to the diffusion of chloride ions. This figure also points out that, although there is a significant increase in chloride diffusion with increasing w/s ratio for the three cement systems, the effect is more marked in the blended fly ash and slag pastes

than in the OPC pastes.

Chloride diffusion coefficients are shown to diminish as the capillary porosity diminishes for carbonated and non-carbonated OPC, PFA and BFS pastes (Figure 6.22). However, the chloride diffusion coefficients diminish much more rapidly for carbonated pastes than for non-carbonated pastes. Furthermore, the chloride diffusion coefficients for the carbonated pastes are much higher than those of the corresponding non-carbonated pastes for the same capillary porosity. Figures 6.21 and 6.22 also indicate that, non-carbonated slag pastes are slightly less permeable to the diffusion of chloride ions than fly ash pastes, the reverse being true for carbonated pastes.

#### 6.4.2.2 Oxygen Diffusion

The oxygen diffusion coefficients obtained using Equation 5.8 for carbonated OPC, OPC/30%PFA and OPC/65%BFS pastes at w/s ratios of 0.5 and 0.6 are shown in Table 6.5.

Figure 6.23 shows the average values of the oxygen diffusion coefficient for the three cement systems. This plot demonstrates, that compared with non-carbonated pastes of same w/s ratio, the carbonated pastes for the three cement systems are more permeable to the diffusion of the neutral oxygen molecule. It can also be seen (from this figure) that for w/s ratios of 0.5 and 0.6 investigated, the effect of carbonation on oxygen permeability is more marked in pastes with a higher w/s ratio of 0.6 than in pastes of 0.5 w/s ratio. Furthermore, at a given w/s ratio, the permeability of carbonated pastes to oxygen molecules seem to increase from OPC to OPC/30%PFA and OPC/65%BFS pastes.

## 6.5 DISCUSSION

### 6.5.1 Porosity and Pore Structure

Desorption and MIP techniques both reveal similar information regarding the porosity of carbonated cement pastes. In this study, it has been observed, that generally, there is a marked increase in the volume of coarser pores and a substantial decrease in the total pore volume following the neutralization of the cement paste matrix. This outcome which has been illustrated in Figures 6.4 to 6.18 suggests, that the carbonation reaction generally modifies the pore solution composition and pore structure of the cementitious material in which it occurs. The bulk densities of all the pastes investigated have been shown to increase as a result of carbonation, probably due to the compaction of the matrix and the consequent increase in weight as the solids formed are deposited.

The reduction in total pore volume and the corresponding increase in bulk density may be associated with the reactions that occur during carbonation. When neutralization occurs, the volume of $CaCO_3$ formed exceeds that of the parent hydrate, causing a reduction in the porosity as reported by previous investigations (Bier *et al.*, 1989; Bier, 1986; Hilsdorf *et al.*, 1984). However, this increase in weight and the reduction in total pore volume is accompanied by a substantial increase in the volume of large pores. This unexpected displacement of pores towards coarser ones could be caused to some extent by the dissolution of the $Ca(OH)_2$ crystals present in the large pores followed by the carbonation and nucleation of $CaCO_3$ in the higher moisture content smaller pores where dissolution of the $CO_2$ might be easier. This may tend to rearrange the pore size distribution of the cement pastes as the new solids are deposited. Also, prolonged and accelerated carbonation would cause the decomposition of the C-S-H gel in the matrix forming more silica gel which is very porous. Bier *et al.* (1989) demonstrated that the silica gel formed due to carbonation in cement pastes has a large porosity with a pore size distribution peak at $100 < r < 1000$ nm. This suggests a major transformation in the pore structure with the formation of silica gel since the C-S-H gel contains pores with radii of about 5 nm.

Clearly, the modification in the pore solution composition and pore structure varies between carbonated OPC, OPC/30%PFA and OPC/65%BFS cement systems owing to the differences in their original compositions and amount of cement hydrates prior to carbonation. Figures 6.4 to 6.7 reveal that the increase in capillary porosity is much higher for the blended fly ash and slag pastes than for the OPC pastes, while the reduction in total porosity for the OPC pastes is slightly greater than that for the blended pastes. These variations may be associated with the large amount of $Ca(OH)_2$ and less C-S-H gel present in the non-carbonated OPC pastes, as opposed to the high content of C-S-H gel present in the blended PFA and BFS pastes. Thus following the decomposition of the C-S-H gel, less silica gel is expected to be deposited in the carbonated OPC pastes compared to the high content of silica gel in carbonated fly ash and slag pastes. However, previous investigations (Bier *et al.*, 1989; Bier, 1986) have indicated that no coarsening of the pore structure occurs in carbonated OPC pastes because the C-S-H gel is less involved in the $CO_2$ take up, with large amounts of the $Ca(OH)_2$ being transformed into calcite. Consequently, the 5% increase in the volume of capillary pores in OPC pastes observed in this study could be associated with the artificial carbonation atmosphere (0.03 to 5% by volume of $CO_2$) used.

### 6.5.2 Diffusional Properties

The permeability of the OPC, OPC/30%PFA and OPC/65%BFS pastes to the diffusion of chloride ions is markedly increased as a consequence of carbonation. The effect is more obvious in blended fly ash and slag pastes than in the OPC pastes (Figures 6.21 and 6.22). The similarly-sized neutral oxygen molecule (Figure 6.23) diffuses relatively faster in the carbonated cement pastes than in the non-carbonated cement pastes for the three cement systems. These effects of carbonation on diffusion rates can be linked to the coarsening of the pore structure of these cement matrices since capillary porosity is thought to play a vital role in diffusion and other transport properties in cement pastes, mortars and concretes. However, Figure 6.22 illustrates that for the same capillary porosity, the

chloride ion diffuses relatively faster in the carbonated cement pastes than in the corresponding non-carbonated pastes. This suggests, that as well as the pore structure, other properties such as the binding capabilities of the virgin pastes are probably affected following carbonation. This may be associated with the reduction in the ability of the $C_3A$ phase to bind chloride ions in carbonated cement pastes.

The ratio of diffusion coefficients for carbonated and non-carbonated pastes, ($D_C/D_{NC}$), may be considered as a numerical measure of the effect of the neutralization of cement paste matrix on diffusion. Table 6.6 and Figure 6.24 show the variation of the ratio of chloride diffusion coefficient for carbonated and non-carbonated pastes, ($D_{Cl/C}$)/($D_{Cl/NC}$), with w/s ratio and type of cement matrix. It can be seen from Figure 6.24 that, although this ratio, ($D_{Cl/C}$)/($D_{Cl/NC}$), can be as small as 2 for OPC pastes, it can be as high as 162 and 225 for the blended fly ash and slag pastes respectively. At all w/s ratios investigated, the ratio ($D_{Cl/C}$)/($D_{Cl/NC}$) is greater for the OPC/65%BFS pastes than for the OPC/30%PFA pastes.

Similarly, Table 6.7 and Figure 6.25 show the variation of the ratio of the oxygen diffusion coefficient for carbonated and non-carbonated pastes, ($D_{O/C}$)/($D_{O/NC}$), with type of cement matrix at w/s ratios of 0.5 and 0.6. Figure 6.25 indicates that the ratio, ($D_{O/C}$)/($D_{O/NC}$), of fly ash pastes is greater than that of OPC pastes but less than that of slag pastes at both w/s ratios. Comparing Figures 6.24 and 6.25, it may be suggested that as a result of carbonation, the increase in the permeability of the blended pastes to the diffusion of chloride ions is higher than to the diffusion of neutral oxygen molecules. This is probably due largely to differences in the diffusion rates of the two species in the corresponding non-carbonated cement pastes as reported in Chapter Five.

Oxygen molecules and chloride ions might be expected to diffuse at similar rates in very porous hydrated cement systems owing to their similar sizes. The ratio of oxygen to chloride diffusion coefficients, ($D_O/D_{Cl}$), was considered in Chapter Five as a numerical

measure of the effect of surface charge on chloride diffusion for non-carbonated cement pastes. This ratio, ($D_O/D_{Cl}$), which is shown in Table 6.8 for carbonated cement pastes and reveals values of approximately 1 for most of the cement pastes, is illustrated in Figure 6.26, together with data from Figure 5.11 for non-carbonated pastes. This figure indicates that as the carbonated pastes become more permeable to the diffusion of chloride ions, they provide similar vulnerability to the diffusion of the oxygen molecule. This is due largely to the coarsening of the pore structures of the cement pastes and the reduced ability to bind chloride ions as a consequence of carbonation. Thus the results generally suggest that the rate-controlling factors of diffusion in carbonated OPC, OPC/30%PFA and OPC/65%BFS pastes, are almost the same for negatively charged chloride ions and neutral oxygen molecules.

The neutralization of cement pastes and concrete results in an increased volume of large pores and a reduction in total pore volume, and subsequently an increase in the permeability of these cementitious materials. This study has revealed that the superb qualities of fly ash and slag in resisting the ingress of chloride ions and the diffusion of oxygen molecule are almost completely lost on carbonation. This is due largely to the marked increase in the proportion of coarse pores in these carbonated pastes. It is, therefore, of vital importance to consider the environmental factors and conditions to which concrete would be exposed when incorporating fly ash or slag as partial replacement of cement for the purpose of limiting chloride ingress and other transport properties. It is well known that the process of carbonation lowers the pH of pore solutions thereby causing reinforcement corrosion, while chloride ions cause localised pitting corrosion of steel in concrete. Thus the combined action of carbonation, followed by exposure to chloride ions is a more devastating form of degradation than either process acting separately. The consequence would be a faster pit propagation, which, aided by the reduction in pH, could lead to quite considerable corrosion rates in concrete structures.

# PART II: DRYING OF HYDRATED CEMENT PASTES

## 6.6 INTRODUCTION AND LITERATURE REVIEW

The process of carbonation requires a reasonably dry paste or concrete for easy diffusion of the $CO_2$ gas, as well as enough moisture for the reaction to take place. As outlined in Section 6.2.2, the fastest carbonation rate could be achieved at an intermediate relative humidity of between 60 and 70%. Carbonating the specimens in this investigation involved drying their microstructure from a saturated surface dry condition at a relative humidity of about 65%. The microstructure of the paste phase in concrete is known to play a critical role in controlling the ingress of aggressive agents or chemicals. When concrete is subjected to a desorption atmosphere, the microstructure results in moisture gradients which can cause varying degrees of hydration and porosity.

Researchers (Parrott, 1992, 1987, 1986, 1985, 1981; Bager and Sellevold, 1986b, 1986a; Patel *et al.*, 1985) agree on the fact that drying alters the pore structure of cement paste in concrete. Patel *et al.* (1985) pointed out that drying causes a reduction in the volume of pores less than 36.8 nm diameter and a corresponding increase in the volume of larger pores. However, using PFA blended pastes, the authors showed that for well cured slabs, the capillary porosity was slightly decreased in the central regions. Using low temperature calorimetry, Bager and Sellevold (1986b, 1986a) reported that drying and resaturation of HCP resulted in an increase in the amount of large pores and their continuity due to the collapse of the smaller pores. This effect was more marked with increasing severity of drying down to a relative vapour pressure of 0.58, below which it remained practically constant. Parrott (1986, 1985) modelled the change in pore size distribution that accompanies drying to a given relative humidity, RH, and showed that the small pore volume is reduced for relative humidities down to 0.5 by a factor given by

$$G(RH)=0.7+1.2(RH-0.5)^2 \quad \text{.....(6.4)}$$

while at lower values of relative humidity,

$$G(RH)=0.7 \quad \text{.....(6.5)}$$

Since the total porosity is assumed not to be affected by drying, the reduction in smaller pores results in an increase in the volume of large pores. Parrott (1992) demonstrated that the resulting capillary porosity and water absorption rates in surface concrete were normally greater than those of the underlying material as a result of drying and carbonation.

The literature above points out that drying would affect pore structure and transport properties in concrete and this effect is expected to vary with different materials depending on the composition of the paste. Comparing the effects of carbonation on the properties of these materials without considering the influence of drying may be misleading in some circumstances. Consequently, this part of Chapter Six investigates the influence of drying on pore structure and chloride diffusion of comparable specimens with the intention of providing a better understanding of the effects of carbonation discussed in Part I of this Chapter.

## 6.7 SAMPLE PREPARATION AND EXPERIMENTAL SET UP

The cylindrical samples were prepared and the thin discs obtained as outlined in Section 2.2. The discs were placed in vacuum desiccators containing a saturated solution of $NaNO_2$, similar to that used for controlling the relative humidity of the carbonating samples (Section 6.3.1). The discs were maintained at this relative humidity until they reached near-constant weights. To minimize any carbonation taking place, the air entering

the desiccators was passed through a jar containing a mixture of carbosorb and silica gel to absorb any carbon dioxide gas. Some of the discs were further dried in propan-2-ol and used for MIP, while the rest were saturated in water and used for either chloride diffusion measurement or porosity determination.

## 6.8 RESULTS AND DISCUSSION

### 6.8.1 Pore Structure

A summary of the porosity data obtained for specimens initially dried from a saturated surface dry condition to a near-constant weight at 65% relative humidity is given in Table 6.9. The table shows that values for the bulk density and total pore volume are similar to those of the corresponding non-carbonated virgin specimens in Table 3.1, while the threshold diameters and capillary pore volumes are higher than those in Table 3.1.

The differences in capillary porosity between non-carbonated, partially dried and fully carbonated cement pastes for the three cement systems are illustrated in Figures 6.27 and 6.28 for w/s ratios of 0.5 and 0.6 respectively. These figures indicate that cement systems constituting OPC, OPC/30%PFA and OPC/65%BFS undergo a slight increase in the capillary porosity following drying and resaturation as pointed out by previous investigations (Parrott, 1992; Bager and Sellevold, 1986b, 1986a; Patel *et al.*, 1985). It can also be seen from Figures 6.27 and 6.28 that, in OPC pastes, the capillary porosity of partially dried cement pastes is comparable to that of carbonated pastes. On the other hand, the increase in capillary pore volume for partially dried blended fly ash and slag pastes is small compared to the marked increase incurred as a result of carbonation. Similar observations from mercury intrusion porosimetry measurements are demonstrated in Figures 6.29 to 6.34.

Since drying precedes carbonation, the above observation suggests, that the neutralization process does not seem to alter the capillary pore volume in the OPC pastes, at least not

for the w/s ratios of 0.5 and 0.6 investigated. This suggests that the increase in capillary pore volume observed for carbonated OPC pastes (Part I of this Chapter) was manifested by the initial drying prior to carbonation, and not by the carbonation process itself.

### 6.8.2 Chloride Diffusion

Chloride diffusion coefficients obtained for partially dried cement pastes are shown in Table 6.10 for OPC, OPC/30%PFA and OPC/65%BFS cement systems. It is illustrated (Figures 6.35 and 6.36), that for fly ash and slag cement systems, the partially dried specimens are more permeable to the diffusion of chloride ions than the non-carbonated virgin specimens, but much less permeable compared with the corresponding carbonated cement pastes. The OPC pastes studied seem to suggest a steady increase in chloride diffusivity with initial drying and consequent carbonation.

The ratio of diffusion coefficients for partially dried and non-carbonated cement pastes, $(D_{Cl/D})/(D_{Cl/NC})$, may be considered as a numerical measure or indication of the effect of initial drying on chloride diffusion rates. Table 6.11 shows that the ratio, $(D_{Cl/D})/(D_{Cl/NC})$, varies from an average value of about 2 for OPC pastes, to 4 for fly ash pastes and 14 for slag pastes. This ratio seems to vary between w/s ratios of 0.5 and 0.6 for blended fly ash and slag pastes. The effect of drying on chloride diffusion in blended cement pastes is less significant compared with the effect of carbonation as demonstrated by the ratio, $(D_{Cl/C})/(D_{Cl/NC})$, (Table 6.6) of on average 3.5, 114 and 185 for OPC, OPC/30%PFA and OPC/65%BFS cement systems, respectively.

## 6.9 GENERAL DISCUSSION

It has been shown that partial drying and resaturation of various cement pastes causes a slight coarsening of the pore structure. This increase in volume of large pores may be associated with the collapse of small pores since the total pore volume seems unaltered. The consequence of this modification is the increased permeability of these pastes to the

diffusion of chloride ions. This study has shown, that the permeability of blended pastes is greatly affected by the exposure conditions, more so for the slag pastes than for the fly ash pastes. Partial drying and resaturation of blended cement pastes increases their permeability to chloride ions. However, the magnitude of this effect of drying on chloride ingress is small compared with the marked effect of carbonation. This is not the case with OPC pastes in which the two exposure conditions seem to influence chloride permeability to a similar extent, despite the suggestion that initial drying is solely responsible for the coarsening of the pore structure. This, therefore, confirms the suggestion in Part I, that carbonation seems to alter other properties that influence chloride diffusion in cementitious materials, such as chloride binding and pore connectivity.

Effectively, if the three cement systems were exposed to drying and resaturation without any carbonation, then the blended pastes would still provide better resistance to the ingress of chloride ions. However, if carbonation subsequently occurred, then the OPC pastes would provide better resistance to the ingress of chloride ions than the blended pastes.

The observations clearly indicate that the good qualities associated with blended fly ash and slag pastes in retarding chloride ingress are slightly damaged with drying and/or resaturation, and almost completely lost with carbonation. There is, therefore, need for careful consideration of the environmental conditions to which PFA and slag concrete would be exposed. The marked increase in the permeability of the carbonated fly ash and slag pastes to chloride ions could therefore be associated mainly with neutralization, with initial drying prior to carbonation playing only a minor role. In OPC pastes, however, initial drying and carbonation seem to influence chloride permeability to a similar extent, probably by altering different properties of the original pastes. Moreover, there would be no significant carbonation occurring in saturated specimens without some form of initial drying to allow for the transport of $CO_2$ gas to the carbonation front.

## 6.10 CONCLUSIONS

The neutralization of cement matrices constituting OPC, OPC/30%PFA and OPC/65%BFS generally modifies the pore solution composition, pore structure and associated properties in a number of ways.

(1) There is an increase of about 5% in the proportion of capillary or coarse pores in the OPC paste matrix following carbonation. This is negligible compared with the marked increase of approximately 145% and 230% for blended fly ash and slag pastes respectively.

(2) The $CaCO_3$ formed results in an increase in the bulk density and a corresponding decrease in the total pore volume. This reduction in the total pore volume diminishes slightly with increasing w/s ratio, but is on average about 25% for OPC pastes, compared with 18% and 17% for fly ash and slag blends, respectively.

(3) The diffusion rate of chloride ions through carbonated OPC, OPC/30%PFA and OPC/65%BFS pastes diminishes markedly with decreasing w/s ratio or capillary porosity.

(4) For a given w/s ratio the chloride diffusion rates at 25°C for carbonated OPC/30%PFA and OPC/65%BFS pastes are about two orders of magnitude greater than those of the corresponding non-carbonated pastes. On the other hand, the chloride diffusion rates for carbonated OPC pastes are about 2 to 5 times higher than those of the corresponding non-carbonated pastes.

(5) For w/s ratios of 0.5 and 0.6 investigated, the oxygen diffusion rates for carbonated OPC, OPC/30%PFA and OPC/65%BFS pastes are considerably greater than those of the corresponding non-carbonated pastes. The increase in oxygen diffusion rates

is about one order of magnitude for the blended pastes compared to about 2 to 5 times for the OPC pastes.

(6) The ratio of oxygen to chloride diffusion coefficients is close to 1 for most of the carbonated pastes investigated irrespective of the cement composition or w/s ratio. This supports the view that the two species diffuse at a similar rate in very porous hydrated cement systems, probably due to negligible surface charge effects.

However, initial drying of cement pastes tends to influence their properties in at least two ways.

(7) Drying and resaturation of cement pastes slightly increases the capillary pore volume without any noticeable change in the total pore volume. This increase in coarse pores, which is at the expense of the small pores, is associated with the collapse of these small pores.

(8) The marked increase in permeability of carbonated OPC/30%PFA and OPC/65%BFS pastes to the diffusion of chloride ions is associated mainly with the effect of carbonation, with the initial drying playing only a minor role. In OPC pastes, however, initial drying seems to play a major role in the coarsening of the pore structure and the marked increase in permeability to chloride ions.

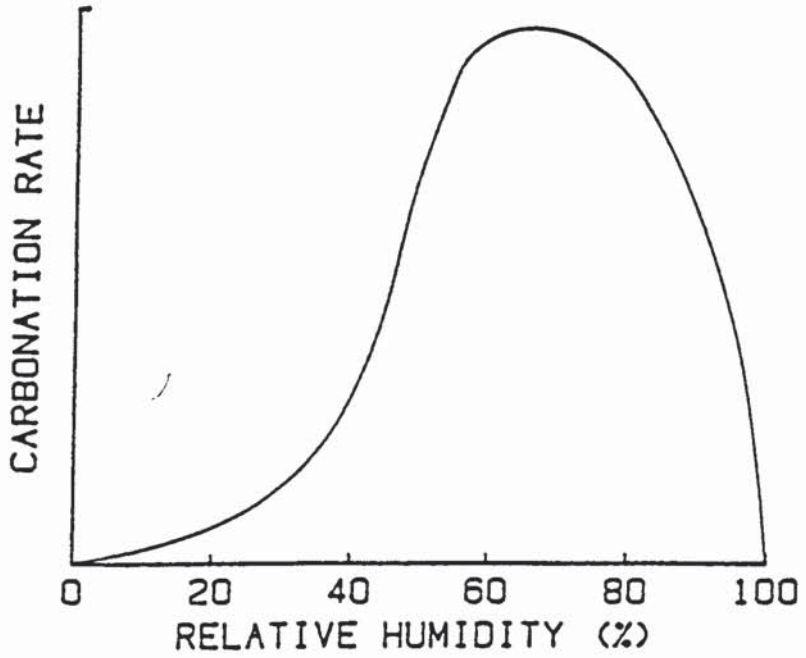


**Figure 6.1: Rate of carbonation of hardened cement paste or concrete as a function of relative humidity (Tuutti, 1982)**

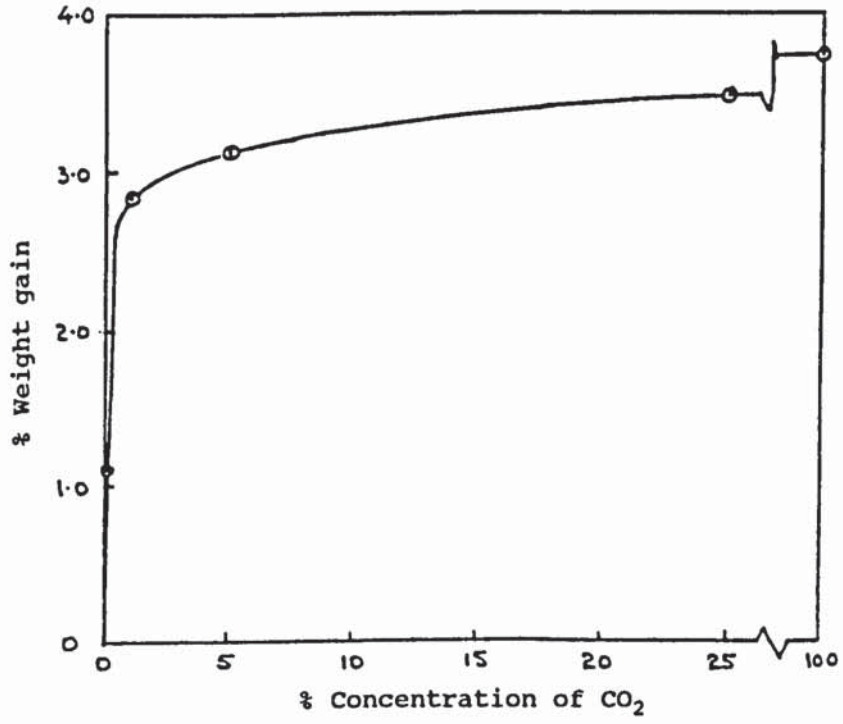


**Figure 6.2: Weight gain due to carbonation at different carbondioxide concentrations (Verbeck, 1958)**

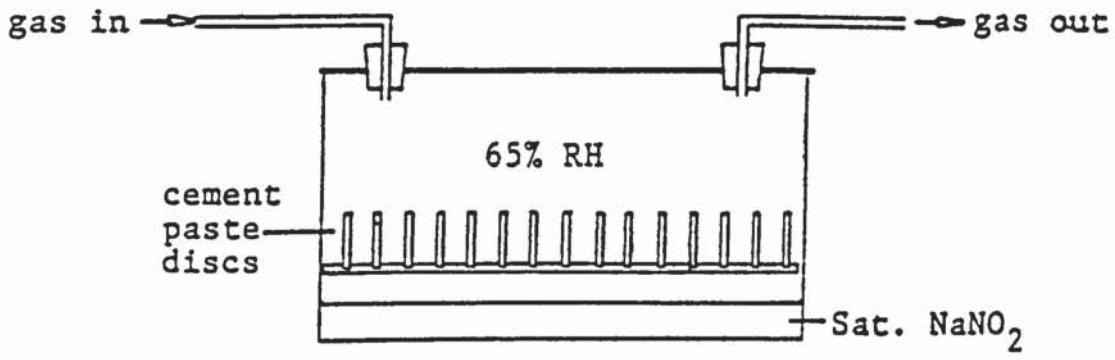


**Figure 6.3: Experimental set-up used for the carbonation of cement pastes**

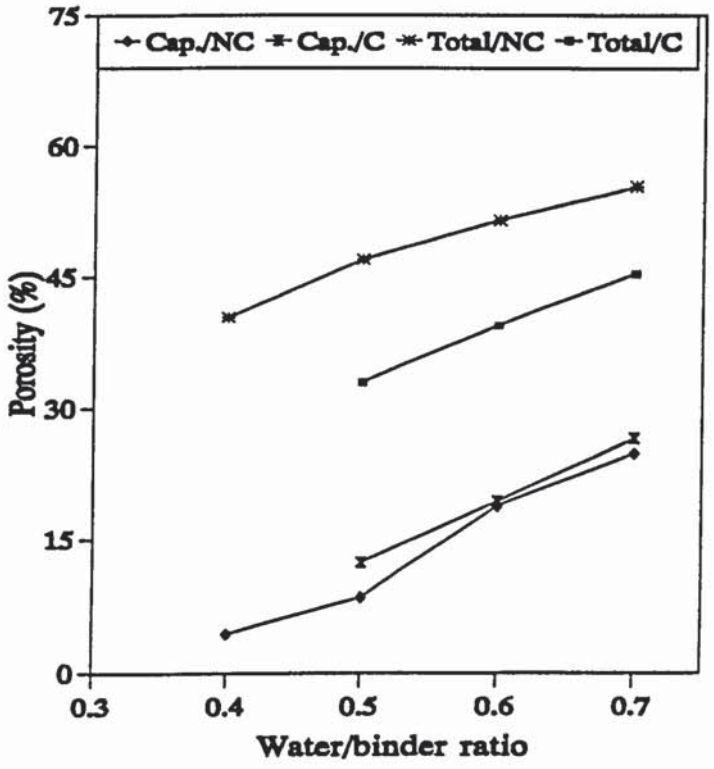


**Figure 6.4: Porosity of carbonated and non-carbonated OPC pastes**

**Table 6.1: Porosity data for fully carbonated cement pastes.**

| Sample | Bulk Density ($g/cm^3$) | Threshold Diameter (μm) | Total Pen. Volume ($cm^3/g$) | Capillary Porosity (%) | Total Porosity (%) |
|---|---|---|---|---|---|
| OPC5C | 2.137 | 0.147 | 0.093 | 12.31 | 32.88 |
| OPC6C | 2.011 | 0.307 | 0.144 | 19.38 | 39.49 |
| OPC7C | 1.924 | 0.642 | 0.201 | 26.57 | 45.52 |
| PFA4C | 2.096 | 0.090 | 0.064 | 7.49 | 32.56 |
| PFA5C | 2.017 | 0.307 | 0.150 | 14.09 | 38.85 |
| PFA6C | 1.899 | 0.502 | 0.184 | 20.66 | 46.15 |
| PFA7C | 1.776 | 0.642 | 0.290 | 33.22 | 52.77 |
| BFS4C | 2.119 | 0.147 | 0.083 | 8.21 | 32.63 |
| BFS5C | 1.984 | 0.188 | 0.169 | 14.36 | 40.16 |
| BFS6C | 1.888 | 0.240 | 0.204 | 23.04 | 46.48 |
| BFS7C | 1.817 | 0.240 | 0.228 | 30.38 | 50.30 |

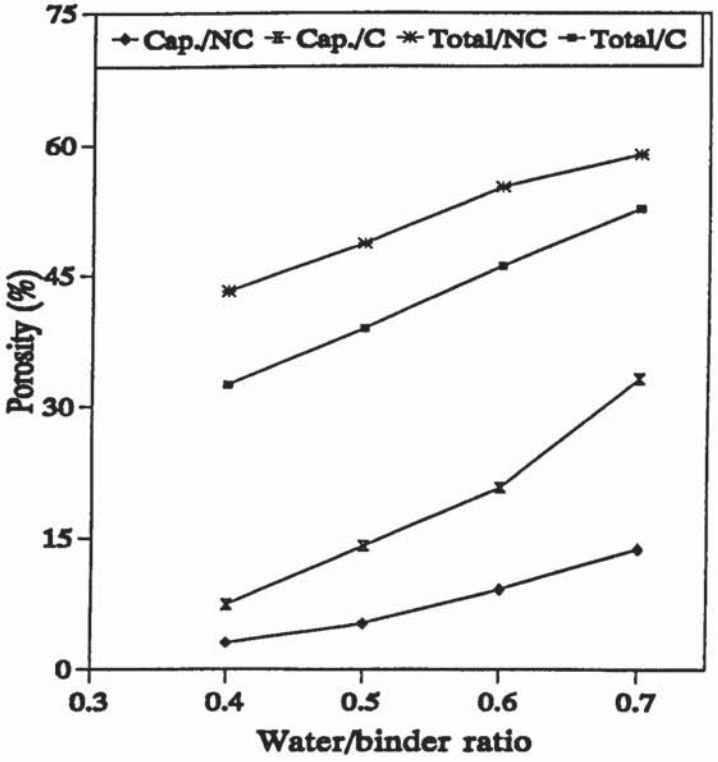


**Figure 6.5: Porosity of carbonated and non-carbonated fly ash pastes**

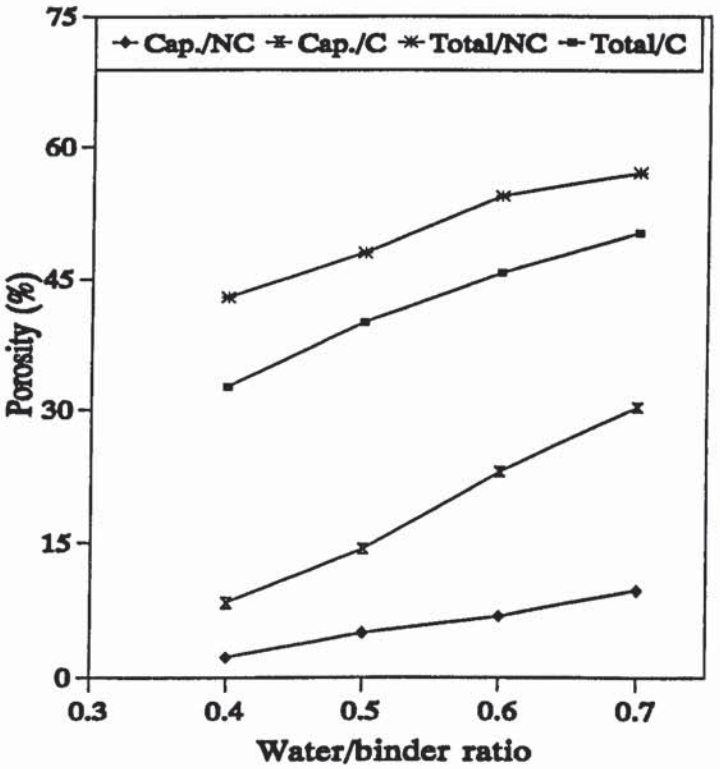


**Figure 6.6: Porosity of carbonated and non-carbonated slag pastes**

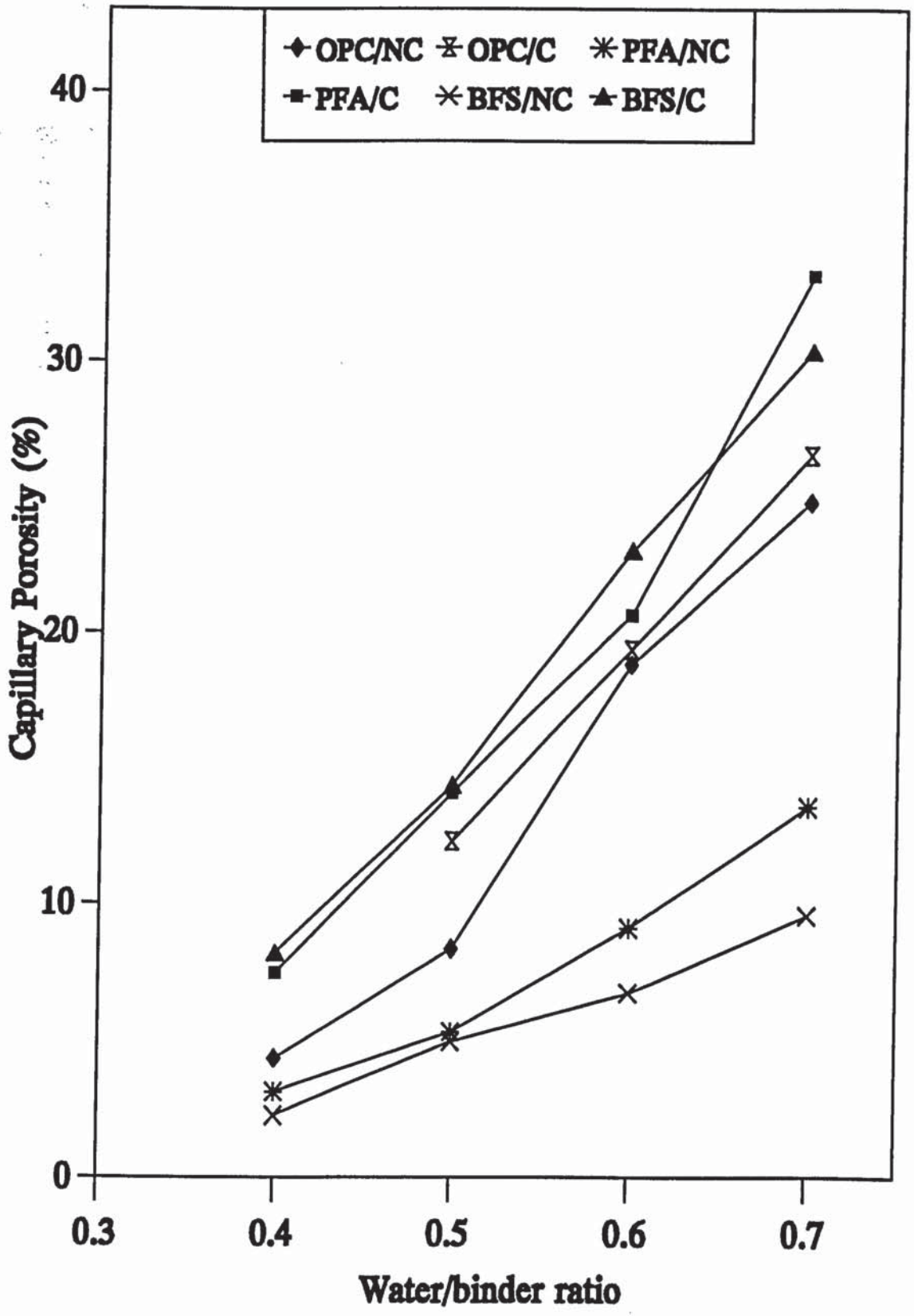


**Figure 6.7: Capillary porosity of hydrated cement pastes**

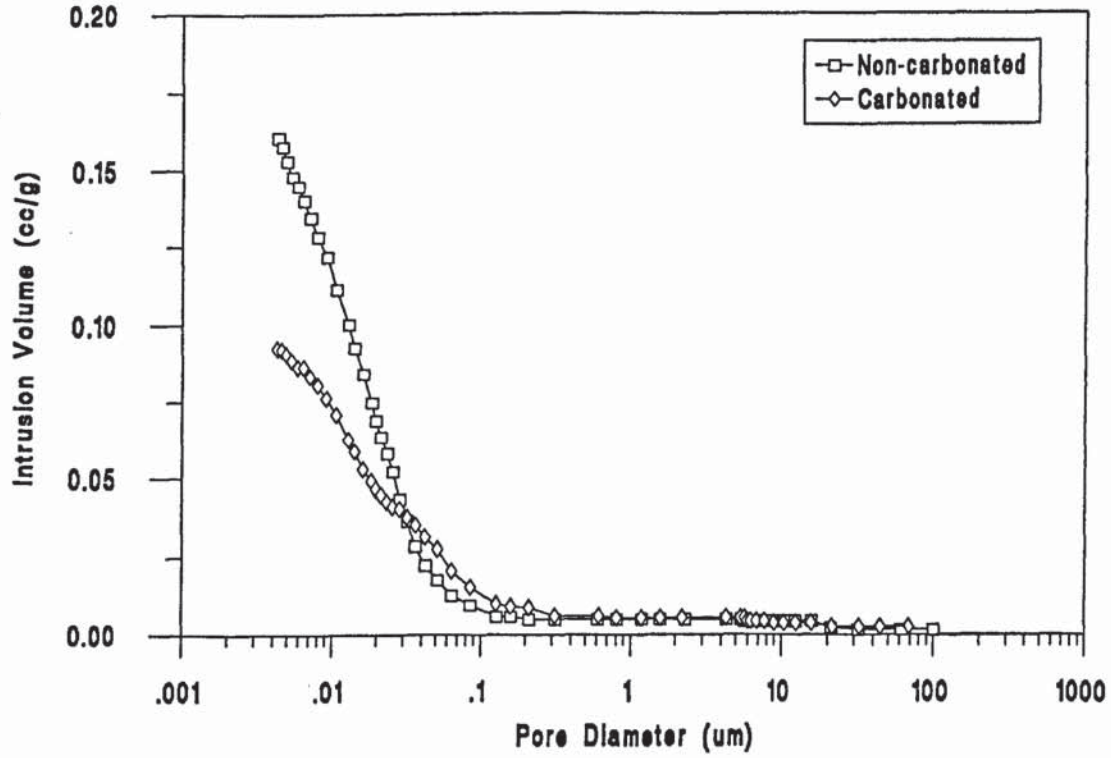


**Figure 6.8: Pore size distribution curves for OPC pastes of 0.5 w/c ratio**

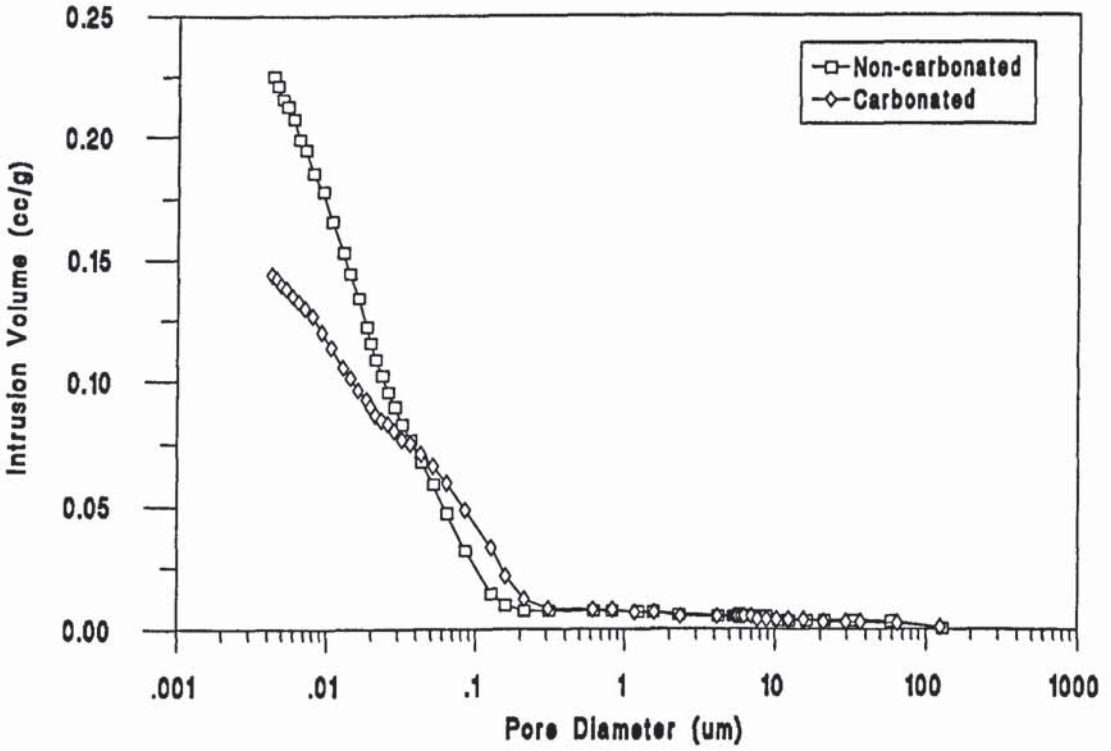


**Figure 6.9: Pore size distribution curves for OPC pastes of 0.6 w/c ratio**

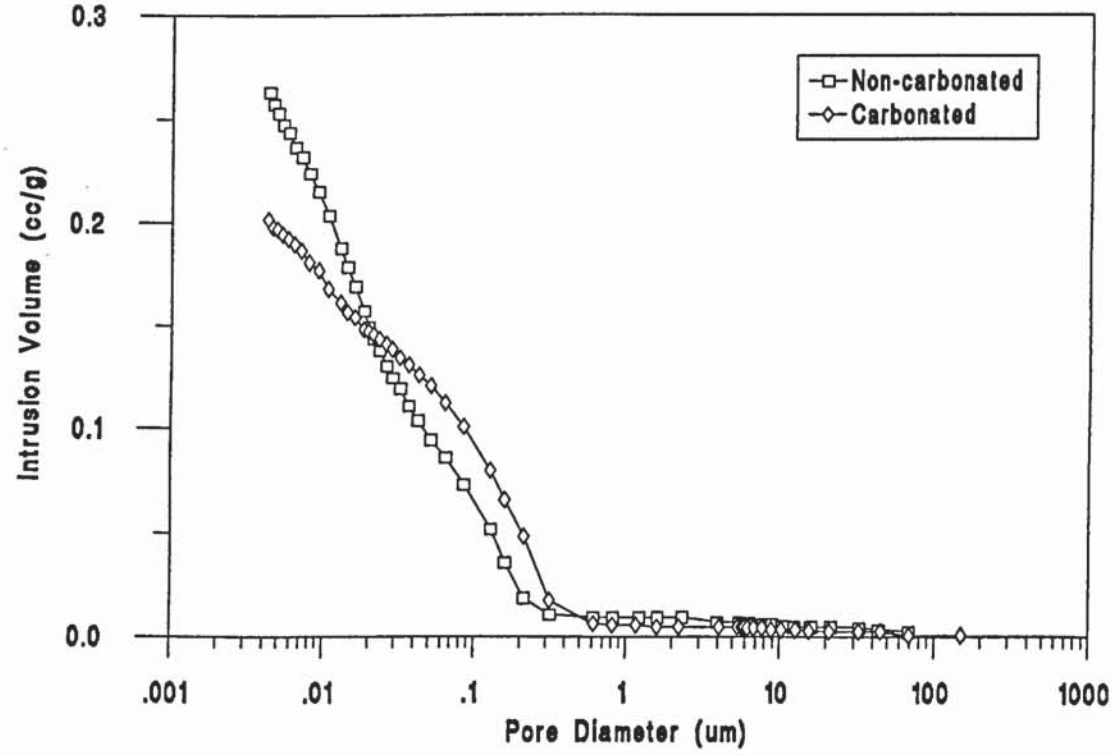


**Figure 6.10: Pore size distribution curves for OPC pastes of 0.7 w/c ratio**

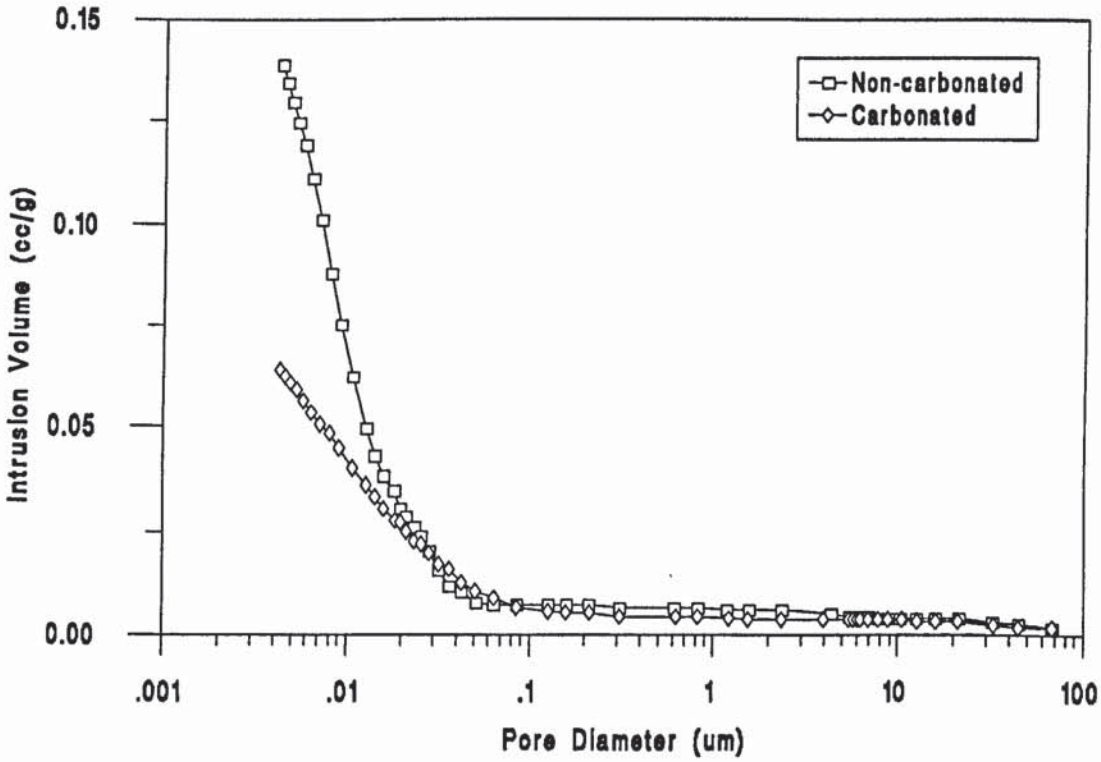


**Figure 6.11: Pore size distribution curves for fly ash pastes of 0.4 w/s ratio**

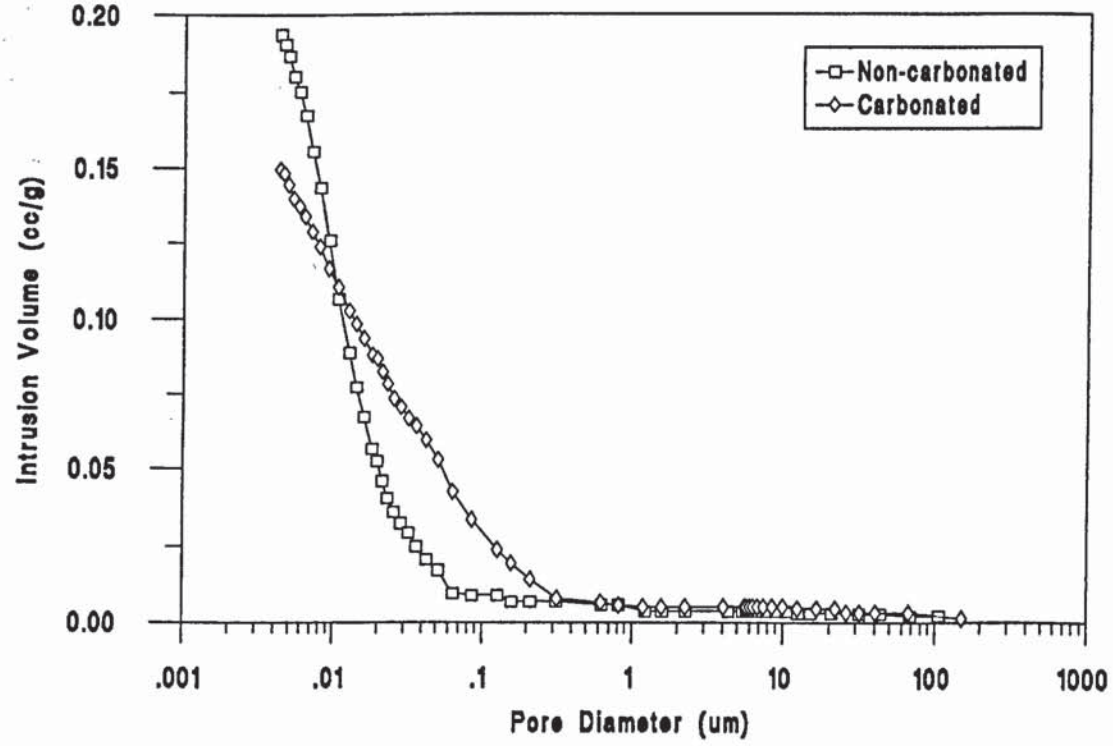


**Figure 6.12: Pore size distribution curves for fly ash pastes of 0.5 w/s ratio**

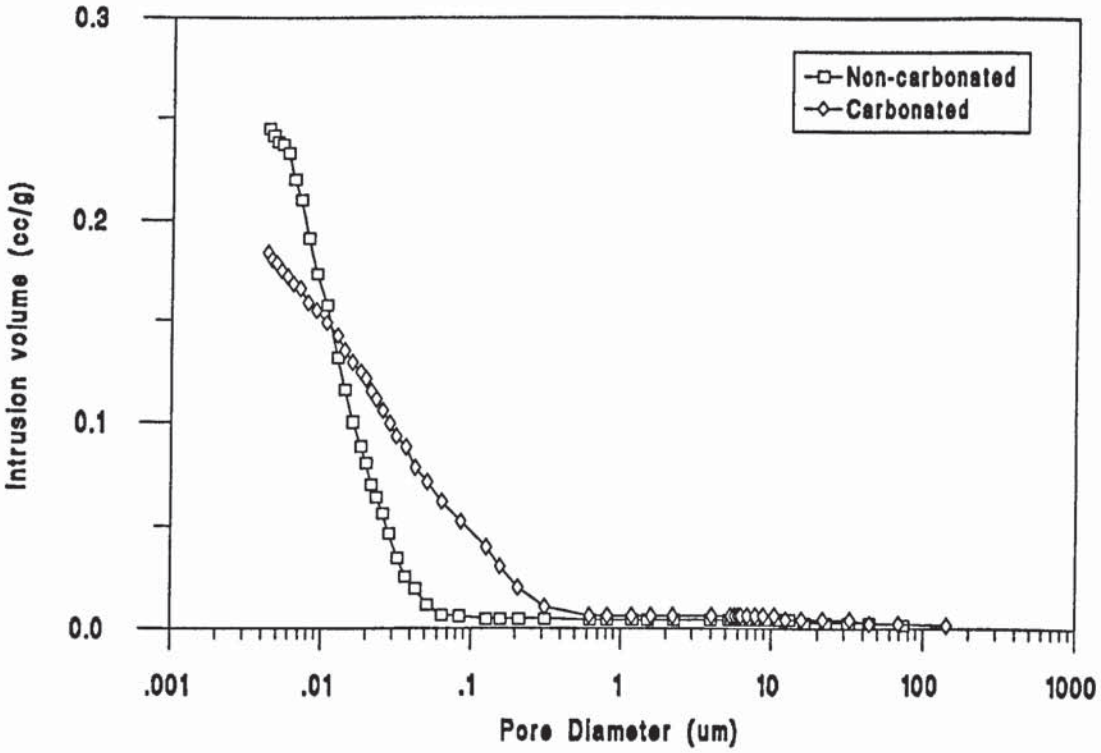


**Figure 6.13: Pore size distribution curves for fly ash pastes of 0.6 w/s ratio**

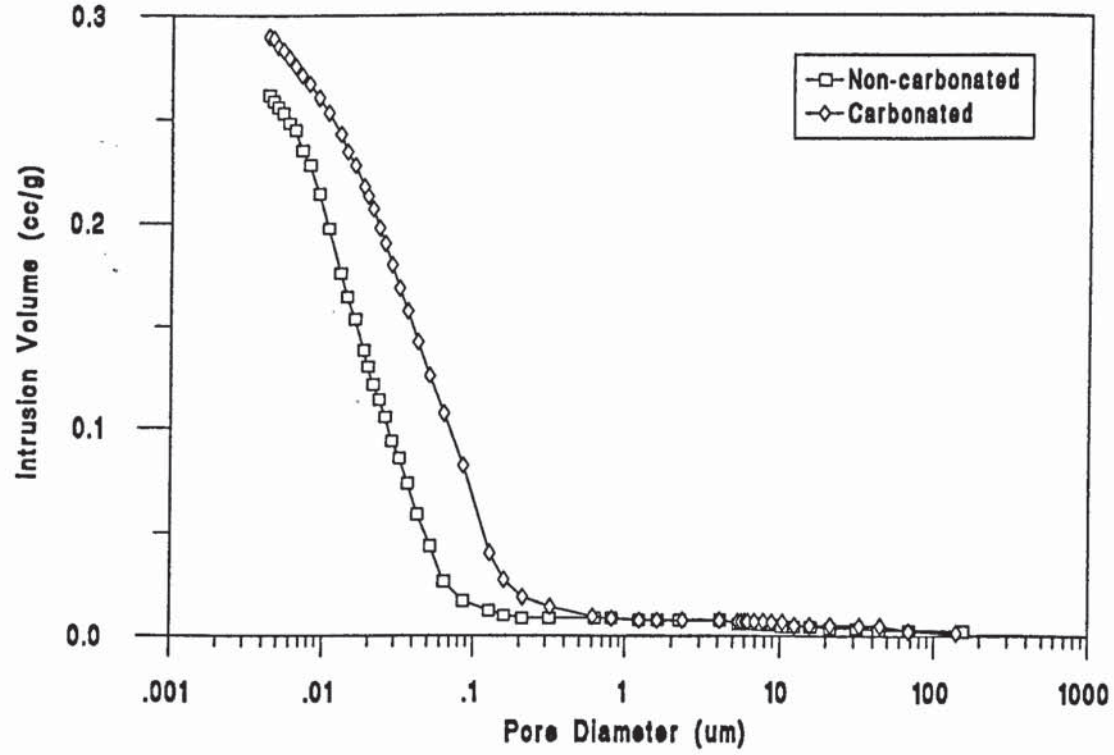


**Figure 6.14: Pore size distribution curves for fly ash pastes of 0.7 w/s ratio**

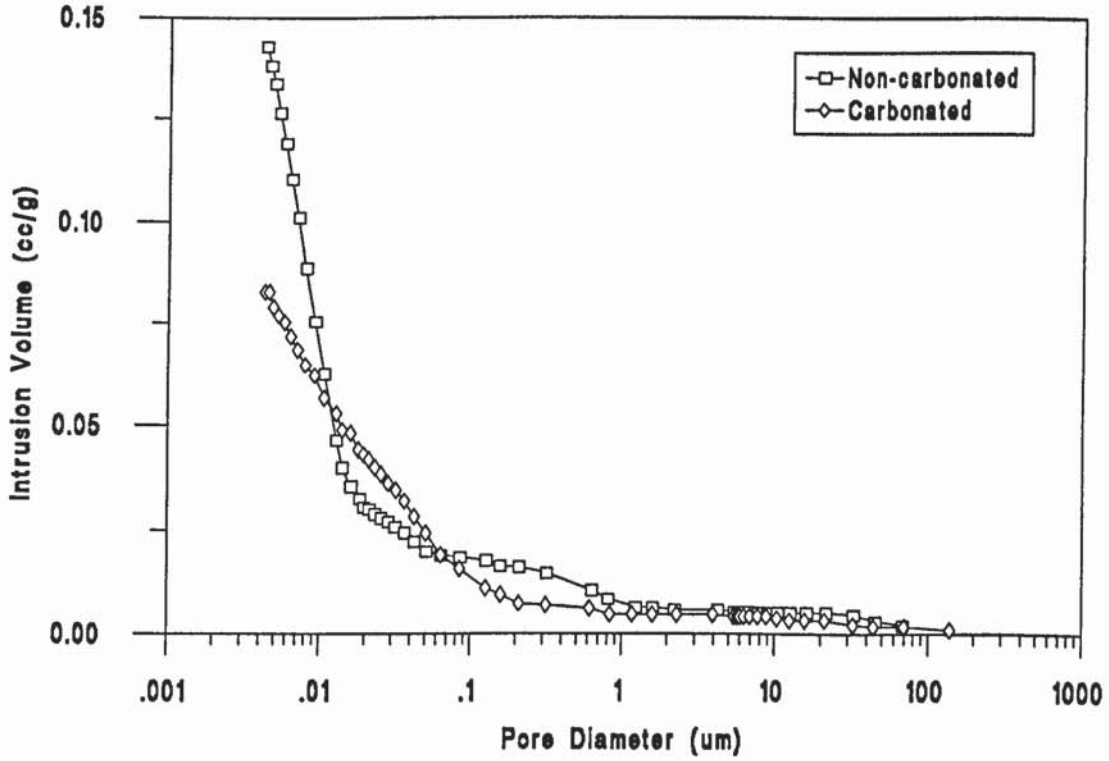


**Figure 6.15: Pore size distribution curves for slag pastes of 0.4 w/s ratio**

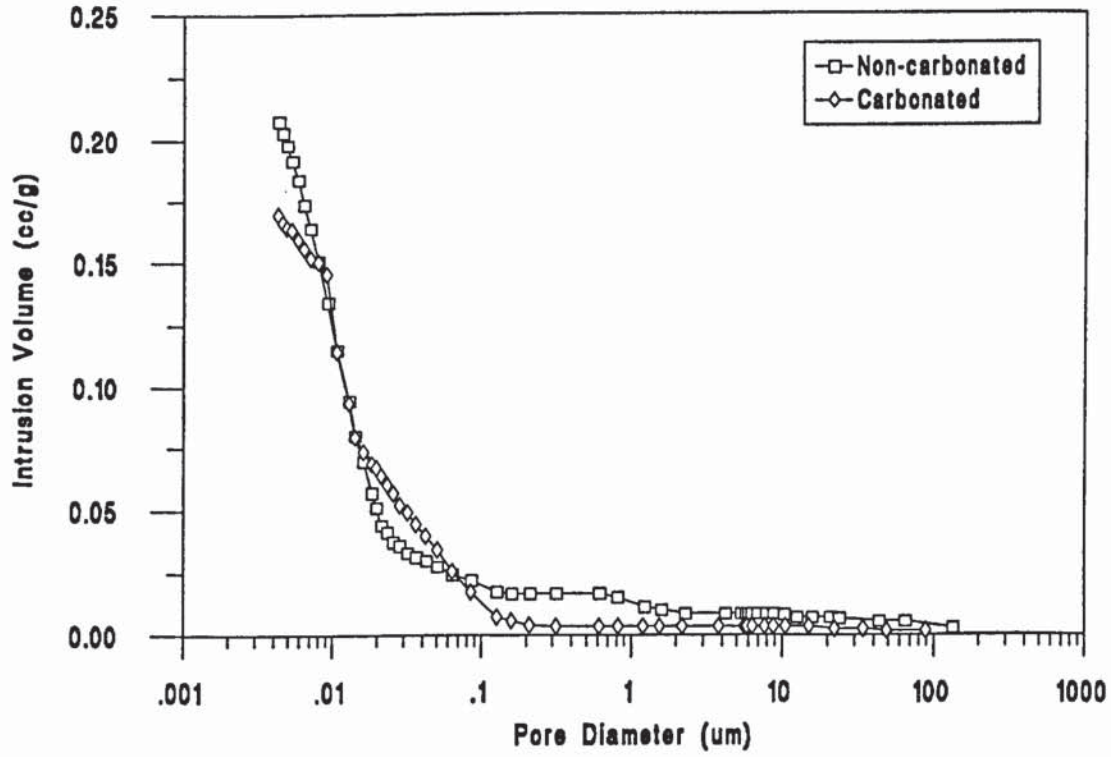


**Figure 6.16: Pore size distribution curves for slag pastes of 0.5 w/s ratio**

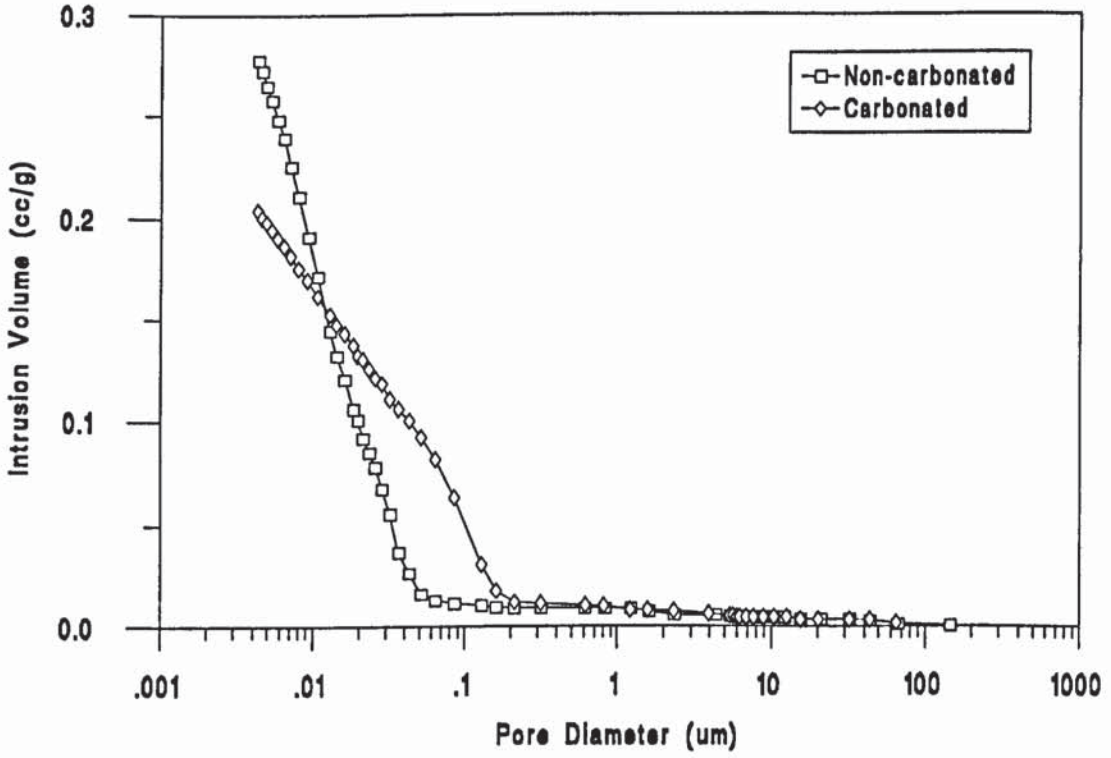


**Figure 6.17: Pore size distribution curves for slag pastes of 0.6 w/s ratio**

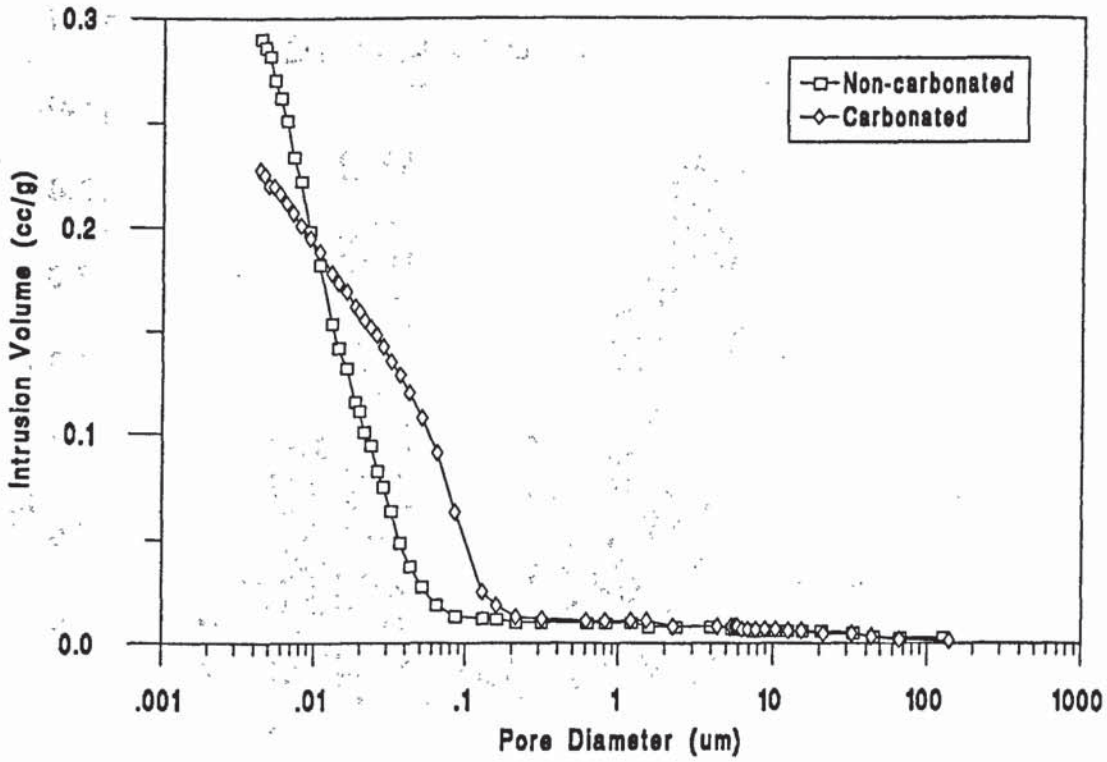


**Figure 6.18: Pore size distribution curves for slag pastes of 0.7 w/s ratio**

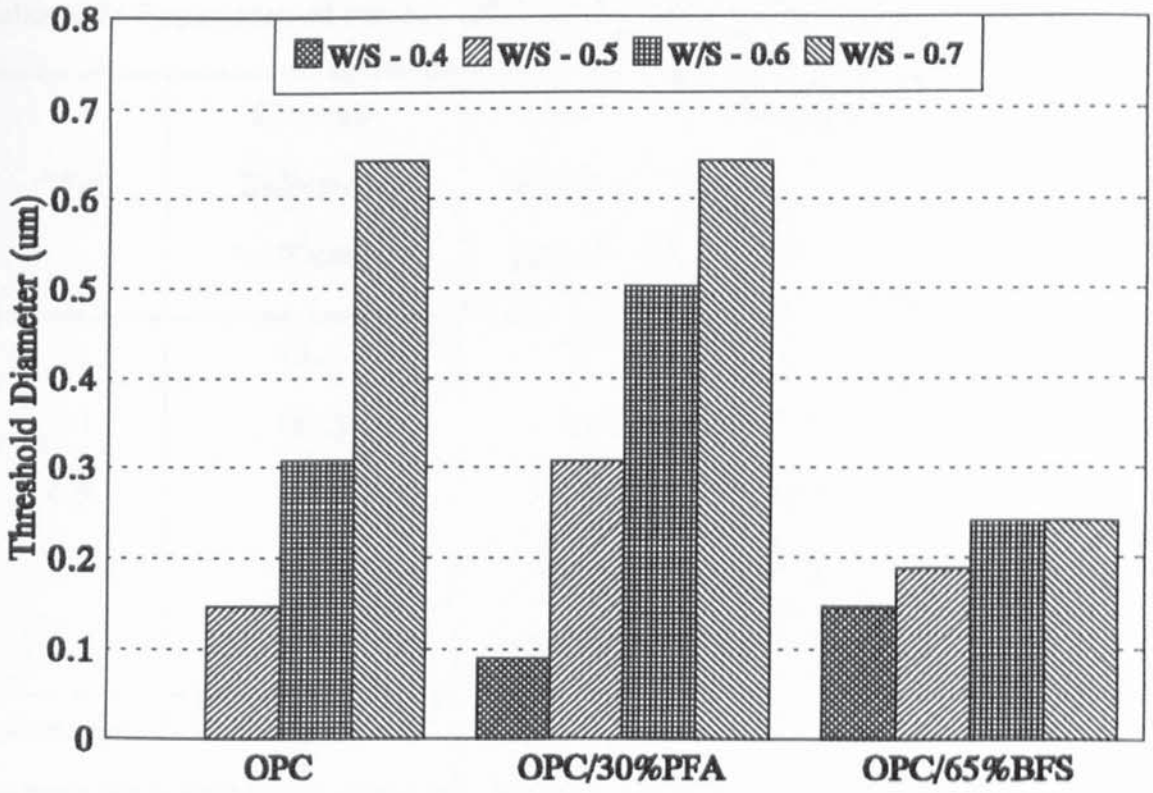


Figure 6.19: Threshold diameters for carbonated cement pastes

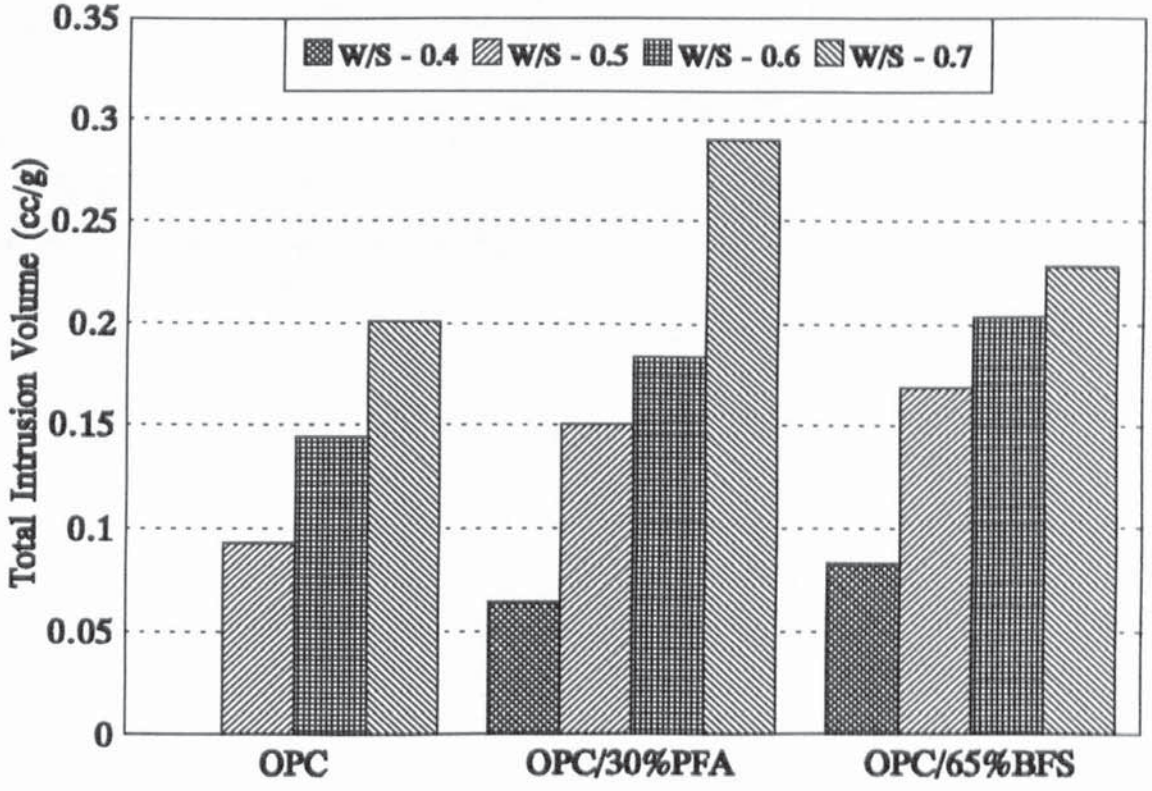


Figure 6.20: Total intrusion volumes for carbonated cement pastes

**Table 6.2: Experimental results obtained for fully carbonated OPC pastes.**

| W/C | Chloride Diffusivity ($x10^{-8}cm^2/s$) | Bulk Density ($g/cm^3$) | Capillary Porosity (%) | Total Porosity (%) |
|---|---|---|---|---|
| 0.5 | 16.48 | 2.125 | 12.38 | 32.80 |
| | 15.29 | 2.130 | 12.09 | 33.05 |
| | 14.39 | 2.131 | 11.80 | 32.83 |
| | 15.80 | 2.125 | 11.93 | 32.68 |
| | 15.93 | 2.125 | 12.28 | 33.06 |
| **Average** | 15.58 | 2.127 | 12.10 | 32.88 |
| 0.6 | 53.80 | 2.007 | 19.30 | 39.63 |
| | 51.01 | 2.010 | 18.72 | 39.71 |
| | 47.96 | 2.010 | 19.55 | 39.63 |
| | 44.84 | 2.009 | 19.72 | 39.54 |
| | 46.06 | 2.020 | 18.38 | 38.93 |
| **Average** | 48.73 | 2.011 | 19.13 | 39.49 |
| 0.7 | 102.23 | 1.931 | 26.03 | 45.19 |
| | 108.93 | 1.916 | 27.26 | 45.75 |
| | 108.31 | 1.926 | 25.88 | 45.17 |
| | 104.93 | 1.917 | 27.40 | 46.01 |
| | 107.74 | 1.924 | 26.27 | 45.49 |
| **Average** | 106.23 | 1.924 | 26.57 | 45.52 |

**Table 6.3: Experimental results for fully carbonated OPC/30%PFA pastes.**

| W/S | Chloride Diffusivity ($x10^{-8}cm^2/s$) | Bulk Density ($g/cm^3$) | Capillary Porosity (%) | Total Porosity (%) |
|---|---|---|---|---|
| 0.4 | 26.55 | 2.096 | 7.71 | 32.77 |
| | 24.31 | 2.104 | 6.91 | 32.06 |
| | 25.37 | 2.096 | 7.58 | 32.60 |
| | 26.04 | 2.094 | 7.31 | 32.48 |
| | 28.05 | 2.090 | 7.96 | 32.90 |
| **Average** | 26.06 | 2.096 | 7.49 | 32.56 |
| 0.5 | 56.80 | 2.014 | 13.70 | 39.08 |
| | 57.15 | 2.016 | 14.88 | 38.81 |
| | 61.84 | 2.017 | 14.24 | 38.67 |
| | 56.30 | 2.020 | 13.58 | 38.88 |
| | 58.08 | 2.020 | 14.07 | 38.79 |
| **Average** | 58.03 | 2.017 | 14.09 | 38.85 |
| 0.6 | 89.87 | 1.895 | 20.54 | 46.19 |
| | 80.51 | 1.894 | 21.18 | 46.45 |
| | 84.23 | 1.908 | 20.88 | 45.77 |
| | 81.42 | 1.892 | 20.40 | 46.60 |
| | 76.02 | 1.906 | 20.30 | 45.75 |
| **Average** | 82.41 | 1.899 | 20.66 | 46.15 |
| 0.7 | 165.27 | 1.779 | 32.75 | 52.35 |
| | 169.10 | 1.785 | 32.67 | 52.29 |
| | 184.69 | 1.767 | 33.77 | 53.16 |
| | 160.94 | 1.775 | 33.29 | 52.93 |
| | 156.15 | 1.775 | 33.62 | 53.12 |
| **Average** | 167.23 | 1.776 | 33.22 | 52.77 |

**Table 6.4: Experimental results for fully carbonated OPC/65%BFS pastes.**

| W/S | Chloride Diffusivity ($x10^{-8}cm^2/s$) | Bulk Density ($g/cm^3$) | Capillary Porosity (%) | Total Porosity (%) |
|---|---|---|---|---|
| 0.4 | 33.96 | 2.116 | 8.29 | 32.80 |
| | 36.45 | 2.117 | 7.98 | 32.75 |
| | 38.68 | 2.120 | 8.04 | 32.57 |
| | 36.62 | 2.124 | 7.88 | 32.44 |
| | 35.95 | 2.118 | 8.84 | 32.61 |
| **Average** | 36.33 | 2.119 | 8.21 | 32.63 |
| 0.5 | 59.84 | 1.986 | 14.40 | 39.74 |
| | 64.72 | 1.980 | 14.38 | 40.61 |
| | 56.41 | 1.981 | 15.02 | 40.36 |
| | 62.76 | 1.989 | 13.93 | 40.21 |
| | 61.53 | 1.986 | 14.06 | 39.86 |
| **Average** | 61.05 | 1.984 | 14.36 | 40.16 |
| 0.6 | 110.21 | 1.896 | 22.21 | 46.00 |
| | 119.92 | 1.889 | 24.02 | 46.64 |
| | 119.68 | 1.896 | 23.38 | 46.27 |
| | 104.76 | 1.878 | 22.70 | 46.58 |
| | 118.00 | 1.883 | 22.90 | 46.93 |
| **Average** | 114.51 | 1.888 | 23.04 | 46.48 |
| 0.7 | 160.74 | 1.814 | 30.88 | 50.52 |
| | 159.85 | 1.814 | 30.30 | 50.29 |
| | 180.06 | 1.805 | 31.38 | 50.88 |
| | 171.53 | 1.818 | 30.44 | 50.42 |
| | 159.29 | 1.833 | 29.17 | 49.38 |
| **Average** | 166.29 | 1.817 | 30.38 | 50.30 |

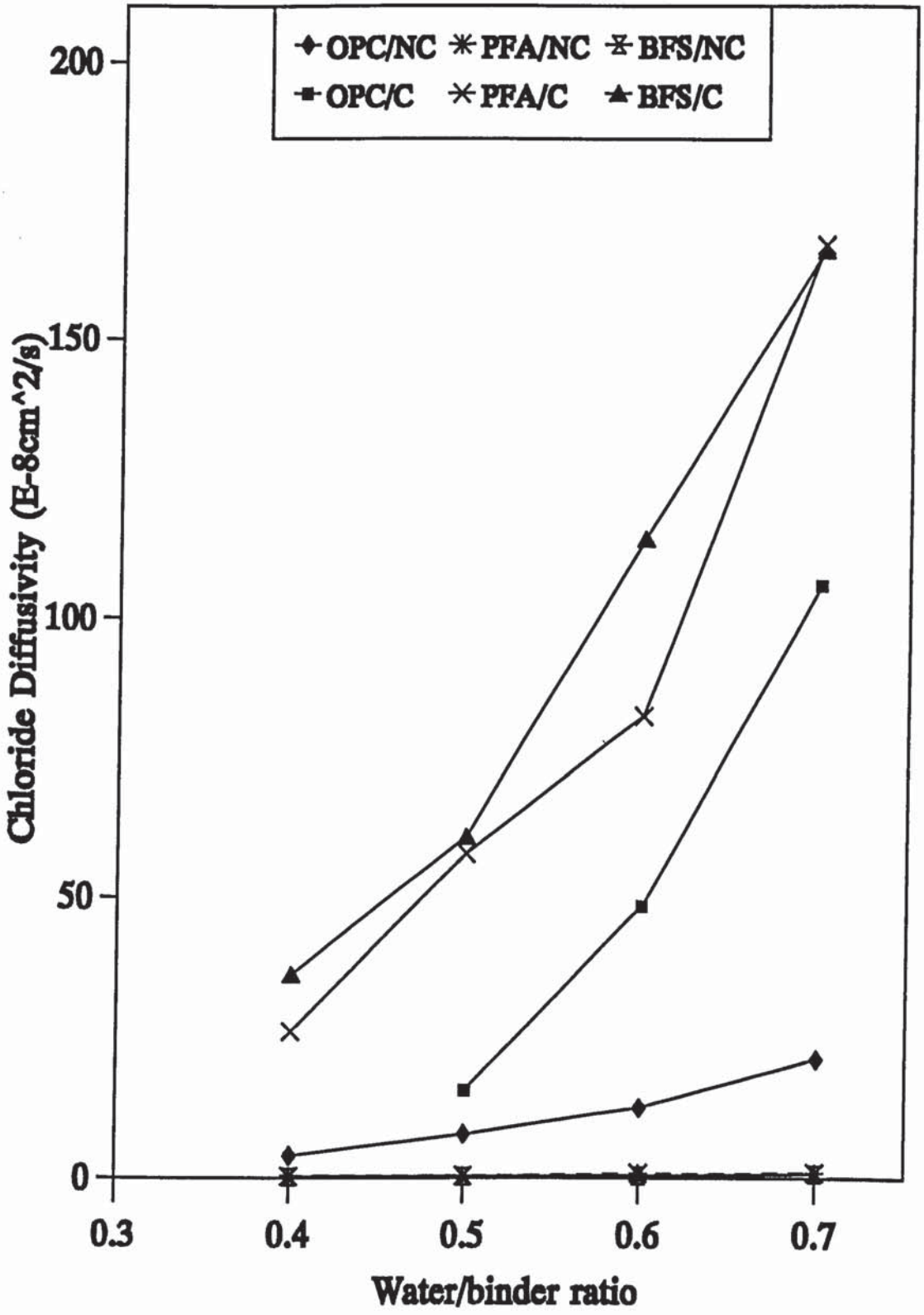


**Figure 6.21: Plot of chloride diffusion coefficient versus w/s ratio**

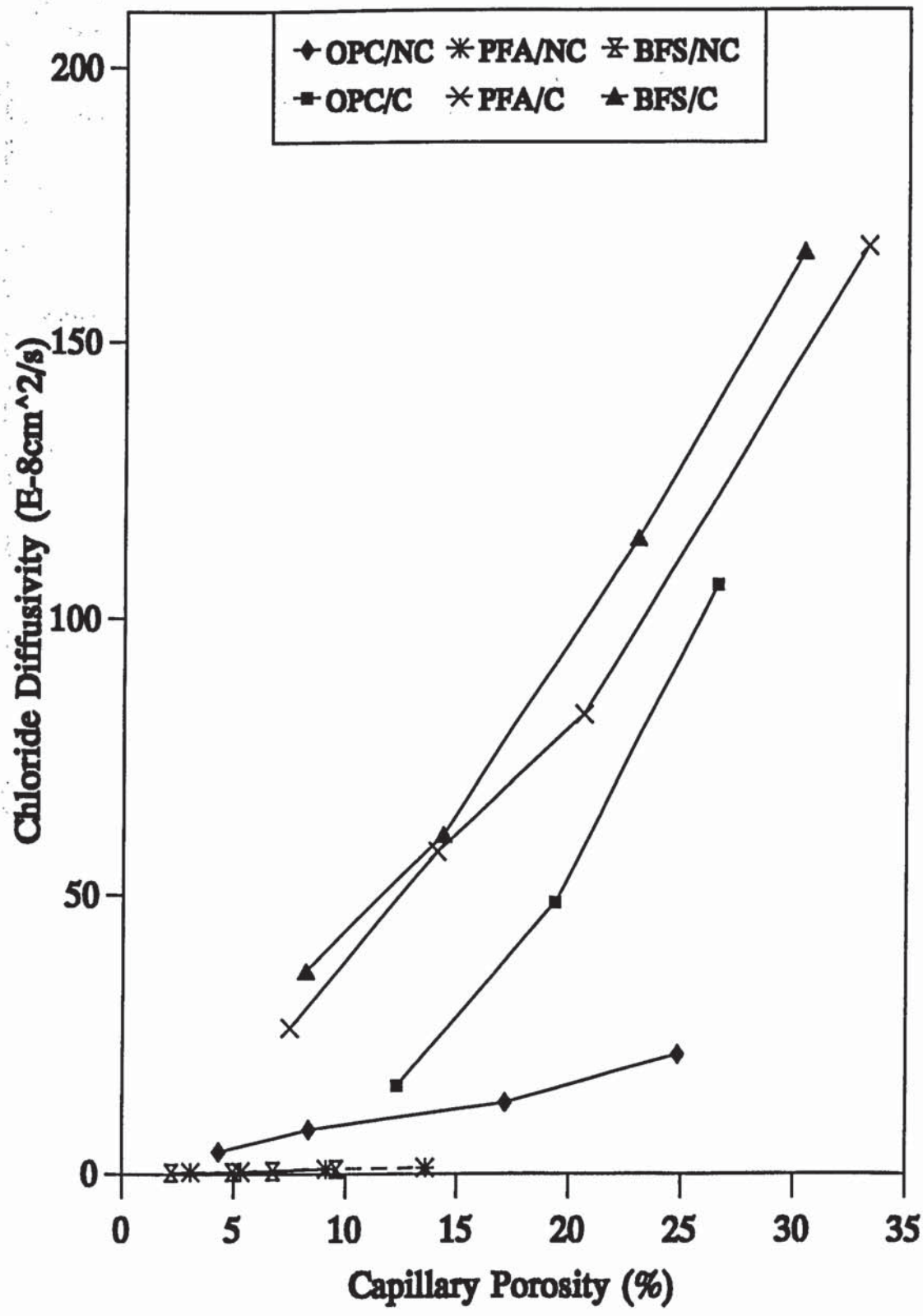


**Figure 6.22: Plot of chloride diffusion coefficient against capillary porosity**

**Table 6.5: Oxygen diffusion coefficients for fully carbonated cement pastes.**

| Sample | Oxygen Diffusivity ($x10^{-8}cm^2/s$) | Bulk Density ($g/cm^3$) | Capillary Porosity (%) | Total Porosity (%) |
|---|---|---|---|---|
| OPC5C | 19.71 | 2.125 | 12.49 | 32.53 |
| | 20.28 | 2.133 | 12.08 | 32.05 |
| | 18.87 | 2.129 | 12.09 | 32.24 |
| | 19.13 | 2.125 | 12.43 | 32.77 |
| | 16.44 | 2.128 | 12.46 | 32.35 |
| **Average** | 18.89 | 2.128 | 12.31 | 32.39 |
| OPC6C | 63.33 | 1.999 | 18.73 | 39.67 |
| | 55.66 | 2.004 | 18.07 | 39.18 |
| | 54.24 | 2.021 | 17.27 | 38.47 |
| | 58.71 | 2.005 | 18.66 | 39.41 |
| | 62.11 | 1.991 | 19.17 | 40.25 |
| **Average** | 58.81 | 2.004 | 18.38 | 39.40 |
| PFA5C | 25.63 | 2.013 | 13.70 | 39.02 |
| | 23.66 | 2.014 | 14.88 | 39.25 |
| | 25.10 | 2.017 | 14.24 | 38.90 |
| | 22.75 | 2.017 | 13.58 | 38.84 |
| | 24.55 | 2.017 | 14.07 | 38.96 |
| **Average** | 24.34 | 2.016 | 14.09 | 39.00 |
| PFA6C | 79.57 | 1.894 | 20.54 | 45.35 |
| | 75.69 | 1.884 | 21.18 | 45.98 |
| | 86.68 | 1.889 | 20.88 | 45.76 |
| | 76.48 | 1.889 | 20.40 | 45.62 |
| | 86.68 | 1.893 | 20.30 | 45.23 |
| **Average** | 81.02 | 1.890 | 20.66 | 45.59 |

**Table 6.5: Continued**

| Sample | Oxygen Diffusivity ($x10^{-8}cm^2/s$) | Bulk Density ($g/cm^3$) | Capillary Porosity (%) | Total Porosity (%) |
|---|---|---|---|---|
| BFS5C | 26.88 | 1.989 | 13.93 | 40.21 |
| | 27.65 | 1.986 | 14.06 | 39.86 |
| | 28.11 | 1.986 | 14.40 | 39.74 |
| | 35.39 | 1.980 | 15.02 | 40.36 |
| | 31.17 | 1.981 | 14.38 | 40.61 |
| **Average** | 29.84 | 1.984 | 14.36 | 40.16 |
| BFS6C | 127.96 | 1.878 | 24.02 | 46.17 |
| | 111.89 | 1.889 | 22.70 | 45.86 |
| | 119.32 | 1.880 | 23.38 | 46.20 |
| | 120.00 | 1.892 | 22.90 | 45.66 |
| | 113.98 | 1.899 | 22.21 | 45.09 |
| **Average** | 118.63 | 1.888 | 23.04 | 45.80 |

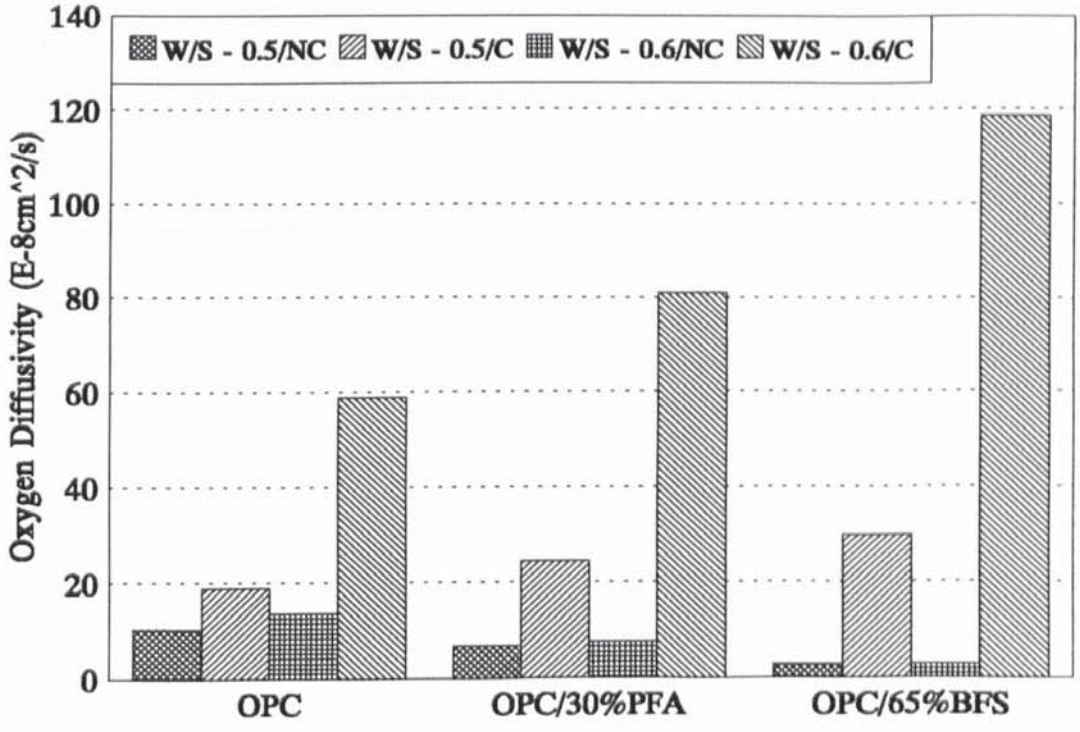


**Figure 6.23: Oxygen diffusion coefficients for hardened cement pastes**

**Table 6.6: Ratio of chloride diffusion coefficients for carbonated and non-carbonated cement pastes.**

| Sample | Chloride Diffusion Coefficient ( $x10^{-8}cm^2/s$ ) | | $(D_{cl/C})/(D_{cl/NC})$ |
|---|---|---|---|
| | Carbonated ($D_{cl/C}$) | Non-carbonated ($D_{cl/NC}$) | |
| OPC5 | 15.58 | 7.80 | 1.997 |
| OPC6 | 48.73 | 12.60 | 3.867 |
| OPC7 | 106.23 | 21.46 | 4.950 |
| PFA4 | 26.06 | 0.39 | 66.82 |
| PFA5 | 58.03 | 0.43 | 134.95 |
| PFA6 | 82.41 | 0.90 | 91.57 |
| PFA7 | 167.23 | 1.03 | 162.36 |
| BFS4 | 36.33 | 0.26 | 139.73 |
| BFS5 | 61.05 | 0.33 | 185.00 |
| BFS6 | 114.51 | 0.51 | 224.53 |
| BFS7 | 166.29 | 0.85 | 192.64 |

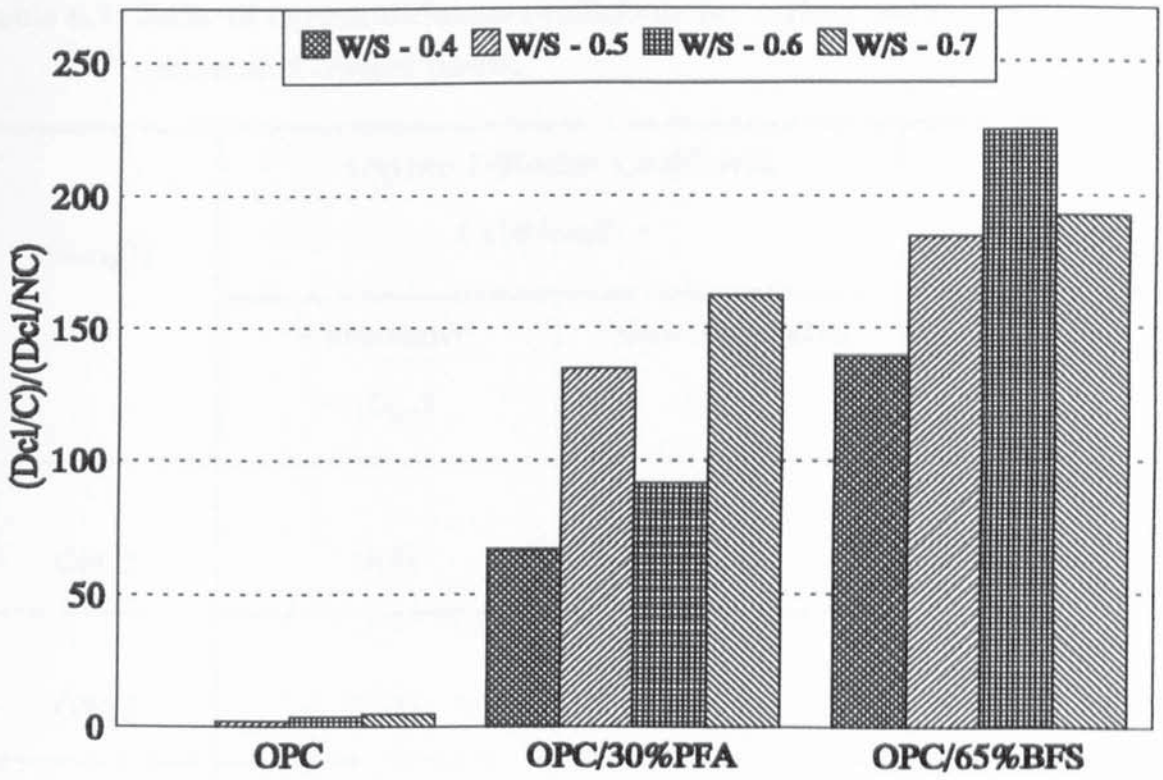


Figure 6.24: Ratio of chloride diffusion coefficients for carbonated and non-carbonated cement pastes

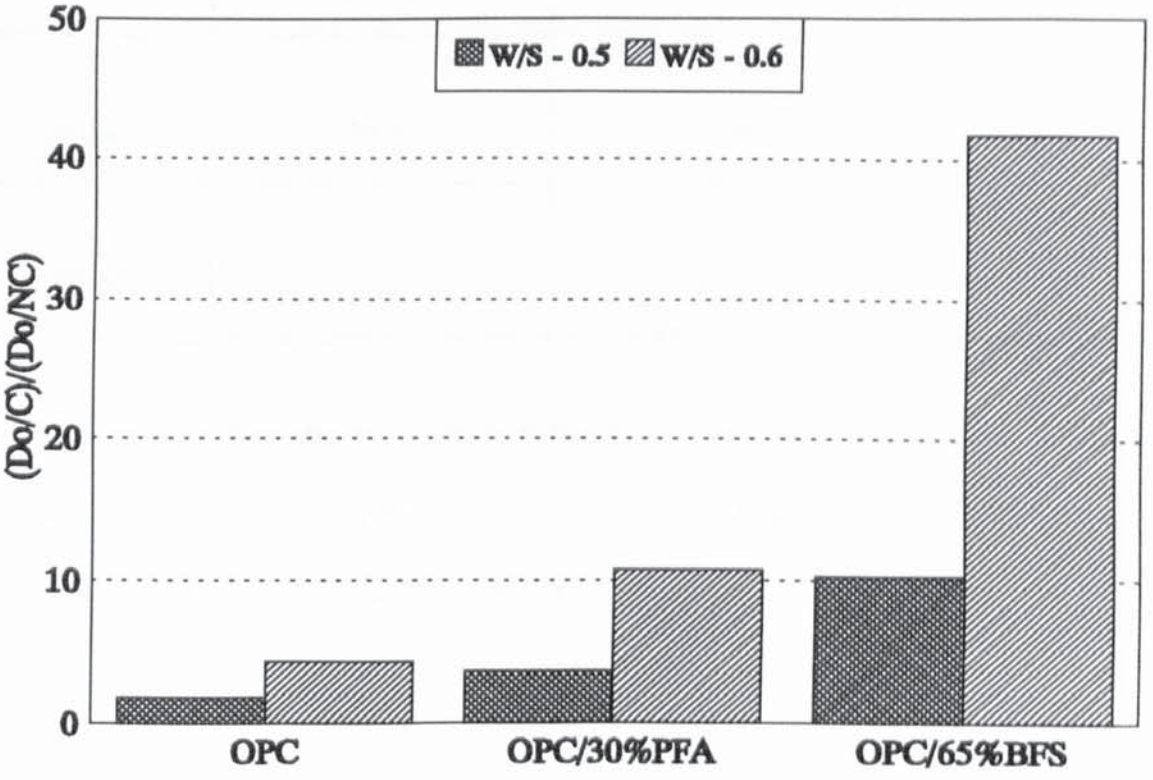


Figure 6.25: Ratio of oxygen diffusion coefficients for carbonated and non-carbonated cement pastes

**Table 6.7: Ratio of oxygen diffusion coefficients for carbonated and non-carbonated cement pastes.**

| Sample | Oxygen Diffusion Coefficient ( $x10^{-8}cm^2/s$ ) | | $(D_{o/C})/(D_{o/NC})$ |
|---|---|---|---|
| | Carbonated ($D_{o/C}$) | Non-carbonated ($D_{o/NC}$) | |
| OPC5 | 18.89 | 10.40 | 1.816 |
| OPC6 | 58.81 | 13.64 | 4.312 |
| PFA5 | 24.34 | 6.67 | 3.649 |
| PFA6 | 81.02 | 7.51 | 10.788 |
| BFS5 | 29.84 | 2.89 | 10.325* |
| BFS6 | 118.63 | 2.84 | 41.771* |

* values show a dramatic increase in ratio $(D_{o/C})/(D_{o/NC})$ for BFS pastes. This is probably due to the fact that the non-carbonated BFS pastes showed fairly constant values of oxygen diffusivity within the range of water/binder ratios investigated.

**Table 6.8: Ratio of oxygen to chloride diffusion coefficients for fully carbonated cement pastes.**

| Sample | Oxygen Diffusivity ( $D_o$ ) ( $x10^{-8}cm^2/s$ ) | Chloride Diffusivity ( $D_{cl}$ ) ( $x10^{-8}cm^2/s$ ) | $D_o/D_{cl}$ |
|---|---|---|---|
| OPC5C | 18.89 | 15.58 | 1.212 |
| OPC6C | 58.81 | 48.73 | 1.207 |
| PFA5C | 24.34 | 58.03 | 0.419 |
| PFA6C | 81.02 | 82.41 | 0.983 |
| BFS5C | 29.84 | 61.05 | 0.489 |
| BFS6C | 118.63 | 114.51 | 1.036 |

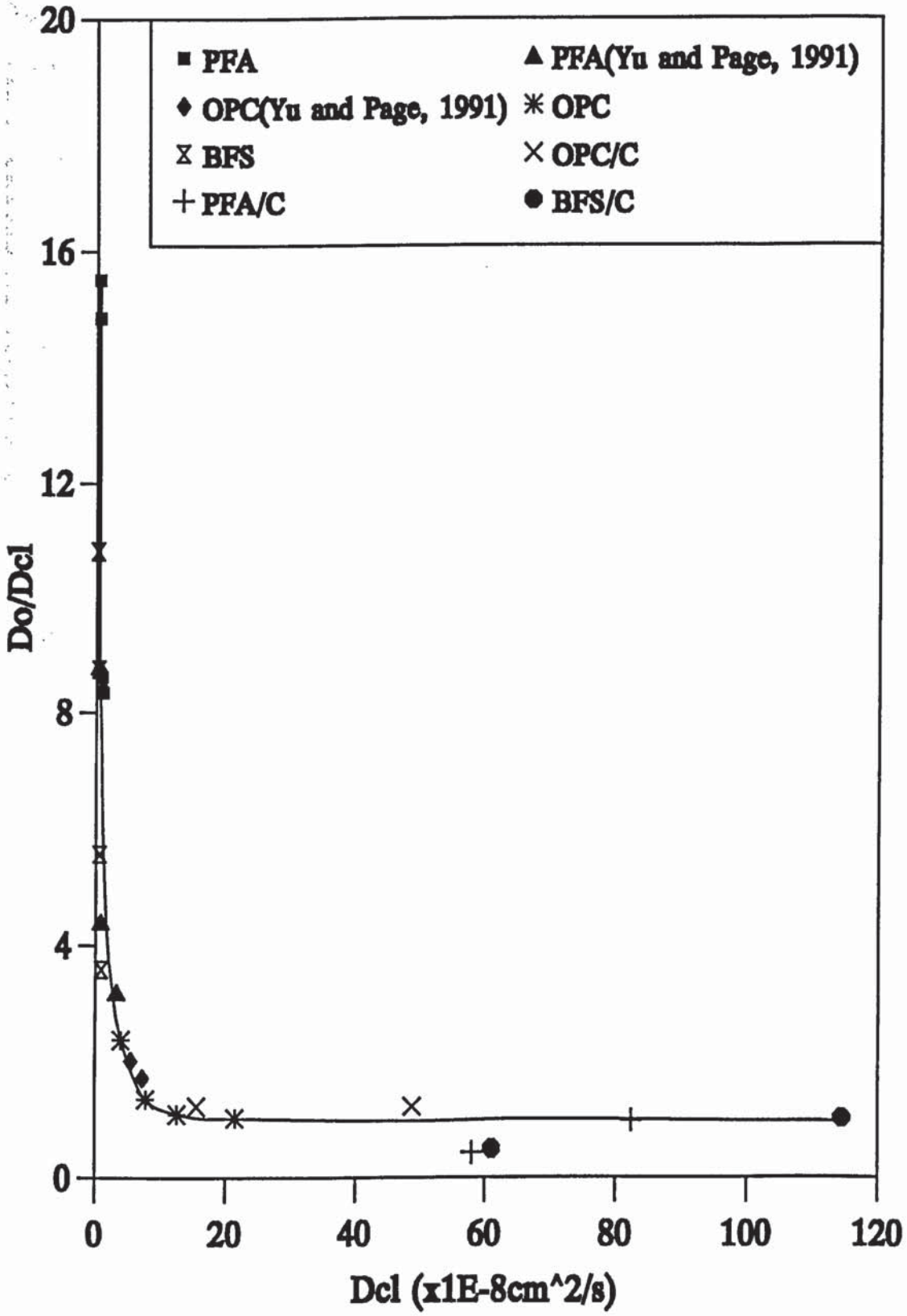


**Figure 6.26: Ratio of oxygen to chloride diffusion coefficients**

**Table 6.9: Porosity data for partially dried hardened cement pastes.**

| Sample | Bulk Density ($g/cm^3$) | Threshold Diameter (μm) | Total Pen. Volume ($cm^3/g$) | Capillary Porosity (%) | Total Porosity (%) |
|---|---|---|---|---|---|
| OPC5NCD | 1.875 | 0.147 | 0.168 | 13.42 | 48.09 |
| OPC6NCD | 1.788 | 0.215 | 0.230 | 20.00 | 53.25 |
| PFA5NCD | 1.840 | 0.075 | 0.209 | 6.50 | 49.87 |
| PFA6NCD | 1.765 | 0.090 | 0.254 | 10.06 | 56.13 |
| BFS5NCD | 1.862 | 0.055 | 0.210 | 6.16 | 49.68 |
| BFS6NCD | 1.784 | 0.115 | 0.272 | 10.50 | 54.95 |

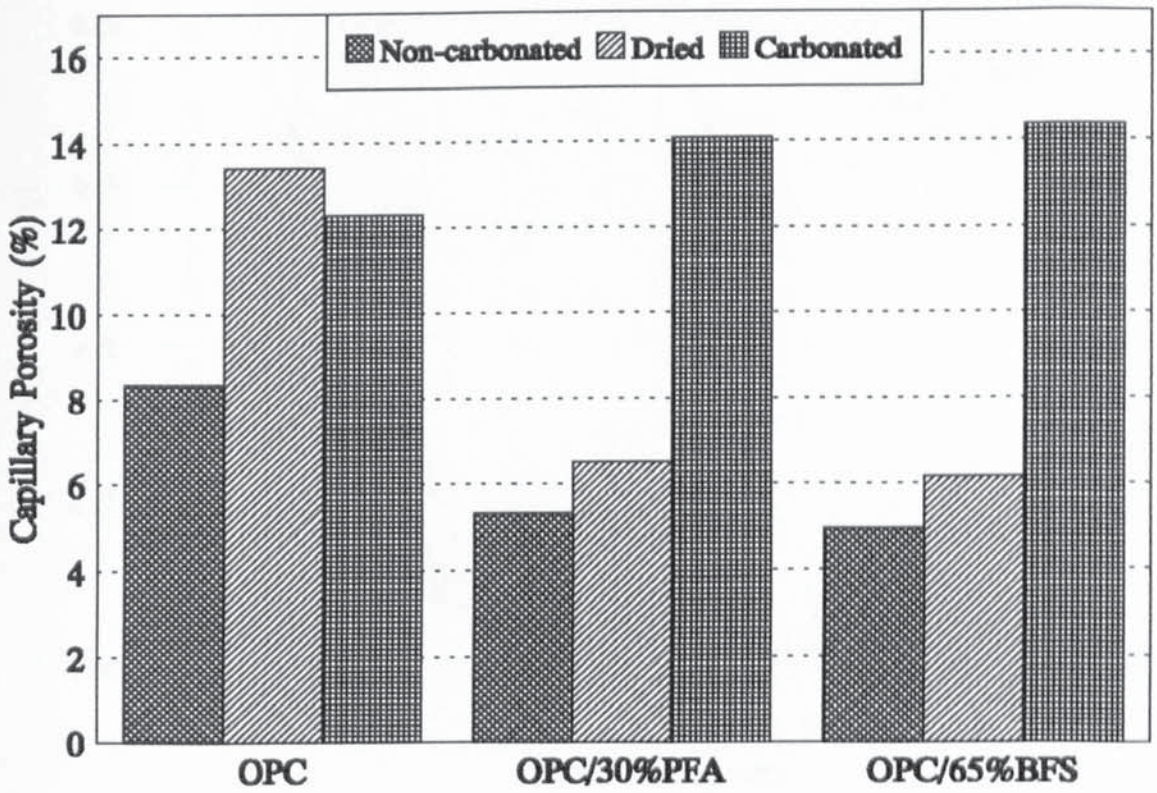


Figure 6.27: Capillary porosity for cement pastes of 0.5 w/s ratio

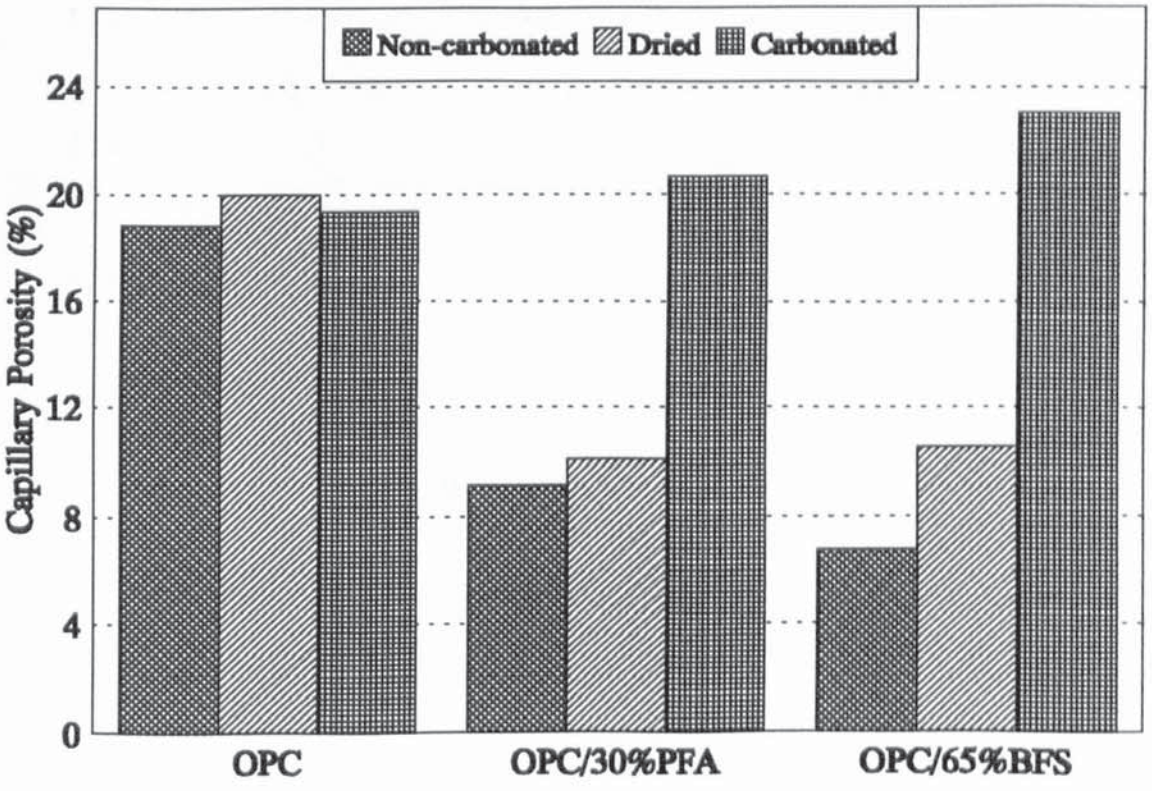


Figure 6.28: Capillary porosity for cement pastes of 0.6 w/s ratio

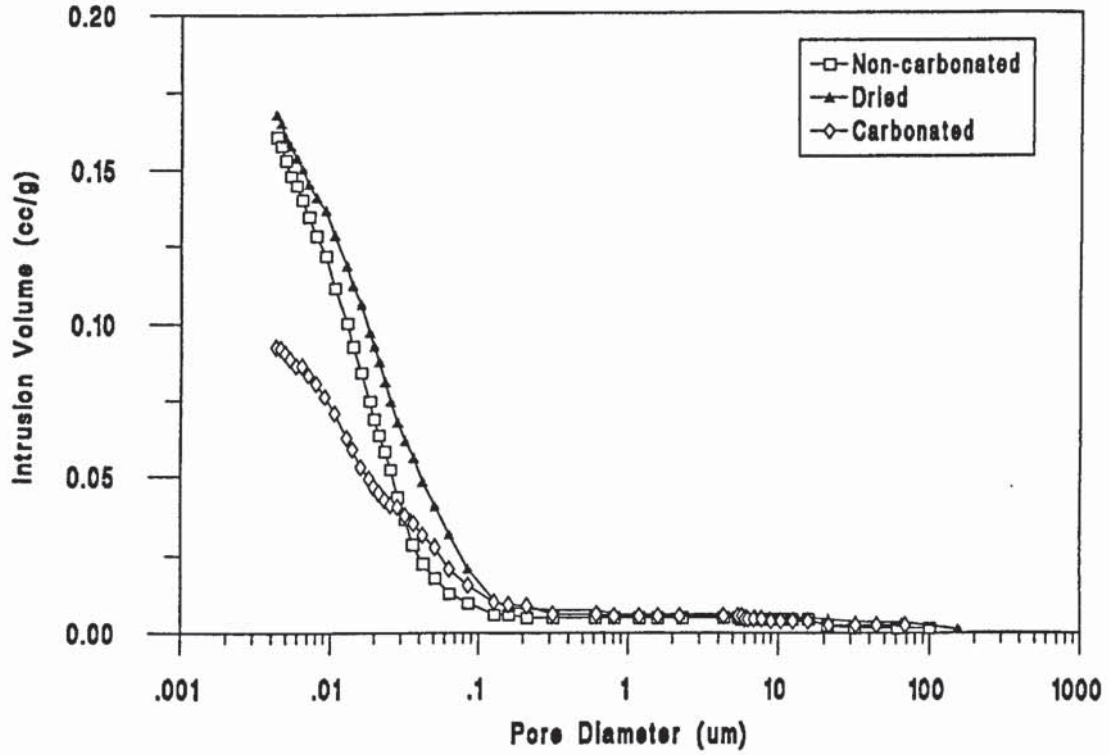


**Figure 6.29: Pore size distribution curves for OPC pastes of 0.5 w/c ratio**

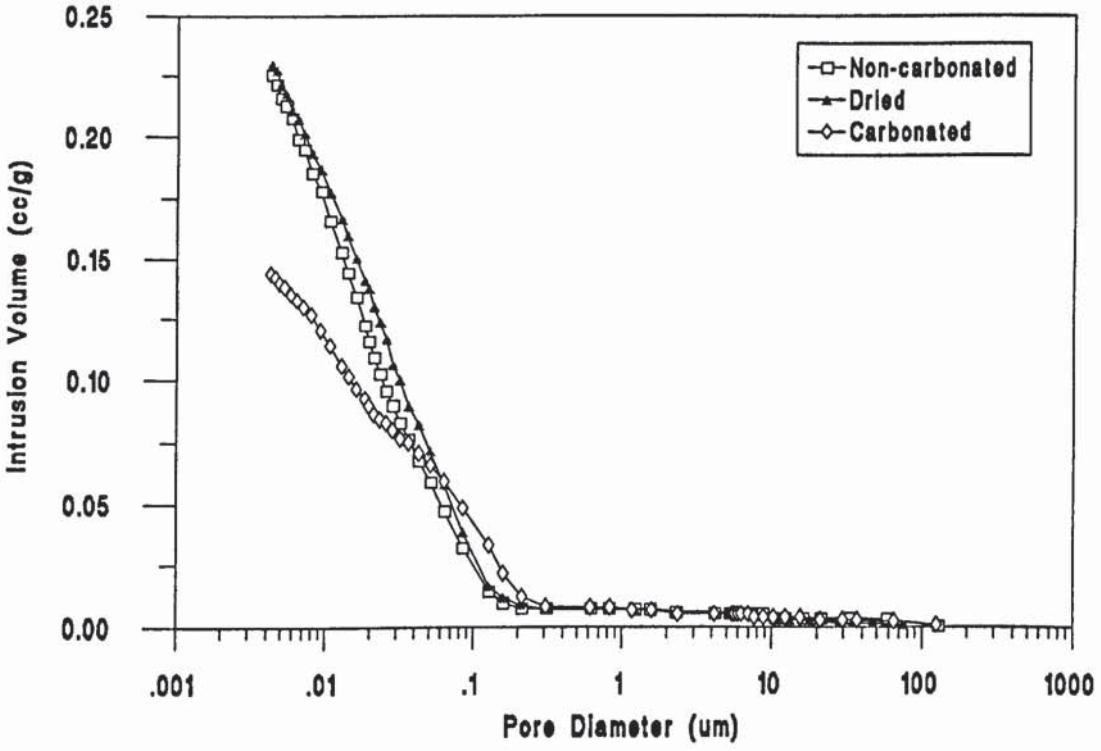


**Figure 6.30: Pore size distribution curves for OPC pastes of 0.6 w/c ratio**

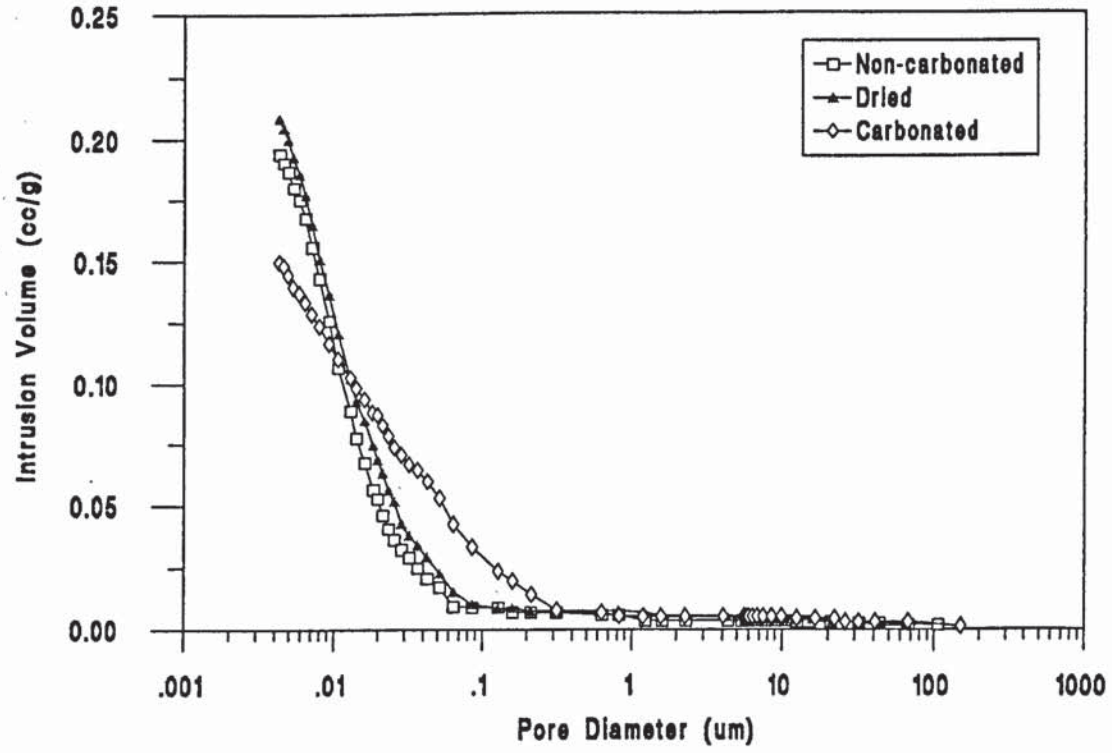


**Figure 6.31: Pore size distribution curves for fly ash pastes of 0.5 w/s ratio**

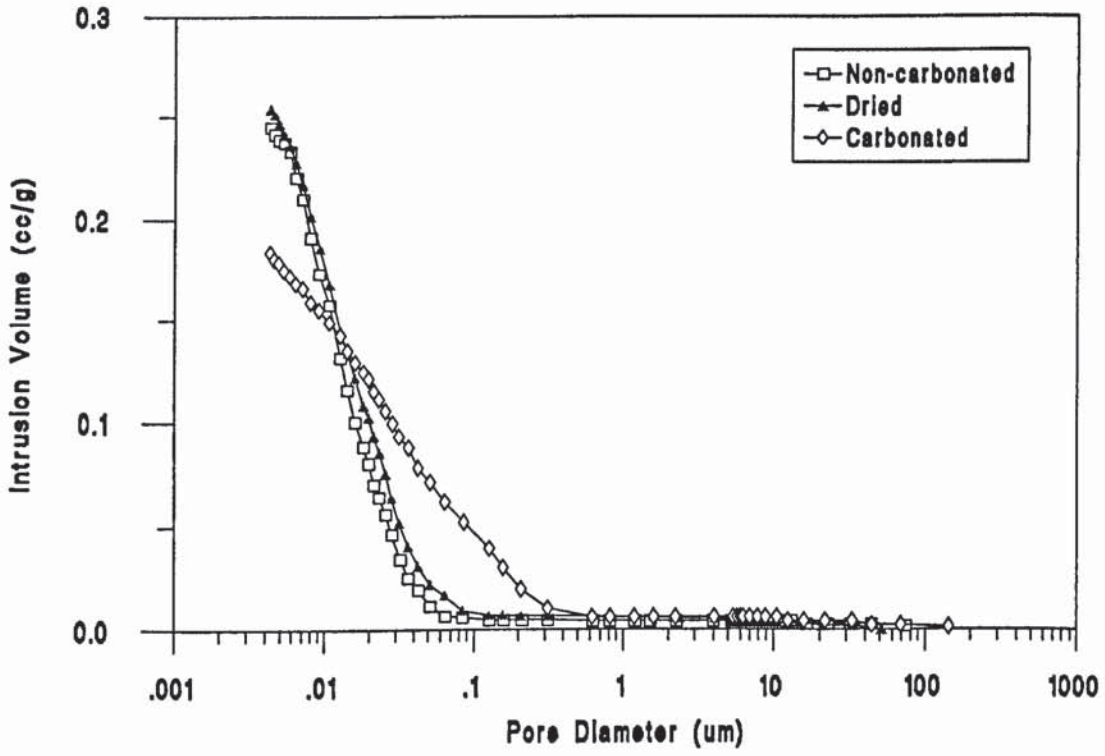


**Figure 6.32: Pore size distribution curves for fly ash pastes of 0.6 w/s ratio**

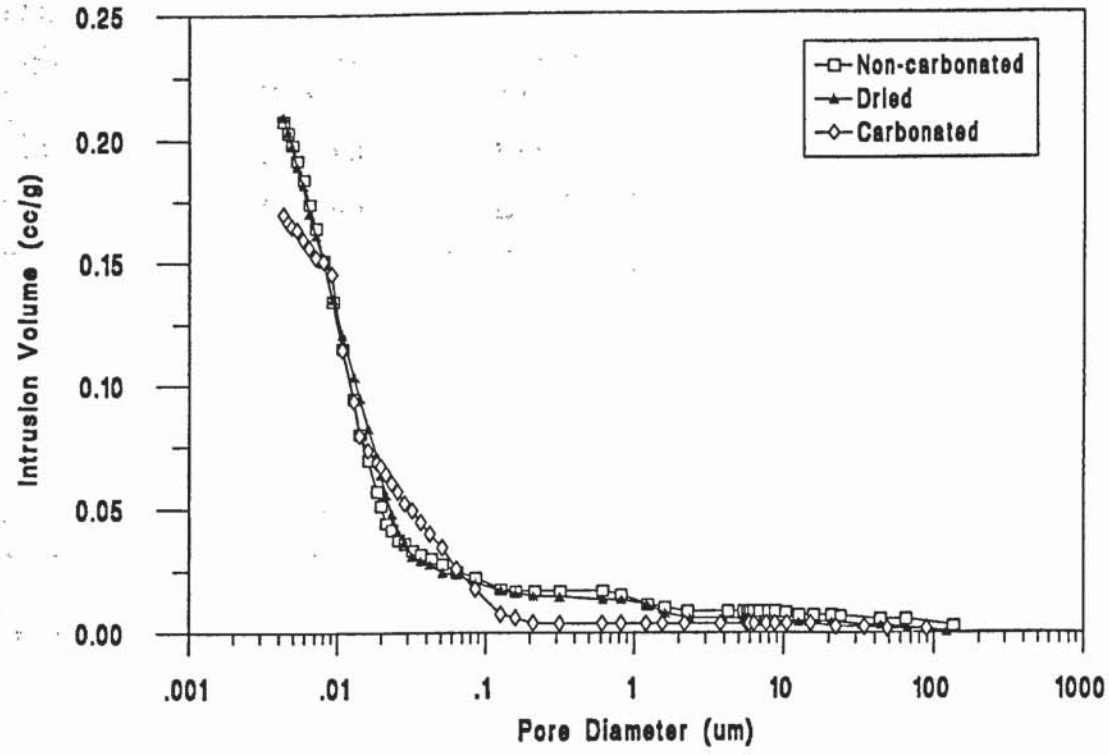


**Figure 6.33: Pore size distribution curves for slag pastes of 0.5 w/s ratio**

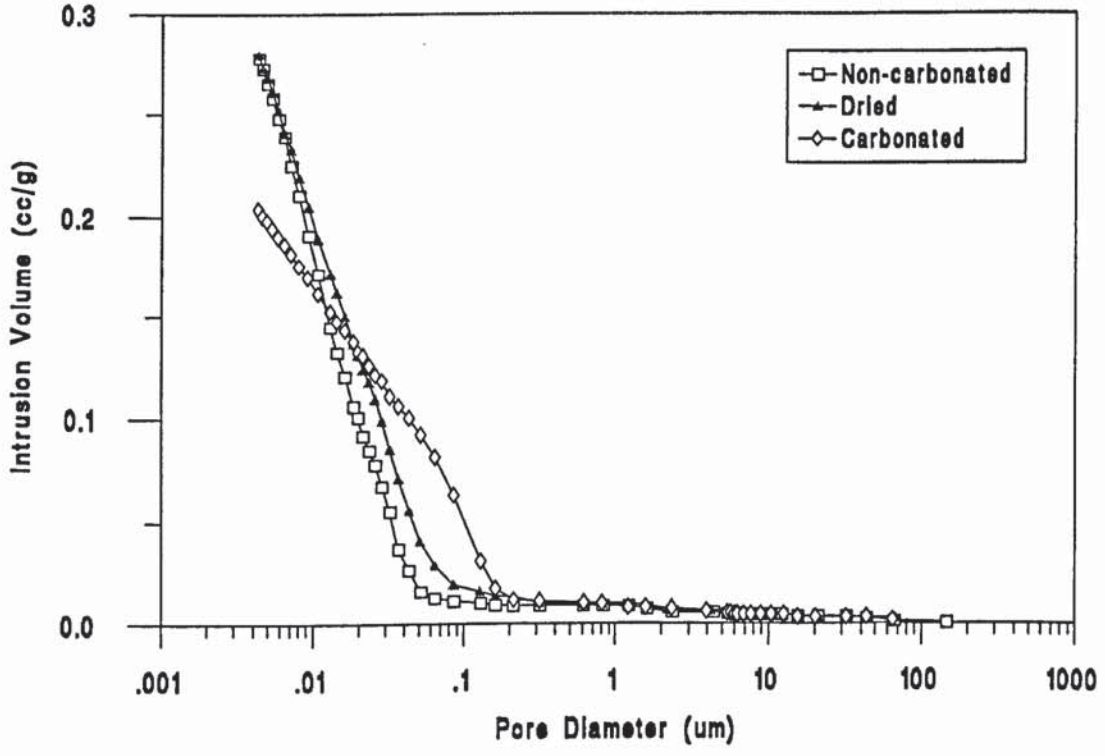


**Figure 6.34: Pore size distribution curves for slag pastes of 0.6 w/s ratio**

**Table 6.10: Experimental results obtained for partially dried cement pastes.**

| Sample | Chloride Diffusivity ($x10^{-8}cm^2/s$) | Bulk Density ($g/cm^3$) | Capillary Porosity (%) | Total Porosity (%) |
|---|---|---|---|---|
| OPC5NCD | 17.36 | 1.877 | 13.41 | 47.88 |
| | 21.39 | 1.867 | 13.67 | 48.35 |
| | 17.00 | 1.874 | 13.43 | 47.83 |
| | 16.74 | 1.876 | 13.46 | 48.19 |
| | 18.41 | 1.879 | 13.14 | 48.18 |
| **Average** | 18.18 | 1.875 | 13.42 | 48.09 |
| OPC6NCD | 27.00 | 1.791 | 19.87 | 53.10 |
| | 24.98 | 1.792 | 20.23 | 53.27 |
| | 28.57 | 1.784 | 19.76 | 52.98 |
| | 31.86 | 1.785 | 20.21 | 53.37 |
| | 29.93 | 1.790 | 19.91 | 53.52 |
| **Average** | 28.47 | 1.788 | 20.00 | 53.25 |
| PFA5NCD | 1.18 | 1.836 | 6.31 | 49.38 |
| | 1.14 | 1.839 | 6.49 | 49.70 |
| | 1.30 | 1.842 | 6.11 | 49.23 |
| | 1.54 | 1.843 | 6.82 | 50.08 |
| | 1.42 | 1.840 | 6.76 | 50.97 |
| **Average** | 1.32 | 1.840 | 6.50 | 49.87 |
| PFA6NCD | 4.46 | 1.760 | 9.91 | 55.96 |
| | 4.16 | 1.766 | 10.25 | 56.86 |
| | 5.20 | 1.760 | 10.69 | 56.07 |
| | 3.80 | 1.763 | 9.54 | 55.96 |
| | 3.82 | 1.778 | 9.93 | 55.78 |
| **Average** | 4.29 | 1.765 | 10.06 | 56.13 |

**Table 6.10: Continued**

| Sample | Chloride Diffusivity ($x10^{-8}cm^2/s$) | Bulk Density ($g/cm^3$) | Capillary Porosity (%) | Total Porosity (%) |
|---|---|---|---|---|
| BFS5NCD | 3.52 | 1.860 | 6.13 | 49.37 |
| | 3.94 | 1.865 | 6.27 | 49.51 |
| | 2.80 | 1.864 | 5.67 | 49.69 |
| | 3.47 | 1.862 | 6.28 | 49.91 |
| | 3.99 | 1.861 | 6.44 | 49.94 |
| **Average** | 3.54 | 1.862 | 6.16 | 49.68 |
| BFS6NCD | 8.84 | 1.793 | 10.06 | 54.39 |
| | 8.56 | 1.788 | 10.48 | 54.58 |
| | 10.37 | 1.792 | 10.00 | 54.43 |
| | 8.96 | 1.775 | 10.60 | 55.57 |
| | 9.56 | 1.772 | 11.35 | 55.80 |
| **Average** | 9.26 | 1.784 | 10.50 | 54.95 |

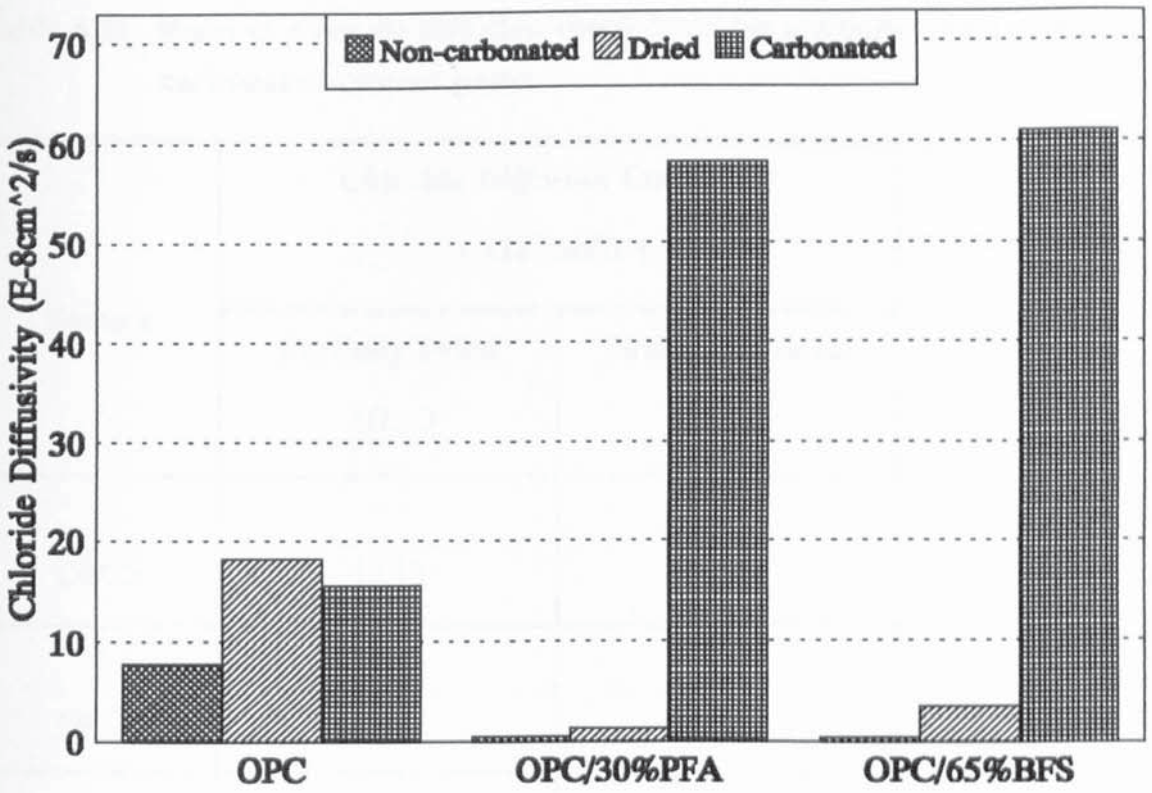


Figure 6.35: Chloride diffusion coefficients for cement pastes of 0.5 w/s ratio

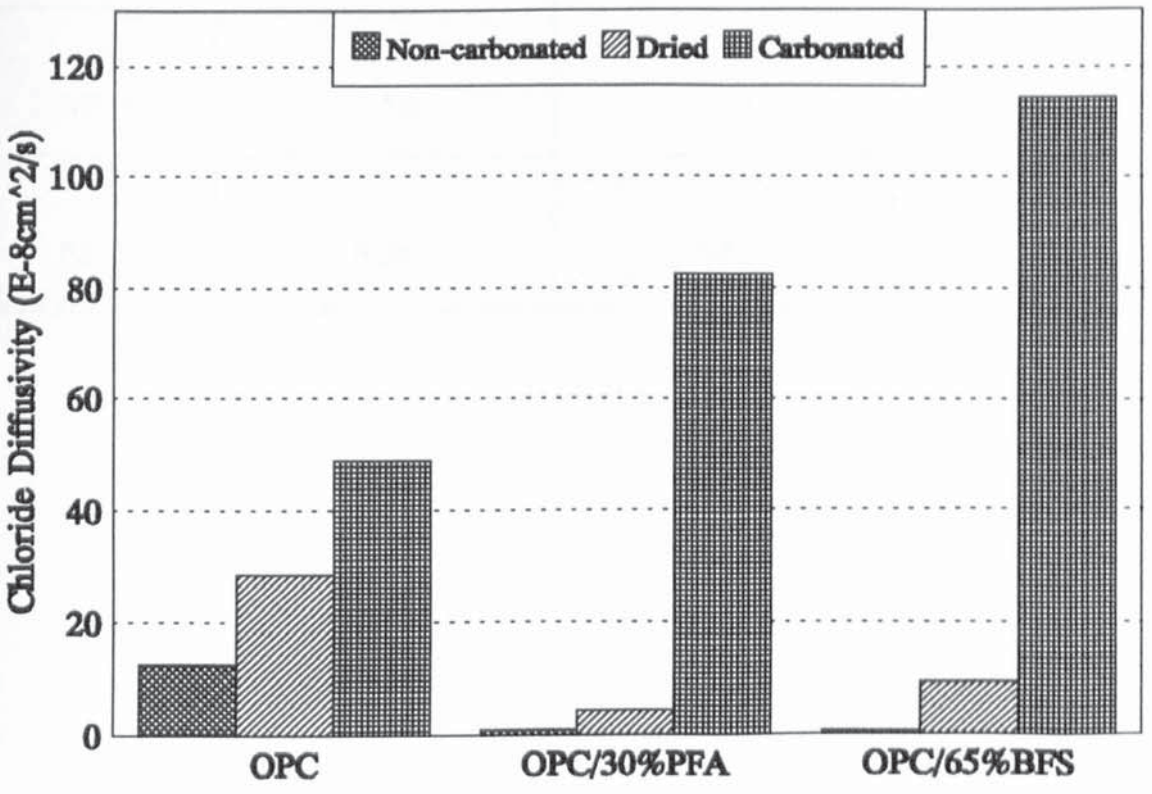


Figure 6.36: Chloride diffusion coefficients for cement pastes of 0.6 w/s ratio

**Table 6.11: Ratio of chloride diffusion coefficients for partially dried and non-carbonated cement pastes.**

| Sample | Chloride Diffusion Coefficient ( $x10^{-8}cm^2/s$ ) | | $(D_{cl/D})/(D_{cl/NC})$ |
|---|---|---|---|
| | Partially Dried ($D_{cl/D}$) | Non-carbonated ($D_{cl/NC}$) | |
| OPC5 | 18.18 | 7.80 | 2.331 |
| OPC6 | 28.47 | 12.60 | 2.260 |
| PFA5 | 1.32 | 0.43 | 3.070 |
| PFA6 | 4.29 | 0.90 | 4.767 |
| BFS5 | 3.54 | 0.33 | 10.727 |
| BFS6 | 9.26 | 0.51 | 18.157 |

# CHAPTER SEVEN

# EFFECT OF PASTE-AGGREGATE INTERFACIAL ZONE ON ION TRANSPORT IN CEMENT COMPOSITES

## 7.1 INTRODUCTION

Concrete may be modelled as consisting of aggregate particles dispersed in a matrix of hardened cement paste. The performance of plain concrete must therefore be governed by the properties of both the hardened cement paste and the aggregate, and by the nature of the interface between them. There is ample evidence to suggest that the structure of the cement matrix in the vicinity of the aggregate surface, is distinctly different from that in the bulk paste. However, the detailed structure of the interfacial zone varies, depending among other factors, on the nature of the cement, the type of aggregates, the presence of admixtures and curing conditions.

Unlike the bulk matrix, the microstructure of the interfacial zone is characterized by coarser crystals, less cement paste, more capillary pores, and preferred orientation of calcium hydroxide crystals. However, the extent to which this so-called "weak link" between cement paste and aggregates, affects fluid transport into concrete and other durability-related properties is not completely understood.

## 7.2 LITERATURE REVIEW

### 7.2.1 Microstructure of the Cement Paste-Aggregate Interfacial Zone

During the manufacture of mortar and concrete, the aggregate particles interact with the surrounding cement paste. As a result, the microstructure of the cement paste in the vicinity of the aggregate particles differs from the microstructure of the bulk matrix.

Farran (1956) was one of the first researchers to study the microstructure of the paste-aggregate interfacial zone. The author examined the nature of the bond between different types of minerals and portland cement paste at normal temperatures and found that the paste-calcite bond strength was higher than those of the rest of the minerals examined. He associated this effect with the "corrosion" of the calcite surfaces as a result of the dissolution of these surfaces. Buck and Dolch (1966) performed a similar study on a more elaborate scale and their observations supported Farran's conclusions. The results of these investigations indicate that at the interfacial zone between cement paste and calcareous aggregates, a kind of chemical reaction occurs in which $Ca(OH)_2$ is produced with a definite orientation towards the aggregate surface.

Using a SEM equipped with an energy dispersive x-ray analyzer (EDAX), Hadley (1972), and later Barnes *et al.* (1979, 1978) studied the micromorphology of the interfacial zone using glass and α-quartz granules as model "coarse aggregates". They reported the formation of a continuous film of cement hydrates consisting predominantly of $Ca(OH)_2$, intermixed with C-S-H and ettringite as a deposition on the glass and α-quartz aggregate surfaces. Initially, their method of study was criticised because the glass and α-quartz aggregates used were considered to be unrepresentive of conventionally used aggregates. However, since their report, evidence from a number of studies involving cement paste-aggregate interfaces in typical concrete systems (Detwiler *et al.*, 1988; Monteiro *et al.*, 1985; Grandet and Ollivier, 1980) have supported their interpretations.

The microstructure of the interfacial zone modelled by Barnes *et al.* (1979, 1978) has been presented in detail by Diamond (1987) as follows:

(i) In the immediate vicinity of the aggregate surface is a "duplex film" of $Ca(OH)_2$ overlayed by or occasionally intermixed with C-S-H. The side of the film in contact with the aggregate is a layer of crystalline calcium hydroxide, approximately 0.5 μm thick. Following this layer is a thin deposit of C-S-H gel,

in the form of short fibres, that extend into the cement paste. The total extent of the duplex film is approximately 1.0 μm.

(ii) Next to the "duplex film" is the "transition zone". This region is relatively larger, approximately 50 μm wide including the "duplex film". Generally, this zone contains a large number of hollow-shell hydration grains, and is enriched in larger $Ca(OH)_2$ crystals and ettringite.

Following the work of Hadley (1972) and Barnes *et al.* (1979, 1978), subsequent models of the microstructure of the interfacial zone have also been characterised by Zimbelmann (1978) and by Yuan and Guo (1988). All three models identify the interfacial zone as comprising two layers, the "duplex film" and the "transition zone". However, Zimbelmann described a third layer, the "intermediate layer", located between the two main layers. These microstructural features of the interfacial zone have also been observed by Struble (1988) and by Scrivener and co-workers (Scrivener *et al.*, 1988; Scrivener and Gartner, 1988; Scrivener and Pratt, 1986).

Recently, Garboczi and co-workers (Garboczi, 1993; Bentz *et al.*, 1992; Garboczi and Bentz, 1991) have used computer simulation to reproduce a digital-image-based model of the interfacial zone described in this section. The authors have shown that an algorithmic growth model, based on a dissolution/diffusion/reaction cycle, can simulate the microstructural developments of cement paste around non-reactive aggregates. The resulting microstructure semi-quantitatively reproduces many real interfacial zone features. Based on the context of the model, the authors have concluded that the main contributions to the interfacial zone in concrete are;

(a) the particle packing effect - random and inefficient packing of large size aggregates;

(b) one-sided growth effect - in the bulk of the paste, hydration products grow into any given area from all directions, but very near to an aggregate, growth occurs from the cement paste matrix side only. As a result, the volume in this side is filled

inefficiently;

(c) bleeding of cement paste near an aggregate surface.

On the average, researchers have shown the interfacial zone thickness to be typically in the region of 20-50 μm, as measured by SEM and 15-25 μm as measured by MIP and computer modelling. This implies that the measured thickness of the transition zone in mortars and concretes depends on the method of measurement used. Researchers (Ping *et al.*, 1991; Monteiro *et al.*, 1985) have pointed out that the thickness of the transition zone is larger for larger aggregates and is also a function of the size and shape of the sand particles. The surface effects originated by the sand particles interfere with those caused by the large aggregates and the intensity of this interference determines the final thickness of the interfacial zone.

### 7.2.2 Porosity of the Interfacial Zone

The microstructure of the interfacial zone, with its coarser and better crystallized hydrates, is expected to have a higher porosity than that of the bulk cement paste. However, opinions vary on the subject. Kayyali (1987) compared the porosity of neat cement pastes to that of pastes in mortars and concrete using MIP and concluded that the interfacial zone was lower in porosity.

Scrivener and co-workers (Scrivener *et al.*, 1988; Scrivener and Gartner, 1988; Scrivener and Pratt, 1986) developed a method for quantitatively characterising the paste-aggregate interfacial zone in cement composites. The authors used a combination of backscattered electron imaging and quantitative image analysis to study the microstructure of the interfacial zone in concrete. The information obtained has been shown to correlate with that obtained by other methods such as X-ray diffractometry and MIP. Some of their results are demonstrated in Figure 7.1 which shows that the amount of anhydrous cement grains is lowest in the vicinity of the aggregates, and increases into the bulk paste. This

figure also indicates that the porosity, is highest at the interface, and decreases with increasing distance into the paste.

It has been demonstrated (Larbi and Bijen, 1991) that the capillary and total porosities of pastes in mortars are higher than those of the corresponding neat cement pastes prepared without sand. The authors pointed out that the modification of the pore structure of cement paste in mortars was more pronounced with increasing volume fraction of sand.

More recently, Snyder and co-workers (Winslow *et al.*, 1994; Snyder *et al.*, 1992) have investigated the porosity of interfacial zones using computer simulation and MIP. Their studies confirmed the findings of previous researchers, that the microstructure of the interfacial zone is more porous than that of bulk paste. Using computer modelling, the authors pointed out that if a sufficient volume of aggregate particles is present, the interfacial zones may overlap and link together, percolating the system (Snyder *et al.*, 1992), as shown in Figure 7.2. Their computer model indicated that for an interfacial zone thickness of about 20 μm, interfacial zone percolation would occur in most typical construction mixes (Winslow *et al.*, 1994). The authors, however, suggested that ultimate effects of this interfacial zone percolation on transport properties and durability were uncertain. Mercury intrusion experiments indicated that the intrusion characteristics of mortars change dramatically at a critical sand content. However, oven drying of samples at 105°C prior to MIP, as adopted in their study, is thought to alter the original pore structure of the paste to a great extent (Moukwa and Aitcin, 1988).

### 7.2.3 Effect of Interfacial Zone on Transport Properties

The findings of previous studies on this subject have been contradictory, to say the least. Roy and co-workers (Malek and Roy, 1988; Wakely and Roy, 1982) reported that the paste-aggregate interfacial zone does not seem to play any major role in determining the permeability of concrete. However, studying the permeability of normal and lightweight

mortars, Nyame (1985) concluded that by increasing the aggregate volume, interfacial effects seem to increase the permeability. Young (1988) stated that the permeability coefficients for concrete are generally about 100 times higher than those for comparable pastes, while for mortars they are 3-10 times higher.

Recently, Larbi and Bijen (1991) investigated the role of the interfacial zone on the transport of fluids in mortars. The authors found out that fluid transport through the "mortar pastes" was comparatively faster than fluid transport through plain cement pastes of the same properties. However, they pointed out that the interfacial zone effect on fluid transport appears to be small relative to the increase in capillary porosity. The authors, therefore, suggested that the paste matrix is the continuous phase in concrete and is mainly responsible for the fluid transport processes in concretes.

This brief literature review has highlighted the microstructure of the paste-aggregate interfacial zone and the role it plays in fluid transport in concrete. The survey shows that in concrete, interfacial zones with distinct microstructural features exist between cement paste and aggregate particles. In general these interfaces contain more calcium hydroxide crystals than the bulk paste matrix. Moreover, the $Ca(OH)_2$ crystals exhibit a preferred orientation with regard to the surface of the aggregate.

While most of the investigations agree on the existence of a relatively high amount of $Ca(OH)_2$ at the interfacial zone, differences in opinion exist on the question of porosity and the resulting permeability. One group of researchers believe that the interface is comparatively higher in porosity than the bulk paste, while others are of contrary opinion.

It is therefore evident, that whereas a great deal of effort has been directed towards the characterization of the interfacial zone, most of the information obtained from these techniques has not been adequately translated to the bulk properties of concrete, such as

the compressive strength and permeability. It is a well established fact that the penetration of chloride ions into concrete is very detrimental as far as corrosion of reinforcement and the service life of the concrete are concerned. Nevertheless, there is very little evidence on the effect of this so-called "high porosity" interfacial zone on diffusion of chloride ions into cement composites. This chapter is therefore directed towards investigating the influence of the interfacial zone in mortars and concrete on the transport of chloride ions.

## 7.3 EXPERIMENTAL PROCEDURE

### 7.3.1 Preliminary Investigation on Volume Fractions

The packing density in a crystal is most conveniently determined by the atomic packing factor (Jastrzebski, 1987), which is defined as the ratio;

$$\frac{\textit{volume of atoms per unit cell}}{\textit{volume of unit cell}} \qquad \text{.....(7.1)}$$

Using Equation 7.1, it can be shown (Appendix A), that the packing factors of a face-centred cubic (FCC) structure and a body-centred cubic (BCC) structure are 74% and 68% respectively.

Preliminary work on the use of glass beads to manufacture mortars involved an initial investigation on the packing factor of the glass beads and the maximum volume fraction achievable. The actual packing factor of the beads was determined by employing Equation 7.1 and using three containers of different volumes as shown in Table 7.1. The calculated packing factors of the beads together with an average value of 65% are shown in Table 7.1. This packing factor of 65%, though smaller than that found by Jastrzebski for FCC and BCC structures, was used as a basis for determining the maximum volume fraction of beads for this investigation. A volume fraction of 60% was found to be the maximum volume concentration of beads at which there was sufficient paste matrix to form the mortar. However, further work revealed that at 60% concentration of beads, it was almost

impossible to get rid of the air bubbles without seriously altering the intended properties of the mortar, mainly through segregation. As such, the maximum volume fraction of 55% of glass beads was adopted and used for this study.

### 7.3.2 Sample Preparation and Experimental Set-up

The mortar specimens used for this investigation were prepared from OPC, glass beads and deionised water. A constant w/c ratio of 0.4 was maintained for all the mixes investigated while the volume fraction or concentration of the beads varied from about 14% to 55%. For each mix, the materials were proportioned by mass, mixed by hand, and then casted and cured as described in Section 2.2 for plain cement pastes. After obtaining the thin discs, the experiment was set up in an identical manner, using similar cells as described in Section 4.3.1.

### 7.3.3 Chloride Diffusivity

Chloride ions diffusing across the thin discs were determined by means of a spectrophotometer as described in Sections 4.3.2 and 2.3.2. The measurements were carried out over a period of about 4-8 weeks depending on the volume fraction of the beads in the mortar under investigation.

The chloride diffusion coefficients of the mortars were calculated as described in Section 4.3.3 and termed, the effective diffusivity, $D_{eff}$. However, the chloride diffusivity through the pastes in the mortars (D) was required to compare the results from various volume concentrations with each other and with those of corresponding plain cement paste.

Chloride diffusivity through pastes in mortars, D, can be modeled by assuming diffusion in a periodic composite as demonstrated by Maxwell (1873) and discussed in Cussler (1984). The author considered a situation where a solid consists of periodically spaced spheres as shown in Figure 7.3, where diffusion can be altered by a tortuous path as shown

in Figure 7.3(a), or by two phases in which diffusion coefficients are different as shown in Figure 7.3(b). If it is assumed that diffusion can take place both in the interstitial region between the spheres and through the spheres themselves, then the effective diffusion coefficient ($D_{eff}$) can be calculated exactly from;

$$\frac{D_{eff}}{D}=\frac{\frac{2}{D_s}+\frac{1}{D}-2\Phi_s(\frac{1}{D_s}-\frac{1}{D})}{\frac{2}{D_s}+\frac{1}{D}+\Phi_s(\frac{1}{D_s}-\frac{1}{D})} \qquad \text{.....(7.2)}$$

in which D and $D_s$ are the diffusion coefficients in the interstitial pores and spheres respectively, and $\Phi_s$ is the volume fraction of the spheres in the composite material.

In an analogous situation, the composite material is the mortar, the spheres are the glass beads, and the interstitial pores are the pores in the cement matrix. First, Equation 7.2 indicates that diffusion does not depend on the size of the aggregate or glass beads in the mortar, but only on their volume fraction. Secondly, the diffusion coefficient ($D_s$) of glass beads is zero since they are impenetrable. Thus substituting for $D_s = 0$ in Equation 7.2 gives;

$$\frac{D_{eff}}{D}=\frac{2(1-\Phi_s)}{2+\Phi_s} \qquad \text{.....(7.3)}$$

Therefore substituting $\Phi_s$ with $\Phi_b$ in Equation 7.3, the chloride diffusivity through pastes in mortars, D, can be calculated from measured $D_{eff}$ as;

$$D=D_{eff}[\frac{2+\Phi_b}{2(1-\Phi_b)}] \qquad \text{.....(7.4)}$$

where $\Phi_b$ is the volume fraction of glass beads.

## 7.4 RESULTS

The effective chloride diffusion coefficients ($D_{eff}$) of the mortars for varying volume fraction of glass beads are shown in Table 7.2. The corresponding chloride diffusivities of the pastes in the various mortars were calculated using Equation 7.4 and also shown in Table 7.2. The capillary porosity of the "mortar pastes" obtained by drying the mortars from a saturated surface dry condition to a near-constant weight at 90.7% RH and the corresponding total porosities obtained are also included in this table. Furthermore, Table 7.2 shows reasonably close consistency between the bulk densities of the replicate mortar specimens, thereby validating the mixing and casting procedures used.

### 7.4.1 Porosity of Paste in Mortars

As the volume of glass beads increases, the proportion of the paste in the mortar decreases. Since the glass beads are non-porous, the amount of pores also decreases by virtue of the decreasing volume of paste. In order to make meaningful comparison, the porosity data obtained in this study has been calculated and presented in Table 7.2 as a percentage by volume of the paste portion of each mortar.

Figure 7.4 shows the variation of the capillary and total porosities of paste matrix with volume fraction of glass beads in the various mortars. This figure indicates a gradual increase in the capillary porosity as the volume fraction of glass beads was increased, particularly at the higher volume fractions where a significant proportion of overlap between the transition zones associated with the various beads would be expected. Furthermore, this figure demonstrates that the total porosity remains approximately constant for the various volume fractions of glass beads, which is expected since a constant w/c ratio of 0.4 was used for all the mortar mixes. Table 7.2 and Figure 7.4 show that the capillary porosity of paste matrix increases by approximately 109% from a value of 4.32% for plain cement pastes to a value of 9.03% for the maximum volume fraction of 55%. A similar observation has been reported by Feldman (1986), and Larbi and Bijen (1991)

for sand mortars, using the MIP technique.

### 7.4.2 Chloride Diffusion through Pastes and Mortars

It may be seen from Figure 7.5 that, for $\Phi_b$ greater than about 30%, the rate of diffusion of chloride ions through mortar pastes increases with increasing volume fraction of glass beads in the various mortars. Table 7.2 and Figure 7.5 indicate that the chloride diffusion coefficient through mortar pastes increases by about 100% from $3.95 \times 10^{-8}$ $cm^2/s$ for plain cement pastes to a value of $7.87 \times 10^{-8}$ $cm^2/s$ for mortar paste with a volume fraction of 55%. This implies that the paste in mortar with glass bead volume fraction of 55% is twice as permeable to the diffusion of chloride ions as plain cement pastes. However, Figure 7.5 demonstrates that the rate of diffusion of chloride ions through mortars is less than that through plain cement pastes and seems to remain fairly constant for most of the volume fractions of glass beads investigated. Thus the increase in chloride diffusivity with increasing volume fraction of glass beads could be associated with the greater capillary porosity of these mortar pastes, probably as a consequence of the increased interfacial zone pores. Larbi and Bijen (1991) reported faster fluid transport through mortar pastes than through plain cement pastes.

## 7.5 DISCUSSION

This study has shown that the capillary porosity and chloride diffusion coefficients in mortar pastes both increase with increasing volume fraction of glass beads, although at different rates. The volume of the interfacial zone around aggregates increases as the volume fraction of aggregates increases. Thus for the same w/c ratio, the porosity of the paste decreases away from the interfacial zone forming a denser paste. It is, therefore, suggested that for chloride ions to diffuse faster in mortar pastes than plain paste, the interfacial zone pores would be expected to form part of the diffusion path. Thus the increased permeability to chloride ions observed in this study for mortar pastes with high volume fraction of glass beads could be associated to the overlapping of the transition

zones of the various beads. Recently, Winslow *et al.* (1994) using MIP suggested the occurrence of percolated interfacial zone pores in concrete. The authors also indicated, using computer modelling, that for an interfacial zone thickness of about 20 μm, interfacial zone percolation will occur in most typical construction concrete. However, the authors used oven-drying at 105°C to evacuate their specimens prior to MIP, which would be expected to alter the pore structure especially the so-called "weak link" or interfacial zone.

Nevertheless, this study has linked the influence of varying the volume fraction of glass beads on both capillary porosity and chloride diffusivity by plotting chloride diffusion coefficients against capillary porosity of mortar pastes as shown in Figure 7.6. This figure illustrates that chloride diffusion coefficient increases with increasing capillary porosity of the mortar pastes. This suggests that interfacial zone pores influence chloride transport to a certain extent since the volume of interfacial zone pores per unit volume of paste increases with increasing glass beads concentration, and the porosity of the paste matrix decreases away from the interfacial zone. However, capillary porosity seems to increase at a faster rate than the chloride diffusivity. This demonstrates that it is not only the amount of capillary pores present that influence chloride transport, but also their connectivity, in this case interfacial zone percolation. Generally, the results in this study suggest that ion transport in mortars and probably concrete are controlled mainly by the cement paste matrix, with interfacial zone pores and interfacial zone percolation considered to play only a secondary role. This suggestion is further reinforced by the close correlation between plain cement pastes with w/c ratios of 0.4 and 0.5 and mortar pastes as demonstrated in Figure 7.6.

On the other hand, chloride transport has been found to be relatively slower in mortars than in corresponding plain cement pastes. This indicates that chloride diffusion coefficients determined for cement paste specimens are representative of corresponding concrete and may only be considered as a slight overestimation of the true diffusion rates

in these concretes.

It must be pointed out, that irrespective of the volume fraction of beads used, ASR gel was not observed or identified at the interfacial zone or cement matrix for the glass bead mortar discs prepared and analyzed as described in Section 2.3.6. Also, Plates 7.1 to 7.4 show the distribution of glass beads within OPC mortars for beads volume fractions of approximately 28%, 38%, 48% and 55% respectively. These plates indicate that the random distribution of glass beads in these mortars is in close agreement with the periodic composite assumed in Section 7.3.3, especially for the higher volume fractions of 48 and 55%.

## 7.6 CONCLUSIONS

(1) The capillary porosity of the paste formed in mortars is higher than that of the corresponding plain cement pastes prepared without glass beads. The capillary porosity has been found to increase with increasing volume fraction of glass beads.

(2) The rate of transport of chloride ions is faster in the mortar pastes than in the corresponding plain cement pastes and also increases with increasing volume fraction of glass beads. On the other hand, chloride transport is comparatively slower in mortars than in plain cement pastes and seemed to remain fairly constant with increasing volume fraction of glass beads. The results suggests that the paste matrix is the continuous phase in mortars and concretes and is mainly responsible for chloride ion transport in these materials.

**Figure 7.1: Microstructural gradients (anhydrous material and porosity) in the interfacial region of concrete (Scrivener et al, 1988)**

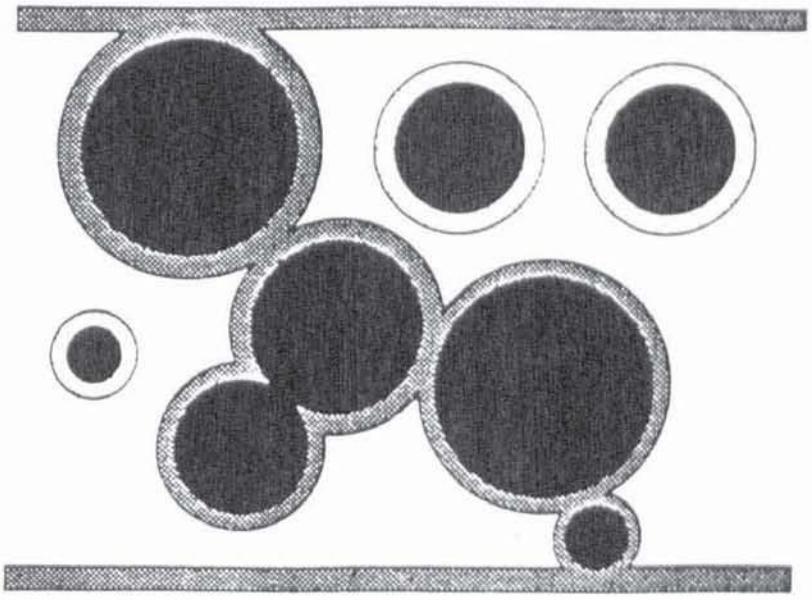

**Figure 7.2: Two-dimensional schematic representation of interfacial zone percolation**

(a) Tortuous diffusion in a porous solid

(b) Diffusion through a spatially periodic composite

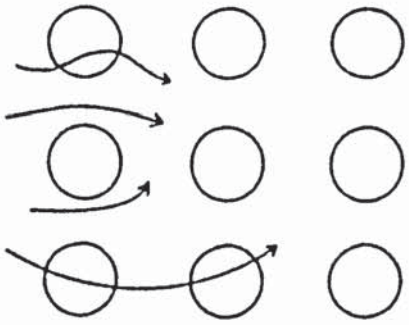

**Figure 7.3: Diffusion in porous media**

**Table 7.1: Packing Factor of Glass Beads**

| Container | A | B | C |
|---|---|---|---|
| Volume of container ($cm^3$) | 122.71 | 136.93 | 161.33 |
| Weight of container (g) | 15.40 | 18.64 | 20.15 |
| Weight of container + beads (g) | 251.66 | 281.40 | 327.60 |
| Volume of beads ($cm^3$) | 80.09 | 89.07 | 104.22 |
| Packing Factor (%) | 0.653 | 0.650 | 0.646 |
| **Average Packing Factor (%)** | **0.650** | | |

**Table 7.2: Experimental results obtained for glass bead mortars with w/c of 0.4.**

| $\Phi_b$ (%) | $D_{eff}$ ($x10^{-8}cm^2/s$) | * Bulk Density ($g/cm^3$) | Capillary Porosity (%) | Total Porosity (%) | Chloride Diffusivity ($x10^{-8}cm^2/s$) |
|---|---|---|---|---|---|
| 0.0 | 4.35 | 1.982 | 4.33 | 40.18 | 4.35 |
| | 3.75 | 1.987 | 4.32 | 40.40 | 3.75 |
| | 3.99 | 1.987 | 4.05 | 40.43 | 3.99 |
| | 4.01 | 1.987 | 4.56 | 40.56 | 4.01 |
| | 3.65 | 1.981 | 4.32 | 40.59 | 3.65 |
| **Average** | 3.95 | 1.985 | 4.32 | 40.41 | 3.95 |
| 14.0 | 3.27 | 2.118 | 4.72 | 39.19 | 4.07 |
| | 3.16 | 2.124 | 4.26 | 38.72 | 3.93 |
| | 3.05 | 2.131 | 4.47 | 40.13 | 3.79 |
| | 3.06 | 2.134 | 4.81 | 39.14 | 3.81 |
| | 2.87 | 2.133 | 4.58 | 39.73 | 3.57 |
| **Average** | 3.08 | 2.128 | 4.57 | 39.38 | 3.83 |
| 28.4 | 2.52 | 2.294 | 4.82 | 37.70 | 4.02 |
| | 2.81 | 2.299 | 5.32 | 38.38 | 4.48 |
| | 2.58 | 2.306 | 5.19 | 37.45 | 4.11 |
| | 3.54 | 2.291 | 5.61 | 38.50 | 5.65 |
| | 2.37 | 2.303 | 4.46 | 37.20 | 3.78 |
| **Average** | 2.89 | 2.299 | 5.08 | 37.85 | 4.41 |
| 37.7 | 2.28 | 2.390 | 5.21 | 38.29 | 4.35 |
| | 3.44 | 2.426 | 5.92 | 37.75 | 6.55 |
| | 2.24 | 2.468 | 4.97 | 36.26 | 4.26 |
| | 3.01 | 2.452 | 5.81 | 36.58 | 5.75 |
| | 2.69 | 2.401 | 5.21 | 38.72 | 5.12 |
| **Average** | 2.73 | 2.427 | 5.42 | 37.52 | 5.21 |

where $\Phi_b$ is the volume fraction of glass beads and * is the bulk density of mortars

**Table 7.2: Continued**

| $\Phi_b$ (%) | $D_{eff}$ ($x10^{-8}cm^2/s$) | * Bulk Density ($g/cm^3$) | Capillary Porosity (%) | Total Porosity (%) | Chloride Diffusivity ($x10^{-8}cm^2/s$) |
|---|---|---|---|---|---|
| 43.0 | 2.67 | 2.435 | 5.69 | 38.40 | 5.69 |
| | 2.82 | 2.487 | 5.98 | 37.03 | 6.01 |
| | 2.51 | 2.451 | 5.50 | 36.69 | 5.34 |
| | 3.20 | 2.428 | 6.39 | 38.63 | 6.81 |
| | 2.88 | 2.423 | 6.49 | 39.28 | 6.14 |
| **Average** | 2.82 | 2.445 | 6.01 | 37.94 | 6.00 |
| 48.0 | 3.02 | 2.483 | 7.16 | 38.96 | 7.21 |
| | 2.88 | 2.466 | 6.98 | 38.54 | 6.87 |
| | 2.68 | 2.457 | 7.44 | 39.39 | 6.38 |
| | 3.14 | 2.460 | 7.51 | 39.58 | 7.48 |
| | 2.74 | 2.467 | 7.23 | 38.69 | 6.53 |
| **Average** | 2.89 | 2.467 | 7.26 | 39.03 | 6.89 |
| 55.0 | 2.64 | 2.570 | 8.79 | 39.89 | 7.48 |
| | 2.59 | 2.582 | 8.41 | 39.16 | 7.33 |
| | 2.72 | 2.567 | 9.09 | 40.80 | 7.71 |
| | 3.14 | 2.570 | 9.94 | 40.69 | 8.89 |
| | 2.80 | 2.572 | 8.92 | 39.71 | 7.92 |
| **Average** | 2.78 | 2.572 | 9.03 | 40.05 | 7.87 |

where $\Phi_b$ is the volume fraction of glass beads and * is bulk density of mortars

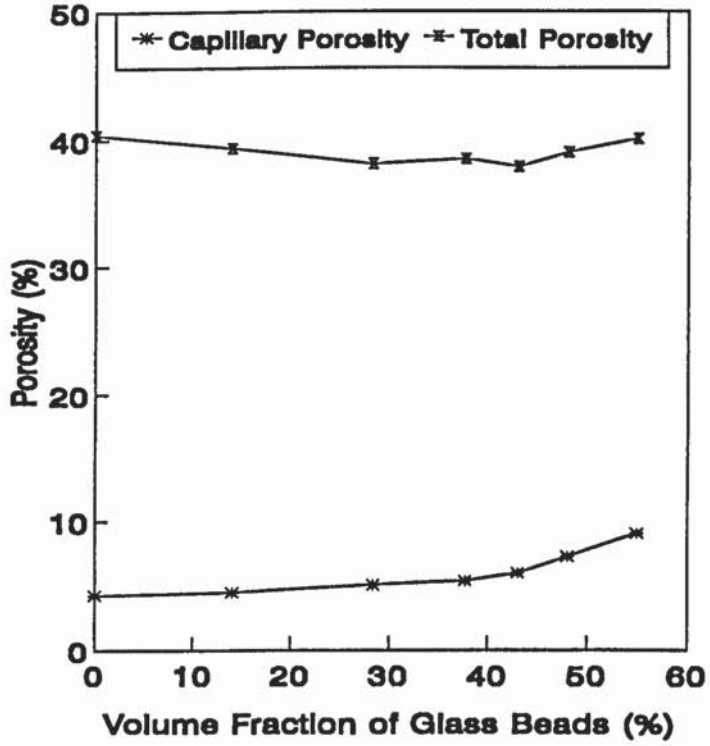


**Figure 7.4: Porosity of paste in mortars with varying volume fraction of glass beads**

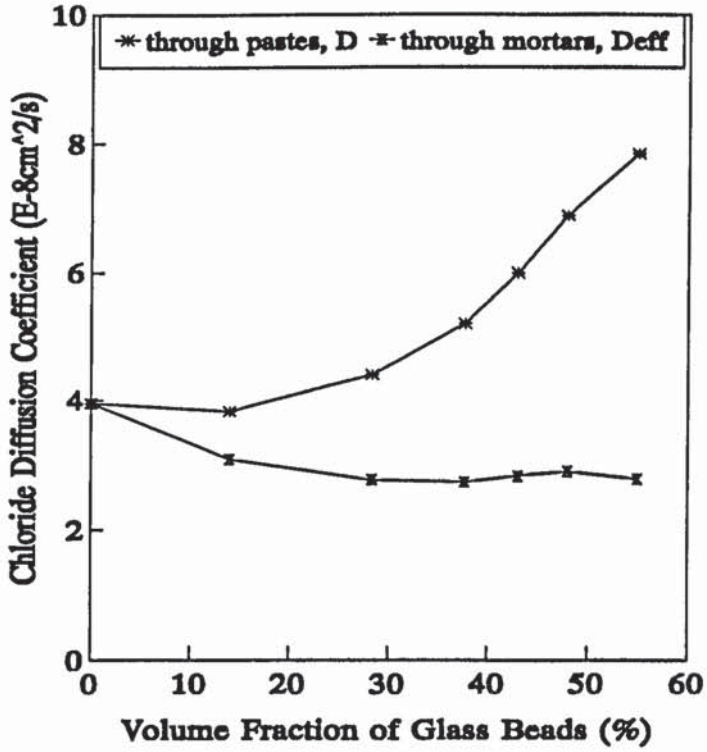


**Figure 7.5: Chloride diffusion coefficients for pastes and mortars with varying volume fraction of glass beads**

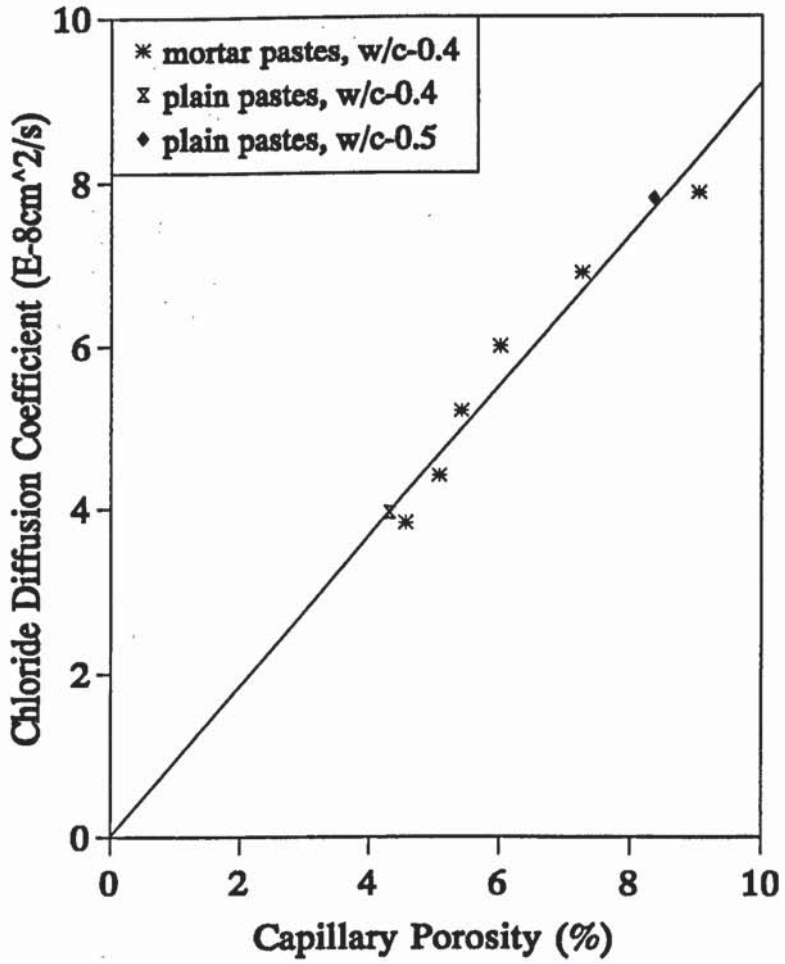


**Figure 7.6: Plot of chloride diffusion coefficient versus capillary porosity for OPC pastes**

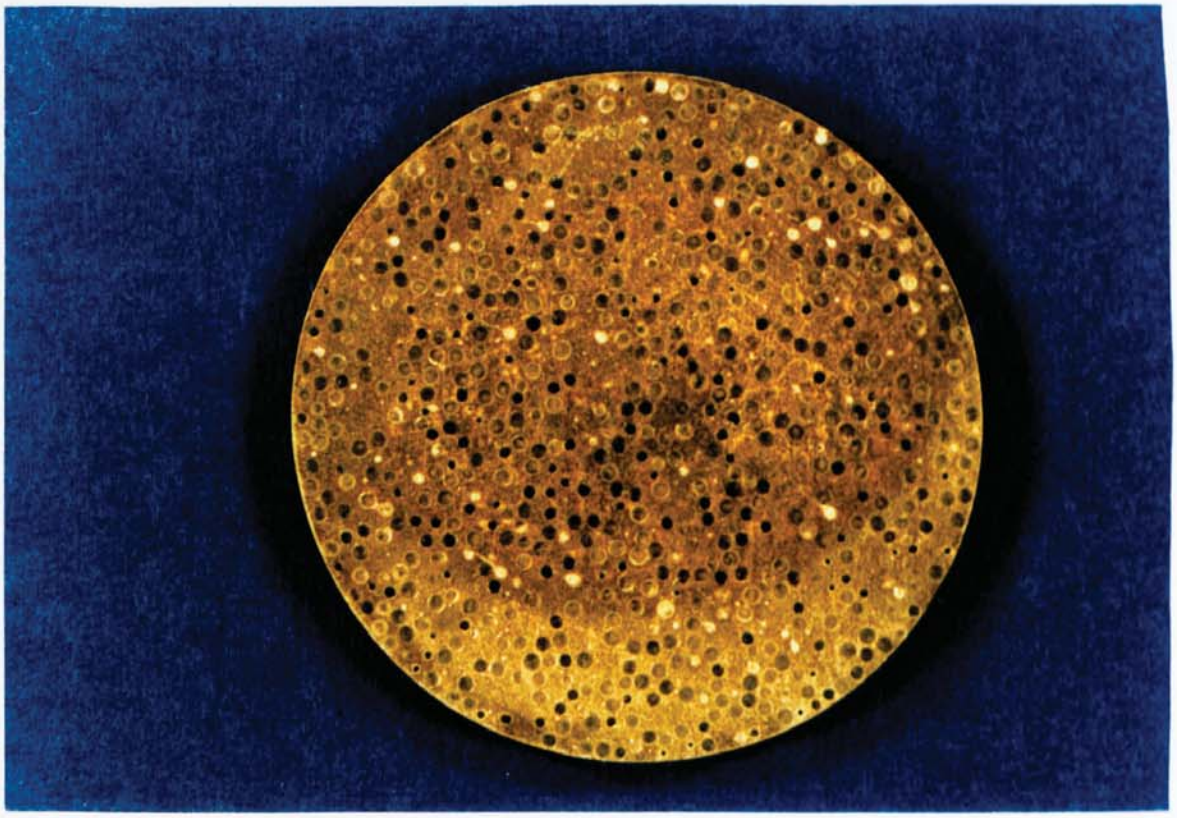

**Plate 7.1: Random distribution of glass beads in OPC mortar constituting approximately 28% volume fraction of beads**

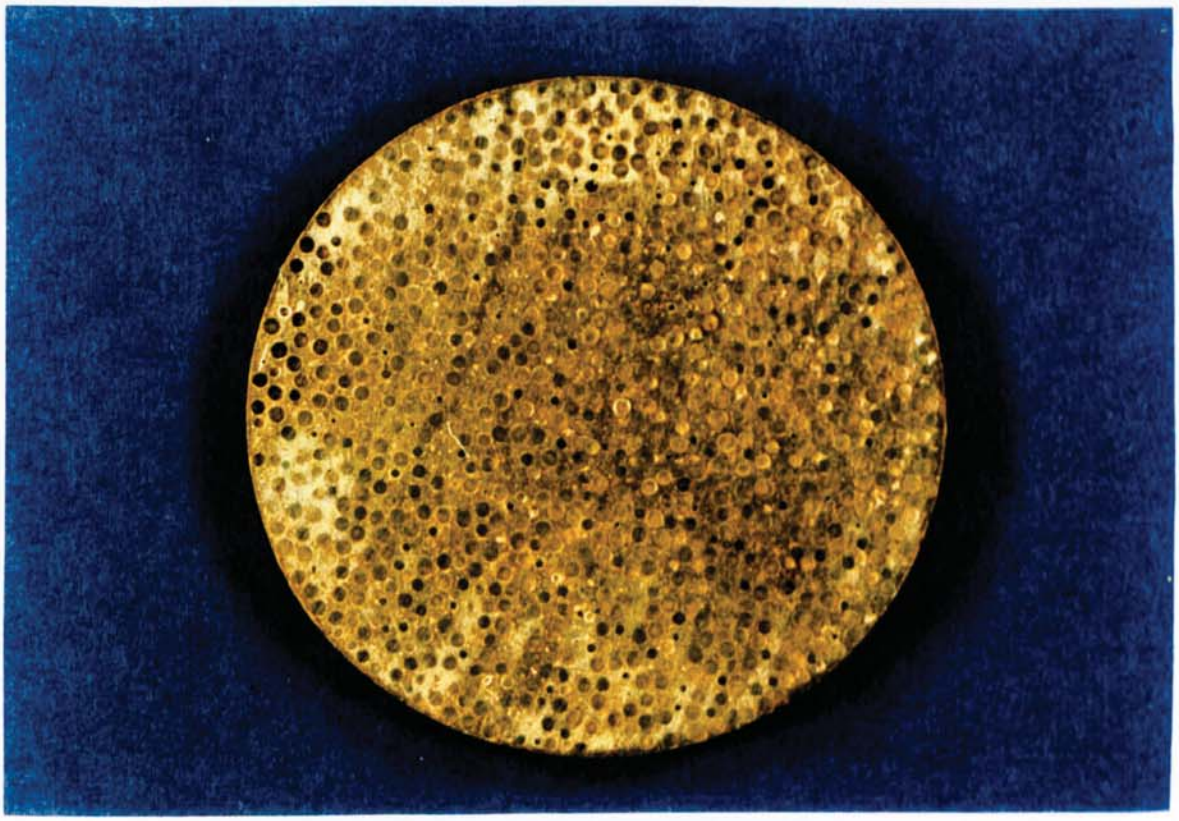

**Plate 7.2: Random distribution of glass beads in OPC mortar constituting approximately 38% volume fraction of beads**

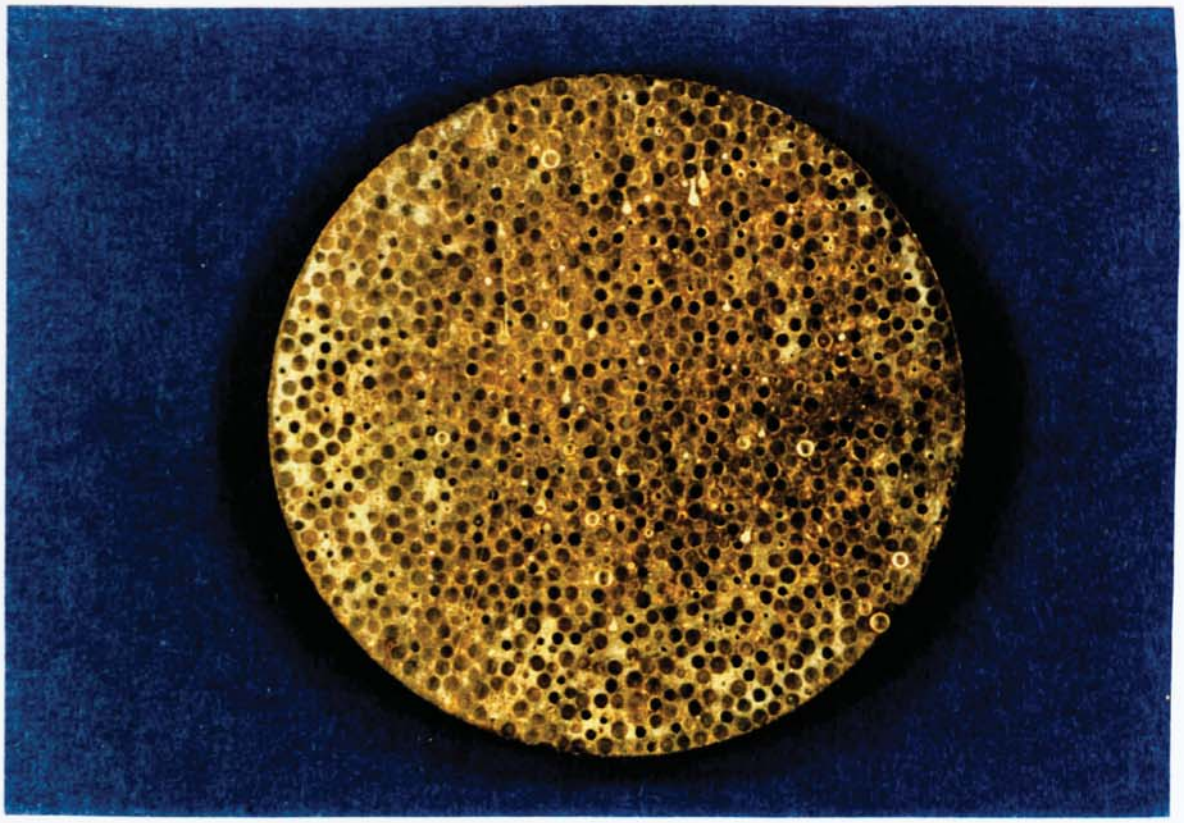

**Plate 7.3: Random distribution of glass beads in OPC mortar constituting approximately 48% volume fraction of beads**

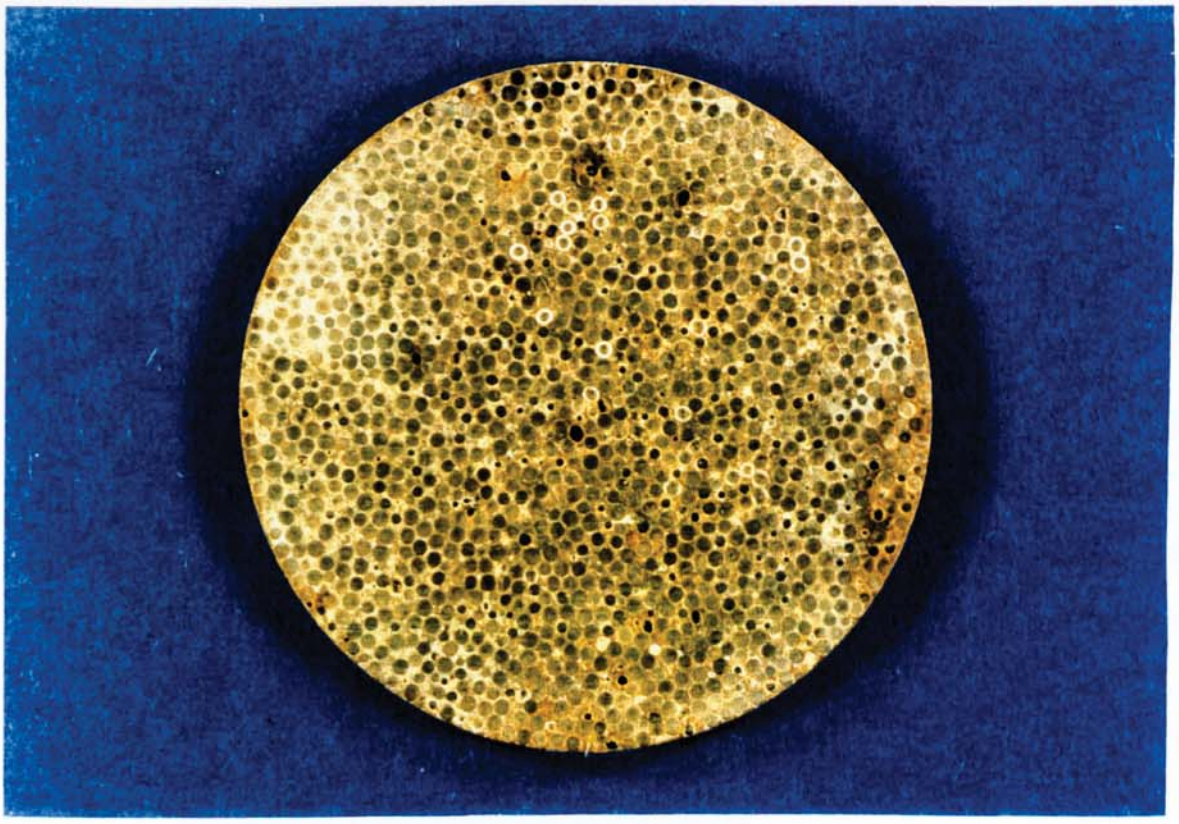

**Plate 7.4: Random distribution of glass beads in OPC mortar constituting approximately 55% volume fraction of beads**

# CHAPTER EIGHT

# GENERAL CONCLUSIONS AND RECOMMENDATIONS FOR FURTHER STUDIES

Detailed conclusions have been presented at the end of each chapter and need not be repeated here. However, it is necessary to provide the general conclusions of the study and provide recommendations for further work which might be required to substantiate some of the views expressed or answer some of the questions raised in this thesis.

## 8.1 CONCLUSIONS

(1) The two techniques employed in this study (desorption and MIP) have revealed compatible information about the pore structure of HCP. The water-vapour desorption of specimens from a saturated surface dry condition to a near-constant weight at 90.7% RH (a measure of coarse capillary porosity) correlates with the threshold diameter and intrusion volume for pores greater than 30 nm using MIP. Similarly, the total porosity obtained by oven-drying specimens at 105°C was related to the total intrusion volume from MIP measurements.

(2) The microcalorimetric measurements of heat flow in porous glasses and hardened cement pastes demonstrate great potential for the low temperature calorimeter developed in this study in characterising the state of pore water in porous materials and providing information regarding the proportion of coarse pores in these materials. This provides an incentive for the further development of the calorimeter and a basis for the interpretation of the mechanical properties of ice formation in porous materials.

(3) In hydrated OPC pastes, the coarse $Ca(OH)_2$ crystals are dispersed throughout the pore system accounting for the high observed values of coarse capillary porosity and continuity of the pores. The use of fly ash and slag as partial replacements for OPC in blended pastes has resulted in a marked reduction in capillary porosity and a slight increase in total pore volume. This is a reflection of the reduced $Ca(OH)_2$ content and greater gel porosity due to the production of additional C-S-H gel associated with the pozzolanic reaction of the fly ash or hydraulicity of the slag.

(4) There is a significant difference in pore structure between hardened fly ash and slag blends, with the fly ash blended pastes indicating higher values of capillary porosity and slightly lower total pore volume. This difference is associated mainly with the variation in chemical composition and physical properties such as fineness and percentage replacement of OPC by fly ash and slag.

(5) This study has established that for any given w/s ratio, the chloride diffusion rates for blended OPC/30%PFA and OPC/65%BFS pastes are about one order of magnitude smaller than those for plain OPC pastes. For blended cement pastes, however, the OPC/65%BFS pastes provides slightly greater resistance to chloride ingress than OPC/30%PFA pastes for a given w/s ratio or given capillary porosity.

(6) Similarly, for a given w/s ratio, the oxygen diffusion rates for blended OPC/30%PFA pastes are about 25% smaller than those for OPC pastes but about 35% higher than those for OPC/65%BFS pastes.

(7) Neutral oxygen molecules and charged chloride ions have similar diffusion coefficients in dilute aqueous solutions and may be expected to diffuse through similar pores in HCP. This study has adopted the ratio of oxygen to chloride diffusion coefficients, ($D_O/D_{Cl}$), as a numerical measure of the effect of the surface

charge on cement hydrates. This ratio increases from values close to 1 in very permeable pastes, to values of around 15 in low-permeability blended fly ash and slag pastes. This supports the view that the diffusion of chloride ions is retarded by the surface charge of the hydrated cement gel in low-permeability pastes. In contrast, the hydrated cement gel in these pastes is much more permeable to the similarly-sized, neutral oxygen molecule.

(8) The neutralization of cement pastes by $CO_2$ ingress results in a slight increase of about 5% in the proportion of capillary pores in the OPC matrix. This is almost negligible compared with a marked increase of approximately 145% and 230% for blended OPC/30%PFA and OPC/65%BFS matrices respectively. The $CaCO_3$ deposited following carbonation results in an increase in the bulk density and a corresponding decrease in the total pore volume for all the cement systems investigated. This reduction in total porosity was on average about 25% for OPC pastes, compared to 18% and 17% for fly ash and slag blends, respectively.

(9) The changes in pore structure associated with carbonation in (8) above influence the rate of transport of oxygen molecules and chloride ions. For a given w/s ratio, the chloride diffusion rates for carbonated OPC/30%PFA and OPC/65%BFS pastes are about two orders of magnitude greater than those of the corresponding non-carbonated pastes, while for carbonated OPC pastes the chloride diffusion rates are about 2 to 5 times higher. Similarly, for w/s ratios of 0.5 and 0.6 investigated, the increase in oxygen diffusion rates following carbonation are about one order of magnitude for the blended pastes compared with 2 to 5 times larger for the plain OPC pastes. These findings suggest that the good qualities of fly ash and slag matrices in retarding chloride ingress and thus reinforcement corrosion are lost on carbonation.

(10) The ratio of oxygen to chloride diffusion coefficients was close to one for most of the carbonated pastes investigated irrespective of the cement matrix composition. This reinforces the view that oxygen molecule and chloride ion diffuse at similar rates in very open-textured porous hydrated cement systems, probably due to negligible surface charge effects or the reduced binding capacity of the carbonated cement hydrates.

(11) This study has established that the marked increase in the permeability of carbonated OPC/30%PFA and OPC/65%BFS pastes to the diffusion of chloride ions is associated mainly with the effect of carbonation, with initial drying prior to carbonation playing only a minor role. In OPC pastes, however, the initial drying for easy $CO_2$ ingress seems to play a similar role in the coarsening of the pore structure and the increase in the permeability of carbonated pastes to chloride ions.

(12) It has been demonstrated that the coarse capillary porosity of the paste formed in model mortars with glass bead aggregates is higher than that of the corresponding plain cement pastes and tends to increase with increasing volume fraction of glass beads in the mortars.

(13) The rate of transport of chloride ions has been shown to be faster in the mortar pastes than in the corresponding plain cement pastes and also to increase with increasing volume fraction of glass beads. On the other hand, overall chloride transport is comparatively slower in mortars than in plain cement pastes and seems to remain fairly constant with increasing volume fraction of beads. The results suggest that the paste matrix is the continuous phase in mortars and concretes and is mainly responsible for the transport of chloride ions and other aggressive substances through these materials.

## 8.2 RECOMMENDATIONS FOR FURTHER STUDIES

It is important that further work is carried out to investigate some of the questions raised in this study and which could not be researched within the timescale available.

The LTC has been shown in this section to be a potentially valuable tool which if fully developed and exploited, could provide useful information regarding porosity and ice formation in HCP and other microporous materials. There is, however, need for further developments to transform the present calorimeter into a more user friendly, sensitive, accurate and reliable equipment. These changes should include improving the control program for controlling the rate of temperature change during cooling-heating cycles and decreasing the minimum temperatures achieved during a cooling run to as low as -55°C.

Significant differences in the proportion of large pores were observed in some cement pastes prior to and after exposure to chloride ions. This was more noticeable in low-permeability pastes and suggests that chloride binding seems to narrow or block some of the large pores. This finding is not conclusive and could be associated with errors in the desorption technique used. Nevertheless, it warrants further investigation on a wide range of well-cured cement pastes, probably using MIP or oxygen diffusion before and after chloride diffusion.

The influence of atmospheric carbon dioxide gas on pore structure and chloride diffusion in OPC, fly ash and slag pastes has been established in this thesis. It is considered important to study the influence of other environmental factors such as the presence of sulphates, on the properties of these cementitious materials. There is evidence (New Civil Engineer, 1986) to suggest that sulphates may build up in the cover zone of concrete over a period of time and influence the ability of the binder to immobilise ingressing chloride ions and potentially reach a concentration which may cause sulphate damage. Thus combined sulphate and chloride attack may affect the three cement systems investigated

and others to varying extents.

Oxygen diffusion rates in OPC/65%BFS pastes were unexpectedly found to remain fairly constant irrespective of the w/s ratio or capillary porosity. Neutral oxygen molecules are expected to diffuse freely through porous systems. Nevertheless, their rate of transport is believed to depend on the connectivity and tortuosity of the pore network. This study could not really account for this behaviour and further work on oxygen diffusivity in slag pastes and other blended pastes is required to provide a better understanding of this phenomenon.

It has been demonstrated that the threshold diameters for carbonated OPC/65%BFS pastes remained fairly constant for different w/s ratios despite an expected increase in the proportion of large pores with increasing w/s ratio. These near-constant values of the threshold diameters could be associated with the diameters of the pore entrances rather than with the average pore sizes themselves. However, this is only a preliminary finding and was neither obvious in non-carbonated OPC/65%BFS nor evident in OPC and fly ash pastes. Thus further investigations could provide a clearer understanding of this observation.

The ratio ($D_O/D_{Cl}$) has been found to be about 1/2 for fully carbonated fly ash and slag pastes with w/s ratios of 0.5 (PFA5C and BFS5C, respectively). This unexpected observation suggests that, in these pastes, chloride ions diffuse twice as fast as oxygen molecules. This behaviour was not observed in other pastes investigated (PFA6C, BFS6C, OPC5C and OPC6C). It could be associated with errors in the preparation of samples or in the experimental measurements. Nevertheless, it would be worthwhile doing some further studies on oxygen and chloride diffusion in carbonated fly ash, slag, microsilica and metakaolin pastes (especially for w/s ratios of 0.5 or less) to substantiate this finding.

This study has established the influence of assumed periodic packing of glass beads in OPC mortars on porosity and chloride ingress. It is envisaged that the use of blended cements comprising materials with greater fineness such as fly ash, slag or microsilica could enhance the efficient packing of the glass beads and improve the microstructure of the interfacial zone to a greater extent than OPC. This may provide greater resistance to the ingress of chloride ions and other aggressive chemicals. Furthermore, computer simulations of these assumed periodic composites could provide a better understanding of aggregate packing effects in mortars and concretes and their influence on the properties of the interfacial zone.

# REFERENCES

**AASHTO Designation T259-80 (1980).** Standard Method of test for resistance of concrete to chloride ion penetration. American Association of State Highway and Transportation Officials, Washington D.C.

**Al-Hussaini, M. J., Sangha, C. M., Plunkett, B. A. and Walden, P. J. (1990).** The effect of chloride ion source on the free chloride ion percentages in OPC mortars. Cement and Concrete Research, Vol.20, No.5, pp. 739-745.

**Amasaki, S. (1984).** Influence of carbonation on properties of concrete. Trans. Japan Concr. Inst., Vol.6, pp. 179-184.

**Andrade, C. and Page, C. L. (1986).** Pore solution chemistry and corrosion in hydrated cement systems containing chloride salts: A study of cation specific effects. British Corrosion Journal, Vol.21, No.1, pp. 49-53.

**Arya, C. and Newman, J. B. (1990).** An assessment of four methods of determining the free chloride content of concrete. Materials and Structures, No.23, pp. 319-330.

**Arya, C., Buenfeld, N. R. and Newman, J. B. (1990).** Factors influencing chloride-binding in concrete. Cement and Concrete Research, Vol.20, No.2, pp. 291-300.

**Atkinson, A. and Nickerson, A. K. (1984).** The Diffusion of ions through Water-Saturated Cement. Journal of Materials Science, Vol.19, pp. 3068-3078.

**Bager, D. H. and Sellevold, E. J. (1986a).** Ice Formation in Hardened Cement Paste: Part I- Room Temperature Cured Pastes with Variable Moisture Contents. Cement and Concrete Research, Vol.16, pp. 709-720.

**Bager, D. H. and Sellevold, E. J. (1986b).** Ice Formation in Hardened Cement Paste, Part II- Drying and Resaturation on Room Temperature cured Pastes. Cement and Concrete Research, Vol.16, pp. 835-844.

**Bager, D. H. and Sellevold, E. J. (1986c).** Ice Formation in Hardened Cement Paste: Part III- Slow Resaturation of Room Temperature Cured Pastes. Cement and Concrete Research, Vol.17, pp. 1-11.

**Bager, D. H. and Sellevold, E. J. (1980).** Ice Formation in Hardened Cement Paste: Part II- Steam Cured Pastes with Variable Moisture Contents. Durability of Building Materials and Componenets, STP 691, edited by Sereda P and Litvan G, ASTM, pp. 439-454.

**Barnes, B. D., Diamond, S. and Dolch, W. L. (1979).** Micromorphology of the interfacial zone around aggregates in portland cement mortar. Journal of American Ceramic Society, Vol.62, No.1-2, pp. 21-24.

**Barnes, B. D., Diamond, S. and Dolch, W. L. (1978).** The contact zone between portland cement paste and glass "aggregate" surfaces. Cement and Concrete Research, Vol.8, pp. 233-244.

**Beddoe, R. E. and Setzer, M. J. (1990).** Phase transformations of water in hardened cement paste - A low-temperature DSC investigation. Cement and Concrete Research, Vol.20, No.2, pp. 236-242.

**Bentz, D. P., Stutzman, P, E. and Garboczi, E. J. (1992).** Experimental and simulation studies of the interfacial zone in concrete. Cement and Concrete Research, Vol.22, No.5, pp. 891-902.

**Bentz, D. P. and Garboczi, E. J. (1991).** Percolation of phases in a three dimensional cement paste microstructural model. Cement and Concrete Research, Vol.21, No.2/3, pp. 325-344.

**Bier, T. A., Kropp, J. and Hilsdorf, H. K. (1989).** The formation of silica gel during carbonation of cementitious systems containing slag cements. ACI Proceedings SP114-69, Trondheim, pp. 1413-1429.

**Bier, T. A. (1986).** Influence of type of cement and curing on carbonation progress and pore structure of hydrated cement pastes. Materials Research Symposium Proceedings, Boston, Vol.85, pp. 1-19.

**British Standard Institutions, BS 4550: 1970, Part 2.**

**British Standard Institutions, BS 8110: 1985, Part 1.** Structural use of Concrete- Code of practice for design and construction.

**Buenfeld, N. R. and Newman, J. B. (1987).** Examination of the three methods for studying ion diffusion in cement pastes, mortars and concretes. Materials and Structures, Vol.20, pp. 3-10.

**Byfors, K. (1986).** Chloride in cement pastes. Nordic Concrete Research, No.4, pp. 27-28.

**Collepardi, M., Marcialis, A. and Turriziani, R. (1972a).** The penetration of de-icing agents in cement pastes. Il Cemento, Vol.69, pp. 143-150.

**Collepardi, M., Marcialis, A. and Turriziani, R. (1972b).** Penetration of Chloride ions into Cement Pastes and Concrete. Journal of American Ceramic Society, Vol.55, No.10, pp. 534-535.

**Crank, J. (1975).** The Mathematics of Diffusion. 2nd Edition, pp. 21, Clarendon Press, Oxford.

**CRC Press (1976).** Handbook of Chemistry and Physics - A Read-Reference Book of Chemical and Physical Data, 57th Edition, Table 16, pp. D227, Edited by R. C. West, Ohio, USA.

**Cussler, E. L. (1984).** Diffusion: Mass transfer in Fluid Systems. Cambridge University Press, pp. 116, 147 and 186-187.

**Daimon, M., Akiba, T. and Kondo, R. (1981).** Through pore size distribution and kinetics of the carbonation reaction of portland cement mortars. Journal of American Ceramic Society, Vol.54, No.9, pp. 423-428.

**Day, R. L. and Marsh, B. K. (1988).** Measurement of Porosity in Blended Cement Paste. Cement and Concrete Research, Vol.18, pp. 63-73.

**Dean, J. A. (1985).** Lange's Handbook of Electrochemistry. McGraw-Hill, New York, 13th Edition, pp. 10.

**Detwiler, R. J., Kjellsen, K. O. and Gjorv, O. E. (1991).** Resistance to Chloride Intrusion of Concrete Cured at Different Temperatures. ACI, Materials Journal, Vol.88, No.1, pp. 19-24.

**Detwiler, R. J., Monteiro, P. J. M., Wenk, H. R. and Zhong, Z. (1988).** The texture of calcium hydroxide near the cement paste-aggregate interface. Cement and Concrete Research, Vol.18, pp. 823-829.

**Defay, R., Progogine, I., Bellemans, A. and Everett, D. H. (1966).** Surface Tension and Adsorption, Longmans, London.

**Dhir, R. K., Jones, M. R. and McCarthy, M. J. (1993).** PFA Concrete: Chloride ingress and corrosion in carbonated cover. Proceedings of Institutution of Civil Engineers, Structures and Buildings, Vol.99, pp. 167-172.

**Dhir, R. K., Jones, M. R. and Ahmed, H. E. H. (1991).** Concrete durability: Estimation of chloride concentration during design life. Magazine of Concrete Research, Vol.43, No.154, pp. 37-44.

**Dhir, R. K., Jones, M. R., Ahmed, H. E. H. and Seneviratne, A. M. G. (1990a).** Rapid estimation of the chloride diffusion coefficient in concrete. Magazine of Concrete Research, Vol.42, No.152, pp. 177-185.

**Dhir, R. K., Jones, M. R. and Ahmed, H. E. H. (1990b).** Determination of total and soluble chlorides in concrete. Cement and Concrete Research, Vol.20, pp. 579-590.

**Diamon, M., Abo-El-Enein, S. A., Hosaka, G., Goto, S. and Kondo, R. (1977).** Pore Structure of Calcium Silicate Hydrate in Hydrated Tricalcium Silicate. Journal of American Ceramic Society, Vol.60, pp. 110-114.

**Diamond, S. (1987).** Cement paste microstructure in concrete: In microstructural development during hydration of cement. Materials Research Society Symposium Proceedings, Vol.85, Edited by L. J. Struble and P. W. Brown, pp. 21-31.

**Diamond, S. (1971).** Pore-Distribution, Measurement and Comparison. Cement and Concrete Research, Vol.1, No.5, pp. 532-545.

**Dorner, H. W. (1984).** A microcalorimetric study of ice formation in cement paste containing chloride. Cement and Concrete Research, Vol.14, pp. 807-815.

**Dorner, H. W. and Setzer, M. J. (1980).** Cement and Concrete Research, Vol.10, pp. 403-411.

**Dullien, F. (1979).** Transport Phenomena in Porous Media and Pore Structure. Academic Press.

**Fagerland, G. (1974).** Non-freezable water contents of porous building materials. Report No.42, Lund Institute of Technology, Sweden.

**Farran, J. (1958).** Contribution mineralogique a l'etude de l'adherence entre les constituants hydrates des ciments et les materiaux enrobes. Rev. Mater. Const. Trav. Publics, Ed. C. 490-491, pp. 155-172.

**Feldman, R. F. and Beaudoin, J. J. (1991).** Pretreatment of Hardened Cement Pastes for Mercury Intrusion Measurements. Cement and Concrete Research, Vol.21, pp. 297-308.

**Feldman, R. F. (1984).** Pore Structure Damage in Blended Cement Pastes caused by Mercury Intrusion. Journal of American Ceramic Society, Vol.67, pp. 30-33.

**Feldman, R. F. (1972).** Density and Porosity Studies of Hydrated Portland Cement. Cement Technology, Vol.3, No.1, pp. 5-9 and 11-14.

**Feldman, R. F. and Sereda, P. J. (1970).** A new Model for Hydrated Portland Cement and its Practical Implications. Eng. J. Canada, Vol.53, pp. 53-59.

**Forrester, J. (1976).** Measurement of carbonation: In Carbonation of Concrete - RILEM International Symposium. Cement and Concrete Association, Paper 2.1, 6 pp.

**Garboczi, E. J. (1993).** Computational materials science of cement based materials. Materials and Structures, Vol.26, pp. 191-195.

**Garboczi, E. J. and Bentz, D. P. (1992).** Computer simulation of the diffusivity of cement-based materials. Journal of Materials Science, Vol.27, pp. 2083-2092.

**Garboczi, E. J. and Bentz, D. P. (1991).** Digital simulation of the aggregate-cement paste interfacial zone in concrete. Journal of Materials Research, Vol.6, No.1, pp. 196-201.

**Gautefall, O. and Havdahl, J. (1989).** Effect of Condensed Silica Fume on the mechanism of chloride diffusion into hardened cement pastes. 3rd International Conference on the use of Fly ASh, Silica Fume, Slag and Natural Pozzolans in Concrete. ACI SP-114, Trondheim, Edited by V. M. Malhotra, Vol.II, pp. 849-860.

**Gautefall, O. (1986).** Effect of Condensed Silica Fume on the diffusion of chloride through hardened cement paste. 2nd International Conference on the use of Fly Ash, Silica Fume, Slag and Natural Pozzolans in concrete. ACI SP-91, Madrid, Spain, pp. 991-997.

**Gjφrv, O. E. and Vennesland, Φ. (1979).** Diffusion of Chloride ions from Sea Water into Concrete. Cement and Concrete Research, Vol.9, pp. 229-238.

**Gjφrv, O. E., Vennesland, Φ. and El-Busaidy, A. H. S. (1976).** Diffusion of dissolved oxygen through concrete. Proceedings of "Corrosion/76", NACE, Houston, Paper No.17, March 17.

**Glasser, F. P., Luke, K. and Angus, M. J. (1988).** Modification of cement pore fluid compositions by pozzolanic additives. Cement and Concrete Research, Vol.18, pp. 165-178.

**Gordon, A. R. (1945).** The diaphragm cell method of measuring diffusion. Ann. N. Y. Acad. Sci., Vol.46, pp. 285.

**Goto, S. and Roy, D. M. (1981a).** Diffusion of ions through Hardened Cement Pastes. Cement and Concrete Research, Vol.11, No.5, pp. 751-757.

**Goto, S. and Roy, D. M. (1981b).** The Effect of Water/Cement ratio and Curing Temperature on the Permeability of Hydrated Cement Pastes. Cement and Concrete Research, Vol.11, pp. 575-580.

**Grandet, J. and Ollivier, J. P. (1980).** Nouvelle methode d'etude des interfaces ciments-granulats. Proceedings of 7th International Conference on Chemistry of Cements, paris, Vol.III, pp. VII 85-89.

**Gregg, S. and Sing, K. (1967).** Adsorption, Surface Area and Porosity. Academic Press.

**Hagley, D. (1972).** The nature of paste-aggregate interface. Ph.D Thesis, Purdue University.

**Hamada, M. (1968).** Principal paper - Neutralization of concrete and corrosion of reinforcing steel. 5th International Symposium on Chemistry of Cement Proceedings, Tokyo, Vol.3, pp. 343-369.

**Hansen, T. C., Jensen, H. and Johannesson, T. (1986).** Chloride diffusion and corrosion initiation of steel reinforcement in fly ash concretes. Cement and Concrete Research, Vol.16, No.5, pp. 782-784.

**Hansson, C. M (1984).** Comments on electrochemical measurements of the rate of corrosion of steel in concrete. Cement and Concrete Research, Vol.14, pp. 574-584.

**Hansson, C. M., Strunge, H., Markussen, J. B. and Frolund, T. (1985a).** The effect of cement type on the diffusion of chloride. Nordic Concrete Research, Publication No.4, pp. 70-80.

**Hansson, C. M., Frolund, Th. and Markussen, J. B. (1985b).** The effect of chloride cation type on the corrosion of steel in concrete by chloride salts. Cement and Concrete Research, Vol.15, No.1, pp. 65-73.

**Haque, M. N. and Kawamara, M. (1992).** Carbonation and chloride-induced corrosion of reinforcement in fly ash concretes. ACI Materials Journal, Vol.89, No.1, pp. 41-48.

**Hilsdorf, H. K., Kropp, J. and Gunter, M. (1984).** Carbonation, Pore Structure and Durability, Proceedings RILEM seminar, Hanover, pp. 182-196.

**Hoffman, D. W. (1984).** Changes in structure and chemistry of cement mortars stressed by sodium chloride solution. Cement and Concrete Research, Vol.14, pp. 49-56.

**Holden, W. R., Page, C. L. and Short, N. R. (1983).** The influence of chlorides and sulphates on durability of reinforcement in concrete. International Conference on Corrosion of Reinforcement in Concrete Construction, Edited by A. P. Crane, Soc. of Chem. Industry, pp. 143-150, London, UK.

**Kawamara, M., Kayyali, O. A. and Haque, M. N. (1988).** Effect of fly ash on pore solution composition of mortars with and without fly ash. Cement and Concrete Research, Vol.18, pp. 763-773.

**Kayyali, O. A. (1989).** Porosity and compressive strength of cement pastes in sulphate solution. Cement and Concrete Research, Vol.19, pp. 423-433.

**Kayyali, O. A. and Haque, M. N. (1988).** Effect of carbonation on chloride concentration in pore solution of mortars with and without fly ash. Cement and Concrete Research,

Vol.18, No.4, pp. 636-648.

**Kayyali, O. A. (1987).** Porosity of concrete in relation to the nature of the paste-aggregate interface. Materials and Structures, Vol.20, pp. 19-26.

**Kondo, R., Satake, M. and Ushiyama, H. (1974).** Diffusion of various ions in Hardened Portland Cement", Cement Association of Japan, 28th General Meeting, Tokyo, pp 41-43.

**Kondo, R., Daimon, M. and Akiba, T. (1968).** Mechanisms and kinetics on carbonation of hardened cement. 5th International Symposium on Chemistry of Cement Proceedings, Vol.3, Supplementary paper III-116, Tokyo, pp. 402-409.

**Konecny, L. and Naqvi, S. J. (1993).** The effects of different techniques on the pore size distribution of blended cement mortars. Cement and Concrete Research, Vol.23, No.3, pp. 1223-1228.

**Larbi, J. A. and Bijen, J. M. J. M. (1991).** The role of the cement paste-aggregate interfacial zone on water absorption and diffusion of ions and gases in concrete. Ph.D Thesis at the Technical University of Delft, Netherlands.

**Lawrence, C. D (1986).** Permeability and protection of reinforced concrete. Cement and Concrete Association, Reprint 6/86.

**Le Sage de Fontenay, C. and Sellevold, E. J. (1980).** Ice Formation in Hardened Cement Paste. Part-I: Mature Water Saturated Pastes. Durability of Building Materials and Componenets, STP 691, edited by Sereda P and Litvan G, ASTM, pp. 425-438.

**Li, S. and Roy, D. M. (1986).** Investigation of Relationship between Porosity, Pore Structure, and Chloride diffusion of Fly Ash and Blended Cement Pastes. Cement and Concrete Research, Vol.16, pp. 749-759.

**Lingane, J. J. (1967).** Controlled Potential Electroanalysis: in Coulometry in Analytical Chemistry. Edited by Milner G W C ang Phillips G, Pergamon Press Ltd, Oxford, pp. 172-186.

**Lingane, J. J. (1958).** Electroanalytical Chemistry. Interscience Publishers, New York, pp. 227-229.

**Litvan, G. (1976).** Variability of the Nitrogen Surface Area of Hydrated Cement Paste. Cement Concrete Research, Vol.6, No.1, pp. 139-144.

**Malek, R. I. A., Roy, D. M. and Fang, Y. (1989).** Pore structure, Permeability and Chloride Diffusion in Fly Ash- and Slag-containing Pastes and Mortars. Material Research Symposium Proceedings, Vol.137, pp. 403-411.

**Malek, R. I. A, and Roy, D. M. (1988).** The permeability of chloride ions in fly ash-cement pastes, mortars and concretes. Materials Research Society Symposium Proceedings, Vol.114, pp. 325-334.

**Malek, R. I. A., Roy, D. M. and Licastro, P. H. (1987).** The Diffusion Chloride ions in Fly Ash/Cement Pastes and Mortars. Material Research Symposium Proceedings, Vol.85, pp. 223-233.

**Manns, W. and Wesche, K. (1968).** Variations in strength of mortars made of different cements due to carbonation. 5th International Symposium on Chemistry of Cement Proceedings, Tokyo, Vol.3, pp. 385-393.

**Marsh, B. K. and Day, R. L. (1985).** Some difficulties in the assessment of Pore Structure of high performance Blended Cement Pastes. Material Research Symposium Proceedings, Vol.42, pp. 113-121.

**Marsh, B. K., Day, R. L. and Bonner, D. G. (1985).** Pore Structure Characteristics Affecting the Permeability of Cement Paste containing Fly Ash. Cement and Concrete Research, Vol.15, pp. 1027-1038.

**Mayer, A. (1968).** Investigations of the carbonation of concrete. 5th International Symposium on Chemistry of Cement Proceedings, Tokyo, Vol.3, pp. 394-401.

**Mehta, P. K. (1980).** Durability of concrete in marine environment: A review. ACI Publication, SP-65, pp. 1-20.

**Midgley, H. G. and Illston, J. M. (1984).** The Penetration of Chlorides into Hardened Cement Pastes. Cement and Concrete Research, Vol.14, pp. 546-558.

**Midgley, H. G. and Illston, J. M. (1980).** Effect of Chloride Penetration on the properties of Hardened Cement Pastes. Proceedings of the 7th International Congress on

Chemistry of Cement, Vol.III, pp. 101-103, Paris.

**Monfore, G. E. and Verbeck, G. J. (1960).** Corrosion of prestressed wire in concrete. ACI Journal, Proceedings, Vol.57, No.5, pp. 491-516.

**Monteiro, P. J. M., Maso, J. C. and Ollivier, J. P. (1985).** The aggregate-mortar interface. Cement and Concrete Research, Vol.15, pp. 953-958.

**Moukwa, M. and Aitcin, P. C. (1988).** The effect of Drying on Cement Paste Pore Structure as Determined by Mercury Porosimetry. Cement and Concrete Research, Vol.18, No.5, pp. 745-752.

**Nagataki, S., Ohga, H. and Kim, E. (1986).** Effect of conditions on carbonation and corrosion of fly ash concrete. ACI Proceedings SP-91, Madrid, Vol.1, pp. 521-540.

**Neville, A. M. and Brooks, J. J. (1987).** Concrete Technology. 1st Edition, Longman Group UK Limited.

**New Civil Engineer (1991).** Heavy snow emphasises de-icing deficiences. 14th February.

**New Civil Engineer (1989).** Cause for concern: Problem projects, 14th December.

**New Civil Engineer (1986).** Symptoms of Sulphates, 10th July.

**Newton, C. J. (1988).** The effect of concrete coatings on pipeline corrosion. D. Phil. Thesis, Oxford University.

**Ngala, V. T., Page, C. L., Parrott, L. J. and Yu, S. W. (1995).** Diffusion in cementitious materials: II- Further investigations of chloride and oxygen diffusion in well-cured OPC and OPC/30%PFA pastes. Cement and Concrete Research, Vol.25, No.4, pp. 819-826.

**Nyame, B. K. (1985).** Permeability of normal and lightweight mortars. Magazine of Concrete Research, Vol.37, No.130, pp. 44-48.

**Ost, B. and Monfore, G. E. (1966).** Penetration of Chloride into Concrete. J. PCA Res. and Dev. Lab., Vol.9, pp. 46-52.

**Ottewill, R. H. (1983).** Phil. Trans. R. Soc., A310, pp. 67.

**Page, C. L. and Lambert, P. (1987).** Kinetics of Oxygen Diffusion in Hardened Cement Pastes. Journal of Material Science, Vol.22, pp. 942-946.

**Page, C. L. and Lambert, P. (1986).** Analytical and electrochemical investigations of reinforcement corrosion. Transport and Road Research Laboratory (TRRL), Report No.30, 30 pp.

**Page, C. L. and Treadaway, K. W. J. (1982).** Aspects of the Electrochemistry of Steel in Concrete. Nature, Vol.297, No.5862, pp. 109-115.

**Page, C. L., Short, N. R. and El Tarras, A. (1981).** Diffusion of Chloride ions in Hardened Cement Pastes. Cement and Concrete Research, Vol.11, pp. 395-406.

**Parrott, L. J. (1992).** Variations of water absorption rate and porosity with depth from an exposed concrete surface: Effects of exposure conditions and cement type. Cement and Concrete Research, Vol.22, No.6, pp. 1077-1088.

**Parrott, L. J. (1975).** Increase in creep of hardened cement paste due to carbonation under load. Magazine of Concrete Research, Vol.27, N0.92, pp. 179-181.

**Parrott, L. J. (1987).** Measurement and modelling of porosity in drying cement paste. Materials Research Society Symposium Proceedings, Vol.85, pp. 91-104.

**Parrott, L. J. (1986).** Modelling the development of microstructure. Proceedings of Engineering Foundation Conference on Cement Manufacture and Use, Hennicker, pp. 43-73.

**Parrott, L. J. (1985).** Mathematical modelling of microstructure and properties of hydrated cement. NATO ASI Series E: Applied Science, No.95, pp. 213-228.

**Parrott, L. J. (1983).** Thermogravimetric and Sorption Studies on methanol Exchange in Alite Paste. Cement and Concrete Research, Vol.13, pp. 18-22.

**Parrott, L. J. (1981).** Effect of Drying history upon the Exchange of Pore Water with Methanol and upon subsequent Methanol Sorption behaviour in Hydrated Alite Paste. Cement and Concrete Research, Vol.11, No. 5, pp. 651-658.

**Parrott, L. J., Hansen, W. and Berger, R. (1980).** Effect of First Drying upon Pore Structure of Hydrated Alite. Cement and Concrete Research, Vol.10, No.5, pp. 647-655.

**Patel, R. G., Parrott, L. J., Martin, J. A. and Killoh, D. C. (1985).** Gradients of microstructure and diffusion properties in cement paste caused by drying. Cement and Concrete Research, Vol.15, No.2, pp. 343-356.

**Pihlajavaara, S. E. (1976).** Carbonation, engineering properties and effects of carbonation on concrete structures - General Report. Carbonation of Concrete - RILEM International Symposium, Cement and Concrete Association, paper 4.1.

**Pihlajavaara, S. E. (1968).** Some results of the effect of carbonation on the porosity and pore size distribution of cement paste. Materiaux et Construction, Vol.1, No.6, pp. 521-526.

**Poulsen, E. (1990).** The chloride diffusion characteristics of concrete: Approximate determination by linear regression analysis. Nordic Concrete Research, Publication No.9, pp. 124-133.

**Powers, T. C. (1962).** A hypothesis on carbonation shrinkage. Journal of Portland Cement Association Research and Development Laboratory, Vol.4, No.2, pp. 40-50.

**Powers, T. C. (1958).** Structural and Physical properties of Hydrated Cement Paste Journal of American Ceramic Society, Vol.41, No.1, pp. 1-6.

**Powers, T. C., Copeland, L. E., Hayes, J. C. and Mann, H. M. (1954).** Permeability of Portland Cement Paste. Proceedings of American Concrete Research Institute, Vol.51, No.3, pp. 285-298.

**Powers, T. C. and Brownyard, T. L. (1947).** Journal of American Concrete Institute Proceedings, Vol.43.

**Ramachandran, V. S. (1971).** Possible states of chlorides in hydration of tricalcium silicate in the presence of calcium chloride. Materiaux et Constructions, Vol.4, No.9, pp. 3-12.

**Regourd, M. (1976).** Carbonation accelere et resistance des ciments aux eaux aggressives. Carbonation of Concrete - RILEM International Symposium, Cement and Concrete

Association, paper 5.3, 4 pp.

**RILEM Draft Recommendation CPC-18 (1984).** Measurement of hardened concrete carbonation depth. Materiaux et Constuction, Vol.17, No.102, pp. 435-440.

**Roy, D. M. (1986).** Mechanisms of Cement Paste Degradation due to Chemical and Physical Factors. Proceedings of 8th International Congress on Chemistry of Cement, Vol.I, pp. 362-380.

**Roy, D. M., Kumar, A. and Rhodes, J. P. (1986).** Diffusion of Chloride and Cesium ions in Portland Cement Pastes and Mortars containing Blast Furnace Slag and Fly Ash. Proceedings of the 2nd International Conference on Fly Ash, Silica Fume, Slag and Natural Pozzolans in Concrete, Madrid, Spain, Vol.2, pp. 1423-1444.

**Kumar, A. and Roy, D. M. (1986).** Diffusion and Pore Structure in Portland Cement Pastes blended with low Calcium Fly Ash. Material Research Symposium Proceedings, Vol.65, pp. 227-234.

**Sauman, Z. (1972).** Effect of carbondioxide on porous concrete. Cement and Concrete Research, Vol.2, No.5, pp. 541-549.

**Sauman, Z. (1971).** Carbonization of porous concrete and its main binding components. Cement and Concrete Research, Vol.1, No.6, pp. 645-662.

**Scrivener, K. L., Crumble, A. K. and Pratt, P. L. (1988).** A study of the interfacial region between cement paste and aggregate in: In Bonding in Cementitious Materials. Materials Research Society Symposium Proceedings, Vol. 114, Edited by S. Mindness and S. Shah, pp. 87-88.

**Scrivener, K. L. and Gartner, E. M. (1988).** The characterization and quantification of cement and concrete microstructures: In Bonding in Cementitious Materials. Materials Research Society Symposium Proceedings, Vol. 114, Edited by S. Mindness and S. Shah, pp. 77-85.

**Scrivener, K. L. and Pratt, P. L. (1986).** A preliminary study of the microstructure of the cement-sand bond in mortars. 8th International Conference on the Chemistry of Cement, Rio de Janeiro, Vol.III, pp. 466-471.

**Sellevold, E. J. and Bager, D. H. (1980).** Low Temperature Calorimetry as a Pore Structure Probe. Proceedings of the 7th International Congress on Chemistry Cement, Paris, Vol.4, pp. 394-399.

**Sergi, G., Yu, S. W. and Page, C. L. (1992).** Diffusion of Chloride and Hydroxyl ions in Cementitious Materials exposed to a Saline Environment. Magazine of Concrete Research, Vol.44, pp. 63-69.

**Sergi, G. (1986).** Corrosion of Steel in Concrete - Cement Matrix Variables. PhD Thesis, Aston University, UK.

**Shi, D. and Winslow, D. N. (1985).** Contact Angle and Damage during Mercury Intrusion into Cement Paste. Cement and Concrete Research, Vol.15, pp. 645-654.

**Snyder, K. A., Winslow, D. N., Bentz, D. P. and Garboczi, E. J. (1992).** Interfacial zone percolation in cement-aggregate composites: In Interfaces in Cementitious Composites. Proceedings of the International Conference held by RILEM, Toulouse, France, pp. 259-268.

**Struble, L. (1988).** Microstructure and fracture at the cement paste-aggregate interface. Materials Research Society Symposium Proceedings, Vol. 114, Edited by S. Mindness and S. Shah, pp. 11-20.

**Suzuki, K., Nishikawa, T. and Ito, S. (1985).** Formation and carbonation of C-S-H in water. Cement and Concrete Research, Vol.15, No.2, pp. 213-224.

**Tang, L. and Nilsson, L-O. (1992).** Rapid determination of chloride diffusivity in concrete by applying an electric field. ACI Materials Journal, Vol.89, No.1, pp. 49-53.

**Taylor, H. F. W. (1984).** Studies on the chemistry and microstructure of cement pastes. Proceedings of British Ceramic Society, Vol.35, pp. 65-82.

**Thomas, M. D. A. and Matthews, J. D. (1992).** Carbonation of fly ash concrete. Magazine of Concrete Research, Vol.44, No.160, pp. 217-228.

**Treadaway, K. W. J., Macmillan, G., Hawkins, P. and Fontenay, C. (1983).** The influence of concrete quality of carbonation in Middle Eastern conditions - A preliminary study. Corrosion of Reinforcement in Concrete Construction, Proc. Soc. of Chem. Industry,

London, pp. 101-118.

**Tritthart, J. (1989).** Chloride binding in cement: II- The influence of hydroxide concentration in the pore solution of hardened cement paste on chloride binding. Cement and Concrete Research, Vol.19, No.5, pp. 683-691.

**Tuutti, K. (1980).** Service-life of structures with regard to corrosion of embedded steel. ACI Publication, SP-65-13, pp. 223-236.

**Tuutti, K. (1982).** Corrosion of steel in concrete. Swedish Cement and Concrete Institute, S-100 44-CBI, Forskning Research fo. 4.82, Stockholm.

**Ushiyama, H. and Goto, S. (1974).** Diffusion of various ions in hardened portland cement paste. 6th International Congress on Chemistry of Cement, Moscow, Vol.II-1, pp. 331-337.

**Verbeck, G. J. (1975).** Mechanisms of corrosion of steel in concrete. ACI Publication, SP-49-3.

**Verbeck, G. J. (1958).** Carbonation of hydrated portland cement. ASTM Special Publication, No.205, pp. 17-36.

**Vogel, A. I. (1978).** A Textbook of Quantitative Inorganic Analysis. 4th Edition, Revised by Basset J et al, Longman, London, pp. 754-755.

**Wakely, L. D. and Roy, D. M. (1982).** A method of testing the permeability of between grout and rock. Cement and Concrete Research, Vol.12, pp. 533-534.

**Wallbank, E. J. (1989).** The Performance of Concrete in Bridges - A Survey of 200 Highway Bridges. A Report prepared for the DoT by G. Maunsell and Partners.

**Whiting, D. (1981).** Rapid determination of the chloride permeability of concrete, Report No. FHWA/RD-81/119.

**Winslow, D. N., Cohen, M. D., Bentz, D. P., Snyder, K. A. and Garboczi, E. J. (1994).** Percolation and pore structure in mortars and concrete. Cement and Concrete Research, Vol.24, No.1, pp. 25-37.

**Winslow, D. N. and Diamond, S. (1970).** A Mercury Poosimetry Study of the Evolution of Porosity in Portland Cement. Journal of Materials, Vol.5, No.3, pp. 564-585.

**Young, J. F. (1988).** A Review of the Pore Structure of Cement Paste and Concrete and its influence on Permeability. Concrete Permeability, ACI, SP-108, pp. 1-18.

**Yu, S. W. and Page, C. L. (1991).** Diffusion in Cementitious Materials:-Comparative Study of Chloride and Oxygen Diffusion in Hydrated Cement Pastes. Cement and Concrete Research, Vol.21, pp. 581-588.

**Yu, S. W. (1990).** Ionic and Molecular Diffusion in Cementitious Materials. PhD Thesis, Aston University in Birmingham, UK.

**Yuan, C. Z. and Guo, W. J. (1988).** Effect of bond strength between aggregate and cement paste on the mechanical behaviour of concrete. Materials Research Society Symposium Proceedings, Vol.114, Edited by S. Mindness and S Shah, pp. 41-47.

**Zimbelmann, R. (1978).** The problem of increasing the strength of concrete. Betonwerk + Fertigteil - Technik, Heft 2, pp. 89-96.

# APPENDICES

# APPENDIX A: ATOMIC PACKING IN MATERIALS

The density of packing in a crystal is most conveniently determined by the atomic packing factor, which is defined in Equation 7.1 as:

$$\frac{\text{volume of the atoms per unit cell}}{\text{volume of the unit cell}}$$

Knowing the type of unit cell for a particular crystalline solid, we can estimate the atomic packing factor as above.

### (i) Face-Centred Cubic (FCC) Structure

The FCC structure is shown in Figure AA.1 and the number of atoms per unit cell can be estimated as follows: 8 atoms in the corner of the cube that are shared by 8 unit cells, since the unit cells extend in three directions. However, each atom at the face is shared only between 2 adjacent unit cells (Figure AA.1).

Thus the total number of atoms per unit cell is

$$(8 \times 1/8) + (6 \times 1/2) = 4$$

The lattice constant (a) is related to the atomic radius (r) by considering the projection of a face diagonal of an FCC crystal as shown in Figure AA.1(b).

Thus $$(4r)^2 = a^2 + a^2$$

and $$a = 4r/\sqrt{2}$$

The volume of atoms per unit cell is

$$4 \times 4\pi r^3/3 = 16\pi r^3/3$$

and the volume of the unit cell (V) is

$$V = a^3 = (4r/\sqrt{2})^3 = 32r^3/\sqrt{2}$$

Thus the packing factor of FCC structure is

$$(16\pi r^3/3)/(32r^3/\sqrt{2}) = \pi\sqrt{2}/6 = 0.74$$

which is equivalent to 74%

**(ii) Body-Centred Cubic (BCC) Structure**

The BCC structure is shown in Figure AA.2 and the number of atoms per unit cell can be estimated as follows: 8 atoms in the corners are shared by 8 unit cells and 1 atom totally within the unit cell.

Hence number of atoms per unit cell is

$$(8 \times 1/8) + 1 = 2$$

Figure AA.2(b) shows the planar view of diagonal plane AEGC and

Thus $(4r)^2 = a^2 + (a\sqrt{2})^2 = 3a^2$

with $a^2 = 16r^2/3$ and $a = 4r/\sqrt{3}$

Volume of atoms per unit cell is

$$2 \times 4\pi r^3/3 = 8\pi r^3/3$$

Volume of unit cell (V) is

$$V = a^3 = (4r/\sqrt{3})^3 = 64r^3/(3\sqrt{3})$$

Thus the packing factor of BCC structure is

$$[8\pi r^3/3]/[64r^3/(3\sqrt{3})] = \pi\sqrt{3}/8 = 0.68 \text{ or } 68\%$$

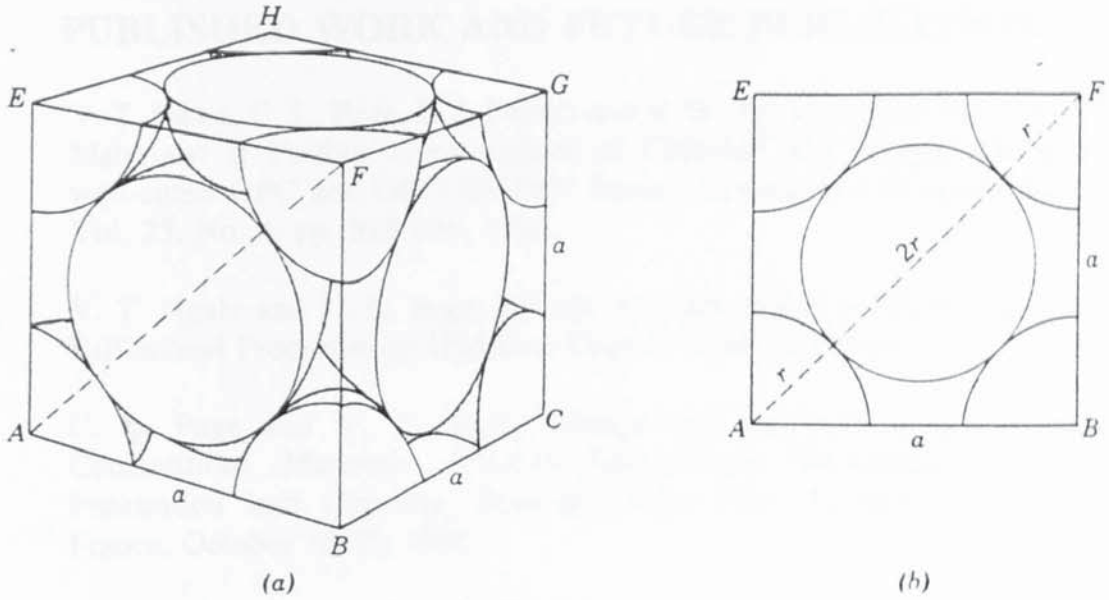


**Figure AA.1: FCC Structure (a) Three dimensional view**
**(b) Projection of the face AEFB**

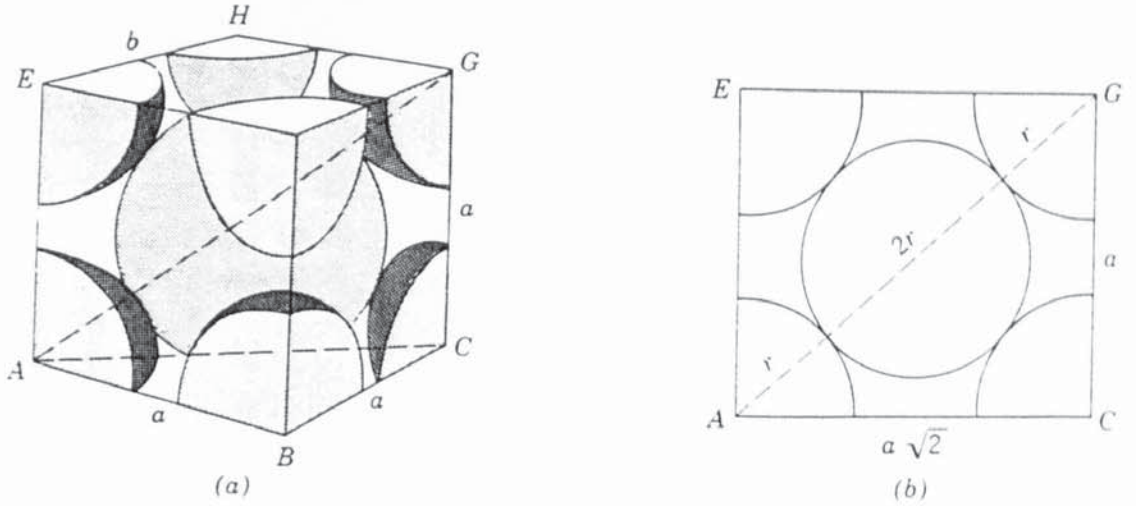


**Figure AA.2: BCC Structure (a) Three-dimensional view**
**(b) Planar view of diagonal plane AEGC**

# APPENDIX B:

# PUBLISHED WORK AND FUTURE PUBLICATIONS

1 V. T. Ngala, C. L. Page, L. J. Parrott and S. W. Yu. Diffusion in Cementitious Materials: II Further investigations of Chloride and Oxygen Diffusion in well-cured OPC and OPC/30%PFA Pastes. Cement and Concrete Research, Vol. 25, No. 4, pp. 819-826, 1995.

2 V. T. Ngala and C. L. Page. Effects of Carbonation on Pore Structure and Diffusional Properties of Hydrated Cement Pastes. In press.

3 C. L. Page and V. T. Ngala. Steady-state Diffusion Characteristics of Cementitious Materials. RILEM International Workshop on Chloride Penetration into Concrete, Domaine Saint Paul, St.-Remy-les-Chevreuse, France, October 15-18, 1995.

4 V. T. Ngala and C. L. Page. Influence of the paste-aggregate interfacial zone pore structure and chloride diffusion in glass bead mortars. To be published.

Cement and Concrete Researech Journal, Volume 25, Number 4, pp. 819-826
May, 1995

# Diffusion in Cementitious Materials: II Further investigations of Chloride and Oxygen Diffusion in well-cured OPC and OPC/30%PFA Pastes

V. T. Ngala, C. L. Page, L. J. Parrott and S. W. Yu
Department of Civil Engineering, Aston University, Birmingham, UK

RILEM International Workshop on Chloride Penetration into Concrete
(St Remy les Chevreuse, France, October 1995)

# Steady-State Diffusion Characteristics of Cementitious Materials

C L Page and V T Ngala
Department of Civil Engineering, Aston University, Birmingham, UK